MOLECULAR BASES UNDERLYING THE SENSITIVITY OF THE CAPSAICIN RECEPTOR: TRPV1

A Thesis Submitted in Satisfaction of the Requirements for the

Degree of Doctor of Philosophy of Imperial College London

by

Cleoper Paule

Sensory Processing Group

Imperial College

Chelsea and Westminster Hospital Campus

London

ABSTRACT

Individual human beings report highly variable pain experiences following exposure to the same noxious stimulus, including noxious heat. A series of missense single nucleotide polymorphisms (SNPs) have been found in the human noxious heat transducer, transient receptor potential vanilloid type 1 ion channel (hTRPV1), which responds to, exogenous, and endogenous, vanilloids, protons, and depolarisation. The aim of this project was to examine the effect of SNPs on the sensitivity of hTRPV1 to certain activators.

The three most frequently occurring SNPs (I315M, T469I, V585I) were used to generate 4 haplotypes: $hTRPV1_{112}$ (V585I); $hTRPV1_{121}$ (T469I); $hTRPV1_{211}$ (I315M); and $hTRPV1_{222}$ (I315M, T469I, V585I). The responses of these haplotypes to these activators were compared to the responses of the "wild type" hTRPV1 ($hTRPV1_{111}$, I315, T469, V585) using whole-cell patch-clamp recordings from HEK293 cells which transiently-expressed the relevant ion channels. Site-directed mutagenesis was used to confirm the role of the SNPs in altering the sensitivity of hTRPV1 to the activators applied.

In addition, in control experiments, several important collateral issues were investigated, namely: (a) the effect of the solvent, dimethyl sulphoxide (DMSO), on untransfected, and transfected, cells, respectively; and (b) the extent to which acid-sensing ion channels, constitutively-expressed by HEK293 cells, compromised the assessment of the proton-evoked responses of hTRPV1. The techniques employed included: the co-transfection of the cells with vector carrying the coding region of the green fluorescent protein (GFP) gene; the reverse transcriptase polymerase chain reaction; immunocytochemistry; the cobalt uptake assay; and whole-cell patch-clamp recordings.

The pharmacological and biophysical properties of the DMSO-evoked, and capsaicin-evoked, responses were similar. Furthermore, DMSO desensitised TRPV1. Acid-sensing ion channels were sensitive to the diuretic, amiloride (30μM).

However, amiloride increased hTRPV1-mediated responses evoked by noxious heat but not capsaicin.

$hTRPV1_{222}$ showed a higher sensitivity than $hTRPV1_{111}$ to capsaicin, and heat. Thus, when capsaicin was applied, the EC_{50} of $hTRPV1_{111}$ and $hTRPV1_{222}$ was 817 nM and 89 nM, respectively. The activation thresholds when heat was applied to $hTRPV1_{111}$ and $hTRPV1_{222}$ were 44.5±0.31 ^{o}C, and 42.3±045 ^{o}C, respectively). However, $hTRPV1_{111}$ was more sensitive to depolarisation than $hTRPV1_{222}$, with the $V_{1/2}$ at 37^{o}C for $hTRPV1_{111}$ and $hTRPV1_{222}$ being 42.3 mV and 83.3 mV, respectively. Furthermore, no differences were found between the proton-and anandamide- sensitivity of $hTRPV1_{111}$ and $hTRPV1_{222}$. The sensitivities of $hTRPV1_{121}$ to heat and depolarization were similar to those of $hTRPV1_{222}$, but different from those of $hTRPV1_{111}$. Furthermore, the sensitivity of $hTRPV1_{112}$ and $hTRPV1_{211}$ were similar to that of $hTRPV1_{111}$, but different from that of $hTRPV1_{222}$ and $hTRPV1_{121}$. Charge-neutralising and conserving mutations at position 469 produced clones with similar sensitivities to $hTRPV1_{121}$ and $hTRPV1_{111}$, respectively.

The studies undertaken established, first, that DMSO is able to activate TRPV1. Second, the non-synonymous SNP at position 469 in hTRPV1 alters the sensitivity of the ion channel to vanilloids, heat, and depolarisation. These findings suggest that missense SNPs in hTRPV1 may contribute to the development of different pain experience in humans in response to the same noxious stimulus. Accordingly, regard must be had to SNPs found in hTRPV1 when attempting to develop analgesics for pain which depends on TRPV1 activation and in treating that pain. Finally, the finding that the T469I mutation increased the sensitivity of the molecule to heat, but reduced its sensitivity to depolarisation, suggests that the various sensors in TRPV1 may be coupled allosterically rather than directly.

ACKNOWLEDGEMENT

I wish to take this opportunity of thanking all those people who have made it possible for me to spend four years discovering that there is more to chillies than is apparent in my local curry-house and who have been there to support me and make those years as enjoyable as they have been interesting and intellectually rewarding.

My first thanks must go to Dr. Istvan Nagy who has spent these last few years putting up with my mad rantings about Jelly Beans, Subway Sandwiches and Chinese takeaways but most importantly for giving me this opportunity to work with him. His love for science and his constant insistence to aim for the highest standards has given me the necessary foundation to be passionate about my own work and to believe in my own ability. I am deeply grateful to him.

Thanks to Dr. John White for his friendship and endless supply of warm dinners and glasses of wine. His company and his constant presence during the late nights while I was recording from cells made it more bearable, especially when I was really sleepy, hungry and fed-up. My pure addiction to "one more" -- one more cell, because one more cell will make, or break, it -- will forever haunt me and make me smile.

I wish to express my appreciation to Dr. John B. Davis, for his always valuable assistance, his challenging ideas, and generous support of my work. Thanks to Dr. Andy Photiou and Dr. Laki Buluwela for allowing me to hang out in their lab and for admitting me to their inner circle where I learned the fascinating complexities of site-directed mutagenesis.

A very big "thank you" is due to all the people in the laboratories at Chelsea and Westminster Hospital. Their laughter, good company, and continuous supply of jokes and Starbucks, have always been appreciated.

My deepest debt of gratitude is owed to my nearest and dearest. Thanks to my parents for providing me with endless love, support, and for a roof to sleep under. Thanks to my three wonderful sisters, especially to Annabelle, who has kept me grounded and sane with words of encouragement during the very testing time of writing this thesis. Finally, to Gurpreet Singh, without whom I would have been lost; just you and I against the world!

Cleoper Paule

Sensory Processing Group
Imperial College
Chelsea and Westminster Hospital Campus
London

CONTENTS

Abstract 3
Preface 5
Table of content 6
List of figures and tables 11
List of abbreviations 16

Chapter 1
The Capsaicin Receptor: from chillies to pain

1.1 Introduction 20
1.1.1 Pain as a blessing and a burden 21
1.1.2 Development of acute pain 22
1.1.3 Development of prolonged and chronic pain 23
1.2 Differences in pain perception 25
1.2.1 Cultural and social influences 25
1.2.2 Biological factors 26
1.2.2.1 Sex and Gender 26
1.2.2.2 Psychological status 27
1.2.2.3 Ethnicity 28
1.2.2.4 Genetically-defined factors 28
1.2.2.4.1 Polymorphisms 29
1.3 TRPV1 32
1.3.1 Structure of TRPV1 32
1.3.2 TRPV1 multimeric structure 33
1.3.2a TRPV1 splice variants 35
1.3.3 TRPV1 activators 36
1.3.3.1 Vanilloids 36
1.3.3.2 Anandamide 37
1.3.3.3 Protons 37
1.3.3.4 Heat 38
1.3.3.5 Voltage-dependent activation 39
1.3.3.6 Post-translational modification 39
1.3.4 Expression and distribution of TRPV1 40
1.3.4.1 Expression by primary sensory neurons 40
1.3.4.2 Expression in the central nervous system 40
1.3.4.3 Expression by non-neuronal cells 41
1.3.5 The role of TRPV1 in physiological and pathological conditions 42
1.3.5.1 Pain 42
1.3.5.2 TRPV1 and inflammatory pain 42
1.3.5.3 TRPV1 and neuropathic pain 43
1.3.5.4 Visceral hyper-reflexia and pain 44
1.3.5.5 Diabetes 44
1.3.6 TRPV1 polymorphisms 46

1.4 Aims and objectives 52

1.4.1 Hypothesis 52
1.4.2 Aim 52
1.4.3 Objectives 52

Chapter 2
Experimental techniques and protocols

2.0 Introduction 54
2.1 Cell Culture 54
2.1.1 Cell culture of DRG neurons 57
2.1.1.1 Theory of DRG neurons in culture 57
2.1.1.2 Culturing DRG neurons 60
2.1.2 Cell culture of HEK293 cells 65
2.1.2.1 Theory of technique 65
2.1.2.2 Culturing HEK293 cells 66
2.2 Transfection 69
2.2.1 Background to the purpose of transfection 69
2.2.1.1 Cloning of DNA 69
2.2.1.2 Theory of transfection 72
2.2.1.3 Transient transfection 75
2.3 Site-directed mutagenesis 78
2.3.1 Theory behind site-directed mutagensis 78
2.3.2 Site-directed mutagenesis: practical approach 84
2.4 Agonist-activated cobalt uptake 91
2.4.1 Theory of agonist-activated cobalt uptake 91
2.4.2 Practical application of agonist-activated cobalt uptake 96
2.4.2.1 Data analysis of agonist-activated cobalt uptake 97
2.4.2.2.1 Data analysis for hTRPV1-transfected HEK293 cells 99
2.4.2.2.2 Data analysis for mouse DRG culture 101
2.5 Whole-cell patch-clamp recordings 103
2.5.1 Introduction to whole-cell patch-clamp recording 103
2.5.2 Biophysics of whole-cell patch-clamp technique 108
2.5.2.1 Ion channels 108
2.5.2.2 Lipid bilayer 113
2.5.2.2.1 Compensating the capacitive transients 113
2.5.2.3 Ionic distribution 114
2.5.2.3.1 Compensating for series resistance 117
2.5.3 Practical components of whole-cell patch-clamp recordings 119
2.5.3.1 Solutions 120
2.5.3.2 Patch Electrodes 120
2.5.3.3 Perfusion system and drug application 122
2.5.3.4 Obtaining whole-cell patch-clamp configuration 126

2.5.4 Recording protocols and data analysis 127
2.5.5 Capsaicin-evoked activation 127
2.5.6 Anandamide-evoked activation 128
2.5.7 Proton-evoked activation 128
2.5.8 Heat-evoked activation 129
2.5.8.1 Analysis of heat-sensitivity 130
2.5.8.2 Biophysics of heat-sensitivity 130
2.5.8.3 Analysis of heat-induced response 134
2.5.8.4 Comparison of analysing heat-induced responses by the two methods 145
2.5.9.1 Current-voltage relationship of the TRPV1agonist-evoked responses 150
2.5.10 Voltage-dependence 152
2.5.10.1 Biophysics of voltage-dependence 152
2.5.10.2 Untransfected HEK293 cells and voltage-dependence 155
2.5.10.2.1 Study design and practical application 155
2.5.10.2.2 Response of untransfected cell to changing the membrane potential 157
2.5.10.3 TRPV1-transfected HEK293 cells and voltage-dependent acyivity 158
2.5.10.3.1 Study design 158
2.5.10.3.2 Practical application 163
2.5.10.3.3 Response of TRPV1-transfected cell to voltage-dependence 163
2.6 Statistical Analysis 171
2.6.1 Descriptive statistics 171
2.6.1.1 Central tendency 171
2.6.1.2 Variability 172
2.6.1.3 Distribution 174
26.1.4 Sampling distribution of the mean 176
2.6.2 Inferential statistics 179
2.6.2.1 Estimation statistics 179
2.6.2.1.1 Parameter estimation 179
2.6.2.1.1.1 Linear regression model 179
2.6.2.1.1.1a Correlation coefficient of a linear regression 180
2.6.2.1.1.2 Non-linear regression model 181
2.6.2.1.1.2a Gaussian distribution 181
2.6.2.1.1.2b Sigmoid curve 183
2.6.2.1.1.2c Boltzmann curve 184
2.6.2.1.1.3 The goodness of fit of nonlinear regression 185
2.6.2.1.1.4 Confidence intervals 185
2.6.2.2 Hypothesis testing 186
2.6.2.2a Statistical errors: type I and type II error 187
2.6.2.2b Power analysis 188
2.6.2.2.1 Parametric tests 189
2.6.2.2.1a Test for normality of the distribution 190
2.6.2.2.1b Test for equal variance 191

2.6.2.2.1.1 Comparing the means of data 193
2.6.2.2.1.1a Student t-test 193
2.6.2.2.1.1b ANOVA 195
2.6.2.2.1.1c Post hoc tests 197

Chapter 3
DMSO activates TRPV1

3.1 Introduction 201
3.2 Methods 201
3.2.1 Whole-cell patch-clamp recordings 201
3.2.1.1 Application of 0.2% DMSO 203
3.2.1.2 Application of 0.2% DMSO in the presence of capsazepine 203

3.2.2 Cobalt-uptake of hTRPV1$_{111}$-transfected HEK293 cells 204
3.2.2.1 0.2% DMSO application 204
3.2.2.2 0.2% DMSO application in the presence of capsazepine 205
3.2.2.3 Repeated applications of capsaicin and DMSO in the presence and absence of calcium ions. 207
3.2.2.4 Application of capsaicin dissolved in varying percentages of DMSO 209
3.2.2.5 Cobalt-uptake on cultured DRG neurons 209

3.2.3 Statistical analysis 210

3.3 Results 211
3.3.1 Properties of DMSO-evoked hTRPV1-mediated currents 211
3.3.2 The effect of DMSO on cobalt-uptake 217
3.3.3 DMSO-evoked desensitisation in the presence of calcium ions. 220
3.3.4 Effect of DMSO on the capsaicin-evoked hTRPV1 activation 225
3.3.5 DMSO-evoked responses in DRG cultures 227
3.4 Discussion 230

Chapter 4
Constitutive and acid sensitivity of HEK293 cells

4.1 Introduction 236
4.2 Methods 236
4.2.1 Whole-cell patch-clamp recordings of hTRPV1-transfected HEK293 cells 236
4.2.1.1 Proton application in the absence and presence of amiloride 238 239
4.2.1.2 Capsaicin application in the absence, and presence, of amiloride 239
4.2.1.3 Heat application in the absence and presence of amiloride
4.2.2 Statistical analysis 240
4.3 Results 241
4.3.1 Proton-evoked responses in untransfected HEK293 cells 241
4.3.2 The effect of amiloride on hTRPV1-mediated responses in hTRPV1-tranfected cells 243
4.3.2.1 The effect of amiloride on proton-evoked responses 243
4.3.2.2 The effect of amiloride on capsaicin-evoked responses 245
4.3.2.3 The effect of amiloride on heat-evoked responses 247
4.4 Discussion 250

Chapter 5
Naturally occurring polymorphism in human TRPV1 gene alters the sensitivity of the ion channel

5.1 Introduction 254
5.2 Method 255
5.3 Results 255
5.3.1 Comparative analysis of $hTRPV1_{111}$-, and $hTRPV1_{222}$-, mediated responses to various activators 255
5.3.1.1 *Comparison of responses to capsaicin* 255
5.3.1.2 *Comparison of responses to anandamide* 260
5.3.1.3 *Comparison of responses to protons* 262
5.3.1.4 *Comparison of responses to heat* 266
5.3.1.5 *Comparison of responses to voltage-dependent activation* 269
5.3.1.6 *Summary of comparisons of responses of $hTRPV1_{111}$ and $hTRPV1_{222}$ to various to TRPV1 activators* 272
5.3.2 The relationship between heat and voltage for $hTRPV1_{111}$ and $hTRPV1_{222}$ 274
5.3.2.1 The heat threshold depends on the holding potential 274

5.3.3 Comparative analysis of hTRPV1$_{211}$-, hTRPV1$_{121}$- and hTRPV1$_{112}$-, mediated responses 276
5.3.3.1 Responses of TRPV1$_{211,}$ hTRPV1$_{121,}$ and hTRPV1$_{112}$ to heat 276
5.3.3.2 Response of hTRPV1$_{121}$ to voltage-dependent activation 278
5.3.4 Comparative analysis of hTRPV1 $_{121\text{-}S}$ and hTRPV1$_{121\text{-}A}$ mediated responses 280
5.3.4.1 Responses of mutants to heat 280
5.4 Discussion 282

Chapter 6
Summary of results and conclusions

6.1 Summary 291
6.2 DMSO activates TRPV1 291
6.3 Amiloride affects TRPV1-mediated responses 293
6.4 Polymorphisms alter the sensitivity of hTRPV1 to various activators 295

REFERENCES **297**

FIGURES AND TABLES

Chapter 1: The Capsaicin Receptor: from chillies to pain

Figure 1.1 Membrane topology of TRPV1
Figure 1.2 Membrane topology and approximate location of the 7 missense SNP's found in hTRPV1 receptor
Table 1.1 Seven missense SNPs found in hTRPV1 by Davis and colleagues (unpublished data).
Table 2.2 5 haplotypes of hTRPV1, where isoleucine (I), threonine (T) and valine (V) are substituted by a different amino acid within a specified position.

Chapter 2. Experimental techniques and protocols

Figure 2.1 Cross-section of the spinal cord and surrounding structures
Figure 2.2 The spinal segments of a mouse.
Figure 2.3 Map of pcDNA3.1v5-HIs-TOPO vector.
Figure 2.4 Location of mutagenic primers for site-directed mutagenesis of codon 469 on the hTRPV1 gene.

Figure 2.5 Complementary DNA sequence between bases 1021-1660 of the open reading frame of the human TRPV1 and the location of the primer pair flanking the region of site directed mutation.
Figure 2.6 Sequencing data of site directed mutation of codon 469 of the human TRPV1 gene
Figure 2.7 General procedure when carrying out cobalt-uptake assay to investigate functional TRPV1 activity in TRPV1-expressing cells.
Figure 2.8 Analysis of cobalt-uptake assay on hTRPV1-transfected HEK293 cells
Figure 2.9 Analysis of cobalt-uptake assay on mouse DRG cells.
Figure 2.10 The main components of a two-electrode voltage-clamp set-up.
Figure 2.11 Diagram of the main components of a patch-clamp configuration using one electrode
Figure 2.12 The Ag/AgCl electrode. Currents are able to flow in both direction of the electrode.
Figure 2.13 Four configurations of patch-clamp technique.
Figure 2.14 Ohm's law. Ohm's law states that there is a linear relationship between current *I* and voltage *V*.
Figure 2.15 Schematic diagram of an idealised single channel recording
Figure 2.16 Ion channels as a parallel circuit.
Figure 2.17 A single membrane ion channel as circuit
Figure 2.18 The main components of a patch-clamp set-up
Figure 2.19 Schematic diagram of the fabrication of patch electrodes using a two-stage vertical puller.
Figure 2.20 Perfusion system of the electrophysiology set-up.
Figure 2.21 Thermo-TRP channels respond to a wide range of temperatures
Figure 2.22 Schematic diagram of a typical Arrhenius plot.
Figure 2.23 Arrhenius plot of heat-induced response in hTRPV1-transfected cells
Figure 2.24 Whole-cell membrane current induced by heat ramp and its Q_{10} in an untransfected HEK293 cell.
Figure 2.25 A whole-cell membrane current induced by a heat ramp and its Q_{10} in TRPV1-transfected HEK293 cell.
Figure 2.27 Q_{10} values of untransfected HEK293 cells and hTRPV1-transfected HEK293 cells between 37-51 ^{o}C.
Figure 2.28 Q_{10} values and activation energy the slow rising phase (37-43 ^{o}C) and the fast (46-51 ^{o}C) from hTRPV1-transfected HEK293 cells.
Figure 2.29 Heat activation threshold of first and second analysis of data.
Figure 2.30 Voltage-dependent activation of untransfected HEK293 cells.
Figure 2.31 Data analysis of voltage-dependence of hTRPV1-mediated response
Figure 2.32 Typical conductance-voltage relationships of a $TRPV1_{111}$-transfected HEK293 cell

Figure 2.33 V-G/G_{max} relationship of conductances
Figure 2.34 V-G/G_{max} relationship showed on fig 2.32, fitted with two Boltzmann functions.
Figure 2.35 V-G relationship of voltage-activated current in untransfected cell and hTRPV1-transfected cell
Figure 2.36 Average V-G/Gmax relationship of $hTRPV1_{111}$ and $hTRPV_{222}$
Figure 2.37 Normal distribution curve and the Empirical Rule
Figure 2.38 The spread of the sampling distribution of the mean
Figure 2.39 Sigmoidal dose response curve.
Figure 2.40 Boltzmann curve
Figure 2.41 Types of statistical errors associated with hypothesis testing.
Table 2.1 Seven haplotypes of hTRPV1. Haplotypes 1-5 were made by Davis and co-workers.
Table 2.2 TRP channels and their Q_{10} values as found in various studies.

Chapter 3. DMSO activates TRPV1

Figure 3.1 Sequence of treatment steps performed to investigate capsazepine on capsaicin-evoked, and DMSO-evoked, capsaicin-evoked cobalt-labelling.
Figure 3.2 Sequence of treatments steps investigates the effect of successive applications of capsaicin and DMSO.
Figure 3.3 DMSO-evoked responses in untransfected cells and hTRPV1-transfected cells using whole-cell patch-clamp recordings.
Figure 3.4 The effect of capsazepine on capsaicin-evoked activation of hTRPV1-transfected cells using whole-cell recordings.
Figure 3.5 The effect of capsazepine on 0.2% DMSO-evoked currents in hTRPV1-transfected cells using whole-cell recordings.
Figure 3.6 Grey scale images of cells following cobalt-uptake assay of untransfected cells in response to 500 nM capsaicin and 0.2% DMSO application.
Figure 3.7 Grey scale images of cells following cobalt-uptake assay Cobalt-uptake images of hTRPV1-transfected cells in response to 500 nM capsaicin and 0.2% DMSO application.
Figure 3.8 The effect of capsaicin (500nM), capsazepine (5μM) and DMSO (0.2 %) on hTRPV1-transfected cells using cobalt-uptake
Figure 3.9 Repeated application of capsaicin and DMSO in hTRPV1-transfected cells in the presence, and absence, of 2 mM $CaCl_2$ using the cobalt-uptake assay.
Figure 3.10 The effect of the percentage of DMSO content in capsaicin on hTRPV1-mediated capsaicin responses assessed by the cobalt-uptake assay
Table 3.2 Protocols of cobalt-uptake assay to investigate the effect of capsazepine (Cpz) on capsaicin-evoked, and DMSO-evoked, cobalt-labelling.
Table 3.3 Protocols of cobalt-uptake assay to investigate the effect of repeated applications of capsaicin and DMSO.

Chapter 4. Constitutive and acid sensitivity of HEK293 cells

Figure 4.1 Untransfected HEK293 cells constitutively express proton-responding ion channels.

Figure 4.2 Proton-evoked responses of hTRPV1-transfected HEK293 cells in the absence, and presence, of amiloride.

Figure 4.3 Proton concentration–response curve of hTRPV1-transfected HEK293 cells in the absence, and presence, of amiloride.

Figure 4.4 Whole-cell patch-clamp recordings of hTRPV1-mediated responses to 10 μM capsaicin in the absence and presence of amiloride buffer.

Figure 4.5 Concentration response curves of hTRPV1 to capsaicin in the absence and presence of 30 μM amiloride.

Figure 4.6 Heat-evoked responses of hTRPV1-transfected cells in the absence, and presence, of amiloride (part I).

Figure 4.7 Heat-evoked response of untransfected cell in standard buffer.

Figure 4.8 Heat-evoked responses of hTRPV1-transfected cells in the absence, and presence, of amiloride part (II)

Chapter 5. Naturally occurring polymorphism in human TRPV1 gene alters the sensitivity of the ion channel

Figure 5.1 Capsaicin-evoked responses of $hTRPV1_{111}$-transfected, and $hTRPV1_{222}$-transfected, HEK293 cells.

Figure 5.2 Current-voltage relationship of 1 μM capsaicin-evoked current of $hTRPV1_{111}$ and $hTRPV1_{222}$

Figure 5.3 Anandamide-evoked responses in $hTRPV1_{111}$-transfected, and $hTRPV1_{222}$-transfected, HEK293 cells.

Figure 5.4 Proton-evoked responses of $hTRPV1_{111}$-transfected and $hTRPV1_{222}$-transfected, HEK293 cells.

Figure 5.5 Current-voltage relationship of pH 5-evoked currents of $hTRPV1_{111}$ and $hTRPV1_{222}$.

Figure 5.6 Heat-evoked responses of $hTRPV1_{111}$-transfected and $hTRPV1_{222}$-transfected,

Figure 5.7 Current-voltage relationship of heat-evoked currents of $hTRPV1_{111}$ and $hTRPV1_{222}$.

Figure 5.8 Voltage-evoked response of $hTRPV1_{111}$-transfected, and $hTRPV1_{222}$-transfected HEK293 cells using symmetrical Na+ concentrations (130 mM).

Figure 5.9 Summary of reversal potential obtained from current-response curves of $hTRPV1_{111}$-transfected and $hTRPV1_{222}$-transfected, HEK293 cells evoked by various TRPV1 activators using normal extracellular and intracellular solution.

Figure 5.10 Heat activation threshold of $hTRPV1_{111}$ and $hTRPV1_{222}$ at four different holding potentials.

Figure 5.11 Heat responses of $hTRPV1_{111,}$ $hTRPV1_{222,}$ $hTRPV1_{121,}$ $hTRPV1_{211}$ and $hTRPV1_{112}$

Figure 5.12 Voltage-dependent activation of $hTRPV1_{111,}$ $hTRPV1_{222}$, and $hTRPV1_{121}$.

Figure 5.13 Heat-activation threshold of $hTRPV1_{111,}$ $hTRPV1_{222,}$ $hTRPV1_{121,}$ $hTRPV1_{121\text{-}S}$, and $hTRPV1_{121\text{-}A}$.

Figure 5.14 Amplitude of currents at 48°C of $hTRPV1_{111,}$ $hTRPV1_{222,}$ $hTRPV1_{121,}$ $hTRPV1_{121\text{-}S}$, and $hTRPV1_{121\text{-}A}$

Table 5.1 5 haplotypes of hTRPV1, where isoleucine (I), threonine (T) and valine (V) are substituted by a different amino acid within a specified position.

Table 5.2 Summary of responses of $hTRPV1_{111}$-transfected and $hTRPV1_{222}$-transfected, HEK293 cells evoked by various TRPV1 activators.

ABBREVIATIONS

1-ANOVA	One way analysis of variance
Ag/AgCl	Silver wire coated with silver-chloride
AMPA	Alpha-amino-3-hydroxy-5-methyl-4-isoxazole propionate
ASIC	Acid-Sensing Ion Channel
ATP	Adenosine triphosphate
BK	Bradykinin
Ca^{2+}	Calcium ions
$CaCl_2$	Calcium chloride
CB1	Cannabinoid 1
cDNA	Complementary DNA
CGRP	Calcitonin Gene-Related peptide
CNS	Central nervous system
Co^{2+}	Cobalt ions
$CoCl_2$	Cobalt chloride
DMSO	Dimethyl
DNA	Deoxyribonucleic acid
D-PBS	Dulbecco's Phosphate Buffered Saline
DRG	Dorsal root ganglion
EC_{50}	Half maximal effective concentration
ECACC	European Collection of Cell Cultures
EDTA	Ethylenediaminetetraacetic acid-tetrasodium
G6PD	Glucose 6-phosphate dehydrogenase
GAPDH	Glyceraldehyde-3-phosphate dehydrogenase
GDNF	Glial cell derived neurotrophic factor
GFP	Green fluorescent protein
HEK	Human Embryonic Kidney cells
HEPES	4-(2-hydroxyethyl)-1-piperazineethanesulfonic acid
hTRPV1	Human Transient Receptor Potential Vanilloid type 1
IASP	International Association for the Study of Pain
KCl	Potassium Chloride
LSD	Least significant difference
MES	2-(N-Morpholino)ethanesulfonic acid sodium
$MgCl_2$	Magensium Chloride
mRNA	Messenger RNA
NaCl,	Sodium Chloride
NADA	N-arachidonoyl-dopamine
NAEs	N-acylethanolamines
NGF	Nerve growth factor
NMDA	N-methyl-D-aspartic acid
OLDA	N-oleoyldopamine
OPRM1	mu-opioid receptor gene

PBS	Phosphate Buffered Saline
PGE2	Prostaglandin E2
$pH_{0.5}$	Half-maximal pH
PIP2 or PtdIns(4,5)P2	Phosphatidylinositol 4,5-Bisphosphate
PKA	cAMP-dependent protein kinase
PKC	Protein kinase C
RT-PCR	Reverse Transcription-Polymerase Chain Reaction
rTRPV1	Rat transients Receptor Potential Vanilloid type 1
RTX	Resiniferatoxin
SDM	Site -Directed Mutagenesis
SEM	Stand Error of Mean
SIC	Stretch-inactivated channel
SNP	Single Nucleotide Polymorphism
TM	Transmembrane
TRPA1	Transient receptor potential subtype A1
TRPM8	Transient receptor potential cation channel, subfamily M, member 8
TRPV1	Transients Receptor Potential Vanilloid type 1
$TRPV1_{VAR}$	TRPV1 splice variant
$V_{1/2}$	Half activation potential
VR.5'sv	TRPV1 5' splice variant

Twenty years from now you will be more disappointed by the things that you didn't do than by the ones you did do. So throw off the bowlines. Sail away from the safe harbour. Catch the trade winds in your sails. Explore. Dream. Discover.

Mark Twain

Chapter 1

THE CAPSAICIN RECEPTOR: FROM CHILLIES TO PAIN

1.1 Introduction

The capsaicin receptor, the transient receptor potential vanilloid type-1 receptor (TRPV1), is a non-selective cationic channel (Caterina et al., 1997). TRPV1 is expressed by the great majority of nociceptive primary sensory neurons within the dorsal root, and trigeminal ganglia predominately in small diameter cells (Caterina et al., 1997; Tominaga et al., 1998). Intense TRPV1 immunoreactivity has also been observed in both the peripheral, and central, terminals of primary sensory neurons (Szallasi and Blumberg, 1999; Tominaga and Caterina, 2004). In addition to small diameter primary sensory neurons, TRPV1 is also expressed in neurons in various areas in the brain including the cortex, hypothalamus, and hippocampus (Starowicz et al., 2007; Cristino et al., 2006; Sasamura et al., 1998; Mezey et al., 2000; Roberts et al., 2004). Non-neuronal tissues expressing TRPV1 include epithelial cells of the skin, urinary bladder, kidney and mast cells (Denda et al., 2001; Birder et al., 2002; Sanchez et al., 2001; Stander et al., 2004).

TRPV1 belongs to a unique group of ion channels which can be activated by multiple stimuli. TRPV1 responds to at least 5 groups of activators which include: ligands, such as capsaicin, the pungent agent of chilli pepper; acidification; heat above 43ºC; post-translational modification, such as phosphorylation; and depolarisation (Caterina et al., 1997; Tominaga et al., 1998; Voets et al., 2004; Zygmunt et al., 1999). TRPV1 is regarded as a noxious heat transducer in primary sensory neurons because many of its activators, including capsaicin, heat above 43^{o}C and protons, evoke a burning pain sensation when they activate TRPV1 expressed in these cells. TRPV1 is expressed in various neurons other than primary sensory neurons, as well in non-neuronal cells, which suggests that TRPV1 may be involved in a series of physiological and pathological processes. However, initiating, and maintaining pain sensation is still regarded as the main function of TRPV1.

1.1.1 Pain as a blessing and a burden

The International Association for the Study of Pain (IASP: 1979), defines "pain" as an unpleasant sensory and emotional experience associated with actual, or potential, tissue damage, or described in terms of such damage. The pain experience develops in a process called nociception which exists in the entire animal kingdom. Nociception involves the processing of signals arising from the inner, or outer, environment of the organism and their interpretation by the nervous system as presenting a threat to the integrity of the tissues, and ultimately, the integrity of the whole organism. Nociception leads to the experience of pain in humans while animals exhibit "pain-related behaviour". Nociception serves as a warning signal to the organism of an impending danger and, therefore, it is biologically beneficial and absolutely essential for survival. However, both in humans and in animals, nociception may sometimes have no biological function and may not serve as a survival tool. On the contrary, in those circumstances, it may ruin the quality of life. Thus, while pain with a biological function is called "physiological pain", pain without that function is called "pathological pain".

Physiological pain develops in two circumstances: (1) when the thermal, mechanical, or chemical, characteristics of the environment change in a way which threatens the integrity of tissues; or (2) when changes in these characteristics results in actual tissue damage. While the first type of pain is called "acute pain" and can last for seconds, the second type is called "prolonged pain" and can last for days, or even weeks. On the one hand, the obvious function of acute pain is to generate a warning signal or a flight reaction, while, on the other hand, the function of prolonged pain is to promote healing through quiescence, by promoting avoidance of contact and use of the injured tissue.

Pathological pain or chronic pain is usually associated with injury which cannot heal. Such pain is found in rheumatoid arthritis, nerve injury, osteoarthritis or cancer-induced tissue damage. Pathological pain can also develop after successful healing of the original injury and may last for years. The IASP defines chronic pain as "pain which has persisted beyond normal tissue healing time", which is taken, in the absence of other criteria, to be three months. The great majority of prolonged and chronic, pain is associated with peripheral events and can be of either inflammatory, or neuropathic, origin. As the names imply, inflammatory pain is related with inflammation of tissues, while neuropathic pain is associated with physical, metabolic injury, or infection of neurons in the peripheral nervous system. In addition, chronic pain may also have a central (central nervous system) origin.

1.1.2 Development of acute pain

Acute pain develops as a consequence of activation of specialised molecules called transducers which are expressed by nociceptive primary sensory neurons. These transducers respond to changes in the thermal, mechanical and/or chemical characteristics of the environment which have the potential of damaging the integrity of the tissues. The known transducers, including TRPV1, are cationic channels. As a result of the effect of changes in the thermal, mechanical, and chemical, characteristics of the environment, the open probability of transducers is increased which results in depolarising inward currents due to the influx of cations. These inward currents produce a generator potential which leads to the generation of action potentials, if and when the membrane depolarisation reaches the threshold for activation of voltage-sensitive sodium channels. The action potentials are propagated along thinly myelinated Aδ (conduction velocity within the range of 5-25 m/s), or unmyelinated C (conduction velocity within the range of 0.5-2 m/s), primary sensory fibers into the dorsal horn of the spinal cord. The action potentials induce the release of neurotransmitters, such as glutamate, from the spinal terminals of these nociceptive primary sensory neurons. Glutamate acts mainly on the ionotropic class of glutamate receptors to produce inward currents in secondary sensory neurons. The

receptor involved in this process is the alpha-amino-3-hydroxy-5-methyl-4-isoxazole propionate (AMPA) type of glutamate receptors. The current flowing through the AMPA receptor initiates action potential generation in the secondary sensory neurons, which have ascending axons. These axons project from laminae I and IV *via* the spinothalamic tract and the spinal lemniscal tract where they terminate at the ventral posterior nuclei of the thalamus and release transmitters to generate action potentials in tertiary sensory neurons (Warren et al., 2006). These tertiary sensory neurons project to the somatosensory cortex, where the information is processed and that processing results in the perception of acute pain sensation.

1.1.3 Development of prolonged and chronic pain

Prolonged, and chronic, pain develops in a 're-tuned' nervous system. This re-tuning is the result of plastic changes induced by pathological processes and includes so-called peripheral sensitisation and central sensitisation. These sensitisations result in an increased excitability of nociceptive neurons. In addition, sensitisation also induces the recruitment of otherwise silent nociceptive-specific neurons, some non-nociceptive neurons, and glial cells (Schmidt et al., 1995; Xu et al., 2000). Thus, prolonged and chronic pain is not a simple repetition of acute pain. Consequently, the prolonged, and chronic, pain experiences are qualitatively different from the acute pain experience. Since the great majority of prolonged, and chronic, pain has a peripheral origin, it is reasonable to assume that central sensitisation and the recruitment of silent nociceptive, non-nociceptive neurons, and glial cells in the central nervous system, are initiated and maintained by increased activity and excitability of primary sensory neurons (Woolf and Costigan, 1999).

Two major types of pathological pain sensations are experienced in prolonged, and chronic pain, namely: hyperalgesia where there is an increase in pain responses to noxious stimuli; and allodynia where pain responses are evoked by normally innoxious stimuli. The modalities of both hyperalgesia and allodynia may be either mechanical or thermal. Since the great majority of prolonged, and chronic, pain diseases have a peripheral origin, it is reasonable to assume that the transducers,

which result in the development of acute mechanical, or thermal, pain sensations, are also involved in the development of mechanical, and thermal, pathological pain sensations, respectively. Indeed, it has been shown, for example that TRPV1 -the acute activation of which results in burning pain sensation- is necessary for the development of heat hyperalgesia in certain pathological conditions (Davis et al., 2000; Caterina et al., 2000)

1.2 Differences in pain perception

The extent and nature of the pain experienced following noxious stimuli varies greatly between individuals. Human beings show large differences in their pain thresholds and individual tolerance to pain. Individuals also exhibit differences in their response to analgesic drugs and their susceptibility to clinical pain syndromes. Pain perception is a personal experience and is influenced by many factors, including cultural and social factors, and biological factors. These factors are able to interact, making pain perception a complex mechanism. Understanding the mechanisms that influence pain perception is especially important to comprehend the development of various types of pain and to develop novel analgesic regimes which are more efficacious then the currently available treatments.

1.2.1 Cultural and social influences

The extent to which the subjective experience of pain by individuals is affected by cultural and social influences has been the subject of considerable study in recent years. Cultural influences refer to values, beliefs and practices of a particular group which are learned and shared and which guide thinking and decisions of action in a given society (Chang et al., 2006). According to classical studies by Zborowski and Herzog (1952), each culture has its own language of distress which is expressed both verbally and non-verbally. For example, cultural attitudes of pain in childbearing women have been reported to affect perception, expression and treatment to pain (Callister et al., 2003; Cheung, 1994; Lee and Essoka, 1998). Higher pain ratings and more pain-like behaviours were seen in women living in the Middle East than women living in Western Europe. However there was no difference in coping style of labour pain (Weisenberg and Caspi, 1989). Moreover, labour pain perception was rated more highly by Anglo women, followed by East Indian women, next Hutterite (Amish or Mennonites) women and finally, among Ukraine women (Morse and Park., 1988)

The religious orientation of an individual also influences pain perception (Low, 1997). In a chronic pain sufferer, religious belief can positively impact upon health, longevity and recovery from physical illness (Carone and Barone, 2001; Rippentrop et al., 2005).

1.2.2 Biological factors

Biological factors can be subdivided into several categorises: sex and gender; psychological status; ethnicity; and genetically-defined factors.

1.2.2.1 Sex and Gender

The term ‘sex’ relates to the biology and medicine of male and female, whereas the term ‘gender’ is used in a social and cultural context (Diamond, 2002). While sex is primarily a biological fact, sex in the context of the gender role of a man or a woman in culture and in society is different. Gender role modelling is the process in which individuals are socialised into masculine and feminine models of behaviour (Moore et al., 2005). Furthermore, gender roles are based on a stereotype which refers to socially shared beliefs that sex determines certain qualities (Chang et al., 2006). These definitions of “sex” and “gender” are terms of art employed in the context of these studies.

Gender differences in pain perception may arise from a variety of differences in cognitive and emotional ways of dealing with pain and in social or occupational roles (Miller and Newton, 2006). Females have lower pain thresholds, greater abilities to discriminate pain and are less tolerant to noxious stimuli than males (Feine et al., 1991; Lautenbacher and Rollman, 1993; Wise et al., 2002; Riley et al., 1998). Women have also been shown to experience a variety of more recurrent pain then men (Unruh, 1996).

Sex differences in response to opoid analgesia in clinical and experimental findings have also been studied (Fillingim and Gear, 2002). In rodent studies, greater opioid analgesia was found in males when compared to females (Kest et al., 2000; Craft, 2003). This difference may be explained by genetic factors which control sex differences in antinociceptive responses in rodents (Barret et al., 2002; Mogil et al., 2000). Conversely, human studies show that females exhibit greater opioid analgesic responses (Sarton et al., 2000; Dahan et al., 1998). Sex hormones and their respective receptors are widely disturbed in the central nervous system (CNS) and have been shown to modulate pain sensitivity (McEwen et al., 1998; Aloisi and Bonifazi, 2006).

Overall, there is a general consensus amongst scientists that sex and gender differences in pain warrant greater attention in pain research and in the development of analgesics.

1.2.2.2 Psychological status

Pain perception can be greatly influenced by psychological aspects such as situational and emotional factors. For example, major depression and impaired functional status has been recently shown to contribute independently to poorer quality of life in cancer patients (Wedding et al., 2008). Furthermore, emotional and social functioning were shown to predict depression, whereas, emotional and physical functioning were key predictors of anxiety (Lue et al., 2008).

Medical areas which use psychological assessment significantly aid in the diagnosis and treatment of patients suffering from psychiatric and neurological disturbances, circulatory diseases (especially hypertension), diabetes, chronic pain, sexual dysfunctions, and gastrointestinal problems (Granick, 1983)

1.2.2.3 Ethnicity

Several researchers have shown that ethnic differences influence the clinical appearance of pain experience (Riley et al., 2002; Rahim-Williams et al., 2007; Hastie et al., 2005). Including the severity of pain associated with medical conditions such as arthritis (Creamer et al., 1999), postoperative pain (Faucett et al., 1994), joint pain (Rantanen et al., 1998), and the treatment of conditions such as low back pain (Taylor et al., 2005). Ethnic differences have also been seen in the responses to multiple experimental pain stimuli. For example, African Americans show significantly higher ratings in intensity and unpleasantness for supra-threshold heat stimuli than Caucasians (Campbell et al., 2005). A recent study has shown that ethnic identity predicts experimental pain sensitivity across multiple noxious stimuli (Rahim-Williams et al., 2007). The difference in pain perception experienced by various ethnic groups indicates that genetic factors may play a major role in the development of pain.

1.2.2.4 Genetically-defined factors

It is likely that environmental factors account for a substantial part of the variability in pain perception amongst individuals. However, Mogil and colleagues (1999) have shown significant strain differences in basal responses to all nociceptive assays in rodents. This suggests that genetic factors are also likely to influence the perception of pain

Recently there has been a surge in research to elucidate the genetics of pain. This will undoubtedly assist in the development of analgesics for individuals. However, as there are thousands of genes which have been implicated in pain variability in humans, it is essential to prioritise candidate genes.

1.2.2.4.1 Polymorphisms

Naturally occurring mutations (polymorphisms) have also been shown to result in different experiences of pain among individuals. 'Poly' means many. 'Morph' means form. Hence, 'polymorphism' refers to a type of genetic variation, specifically a discontinuous variation, which occurs within species in which distinct forms exist in the same population. Polymorphisms are a result of the evolutionary process which are heritable and are adapted by natural selection. Polymorphic genes are genes that have different forms of the DNA sequence, which arise through mutations. These variants of genes are called *alleles* and a *haplotype* is a combination of alleles that are inherited together. Although most SNPs are found in all human populations, the allelic frequencies (a measure of the relative frequency of an allele in a population) differ among continents.

An example of a genetic polymorphism relevant to opiate sensitivity is the cytochrome P450 (CYP) enzyme. The analgesic effect of the opioid codeine depends on the metabolic activation by CYP 2D6 enzyme which is known to exhibit genetic polymorphisms. These polymorphisms result in allelic variants which may be classified on the basis of the level of activity of CYP 2D6 enzyme and, in turn, the production of active opioid (Wuttke et al., 2002; Weinshilboum et al., 2003; Evans et al., 2003; Bradford, 2002; Gaedigk et al., 2002; Wan et al., 2001). The allelic frequencies of CYP 2D6 enzyme varies among ethnic groups. Generally, for European Caucasians, the functional group of alleles is predominant, with a frequency of 71%. In Asians, functional alleles represent only ~ 50% of the frequency of CYP 2D6 alleles (Bradford, 2002).

There are different types of genetic mutations, such as: (i) *deletions* where bases are removed; (ii) *insertions*, were bases are added; (iii) *inversions*, were a nucleotide sequence is reversed; and (iv) *substitutions*, were bases are replaced with another. Not all genetic mutations result in a change to the amino acid sequence of the protein. This is either due to the mutation occurring in the intron and is referred to as silent or neutral mutations. Or that the mutation appears in the exon but does

not alter the translation of the final amino acid sequence. This type of mutation may also be described as a silent mutation but more appropriately referred to as a synonymous substitution.

It has been estimated that the human genome consist of more than 3 billion base pairs. About 99.9% of the human genome is identical in all individuals. Of the 0.1% difference between individuals, the most common source of genetic variation in the human genome is from single nucleotide polymorphisms (SNPs; pronounced 'snips'). A SNP is a single nucleotide substitution of one base for another and is usually observed in the general population at a frequency greater than 1%. A substitution which results in a codon (three nucleotides which codes for specific amino acid) to code for a different amino acid is referred to as missense SNP or nonsynonymous substitution. Furthermore, a missense SNP may or may not alter the protein function (Human Genome Project, 2008).

An example of a missense SNP which alters the protein function is the A118G SNP of the human mu-opioid receptor gene (OPRM1), which occurs in in ~10-20% of the population, and is tightly linked with sensitivity to noxious pressure. Missense SNPs are usually abbreviated based on the amino acid and the amino acid position, i.e., in this particular example glycine is replaced with alanine at codon 118. Individuals with this allele variant have significantly higher pressure pain thresholds than those with the common allele at position 118 (Fillingim et al., 2005). Furthermore, the OPRM1 receptor is the primary site of action for opioids (morphine, heroin, methadone and endogenous beta-endorphin). Individuals with this allele show a response to opioids which is ~3-fold more potent than the response found in those with the common allelic form of the receptor (Bond et al., 1998). Consequently, addiction to opioids has also been linked to this rare allele, and it may contribute to vulnerability to opioid dependence (Szeto et al., 2001; Ide et al., 2004).

Polymorphisms can also affect individual's susceptibility to both dose-dependent, and dose-independent, adverse drug reactions. For example, a deficiency

in the X-linked gene for glucose 6-phosphate dehydrogenase (G6PD) causes haemolysis in response to drugs taken for malaria (Martini et al., 1996).

It is therefore essential that scientists should in the future design studies to further elucidate the role of genetic factors in relation to pain perception. Moreover, understanding the role of naturally occurring polymorphisms in pain-related genes may explain individual variability to pain. This may, in turn, aid in designing better, and more specific, analgesics for individuals.

As discussed above, the screening of genes for molecules which are involved in the development of various types of pain has identified several molecules. Some of these molecules, such as sodium channels, are involved in action potential generation. Others, such as various protein kinases and transcription factors, are involved in transcriptional, and post-translation, processes which underlie peripheral and central sensitisation. In addition to these molecules, transducers, including TRPV1, have been assumed to be the 'driving force', responsible for the initiation and maintenance of sensitisation, and ultimately for the development of the pain experience.

Among the molecules which are regarded as constituting the "driving force", the capsaicin receptor, TRPV1, seems to be one of the most important, because it occupies a strategic position in the pain pathways which are responsible for the development of pain experience of peripheral origin. TRPV1 is expressed by almost all primary sensory neurons which are responsible for the detection of acute noxious stimuli and which are sensitised during the development of prolonged and chronic pain sensation. Furthermore, studies of genetically engineered mice which are deficient in TRPV1 revealed that the development of inflammatory heat hyperalgesia depends on this receptor. While the TRPV1 knock-out animals failed to develop inflammatory heat hyperalgesia, they retained their ability to respond to acute noxious stimuli. Therefore, pharmaceutical companies continue to show great interest in TRPV1.

1.3 TRPV1

1.3.1 Structure of TRPV1

Caterina and colleagues cloned and identified the TRPV1 in rat (Caterina et al., 1997). The rat TRPV1 gene contains an open reading frame of 2,514 nucleotides that encodes a protein of 838 (human: 839) amino acids with a predicted relative molecular mass of 95,000. TRPV1 has six transmembrane domains with three ankyrin repeats present in the N-terminal region. Both the C- and N-terminals are located within the cell. The pore loop of TRPV1 is located at the intracellular side of the membrane between transmembrane (TM) domains 5 and 6.

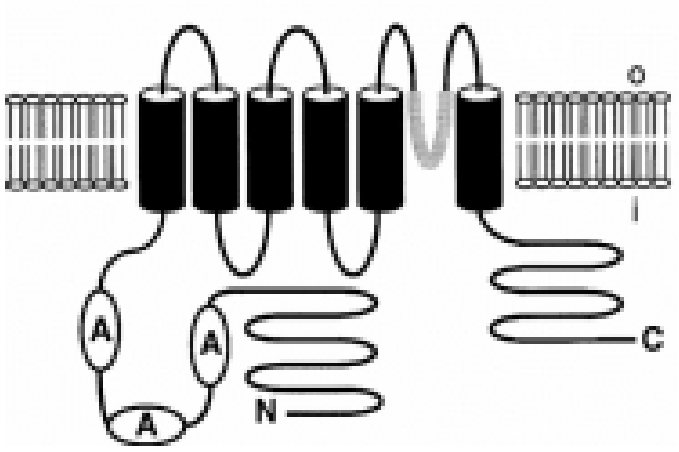

Figure 1.1 Membrane topology of TRPV1. (Taken from Caterina et al., 1997)

Ankyrin repeat domains are thought to interact with cytosolic proteins (Clapham, 2003). Calmodulin, a calcium binding protein which is involved in regulation of channel function, is one such protein which has been shown to bind to the ankyrin repeats (Rosenbaum et al., 2004). Mutations in the ankyrin repeat region result in rapidly diminishing responses to ligands (Lishko et al. 2007).

The N-terminus of the TRPV1 does not exhibit a strong homophilic interaction and does not associate with other full-length TRPV1 subunits (Hellwig et al., 2005). However, studies on an N-terminal splice variant (VR.5'sv) have shown the importance of this region in the formation of functional receptors because VR.5' lacks responses to typical TRPV1 stimuli (Schumacher et al., 2000). In addition to the possible role of the N-terminus in the formation of functional receptors, recent findings suggest that this region may be involved in defining the responsiveness of the molecule. Sharif Naeini and co-workers (2006) reported that an N-terminus variant of TRPV1 may gain osmosensitivity. Furthermore, Brauchi and colleagues' (2007) findings suggest that the heat sensor is located in the N-terminal region. The N-terminal has also been shown to bind the channel function modulator, calmodulin (Rosenbaum et al., 2004).

The C-terminus displays homophilic interactions. Amino acids at position E684 and R721 are molecular determinants of the TRPV1 assembly into functional channels (Garcia-Sanz et al., 2004). Calmodulin has been shown to bind to this region, in a Ca2+-independent manner (Numazaki et al., 2003). Mutations in this region result in a Ca^{2+}-dependent functional loss of responsiveness to capsaicin (Liu et al., 2004). Moreover, a reduced sensitivity to capsaicin, protons and heat responses was seen in TRPV1 receptors with a truncated C-terminus (Vlachova et al., 2003).

1.3.2 TRPV1 multimeric structure

The functional TPRV1 channel is a multimer both in dorsal root ganglion neurones and in heterologous expression systems, with a tetramer as the predominant form. In the tetramer, the TRPV1 monomers appear to assemble with fourfold-symmetry around a central aqueous pore (Kedei et al., 2001; Kuzhikandathil et al., 2001). TRPV1 channel subunits do not combine arbitrarily. On the contrary, they appear to predominantly assemble through an interaction of protein moieties located between transmembrane segments 1-6. Both cytosolic termini and transmembrane segments synergistically contribute to the overall affinity between TRPV1 channel subunits and control the selectivity of homo- and heteromeric assembly of the pore-

forming subunits. Thus, inter-subunit interaction between TRPV1 subunits also involves the transmembrane portion of the protein. This is consistent with the fact that the hexahelical channel subunits that are flanking the pore probably come into close contact with their transmembrane segments 5 and 6 and also their pore loops to stabilise the closed pore conformation of the inactive channel complex or to maintain the selectivity filter upon gating (Hellwig et al., 2005).

As a heteromer TRPV1, in addition to splice variants, could be assembled with other TRP molecules. For example, TRPV1 can form heteromer with the transient receptor potential vanilloid type 3 (TRPV3) that does not respond to capsaicin, but does respond to heat with a threshold of about 39ºC. TRPV3 is co-expressed in dorsal root ganglion neurones with TPVR1. The association of TRPV1 to TRPV3 may modulate the responses of the former, because of the different sensitivity of the molecules (Smith et al., 2002). Other members of the TRPV family may also form heteromers with TRPV1. Indeed Rutter et al. (2005) have reported that the high threshold heat-sensitive TRPV channel, TRPV2 may form heteromers in a small sub-population of primary sensory neurons. Cheng and colleagues (2007) have shown that TRPV1, TRPV2, TRPV3 and TRPV4 form heteromers when co-transfected and that the responses of the heteromeric channels had properties "inherited" from the sub-units. However, others found that TRPV channels prefer to form homomers in transfection systems (Hellwig et al., 2005). Nevertheless, the probability that TRPV1 forms heteromers with sub-units which modify its responses may contribute to functional diversity (Nagy and Rang, 1999).

1.3.2a TRPV1 splice variants

Several TRPV1 splice variants have been found since it was first cloned. The function of the majority of these variants, remains unknown. Splice variants of the same genes are mainly expressed in the same tissue and may act as regulators of each other. Moreover, splice variants which lack an important region of the protein can function as dominant-negative molecules and inhibit the activity of the full-length protein. TRPV1 splice variants include: TRPV1b; the TRPV1 5' splice variant; the $TRPV1_{VAR}$ channel; and stretch-inactivated channel (SIC) TRPV1 channel.

The human receptor splice variant, hTRPV1b forms a functional ion channel that can be activated by heat (threshold ~ 47 ^{o}C) but not by capsaicin or protons (Lu et al., 2005). However, when rat TRPV1b is co-expressed with rat TRPV1 in transfected HEK293 cells, TRPV1b acts as an inhibitory modulator of TRPV1 (Vos et al., 2006).

The TRPV1 5' splice variant (VR.5'sv) has been found to be predominantly expressed in the dorsal root ganglia. It is insensitive to noxious heat, capsaicin, the ultra potent vanilloid, resiniferatoxin, and protons (Schumacher et al., 2000; Sanchez et al., 2001). However, co-expression of VR.5'sv with TRPV1 results in inhibitory modulation of TRPV1 (Eilers et al., 2007)

The human renal splice variant $TRPV1_{VAR}$ (Tian et al., 2006) has been shown to have the capacity to act as either a potentiator, or inhibitor, of rat TRPV1 activity, depending on the cell line used for expression. A potentiating effect is seen when $TRPV1_{VAR}$ is cotranfected with TRPV1 in HEK293 cells. However, when Cos-7 epithelial cells are used, a dominant-negative effect is seen. Furthermore, when $TRPV1_{VAR}$ is transfected alone in these cells, no response was seen during the application of resiniferatoxin (Tian et al., 2006). The mechanism of $TRPV1_{VAR}$ inhibitory and potentiating effect on TRPV1 activity has not yet been elucidated.

The SIC TRPV1 is a non-selective, cation, channel, also expressed in the kidney, and codes a 563 amino acid protein with the topology of a putative six transmembrane segments. The N-terminal sequence of SIC is essentially identical to TRPV1. However its C-terminal is similar to TRPV4 (Xue et al., 2001). SIC cannot be activated by any classical TRPV1 activators and its activation is blocked by mechanical stimuli (Suziki et al., 1999).

1.3.3 TRPV1 activators

TRPV1 can be activated by a number of endogenous, and exogenous, activators, including ligands, protons, heat, voltage, and post-translation modification.

1.3.3.1 Vanilloids

Capsaicin is one of the first known natural algogens and is the active compound in hot chilli peppers causing a burning pain sensation (Thresh, 1846). It belongs to the family of vanilloids, which is characterised by the presence of a vanilloid moiety (Nelson, 1919). Before the TRPV1 ion channel was given the name by which it is universally known today, it was referred to as the capsaicin receptor because capsaicin activates TRPV1 selectively.

Other vanilloids such as resiniferatoxin (RTX), the ultrapotent capsaicin analog, derived from the cactus-like *Euphorbia resinifera*, are also able to activate the receptor (Szallasi et al., 1989; Szallasi and Blumberg, 1990a). Moreover RTX, is 3-4 orders of magnitude more potent than capsaicin (Szallasi and Blumberg, 1990b) .

1.3.3.2 Anandamide

A great number of endogenous compounds have been suggested to directly open TRPV1. These endogenous agents include: anandamide (Zygmunt et al. 1999); N-arachidonoyl-dopamine (NADA: Huang et al., 2002); N-oleoyldopamine (OLDA: Chu et al., 2003); lipoxygenase products, such as 12- and 15-(S)-HPETE (Hwang et al., 2000); and unsaturated C18 N-acylethanolamines (Movahead et al., 2005).

In addition to activation of TRPV1, anandamide is also able to activate the CB1 receptor (Schuel et al., 1994; Di Marzo et al., 1994) and it is therefore of major interest. Anandamide belongs to a group of bioactive lipids, the long chain C18 N-acylethanolamines (NAEs). Other members of this group are also able to activate and modulate TRPV1 activity (Movahead et al., 2005).

The ability of anandamide to activate TRPV1 in normal physiological conditions is very limited. This is essential to prevent unnecessary activation of TRPV1 which would result in pain in absence of pain-inducing stimuli (Ross, 2003; van der Stelt and Di Marzo, 2004). However, in several pathological conditions, such as inflammation and when TRPV1 is activated by other stimuli, the anandamide-evoked effect is potentiated (Olah et al., 2001; Di Marzo et al., 2002; Singh Tahim et al., 2005; Ahluwalia et al., 2003). Furthermore, anandamide-evoked activation of TRPV1 has been shown to contribute to the development of bladder hyperreflexia and hyperalgesia during cystitis (Dinis et al., 2004)

1.3.3.3 Protons

Protons are able to activate TRPV1 directly at pH below 6.5. In addition, proton binding to TRPV1 enhances the apparent binding affinity of capsaicin, and lowers the heat threshold for activation (Caterina et al., 1997; Jordt et al., 2000;

Tominaga and Julius, 2000; Baumann and Martenson, 2000). Apparently, capsaicin-binding and protonation of the channel interact allosterically (Ryu et al., 2003).

In addition to protons, excess positive charges carried by various ions seem also to be able to activate TRPV1. Ahern and colleagues (2005) showed that extracellular Na^{+}, Mg^{2+}, and Ca^{2+} can open the TPRV1 ion channel. Moreover, these extracellular cations can sensitise the ion channel to other activators.

1.3.3.4 Heat

Sensitivity to noxious heat is one the most distinctive features of TRPV1 (Caterina et al., 1997). Heat contributes to TRPV1 activation in two distinct ways. First, heat reduces the threshold for the activation of TRPV1 by all other TRPV1 activators. Second, heat above ~ 43 ºC independently activates TRPV1 (Tominaga et al., 1998). At temperatures < 43 ºC, channel openings are few and brief. However, raising the ambient temperature rapidly increases the frequency of channel openings (Liu et al., 2003). Other activators can reduce the threshold for activation by heat to below body temperature (<37 ºC) with the result that body temperature is sufficient to activate TRPV1 (Caterina et al., 1997; Jordt et al., 2000; Tominaga and Julius, 2000; Baumann and Martenson, 2000). This provides an explanation of ongoing spontaneous pain.

It has been suggested that the ultimate TRPV1 activator is heat, since protons, capsaicin, and indirect activators, such as bradykinin, all reduce the temperature threshold of the channel (Jordt et al., 2000; Babes et al., 2002; Sugiura et al., 2002).

1.3.3.5 Voltage-dependent activation

TRPV1 is a voltage-gated ion-channel (Gunthorpe et al., 2000; Voet et al., 2004; Piper et al., 1998). TRPV1 is activated by depolarisation and changes in the temperature results in a graded shift of the receptors voltage-dependent activation curve. Hence, a tight link between temperature sensing and voltage-dependent gating has been suggested (Voets et al., 2004). However, voltage-dependent activation was recently shown to only partially activate TRPV1 (Matta and Ahern, 2007).

1.3.3.6 Post-translational modification

TRPV1 can be activated directly by vanilloids, heat, protons, and depolarisation. However, gating of this ion channel can also be evoked indirectly. The indirect activators include various inflammatory mediators, which are produced and released during inflammation in tissues (Julius and Basbaum, 2001). These inflammatory mediators, through activating their own target receptors, which are also expressed on nociceptive primary sensory neurons expressing TRPV1, induce activity in the neuron's intracellular second messenger system. That, in turn, results in post-translational modification of TRPV1.

Hydrolysis of phosphotidylinositol 4,5-bisphosphate (PtdIns(4,5)P2 or PIP2) in the cytoplasmic membrane, cAMP-dependent protein kinase (PKA) and protein kinase C (PKC) mediated phosphorylation of the capsaicin receptor, have each been shown to induce opening of TRPV1 (Chuang et al., 2001; Premkumer, 2001).

Hydrolysis of PIP2 can be initiated by the activity of either trkA or bradykinin B2 receptors. Interestingly, while previous data show that PIP2 binding has inhibitory effect on TRPV1 (Chuang et al., 2001), recent data suggest that the effect of PIP2 hydrolysis/binding may depend on certain condition (Lukacs et al., 2007). The PKC-mediated phosphorylation can be induced by activating the bradykinin B2 receptor (Chuang et al., 2001; Premkumar and Ahern, 2000: Vellani et

al., 2001). Activation of prostaglandin E (PGE2) receptors induces PKA-mediated phosphorylation of TRPV1 (Mohapatra and Nau, 2003; Moriyama et al., 2005; Rukwied et al., 2007). Furthermore, treatment with PGE2, or activation of PKA, transiently sensitises capsaicin-activated currents (Lopshire and Nicol, 1998). Similarly, the anandamide-evoked response through TRPV1 is enhanced by PKA (De Petrocellis et al., 2001). TrkA, bradykinin B2 and PGE2 receptors are all expressed on capsaicin-sensitive primary sensory neurons (Lee et al., 2002; Michael et al., 1999; Dray et al., 1988).

1.3.4 Expression and distribution of TRPV1

1.3.4.1 Expression by primary sensory neurons

TRPV1 is predominantly expressed in a sub-population of nociceptive primary sensory neurons (Ahluwalia et al., 2000; Guo et al., 1999; Ichikawa and Sugimoto, 2004; Michael and Priestley, 1999). In peripheral tissues, TRPV1-expressing sensory fibres can be found in the dermis, along the epidermal/dermal junction, epidermis, and also in Meissner's corpuscles (Guo et al., 1999; Pare et al., 2001). In the viscera, TRPV1 immunopositive fibres are found in the mucous membrane, submucous, and muscular layer (Avelino et al., 2002; Ward et al., 2003). TRPV1-expressing fibres also innervate the Langerhans islands in the pancreas (Gram et al., 2007). The central terminals of TRPV1-expressing primary sensory neurons terminate primarily in the superficial dorsal horn of the spinal cord (Guo et al., 1999). However, some TRPV1-expressing fibres can also be found in the deep dorsal horn and around the central canal (Tominaga et al., 1998).

1.3.4.2 Expression in the central nervous system

Several neurons in the central nervous system also express TRPV1. The olfactory nuclei, cerebral and cerebellar cortex, thalamus, hypothalamus, lateral and dorsal septal nuclei, periaqueductal gray, locus coeruleus, substantia nigra, inferior olive, dentate gyrus, and hippocampus express TRPV1 (Starowicz et al., 2007;

Cristino et al., 2006; Sasamura et al., 1998; Mezey et al., 2000; Roberts et al., 2004). TRPV1 expressed in neurons of the thermoregulatory nucleus apparently respond to capsaicin as evidenced by the failure of thermoregulation in animals injected systemically with capsaicin, or when capsaicin is injected directly into the medial preoptic hypothalamic nucleus at neonatal age (Jancso-Gabor et al., 1970).

1.3.4.3 Expression by non-neuronal cells

Some non-neuronal cells have also been shown to express TRPV1, but the function of these ion channels generally remains unknown. TRPV1-expressing cells are found in the inner ear where they include inner and outer hair cells, inner and outer pillar cells, Hensen's cells, spiral ganglion neurons, Scarpa's ganglionic neurons and satellite cells (Balaban et al., 2003; Zheng et al., 2003; Takumida et al., 2005). Both capsaicin and resiniferatoxin increase the threshold for auditory nerve compound action potential generation and reduce the magnitude of cochlear microphonic and electrically evoked oto-acoustic emissions suggesting that capsaicin receptors are functional in the inner ear (Zheng et al., 2003). A sub-population of keratinocytes also expresses TRPV1 which appear to be functional (Ioue et al., 2002; Southall et al., 2003).

A sub-population, at least, of cultured rat gastric epithelial cells express TRPV1, but these ion channels are peculiar in that they are not desensitised or damaged by exposure to capsaicin (Kato et al., 2003). TRPV1 is also found in the basal and superficial layers of the urothelium. These cells are functional as they respond to capsaicin and resiniferatoxin application with a TRPV1-mediated increase in intracellular calcium concentration (Birder et al., 2001).

1.3.5 The role of TRPV1 in physiological and pathological conditions

1.3.5.1 Pain

TRPV1 is well established as a mediator of the pain sensation which results from inflammation. This was demonstrated in behavioural experiments by Davis and colleagues (2000) and Caterina and colleagues (2000) in which TRPV1 knock-mice appear normal in a wide range of behavioural tests, including responses to acute noxious thermal stimuli but lack the ability to develop thermal hyperalgesia after inflammation. Moreover, TRPV1 is required for inflammatory sensitisation to noxious thermal stimuli but not required for normal sensation of noxious heat (Davis et al., 2000).

1.3.5.2 TRPV1 and inflammatory pain

Tissue injury is normally associated with inflammation and inflammatory pain. Inflammatory pain is induced by inflammatory mediators released in the injured tissue, such as PGE2, nerve growth factor (NGF), and bradykinin, acting on nociceptors in peripheral nerve terminals. Another prominent chemical generated in injured tissue is protons which result in tissue acidosis.

The development of hyperalgesia following inflammation involves an increased level of TRPV1 expression as well as the sensitisation of existing TRPV1 channels (Tominaga, 2000). Inflammatory mediators, such as ATP, bradykinin, and NGF, increase the temperature and proton sensitivity of TRPV1 and contribute to enhanced TRPV1 activity (Kwak et al., 2000; Liu et al., 2005; Amaya et al., 2004; Zhang et al., 2005; Cesare et al., 1996; Chuang et al., 2001). Intracellular adenosine triphosphate (ATP) sensitises TRPV1, although there is controversy about whether it is through a direct interaction (Kwak et al., 2000) or, indirectly, through PIP2 synthesis (Liu et al., 2005).

Levels of both NGF and glial cell derived neurotrophic factor (GDNF) increase following inflammation and contribute to inflammatory hyperalgesia via an increase in TRPV1 expression (Amaya et al., 2004). Chuang and colleagues (2001) injected wild-type and TRPV1 knock-mice with bradykinin or NGF and measured paw withdrawal latencies from a radiant heat source before, and after, treatment. Each agent produced substantial sensitisation in wild-type animals but not in the knockout mice, demonstrating that TRPV1 is essential for the development of bradykinin-induced, or NGF-induced, thermal hypersensitivity in vivo.

1.3.5.3 TRPV1 and neuropathic pain

Although the role of TRPV1 in mediating inflammatory pain conditions is well-established, the extent of the involvement of TRPV1 in neuropathic pain conditions remains unknown. There is, however, evidence that, in relation to neuropathic pain, the contribution made by TRPV1 depends on the context of origin of the neuropathic pain condition and, perhaps, even on the species of animal.

Caterina and colleagues (2000) found that in a model of partial spinal nerve ligation, there was no difference between the level of mechanical and thermal nociceptive responses of TRPV1 knock-mice as opposed to wild-type mice. On the other hand, after nerve injury a distinct difference in the regulation of TRPV1 expression is observed (Hudson et al., 2002; Fukuoka et al., 2002; Kanai et al., 2005). After sciatic nerve ligation and intrathecal application of capsazepine, a TRPV1 antagonist, blocks A-delta fibre-evoked responses in the dorsal horn neurones of rats (Kelly et al., 2002).

There is also evidence that the contribution made by TRPV1 to neuropathic pain conditions may even be species dependent. Capsazepine reverses mechanical hyperalgesia in a guinea pig model of partial sciatic nerve ligation, but has no effect in either rat or mouse models of neuropathic pain (Walker et al., 2003). Recently, Christoph and colleagues (2007) reported that in an in vivo rat model of spinal nerve ligation, both intravenous application of the TRPV1 antagonist, thioxo-BCTC, and

intrathecal administration of the antisense oligonucleotide against TRPV1, reduce mechanical hypersensitivity in a similar manner, proving the involvement of TRPV1 in such neuropathic pain conditions in rat (Christoph et al., 2007).

1.3.5.4 Visceral hyper-reflexia and pain

Capsaicin-sensitive sensory fibres are known to have a role in the micturition reflex, because capsaicin instillation first induces contraction, then desensitisation of the urinary bladder (Maggi et al., 1984; Holzer-Petshe and Lembeck; Cheng et al., 1999). Moreover, capsaicin instillation also evokes the expression of the early gene, c-Fos in the dorsal spinal cord, which indicates that nociceptive input reaches second order neurons (Wang and Hassouna, 2000). Recently, Charrua and colleagues (2007) demonstrated that TRPV1 is responsible for both the pain sensation associated with overfilled bladder and the hyper-reflexia associated with inflammation, because bladder distension-evoked spinal c-Fos, expression, and inflammation-evoked hyper-reflexia failed to occur in TRPV1 knock-out mice. However, the extent of the contribution from TRPV1 which is expressed by bladder afferents and by TRPV1 expressed by urothelial cells, to the development of pain and hyper-reflexia, remains to be established.

1.3.5.5 Diabetes

One of the most unexpected putative roles for TRPV1 has been suggested to be in diabetes. Razavi and co-workers (2006) have reported that TRPV1-expressing nerve fibres invade the Langerhans islets in the pancreas. Furthermore, TRPV1 in non-obese diabetic mice, a model for type 1 diabetes, shows polymorphism (P322A and D734E), which results in reduced sensitivity of the molecule to capsaicin. Razavi and colleagues argue that there is a negative feed-back between TRPV1-expressing primary sensory terminals and beta-cells, in which insulin, by increasing the activity of TRPV1 induces the release of neuropeptides, such as substance P and calcitonin gene related peptide (CGRP), which inhibit insulin secretion. Once this regulatory

mechanism is unbalanced due to reduced TRPV1 responsiveness, the anti-inflammatory effect of SP is diminished and insulinitis develops.

Gram and colleagues (2007) have reported recently that systemic injection of capsaicin prevents the development of hyperglycaemia and reduced insulin secretion in Zucker Diabetic Fatty rats, which are regarded as a model of human type 2 diabetes mellitus in certain aspects. The preventive effects of systemic capsaicin injection were accompanied by complete loss of CGRP-, and TRPV1-coexpressing islet-innervating fibers. The authors hypothesise that enhanced release of CGRP that reduces insulin secretion from β cells (Kozlova and Jansson, 2005) from sensitised TRPV1-expressing peptidegic fibres innervating the islets, reduces insulin secretion. The sensitisation could be produced by increased release of inflammatory cytokines from the enhanced amount of adipose tissues (Sopasakis et al., 2005), and/or hyperglycaemia-induced NGF release from the beta cells. Whether TRPV1 itself has any role in the putative enhanced activity of the islet-innervating fibres awaits elucidation.

1.3.6 TRPV1 polymorphisms

The human TRPV1 (hTRPV1) ion channel expresses several naturally occurring polymorphisms. I315M and V585I are missense SNPs which result in a change in the amino acid coded (Hayes et al., 2000: Kim et al., 2004). Similar non-synonymous SNPs are found in hTRPV1 at: P91S, I315M, T469I, T505A and V585I (Xu et al., 2007). The I315M and P91S variants elicit a greater response to capsaicin than wild-type hTRPV1 receptors (Xu et al., 2007). In addition to these human TRPV1 SNPs, rat TRPV1 also show polymorphisms. Recently, two SNPs in the rat TRPV1 have been identified (Razavi et al., 2007). P322A and D734E SNPs have been found in non-obese diabetic mice and these have been shown to underlie the development of insulinitis in these animals (Razavi et al., 2007).

There are many projects involved in identifying SNPs. In 1999, the SNP Consortium (TSC) was established to identify as many individual SNPs in the human genome. Within two years of collaborative efforts of several companies and academic institutions of TSC, ~1.4 million SNPs were published, which exceeded their initial goal of 300,000 SNPs (Sachidanandam et al., 2001).

Dr John Davis and colleagues, at GlaxoSmithKline, have also investigated polymorphisms in TRPV1 on the assumption that mutations in this receptor may result in altered pain sensitivity in humans. For this purpose, these investigators assessed the genetic variations within 94 human DNA samples (62 Caucasians, 16 Asians and 16 African Americans) using double stranded sequencing.

In order to identify SNP in hTRPV1 from these human DNA samples, oligonucleotide specific primers had to be design to anneal with the flanking sequences of the gene. Primers were designed on the genomic accession number of hTRPV1 (AJ272063, AF168787, AC027796 and AC027040), to scan all the coding sequences of the 15 exons for naturally occurring variations in the DNA sequence.

The hTRPV1 contained about 100 bp of intronic sequence flanking each exon: from 0 kb of the promoter sequence to 0.6 kb sequence beyond the stop codon. A total of 20 fragments of ~ 500 bp of each sequence were screened. In total 10 kb was screened.

As a result of this analysis, a total of 48 SNPs within the hTRPV1 gene were observed. Although non-coding SNPs may be involved or effect important mechanisms such as transcription, translation and splicing, coding SNPs are easier to study and are potentially more damaging (Werner, 2003). Davis and colleagues showed that 14 SNPs originated from the coding regions of the gene, of which only 7 were found to be missense SNPs (a change in the amino acid coded) (table.1.1). The 7 missense SNPs identified are as follows (see Fig 1.1): two SNPs in exon 2 were located at the N-terminus of the protein, $hTRPV1_{Q85R}$ and $hTRPV1_{P91S}$. $hTRPV1_{I315M}$ is encoded by a codon located on exon 6 and localised in the region of the ankyrin repeat domains. $hTRPV1_{T469I}$ is encoded by a codon found on exon 9 and is situated on the extracellular loop between TM1 and TM2. $hTRPV1_{T505A}$ is encoded by a codon found on exon 10 and is localised on the intracellular loop between transmembrane 1 and 2. $hTRPV1_{V585I}$ and $hTRPV1_{N738Y}$ are encoded by codons located on exon 12 and exon 14, respectively, and localised on TM5 and the C-terminus of the receptor, respectively. However, due to the small sample size, the observed frequencies are not representative of those that one might expect to find in the population as a whole. SNPs occurring in the population at a minor allele frequency of less than 20% are not likely to be represented. Only three non-synonymous SNP mutations were found in Caucasians and African Americans to produce a frequency of more than 20% which indicates that these SNPs are major alleles. The three most frequently occurring missense SNPs in hTRPV1 in Caucasians and African Americans were found to be: I315M ($hTRPV1_{211}$); T469I ($hTRPV1_{121}$); and V585I ($hTRPV1_{112}$).

Gene Region	Base Change	Position	Amino acid Change	Minor allele freq. in 62 Caucasians	Minor allele freq. in 16 African Americans[1]	Minor allele freq. in 16 Asians[1,2]
Exon 2	A > G	254 bp	Q85R	0.04	0	0.03
Exon 2 (Db)	C > T	271 bp	P91S	0.06	0.19	0.03
Exon 6 (Db)	**C > G**	**945 bp**	**I315M**	**0.28* (17.4)**	**0.53* (8.5)**	**0.16 (2.6)**
Exon 9 (Db)	**C > T**	**1406 bp**	**T469I**	**0.43* (26.6)**	**0.66* (10.6)**	**0.19 (3.0**
Exon 10	A > G	1513 bp	T505A	0.01	0	0
Exon 12	**G > A**	**1753 bp**	**V585I**	**0.31* (19.2)**	**0.59* (9.4)**	**0.19 (3.0)**
Exon 14	G > T	2212 bp	N738Y	0.01	0	0

Table 1.1 Seven missense SNPs found in hTRPV1 by Davis and colleagues (unpublished data). Data were obtained from a sample of 98 humans made up of 62 Caucasians, 16 Asians and 16 African Americans. Bold prints represent the most frequently occurring missense SNPs in hTRPV1. [1] Due to small sample sizes, the observed frequencies are not representative of those which one would expect to find in the population as a whole. SNPs occurring in the population at a minor allele frequency of less than 20% are not likely to be represented in the population. *Appears as a major allele frequency in this population as it is more than 20% and is likely to be present in the population. [2] The 16 Asians were made up of 8 Japanese and 8 Chinese. (Db)- database SNP verified by GlaxoSmithKline sequencing. Number in brackets represents the number of samples with that particular mutation, out of the total sampled population. For example, I315M SNP has a allele frequency of 0.28, which represent 17.4 samples out of the 62 total Caucasians population.

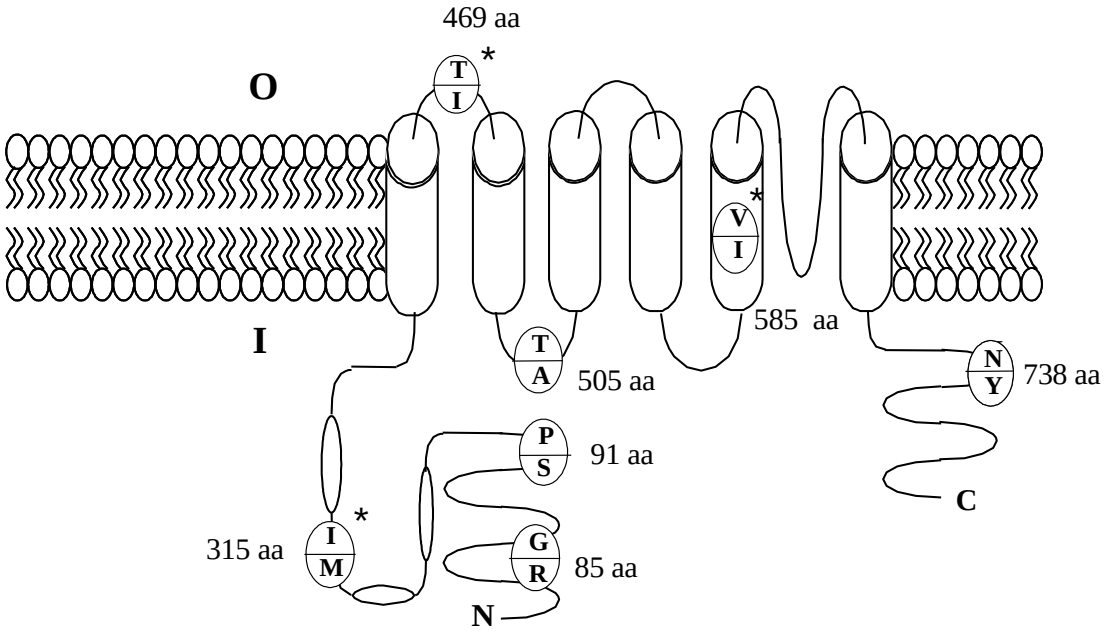

Figure 1.2 Membrane topology and approximate location of the 7 missense SNP's found in hTRPV1 receptor. Key: (A) Alanine; (I) Isoleucine; (M) Methionine; (N) Asparagine; (P) Proline; (Q) Glutamate; (R) Arginine; (S) Serine; (T) Threonine; (V) Valine; (Y) Tyrosine; (O) Outer plasma membrane; and (I) inner plasma membrane. Amino acid position of the SNPs in relation to ion channel membrane also shown. The amino acids are arranged in 6 transmembrane domains (cylinders) which are linked by intra- and extra-cytosolic loops with an additional short hydrophobic loop which connects the 5^{th} and 6^{th} transmembrane domains. Both the N- and C-terminals of TRPV1 are intracellular. The N-terminal is rich in proline and has three ankyrin repeat domains (ovals). * represent the most frequently occurring polymorphs in hTRPV1.

Several polymorphisms were found while cloning the hTRPV1 receptor. Davis and colleagues accordingly searched for hTRPV1 missense SNPs in three ethnic groups (Caucasians, African-Americans, and Asians) to investigate whether the ethnic differences in heat-sensitivity in these groups were due to mutations in their TRPV1. In total, only three non-synonymous SNPs in the hTRPV1 gene in Caucasians and African Americans were found to produce a frequency of more than 20%. Five clones were made; three clones contained single missense SNPs (see table 5.1). These were $hTRPV1_{211}$ (I315M), $hTRPV1_{121}$ (T469I) and $hTRPV1_{112}$ (V585I). Clone $hTRPV1_{111}$ (I315/T469/V585) represented "wild-type", whereas $hTRPV1_{222}$ (I315M/T469I/ V585I) had the combination of all three missense SNPs of hTRPV1 in one clone.

To ascertain whether these mutations produce any functional differences, whole-cell patch-clamp recordings were done during application of each of capsaicin, anandamide, protons and heat, and voltage-dependent activation. $hTRPV1_{111}$ and $hTRPV1_{222}$ were chosen for the first comparison because any differences in the responses, it would be apparent in these two haplotypes, because they show the greatest genetic variability.

	Amino Acid		
Code name.	**Position 315**	**Position 469**	**Position 585**
$hTRPV1_{111}$	I	T	V
$hTRPV1_{211}$	M	T	V
$hTRPV1_{121}$	I	I	V
$hTRPV1_{112}$	I	T	I
$hTRPV1_{222}$	M	I	I

Table 1.2 Five haplotypes of hTRPV1, where isoleucine (I), threonine (T) and valine (V) are substituted by a different amino acid within a specified position.

1.4 Aims and objectives

1.4.1 Hypothesis

Missense single nucleotide polymorphisms (SNPs) in the human noxious heat transducer and transient receptor potential vanilloid type 1 (TRPV1) ion channel are associated with differences in the sensitivity of this ion channel to several of its activators.

1.4.2 Aim

To study the responses of the human TRPV1 polymorphs which appear as major alleles to various TRPV1 activators.

1.4.3 Objectives

1. To compare the responses of wild-type $hTRPV1_{111}$ and $hTRPV1_{222}$ (I315M, T469I and V585I mutations) to: capsaicin; anandamide; heat; protons and voltage-dependent activation, respectively.
2. To identify the SNP, or SNPs, which are responsible for altered sensitivity of $hTRPV1_{222}$ when compared to the responses of $hTRPV1_{111.}$
3. To study the effect of altering the polarity of the amino acids in the positions which are likely to be involved in mediating the differences in responses of $hTRPV1_{111}$ and $hTRPV1_{222}$ to heat-evoked, and voltage-dependent, activation, respectively.

Chapter 2

EXPERIMENTAL TECHNIQUES AND PROTOCOLS

Introduction

The experimental work required for this PhD project was based on various techniques in molecular biology, extending over the areas of: cell culture; agonist-activated cobalt uptake and imaging; electrophysiology; and the use of transgenic animals. Here, the theoretical basis of these techniques is described, as are the protocols which were employed.

2.1 Cell culture

Cell culture is a technique used when cells are grown under controlled conditions. Several different types of cell cultures are routinely performed and can be divided into two groups: primary cell culture and secondary cell culture.

Primary cell cultures can consist of the culture of a complex organ or tissue slice or a defined mixture of cells or highly purified cells isolated directly from the organism. I have used dorsal root ganglia neurons harvested from mice to investigate the effect of DMSO in TRPV1-expressing cells. The isolation of a specific population, or populations, of cells requires several biochemical procedures. The required cells must be dissociated from their parent tissues and from other cell types. Disruption of the extracellular matrix and intercellular junctions that hold the cells together is typically achieved by the use of proteolytic enzymes, such as trypsin and collagenase, or with agents, such as EDTA, that bind, or chelate, the Ca^{2+} on which cell-to-cell adhesion depends. Large cells can be separated from small cells, and dense cells from light cells, by centrifugation (Alberts et al., 2002). Primary cell culture has an advantage in that they closely resemble the function of that cell *in vivo.* However, such cultures suffer from several drawbacks, most notably, the damage which the cells sustain while being harvested and the effect on their normal functioning of their being dissociated from the other tissues with which interact *in vivo* (Mather and Roberts, 1998).

Secondary cell cultures are cultures of established or immortal cell lines. Secondary cell cultures describe the cultures obtained from propagating cells derived from tumours (e.g. Hela) or from cells transformed *in vitro* or from normal embryonic tissue. Secondary cell cultures use propagation techniques, in which cells are propagated *in vitro* for experimental use, such as to express exogenous ion channel proteins. I have used a human embryonic kidney (HEK293) cell line to exogenously express various hTRPV1 haplotypes to investigate their response to various activators.

The fundamental aspect of secondary cell culture technique is the process of growing cells in a confluent monolayer by providing them with anchorage to pass "start" in their cell cycle. Dissociated cells plated on a dish in the presence of appropriate media adhere to the surface, spread out, and divide until a confluent monolayer is formed in which each cell is attached to the dish and contacts its neighbours on all sides. Cells grown *in vitro* also generally exhibit "anchorage dependence of cell division" meaning that they require to be able to adhere to the underlying plate surface in order to divide. A suitable surface to which propagating cells may adhere is constituted by the plastic surface of the culture-dish or T75 flask.

When cells from normal mammalian tissues are cultured in standard conditions, their ability to propagate is confined to a limited number of division cycles – about 50 for typical cells derived from humans. After this, they cease dividing in the process described as "cell senescence". Some cells are capable of avoiding cell senescence to divide indefinitely as "cell lines." These cells have undergone a genetic change that makes them effectively immortal. They will proliferate indefinitely in appropriate conditions and can be propagated as a cell line. Normal cells may similarly be "transformed" to constitute "transformed cell lines" by using a chemical or virus to alter their genetic make-up. The genetic uniformity of a cell line can be improved by cell cloning, in which a single cell is isolated and allowed to proliferate to form a large clone. A "clone" is any such collection of cells that are all descendants of a single ancestor. Such clones offer standardised cells which are ideal for comparative purposes over many experiments (Alberts et al., 2002).

The major advantages of these cloned cells reside in the efficiency with which they may be produced when compared with primary cultures and the consistency and reproducibility of the results which can be obtained from their use. The main disadvantage associated with the use of these cells is that these cells are atypical and their responses are not indicative of those of any other cell type. Moreover, after repeated passaging their characteristics may change and become quite different from those found in the starting population.

Most kinds of animal cells are able to survive, proliferate, and even express differentiated properties in a tissue culture dish in appropriate conditions. Cells require a suitable environment and a medium which contains the necessary nutrients to sustain cell life, as well as various other factors, such as growth factors, which stimulate cell proliferation, and transferrin, which carries iron into cells. These nutrients and other factors were traditionally supplied by constituting a medium comprising specified quantities of small molecules such as salts, glucose, amino acids, and vitamins, together with a poorly defined mixture of macromolecules in the form of animal serum such foetal bovine serum (Alberts et al., 2002). It must also be emphasised that the growth of cells in culture requires a sterile and controlled environment, especially in terms of temperature, oxygen and carbon dioxide.

2.1.1. Cell culture of DRG neurons

2.1.1.1 Theory of DRG neurons in culture

Different kinds of neurons from the peripheral and central nervous system of various kinds of animals have been cultured. These primary neuronal cultures have been used to investigate various molecules involved in the function of neurons. The selection of a particular type of neuron for culture depends on the purpose of the study. In this study, adult mice DRG neurons were chosen because TRPV1 is highly expressed in a population of primary sensory neurons (Caterina et al., 1997; Ahluwalia et al., 2000; Guo et al., 1999; Ichikawa and Sugimoto, 2004; Michael and Priestley, 1999).

Although the term nociceptor is now commomly used to describe nociceptive primary sensory neurons, traditionally it refers to the peripheral terminals of nociceptive A-delta and C afferents. These terminals express receptors for detecting potentially tissue damaging physical and chemical stimuli. However, it is impossible to record ionic currents from these terminals as they are too small (1 µm) for microelectrode penetration (Passmore, 2004). It is also difficult to control *in vivo* experiments as these do not allow for controlled application of chemical stimuli (Kress and Reeh, 1996; Gold et al., 1996). A more practical approach is to identify cell bodies of nociceptive neurons (perikarya), which are found in the DRG, under the assumption that the somatic membranes of the DRGs are also expressed at the nerve terminal at both ends. Furthermore, it is also assumed that the perikarya *in vitro* express all the molecules which are expressed *in vivo*.

The perikarya of primary sensory neurons are located in the spinal ganglia in the vertebral canal before the nerve reaches the spinal cord and are readily dissectible. Dissected neurons can be dissociated into single cell suspensions, plated on glass coverslips and maintained in culture. Dissociation and culturing of neurons involve axotomy close to the cell body. Hence, therefore the predominant phenotype of cultured primary neurons is one of regeneration and inflammation. Studies show that

following injury, primary sensory neurons become hyperexcitable due to the resulting change in the expression of receptors and the release of inflammatory mediators (Dickenson, 1995; Millan, 1999, D'Mello and Dickenson, 2008). In addition, DRG neurons in culture express antinociceptive neuropeptide Y, to the same extent as axotomised DRG *in vivo* (Kerekes et al., 2000).

Despite this, it has been shown that there is no significant difference in the distribution of cell size or neurochemistry of cells from L4/L5 ganglia *in vivo* and in culture (McMahon et al., 1994; Gavazzi et al., 1999). In addition, many sensory neurons in culture are excited by low concentrations of capsaicin and bradykinin, sensitised by prostaglandin E2 and display substance P-like immunoreactivity, each being a characteristic property of nociceptive neurons *in vivo* (Baccaglini and Hogan, 1983; Gold et al., 1996a).

Capsaicin selectively stimulates nociceptors, and sensitises nociceptors. Capsaicin selectively activates and sensitises TRPV1 leading to excitation of primary sensory neurons expressing TRPV1 (Bevan and Yeats, 1991; Oh et al., 1996; Vlachova´ and Vyklicky; 1993). Inflammatory mediators such as ATP and bradykinin greatly potentiate TRPV1-mediated responses (Dai Y et al., 2004, Tominaga et al., 2001; Sugiura et al., 2002; Steen et al., 1995a, 1996; Kress et al., 1992). Subsequent studies have shown that sensory neurons in culture share other similarities with *in vivo* models. Nociceptive neurons are small diameter neurons both in vivo and in vitro (McCarthy & Lawson, 1989, McCarthy & Lawson, 1990; Harper and Lawson, 1985).

Survival and maintenance of the phenotype of cultured DRG neurons requires the addition of nerve growth factor (NGF) to the growth medium. The neurotrophin NGF is a molecule that promotes the survival and differentiation of sensory and sympathetic neurons. NGF has an important influence on the morphological and functional properties of neurons, both *in vitro* and *in vivo.* Whilst DRG cell cultures can survive for few days in the absence of NGF, long term survival can be achieved only with regular treatment of NGF as it promotes the formation of neuronal processes (Levi-Montalcini, 1964; Otten et al., 1983). NGF has been shown to

increase the number of TRPV1-positive neurons in culture and TRPV1 mRNA and protein expression (Anand et al., 2006; Puntambekar et al., 2005; Winston et al., 2001). In the absence of NGF, cultured DRG neurons lose their responsiveness to capsaicin and proton application (Bevan and Winter, 1995; Winter et al., 1988).

The concentration of NGF used by most laboratories is 50 ng ml−1, which has been optimized for ganglion root culture (Levi-Montalcini & Angeletti, 1963). However, although, concentrations even up to 200 ng ml^{-1} have also been used to investigate changes in cultured DRG neurons responses (Winter, 1988). These concentrations are largely in excess of that which is typically present in the extracellular fluid of young rats (about 0.6 ng ml−1; Xia et al., 2000), and thus they more closely correspond to the substantial increases in local NGF levels typically found during tissue inflammation and injury (Ueda et al., 2002). Thus, even though the level of NGF is higher than that found *in vivo*, the data obtained from these experiments are comparative to those *in vitro*.

The primary advantage of cultured DRG neurons is that they facilitate experimental design and enable controlled environment to be established for drug applications as well as efficient wash-out system. This allows accurate pharmacological characterisation of nociceptors. Furthermore, experimental variations are reduced which assists in experimental replication as environmental influences (e.g. temperature, CO_2 content) and the condition of the animal (e.g. hormones, illness and nutrition) are irrelevant (Polikov et al., 2007). In addition, there is an abundance of DRG neurons in a rodent. There are 34 pairs of spinal nerves, each attached to its own DRG.

The most serious limitation on the use of acutely dissociated DRG cultures is that they lack systemic input from the peripheral system and that these cell receptors and other mechanism may not identical to those cells *in vivo*. Several studies have demonstrated a redistribution of channels and receptors in cultured DRG neurons not normally found in intact DRG. (Baccaglini and Hogan, 1983; Cesare and

McNaughton, 1997). Thus, while cultured primary sensory neurons are convenient and cost effective, they can not replace *in vivo* animal studies.

2.1.1.2 Culturing DRG neurons

I employed DRG cultures prepared from wild-type and TRPV1 knock-out adult mice to assess whether DMSO is able to activate native TRPV1 cells (see Chapter Four).

Three wild-type C57BL6/J mice and three knock-out TRPV1 C57BL6/J mice were terminally anaesthetised with an overdose of isoflurane according to the UK Home Office Animal Licensing Laws. Surgical instruments such as forceps, scissors and dissection knives were washed in soap and rinsed in ddH20, before being sprayed with 70% ethanol. Following decapitation, the entire spinal cord was dissected removing as much tissue as possible and pinned to a dissecting board with the dorsal surface facing upwards.

Using a microscope, two longitudinal cuts were made on each side of the spinous process of the vertebra, making it possible to remove the dorsal strip from the spinal column, revealing the meninges which envelop and protect the spinal cord. The meninges consist of three thin layers of tissues: the dura mater, the arachnoid mater and the pia mater (Fig 2.1).

The dura mater and the arachnoid layers where then carefully removed to expose the spinal cord and the DRG with their attached spinal nerves, dorsal and ventral roots. The DRG neurons from the first cervical to the first sacral spinal segments on both sides were carefully dissected out, using a fine pair of tweezers and a pair of microsurgery scissors, under aseptic conditions and collected in a petri dish containing growth medium (Fig. 2.2).

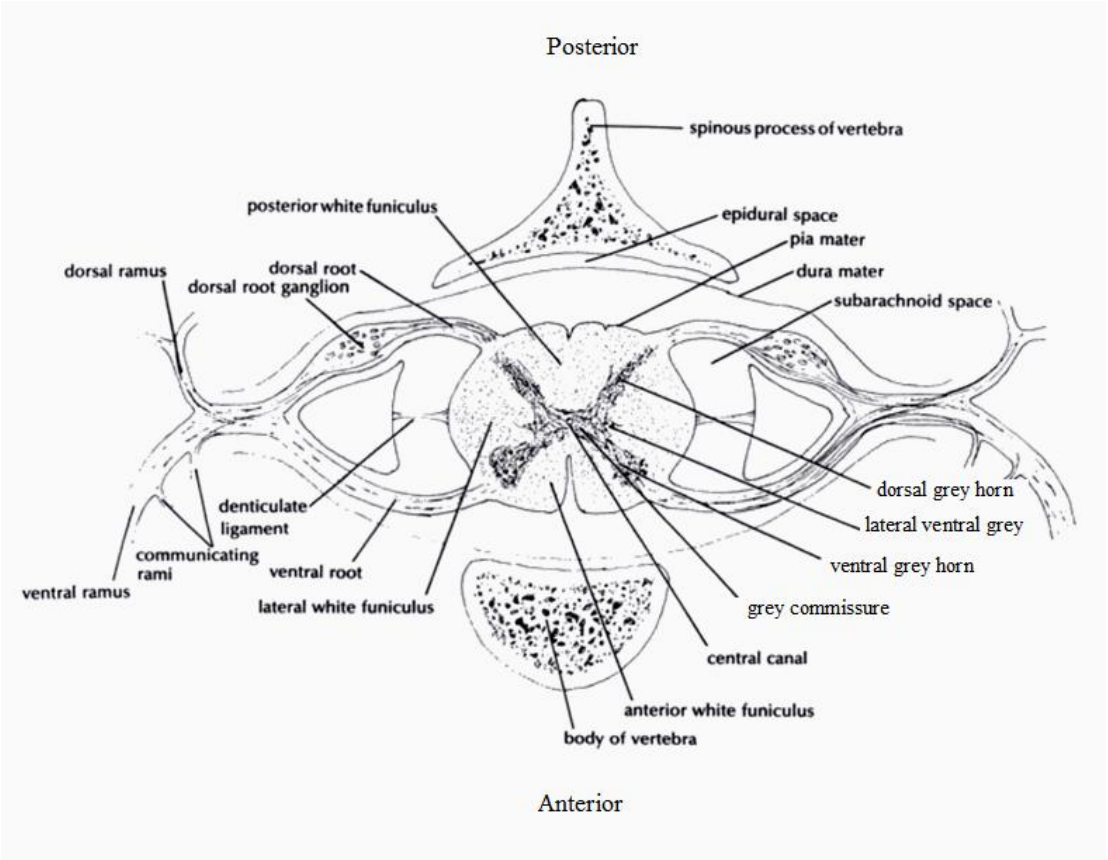

Figure 2.1. Cross-section of the spinal cord and surrounding structures. Each spinal nerve is formed by dorsal (sensory) and ventral (motor) roots which merge with the spinal cord. The dorsal root is a bundle of sensory axons which carries impulses into the spinal cord via a DRG, a small node that contains a collection of cell bodies of the sensory neurons. (Figure taken and adapted from Wingėrd and Stein, 1988)

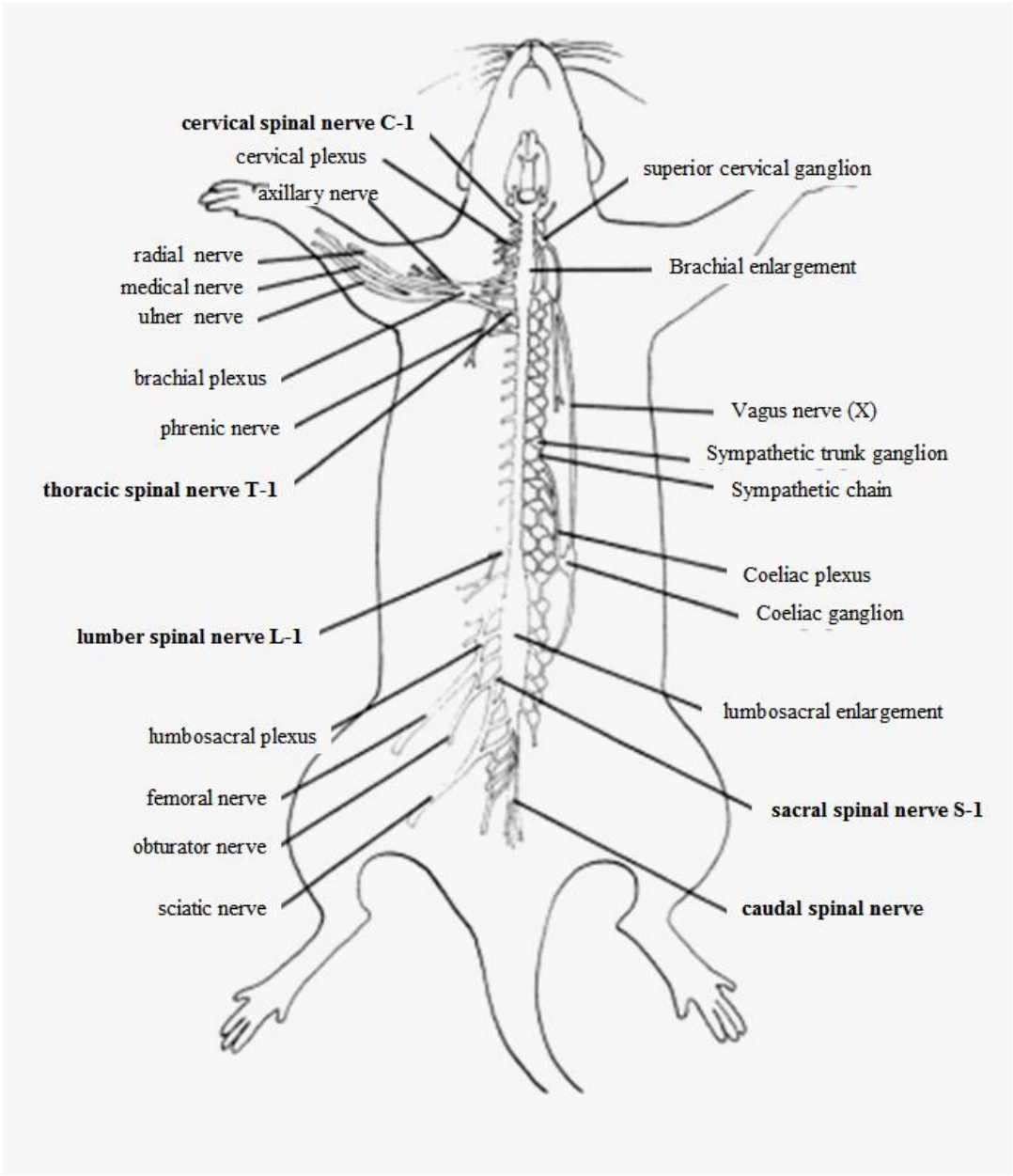

Figure 2.2. The spinal segments of a mouse. There are 34 pairs of spinal nerves that are separated into five regions from which they arise: 8 cervical (C1-8), 13 thoracic (T1-13), 6 lumber (L1-6), 4 sacral (S1-4) and 3 caudal. (Figure taken and adapted from Winger, 1988)

The growth medium which I used contained: Ham's Nutrient Mixture F12 (Sigma) supplemented with 1 mM L-glutamine (Invitrogen), antibiotics (50 units/ml penicillin and 5 µg/ml streptomycin; Invitrogen) and 4% Ultroser G (serum substitute; BioSepra). After collection of the DRGs which were trimmed of excess nerves and roots, the medium was gently removed and replaced with growth medium containing 0.125 % collagenase Type IV (200 units/ml; Sigma or Worthington Biochemical Corporation) for 3 hours in an atmosphere of 95% air and 5% CO_2 at 37 °C. Collagenases are enzymes that break down peptide bonds in collagen, the main protein in connective tissue, allowing the DRGs to soften to permit gentle trituration. Subsequently, the DRGs were washed three times with growth medium to remove traces of collagenase. To minimise the risk of DRGs being removed with the supernatant, in each wash the growth medium was added and the suspension allowed to stand, until the DRGs settled to the bottom and the supernatant was then removed. To achieve a DRGs suspension, mechanical trituration was carried out with a fire-polished (removes sharp edges) Pasteur pipette. The processes of these sensory neurons are removed during this procedure, making the cells appear round in shape. Following addition of nerve growth factor 50 ng ml^{-1} (NGF: Promega, Southampton, UK) the cells were plated on poly-DL-ornithine coated coverslips and cultured for two days at 37°C, 95% air and at 5% CO_2. Each culture contained cells from only one animal. Cells from each animal were plated on 8 coverslips. Cells were used two days after plating.

Prior to plating the cells, the glass coverslips were first coated with adhesion molecules, such as poly-DL-ornithine (Sigma). This organic substrate contains electrically charged poly-amino acids, which by electrostatic interaction favour cell anchoring on the glass coverslips (Ariano et al., 2005). This allows the cells to survive, adhere and maintain their electrical properties, including ion channel availability. Furthermore, the cells must adhere to the coverslip sufficiently to prevent their being washed away during experimental procedures. Coverslips were therefore coated with poly-DL-ornithine by placing them into 0.5 mg/ml poly-DL-ornithine in ddH_20 and placing them on a rotor shaker to agitate the coverslips for 2 hours at room temperature. This allowed the organic substrate to be deposited as a

thin layer on the coverslips. The coverslips were then washed several times with ddH_2O to remove excess poly-DL-ornithine (toxic to cells) and covered with growth medium until use.

2.1.2 Cell culture of HEK293 cells

2.1.2.1 Theory of technique

The HEK293 cell line is a clone of standardised cells which has proved to be particularly accommodating for reliably expressing DNA which has been artificially introduced into the cell in a process called transfection. The HEK293 cell line is derived from HEK293 cells which were transformed by exposing human embryonic kidney cells to sheared fragments of adenovirus type 5 (Ad5) DNA (Graham et al., 1977); and the human-viral junctions of integrated adenovirus type 5 DNA in HEK293 cells have been cloned and sequenced (Louis et al., 1997). Remarkably, it has been found that these cells express significant amounts of protein and mRNA for the neurofilament (NF) subunits NF-M, NF-L, and alpha-internexin, three of the four major NF proteins, with, in addition, small amounts of NF-H, the fourth NF subunit. Subject to very few, apparently aberrant, exceptions, each of these NF proteins is found only in neurons. Hence, the presence of all of these proteins in HEK293 cells is highly suggestive that these cell lines belong to the neuronal lineage (Shaw et al., 2002). It has been suggested that the most likely explanation for this phenomenon is that Ad5 preferentially transforms rare neuronal lineage cells present in human and rodent kidney cultures. It has also been observed that the use of these cells as a non-neuronal control line in transfection studies is inappropriate given their many attributes of developing neurons and neuronal progenitor cells (Shaw et al., 2002).

An important variant of the HEK293 cell line is the HEK293T cell line which provides longer temporal expression of the desired gene product. HEK293T cells stably express an SV40 temperature-sensitive T-antigen. Plasmids containing the SV40 insert are able to replicate copy numbers between 400-1000 plasmids per cell and therefore express higher levels of recombinant proteins. HEK293T cells were the cell line used in this PhD project. However, for simplicity, these cells are simple referred to as HEK293 cells in this thesis.

HEK293 cells have limitations when employed as a model to examine the functioning of various cell types since they are essentially in a category of their own. However, they are highly efficient in expressing a reliable transient transfection. Moreover, they are relatively easy to manage and sustain in culture. They are, therefore, useful where the behaviour of the cell itself is not the subject of study, but rather the protein which is expressed by the transfected DNA. Repeated passaging of these cells results in variations from their original characteristics (Thomas and Smart, 2002; Park et al., 2004, Lee et al., 2001). Therefore, cells passaged >20 times were discarded.

2.1.2.2 Culturing HEK293 cells

HEK293 cells obtained from Dr John B. Davis at GlaxoSmithKline and the European Collection of Cell Cultures (ECACC) were routinely grown as monolayers in growth medium on plastic tissue culture grade T75 flasks for culturing, and on plastic tissue culture grade petri dishes for transfection (Nalg Nunc International), in an atmosphere of 95% air and 5% CO_2 equilibrated at 37 °C.

All cell culture procedures were done under clean and sterile conditions. Glassware and pipette tips were sterilised by autoclaving before use, to remove any contaminating microorganisms, because if left unchecked, these would grow in the culture media and become infected. Autoclaving is carried out using pressurised steam at 121 ^{o}C under 105 kPa for 20 minutes which will destroy microorganisms such as bacteria, viruses, fungi and spores (Wilson and Walker, 2005). Sterile plastic-ware, which is commercially available, was also used (Nalg Nunc International). All procedures were performed under a cell culture hood, which generates a laminar flow of sterile filtered air.

The growth media consisted of minimum essential medium (MEM), 2 mM L-glutamine, MEM non-essential amino acids, 10% foetal bovine serum (FBS), antibiotics (50 units/ml penicillin and 5 µg/ml streptomycin). MEM is patterned after

Eagle's Media and is well suited for the growth of a broad spectrum of mammalian cells. It contains essential amino acids (arginine hydrochloride, cystine, histidine hydrochloride, isoleucine, leucine, lysine hydrochloride, methionine, phenylalanine, threonine, tryptophan, tyrosine and valine), vitamins (choline chloride, calcium pantothenate, folic acid, niacinamide, pyridoxal hydrochloride, riboflavin, thiamine hydrochloride and inositol), inorganic salts (calcium chloride, magnesium sulphate, potassium chloride, sodium bicarbonate, sodium chloride, and sodium phosphate) and glucose. Glutamine is added to the media, as MEM is formulated without this essential amino acid due to its unstable characteristic during long-term storage. The primary function of glutamine in cell culture is to provide a reservoir of nitrogen atoms to synthesise proteins, nucleic acids and other nitrogenous compounds. These, in turn, produce nucleotides, amino acids and vitamins which are necessary for the survival of cells. Glutamine also supports the growth of cells which have high energy demands, as it is also able to function as an alternative energy source for rapidly dividing cells *in vitro* and for cells that use glucose insufficiently (Conrad, 2008). MEM non-essential amino acids (glycine, alanine, asparagines, aspartic acid, glutamic acid, praline and serine) stimulate growth, prolong the viability of cells in culture, and reduce the biosynthetic burden on cells *in vitro.* FBS is rich in albumin, hormones and growth factors which stimulate cellular growth and proliferation. Antibiotics inhibit bacterial growth by inhibiting bacterial protein synthesis, thus ensuring the survival of cells in culture. All of the products described in this paragraph were sourced from Invitrogen U.K.

Sub-confluent cells (70-80%) were obtained after 3–4 days and were harvested using 0.05% trypsin containing 0.53 mM ethylenediaminetetraacetic acid-tetrasodium (EDTA-4Na). EDTA chelates calcium and magnesium ions from intracellular bridges and desmosomes and potentiates the action of trypsin which helps to dissociate the cells from each other and from the flask. Therefore, the cells were briefly washed with 1x Dulbecco's Phosphate Buffered Saline (D-PBS) and treated with trypsin-EDTA (5 minutes at room temperature). Trypsin was inactivated by adding equal amounts of growth media, since bovine serum has a rich source of trypsin inhibitors. Cells were then centrifuged (200g for 5 minutes, at room

temperature) and resuspended in fresh growth medium (to remove any traces of trypsin-EDTA as EDTA has growth inhibitory properties at even low concentrations) before plating into T75 flasks and/or Petri dishes.

2.2 Transfection

2.2.1 Background to the purpose of transfection

One of the major achievements of biological research is the development of cell culture technology and the molecular cloning of genes. These developments have put the investigation of ion channel physiology onto new qualitative level. First, cell culture of cell lines obtained from a single cell produces unlimited supply of cells with uniform properties that can be grown *ex vivo*. Second, molecular cloning of genes has allowed them to express exogenous ion channel proteins, via a transfection, at levels much higher than native cells do. It is therefore possible to investigate ion channel properties under much “cleaner” conditions.

2.2.1.1 Cloning of DNA

DNA may be cloned by first obtaining a fragment of DNA which contains the gene of interest. In our experiments this was the hTRPV1 gene. This DNA is then inserted into the purified DNA genome of a self-replicating genetic element – generally a virus or a plasmid. Plasmids are self-replicating extra-chromosomal circular DNA molecules, distinct from the normal bacterial genome. The term "recombinant DNA technology", refers to the process of the transferring of a DNA fragment of interest from one organism to a self-replicating genetic element, such as a bacterial plasmid. The DNA of interest can then be propagated in a foreign host cell. To "clone a gene," a DNA fragment containing the gene of interest is isolated from chromosomal DNA using restriction enzymes and then united with a plasmid that has been cut with the same restriction enzymes. When the fragment of chromosomal DNA is joined with its cloning vector in the laboratory, it is called a "recombinant DNA molecule." Following introduction into suitable host cells, the recombinant DNA can then be reproduced along with the host cell DNA (Alberts et al., 2004).

Plasmids are self-replicating extra-chromosomal circular DNA molecules because they contain an origin of replication, which allows replication in the host cell independently of the chromosome. Plasmids can carry up to 20,000 bp of foreign DNA. In addition to bacterial plasmids, some other cloning vectors include viruses, bacteria artificial chromosomes *(BACs),* and yeast artificial chromosomes (*YACs*). *Cosmids* are artificially constructed cloning vectors that carry up to 45 kb of foreign DNA and can be packaged in lambda phage particles for infection into *E. coli* cells. BACs utilize the naturally occurring F-factor plasmid found in *E. coli* to carry 100 to 300 kb DNA inserts. A YAC is a functional chromosome derived from yeast that can carry up to 1 MB of foreign DNA. Bacteria are most often used as the host cells for recombinant DNA molecules, but yeast and mammalian cells also are used (Human Genome Project Information, 2008).

In the present study, wild-type hTRPV1 cDNA had been inserted into the plasmid, pcDNA3.1v5-HIs-TOPO by Hayes and co-worker (Invitrogen, Hayes et al., 2004; see Fig 2.3).

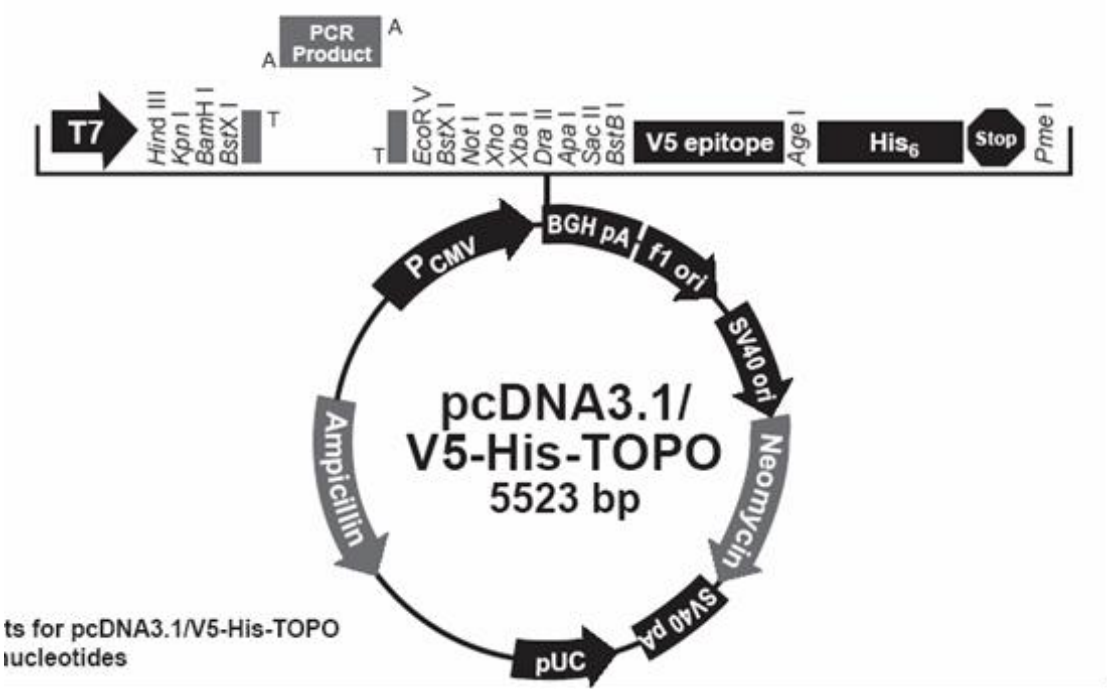

Figure 2.3. Map of pcDNA3.1v5-HIs-TOPO vector. The vector contains key components for cloning. *F1 ORI* insert is the replication origin (ORI) for replication in the host cell. *SV40 ori* (origin), *SV40 pa* (polyadenylation), *pUC* and *T7* inserts enable high levels of replicate copy numbers. CMV or cytomegalovirus promoter insert also achieves high levels of expression. *Neomycin resistance gene* and *ampicillin resistance gene* inserts for selective amplification. To clone a DNA sample, the same restriction enzyme must be used to cut both the vector and the DNA sample. The expanded area above contains a poly-linker region, which is able to recognise several different restriction enzymes. This enables the vector to be used for cloning for a variety of DNA samples. The poly-linker region also contains a section into which the wild-type hTRPV1 cDNA can be inserted, (indicated here as *PCR Product)*. (Taken from http://tools.invitrogen.com/content/sfs/vectors/pc dna3.1v5 histopo_map.pdf.)

2.2.1.2 Theory of transfection

Transfection is the transfer of recombinant genes into cultured mammalian cells. Typically, it involves opening transient pores in the cell plasma membrane to allow the uptake of material. Genetic material (such as supercoiled plasmid DNA or siRNA constructs), or even proteins, such as antibodies, may be transfected. This technique is an important tool for investigating how genetic variations affect the functioning of certain genes. Transfections may be stable (permanant) or transient. A stable transfection requires that the transfected gene should remain in the genome of the cell transfected and its daughter cells. To achieve a stable transfection, another gene must be co-transfected which gives the host cells some selection advantage, such as resistance to a certain toxin to their genome. Addition of the toxin, to which the transfected gene offers resistance, results in only those few cells being able to proliferate, while the others perish. Repeated application of this selection procedure results in only the cells with a stable transfection remaining for further passages. Transient transfections do not require the foreign DNA to be introduced into the nuclear genome. This results in the foreign DNA being lost at the later stage, when the cells undergo mitosis. Typically, expression of the transfected gene can be analysed between 1 and 4 days after induction of the DNA (Felgner et al., 1987).

In the case of my project, transient transfection was the most appropriate method for producing functional human TRPV1 (hTRPV1) polymorphs, in order to assess differences, if any, in their sensitivity to several known activators of TRPV1. The use of transient transfection has it disadvantages because it involves the use of costly transfection reagents and the need to transfect cells each time a clone is required to be expressed. Nevertheless, this method avoids the laborious and time consuming process of establishing stable transfection of several clones.

There are several methods which have been developed for introducing cloned DNA into cultured cells. These include transfection with: (i) calcium phosphate or DEAE-dextran (Pari and Keown, 1997.); (ii) polybrene (Kawai and Nishizawa, 1984;

Chaney et al., 1986); (ii) protoplast fusion (Schaffner, 1980; Rassoulzadegan et al., 1982); (iv) electroporation (Neumann et al., 1982; Zimmermann, 1982); (v) direct microinjection into the nuclei (Capecchi, 1980); and (vi) liposomes (Felgner et al, 1987). However, regardless of the method used to introduce DNA into cells, the efficiency of transfection is dependent on the cell type. Different cultured cell lines vary in their ability to take up and express foreign DNA. Certain cell types and lines are intrinsically easier to transfect than others, although the reason for this is currently unknown (Nikcevic et al., 2003)

I chose the HEK293 cell line to express hTRPV1 as these cells have been extensively used in transfection and have become the mammalian expression system of choice for studying a variety of membrane proteins (Thomas and Smart 2005). Furthermore, HEK293 cells transiently transfected with TRPV1 are routinely used by a large number of laboratories (Caterina et al., 1997; Davis et al., 2000; Jordt et al., 2000; Voets et al., 2004). Hence, transfection of these cells by liposomes was chosen due to its simplicity and high efficiency of transfection to adherent cells (Lipofectamine™ 2000 Transfection Reagent product sheet; Graham Smith, personal communication).

Liposomes are small vesicles made up of phospholipids which consist of hydrophilic heads and lipophilic tails. These vesicles are not only used to deliver foreign DNA to mammalian cells but are also widely used for drug delivery. Liposome-mediated transfection involves the synthetic cationic (positively charged) lipid, N-[1-(2,3-dioleyloxy)propyl]-N,N,N-trimethylammonium chloride (DOTMA; Felgner et al., 1987). Liposomes that contain DOTMA have an overall positive charge, which consequently interact spontaneously with negatively charged nucleic acid molecules, to form lipid-DNA complexes. These complexes, in turn bind strongly to the plasma membrane of the cell due to favourable charge interactions. And with the aid of DOTMA, these complexes facilitate fusion with the plasma membrane of the cell, as both are made up of phospholipid bilayer. This results in both the uptake and expression of the foreign DNA. These synthetic liposomes were

first introduced in 1987 by Felgner and colleagues (Felgner et al., 1987). Consequently, a number and variety of commercially available forms are available, such as Lipofectamine.

Lipofectamine™ (Invitrogen U.K.) is a cationic liposome based reagent that provides high transfection efficiency and high levels of gene expression in a range of mammalian cell types *in vitro*. Optimum transfection efficiency and subsequent cell viability depend on a number of experimental variables, such as cell density, liposome and DNA concentrations, liposome-DNA complexing time, and the presence, or absence, of media components, such as antibiotics and serum (Dalby et al., 2004). PLUS™ reagent by Invitrogen can also be used in conjunction with Lipofectamine to boost the efficiency of transfection. This reagent enhances the cationic lipid-mediated DNA transfection by assisting in the stage where DNA is 'complexed' to the lipids.

Other methods of transfection all suffer from one, or more, problems relating to either cellular toxicity, poor reproducibility, insufficiency of DNA delivery, is simple, highly reproducible, low toxicity, effective for both transient and stable expression of transfected DNA.

However, Lipofectamine does have a number of disadvantages. First, an additional preparation of antibiotic-free and serum-free media is required. The presence of antibiotics in the media during transfection causes cell death. The presence of serum in the media inhibits cationic lipid-mediated transfection (Lipofectamine™ 2000 Transfection Reagent product sheet). Second, the gene of interest must be inserted into a plasmid, prior to transfection.

2.2.1.3 Transient transfection

HEK293 cells expressing hTRPV1 were obtained by transient transfection of subconfluent HEK293 cells using PLUS™ reagent and Lipofectamine™ 2000 reagent (Invitrogen). The $hTRPV1_{111}$ cDNA was cloned in pcDNA3.1/V5-His-TOP vector. The cells were also transfected with a plasmid DNA encoding the Green Fluorescent Protein (GFP), a reporter gene which, when expressed fluoresces green. The co-transfection of cells with the two vectors (TRPV1 and GFP) were carried out to allow efficient selection of cells expressing the transfected genes.

The green fluorescent protein (GFP) is a 27 kDa polypeptide which converts the blue chemiluminescence of the Ca^{2+}-sensitive photo-protein, aequorin, into green light (Chalfie, 1994; Cody et al., 1993). GFP was originally discovered from the Aequoria Victoria jellyfish (Shimomoura et al., 1962). The gene for GFP has been cloned (Prasher et al., 1992) and linked/fused with other genes to produce chimeric proteins when translated, thereby acting as a fluorescent protein tag (Chalfie et al., 1994; Inouye and Tsuji et al., 1994). This technique is a powerful tool in biochemistry and cell biology, because it functions as a non-invasive fluorescent marker in living cells. It has been used in a wide range of applications because it has the ability to function as a cell lineage tracer, a reporter of gene expression, or a measure of protein-protein interactions. Typically, naturally occurring GFP has an absorbance/excitation peak at 395 nm with a minor peak at 475 nm. The emission peak is at 508 nm. The main advantages of using GFP as a gene expression maker are: (i) it can be used in all organisms; (ii) it can be used to target a specific tissue, cell, organelle or protein; (iii) it has good optical properties (visible excitation); and (iv) it is cheap to replicate. In this case, GFP was used as a transfection marker to increase the efficiency of identifying cells to patch-clamp and test for TRPV1 activity. The disadvantages of using GFP as a marker of gene expression are: (i) gene transfection is required; and (ii) strong promoters are needed for sufficient expression for detection, especially in mammalian cells (Tsien, 1998).

The transfection method used has previously been optimised for high efficiency of transfection by GlaxoSmithKline. HEK293 cells were typsinised 1 day before transfection and plated on a 90 mm-diameter plastic Petri dish so that they were 50-70% confluent by the next day when transfection was carried out. On the day of transfection, 0.15 µg of GFP cDNA and 1.5 µg of hTRPV1 cDNA were diluted in serum-free and antibiotic-free Dulbecco's Modified Eagle Medium (D-MEM; Invitrogen) containing Plus^{TM} reagent and were incubated for 15 minutes at room temperature in order to pre-complex DNA with Plus reagent. The reason for transfecting in a 1:10 ratio of GFP to TRPV1 is because cells expressing the green fluorescence under a fluorescent microscope are also more likely to express the gene of interest, TRPV1. However, the expression cassette of a pIRES which contains an internal ribosome entry site with two open reading frames enabling one to translate two genes of interest simultaneously, could be used as an alternative method of cell selection (Trouet et al., 1997). Diluted Lipofectamine reagent was then added to the pre-complexed DNA and incubated for a further 15 minutes at room temperature.

Cells were briefly washed with D-MEM to remove traces of growth medium containing serum and then D-MEM was added to the dish. This was followed by the addition of DNA-Lipofectamine-Plus reagent complexes (final concentration: ~8.7 µg/ml of Lipofectamine reagent and ~8.5 µg/ml of Plus reagent). These were gently which was gently mixed into the medium and incubated at 37°C at 5% CO_2 for 3 hours. After incubation, the transfection medium was removed and replaced with growth medium containing serum and antibiotics and incubated for a further 1 hour.

Transiently transfected cells were typsinised and then plated onto 13-mm poly-DL-ornithine coated glass coverslips as the recording chamber of the electrophysiology machine is of this size.

hTRPV1-tranfected HEK293 cells were used after 24 hours of plating because, being a cationic-mediated transfection, a negative charge forms around the cells, making whole-cell recordings very difficult (Thomas and Smart, 2005). Transfected cells were not used after 72 hours because the culture becomes too

confluent making it difficult to record from a single cell and it has been reported that peak transient expression is generally seen 24-72 hours following transfection (Dalby et al., 2004).

2.3 Site-directed mutagenesis

2.3.1 Theory behind site-directed mutagenesis

Site-directed mutagenesis (SDM) or oligonucleotide-mediated mutagenesis is used to add, delete, or substitute, a nucleotide in a region of DNA with known sequence using synthetic oligonucleotide primers containing the desired mutation. SDM is an invaluable technique for studying gene expression and the protein structure-function relationship of mutated DNA at key residues. It has revolutionised molecular genetic research. This technique was discovered by independent work carried out by Karry B. Mullis (Mullis and Faloona, 1987) and Michael Smith (Gillam et al., 1980; Zoller and Smith, 1983), who later shared the Nobel Prize in 1993 for their contribution to the development of methods within DNA-based chemistry.

The polymerase chain reaction (PCR) is a technique used for amplifying specific segments of DNA. The PCR method was first developed in 1987 by Mullis and co-workers (Mullis and Faloona, 1987; Mullis, 1987; Mullis et al., 1987). The PCR technique derives its name from a key component of the reaction, namely, a heat-stable DNA *polymerase,* which is an enzyme that is not denatured by the repeated heat treatments involved in the reaction. The most widely used enzyme is *Taq* DNA polymerase, an enzyme first isolated from *Thermus aquaticus* (*Taq*), a bacterium which lives in hot springs and which can tolerate high temperatures (optimum temperature 72-74 ^{o}C; Brock and Freeze, 1969). The other essential components of the PCR reaction are: (i) a DNA template that contains the nucleotide target to be amplified; (ii) a pair of primers (synthetic DNA oligonucleotides) that anneal with the flanking sequences of the specific target which are complementary to each strand of the DNA double helix thus determining the boundaries of the amplified product; (iii) dNTPs; and (iv) buffer solution containing Mg^{2+}, which provides a suitable environment for optimum activity and stability of the reaction. Mg^{2+} is used to stabilise dsDNA and contributes to the specificity of primer annealing (Alberts et al., 2004).

A PCR mixture is then placed in a thermal cycler, which is pre-programmed with the following PCR steps:

1. *Denaturation or strand separation*. The parental dsDNA template is separated by a brief heat treatment of the reaction, usually 96°C for 30 seconds.
2. *Annealing of primers*. The reaction is then cooled to the melting temperature of the primers, usually between 55 °C to 60 °C and typically 1 minute is required for every 1kb of DNA to be amplified to anneal to complementary sequences within the DNA template.
3. *Elongation or DNA synthesis*. The reaction is then heated to the optimum temperature of the *Taq* DNA polymerase, usually 72 °C for 3 minutes. This allows the DNA polymerase to elongate both primers downstream of the target DNA sequence as synthesis is in the 5' to 3' direction.

These three steps are then repeated several times, so that, in addition to the parental DNA molecule, the newly synthesised fragment serves also as a template. Thus, for every cycle the amount of DNA synthesised is doubled. Usually 30 cycles of the reaction are required for detectable DNA amplification.

PCR technique has several limitations and disadvantages. First, the target DNA sequence must be known. The region of interest must be previously characterised in order to design specific primers. However, this can be overcome by using degenerate primers if a related gene member has previously been sequenced. Many genes are highly conserved among different species. By aligning the sequences from a number of previously determined related DNA sequences, whose protein products have similar functions (homology), conserved regions can be observed. These conserved regions provide the starting point for designing degenerate PCR primers to unidentified members of the family, instead of using specific PCR primers with a given sequence. Second, product size is short. Typically, PCR product is approximately between 0.1 - 5 kb, compared to cell-based DNA cloning where the

sizes of the cloned fragment is able to reach 2 Mb. Third, amounts of product are limited. A single PCR reaction produces very small amounts of product when compared to cell-based DNA cloning where "scale-up" is possible. Finally, there may be infidelity of DNA replication. DNA replicated *in vitro* has higher copying error rate when compared to DNA replication *in vivo* because of the lack of proof-reading mechanisms of the polymerase. The commonly used *Taq* DNA polymerase has no associated 3'-to-5' exonuclease which has the function of proof-reading. This may result in mis-incorporation during DNA replication. However, an alternative polymerase, such as *Pyrococcus furiosus (Pfu*) DNA polymerase, which has associated 3'-to-5' exonuclease activity, can be used (Cline et al., 1996).

Nevertheless, PCR technique has major advantages. First, the speed and ease of use of the method and a complete reaction can be performed in only a few hours. Initially some time is required to: (a) design and synthesize the primers; and (b) optimise the conditions for the PCR reaction which usually involves altering the annealing temperature for the primers to anneal to the DNA template. Once these two issues have been dealt with, the reaction is quick and simple. For these reasons PCR has revolutionised molecular genetics by allowing rapid cloning and analysis of DNA. Thus, this technique is widely used for the diagnosis of genetic diseases, as well as in basic and clinical research. PCR technique is able to detect a single DNA molecule in a sample and is even able to amplify from a single cell (Li et al., 1988). This technique has been exploited in many applications of forensic science, genetic linkage analysis and molecular palaeontology studies. Futhermore, this technique is able to use degraded and fixed DNA samples, making it suitable for anthropological and palaeontological studies (Strachan and Read, 1999). In addition, PCR has been adapted into other techniques such as DNA sequencing and *in vitro* site directed mutagenesis.

Smith discovered that even if one of the bases of the oligonucleotide primer was incorrect/mis-matched, the primer will still anneal at the correct position of the DNA template and generate an altered/mutated DNA sequence which, in turn, can produce a modified protein (Gillam et al., 1980; Zoller and Smith, 1983).

Previously, SDM required ssDNA as a template to achieve efficient mutagenesis which meant that this was often technically difficult and intensive procedure (Kunkel, 1985; Sugimoto *et al*., 1989; Taylor *et al*., 1985; Vandeyar *et al*., 1988). However, Braman and colleagues in 1996 developed a new method in which they allowed dsDNA to be the starting template for SDM (Braman et al., 1996). The QuikChange SDM kit from Stratagene, utilises this principle (Papworth *et al*., 1996). The key steps used in this kit are as follows.

1. *Mutagenesis reaction*. The plasmid dsDNA of the gene of interest is first placed into a standard PCR reaction mixture (DNA polymerase, dNTPs, and buffer-containing Mg^{2+}) with the mutagenic oligonucleotide primers. These are primers which are complementary to the DNA target sequence except for a base, or a few bases, which will produce either a point mutation, a switch in amino acids, an insertion or a deletion of single or multiple amino acids. The mixture is placed into a thermal cycler set to standard PCR cycle. This involves: (i) denaturation to separate the dsDNA; (ii) annealing to allow the mutagenic primers to anneal to the imperfectly matched DNA strands; and (iii) elongation to allow amplification of the entire plasmid DNA. Two kinds of DNA products result. Half will contain the desired mutated DNA sequence containing staggered nicks (dsDNA break that produces 3’ or 5’ protruding ends). The other half will contain the wild-type DNA sequence (Papworth *et al*., 1996).

2. *Dpn I digestion*. dsDNA template naturally contains methylated strands. Thus incorporation of the mutated primers to the dsDNA template results in unmethylated ssDNA and dsDNA products. The Dpn I endonuclease specifically digest parental methylated non-mutated dsDNA and hemimethylated DNA (where only one of the two strands are methylated), leaving unmethylated dsDNA-containing the desired mutation with staggered nicked ends (Nelson *et al*., 1992).

3. *Transformation*. The unmethylated dsDNA-containing the desired mutation is then transformed into 'competent cells', which not only repairs the staggered nicked ends but results in the amplification of the plasmid DNA with the desired mutation. 'Competent cells', such as *E. coli*, are bacterial cells which possess cell walls that are easily altered when treated with calcium chloride followed by a brief heat shock (Cohen et al., 1972; Mandel and Higa, 1970). This allows the cells to be not only transiently permeable to DNA but also results in genomic incorporation of the foreign DNA.

   DNA must be cloned and then inserted into a plasmid. In the present study, wild-type hTRPV1 cDNA has already been inserted into the plasmid vector, pcDNA3.1v5-HIs-TOPO, which carries genes resistance for the antibiotic, ampicillin. This plasmid can then be propagated by transformation in a bacterial cell in the presence of ampicillin, and left to grow on a nutrient agar plate. Thus, only the bacteria which contain plasmids will survive and replicate into a colony of identical cells. This colony appears as a white plaque on the agar plate. Inoculation of a single colony into culture medium is then carried out. This produces a large number of identical plasmid DNA molecules so that detectable amounts of DNA can be purified for sequencing. Typically a small starter culture of 1.5 mls is sufficient.

4. *Purification of plasmid DNA and sequencing.* The bacteria containing plasmid DNA molecules are then separated from each other using an alkaline lysis extraction method.

   The purified plasmid DNA is then amplified using PCR with primers that flank the region of interest and sequenced to verify that the desired DNA mutation has been achieved.

Once a specific colony has been verified to contain the desired DNA mutation, the plasmid can be re-transformed to produce larger amounts of DNA for transient transfection, thereby allowing investigative analysis of the protein arising from the mutated DNA.

The four step procedure generates mutants with greater than 80% efficiency (Papworth et al., 1996). Furthermore, the use of dsDNA as a template makes this technique a simple, rapid and reliable method, eliminating the need for the time consuming procedure of subcloning into M13-based bacteriophage plasmids (Sambrook et al., 1989).

However, there are disadvantages to this technique. Many of these are similar to the limitations of PCR. First, the design of mutant oligonucleotide primers is critical to the efficiency of the reaction and consequently the target DNA sequence must be known. The length of the mutant oligonucleotide primers is usually more than 25 bases as the primer must be long enough to hybridise to the target DNA sequence. The degree of similarity must be 100% over 10-15 bases at both the 3' and 5' ends, usually the target base/bases are found in the middle of the primer. The sequence of the mutant primer should not generate secondary structures which will inhibit annealing of the primers to subsequent amplification cycles.

The use of the QuikChange Primer Design Programme has made designing mutagenic primers quick and simple. Second, the lack of 3'-to-5' exonuclease associated with the DNA polymerase, such as *Taq* DNA polymerase, increases the

risk of introducing random mutagenesis due to the lack of proofreading activity. However, the QuikChange SDM kit is supplied with an enhanced version of *Pfu* DNA polymerase with associated 3'-to-5' exonuclease activity, *PfuTurbo*® DNA polymerase. This enzyme has a 6-fold higher fidelity in DNA than *Taq* DNA polymerase and is able to amplify plasmid DNA targets up to 15 kb in length (Hogrefe et al., 1997).

2.3.2 Site-directed mutagenesis: practical approach

Originally, I was supplied by Davis and colleagues with five haplotypes: $hTRPV1_{111,}$ $hTRPV1_{222,}$ $hTRPV1_{211,}$ $hTRPV1_{121,}$ and $hTRPV1_{112}$. Due to the initial outcome of my data, I made two additional haplotypes, $hTRPV1_{121\text{-}S}$ and $hTRPV1_{121A}$ (Table 2.1).

		Amino Acid		
	Code name.	**Position 315**	**Position 469**	**Position 585**
1	$hTRPV1_{111}$	I	T	V
2	$hTRPV1_{211}$	M	T	V
3	$hTRPV1_{121}$	I	I	V
4	$hTRPV1_{112}$	I	T	I
5	$hTRPV1_{222}$	M	I	I
6	$hTRPV1_{121\text{-}S}$	I	S	V
7	$hTRPV1_{121\text{-}A}$	I	A	V

Table 2.1 Seven haplotypes of hTRPV1. Haplotypes 1-5 were made by Davis and co-workers. Haplotypes 6-7 were made by me.

Two mutants were made in order to verify whether codon 469 plays an important role in TRPV1-mediated sensitivity. These changed the wild-type codon, by altering the polar amino acid, threonine, to either a non-polar amino acid, alanine (T469A), or another polar amino acid, serine (T469S) (see Fig. 5.2). The $hTRPV1_{111}$ gene was cloned in the mammalian expression plasmid vector pcDNA3.1v5-HIs-TOPO (7.7 Kb). Site directed mutagenesis of codon 469 (bases 1406-1408) of this gene was then performed using the QuikChange XL Site-Directed Mutagenesis kit in accordance with the manufacturer's instruction (Strategene, La Jolla, CA).

The primer pairs used for mutagenesis were designed by the QuikChange Primer Design Programme (www.stratagene.com) and ordered from MWG Biotech, Ebersberg, Germany. The primer pairs were as follows (bases in bold indicate the desired mutation which differs from wild-type sequence; Fig 2.4): TRPV1-T469A, 5'-C TTG CCT CCC TTT AAG ATG GAA AAA **GCT** GGA GAC TAT TTC-3' (sense,) and 5'- GAA ATA GTC TCC **AGC** TTT TTC CAT CTT AAA GGG AGG CAA G-3' (antisense); TRPV1-T469S, 5'-C TTG CCT CCC TTT AAG ATG GAA AAA **TCT** GGA GAC TAT TTC-3' (sense), and 5'-GAA ATA GTC TCC **AGA** TTT TTC CAT CTT AAA GGG AGG CAA G-3' (antisense).

(a) Wild-type hTRPV1

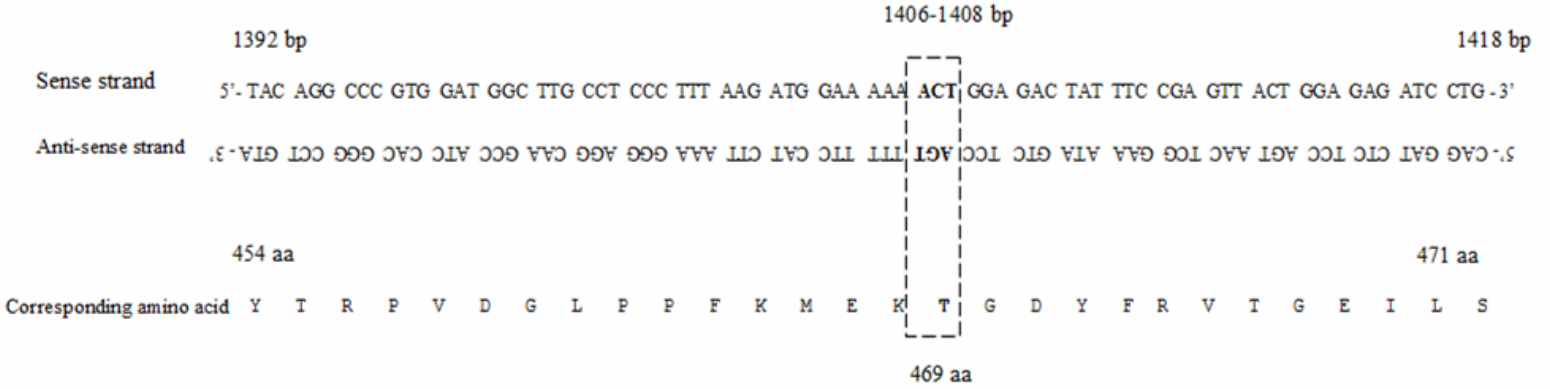

(b) Mutant hTRPV1 T469A (non-polar)

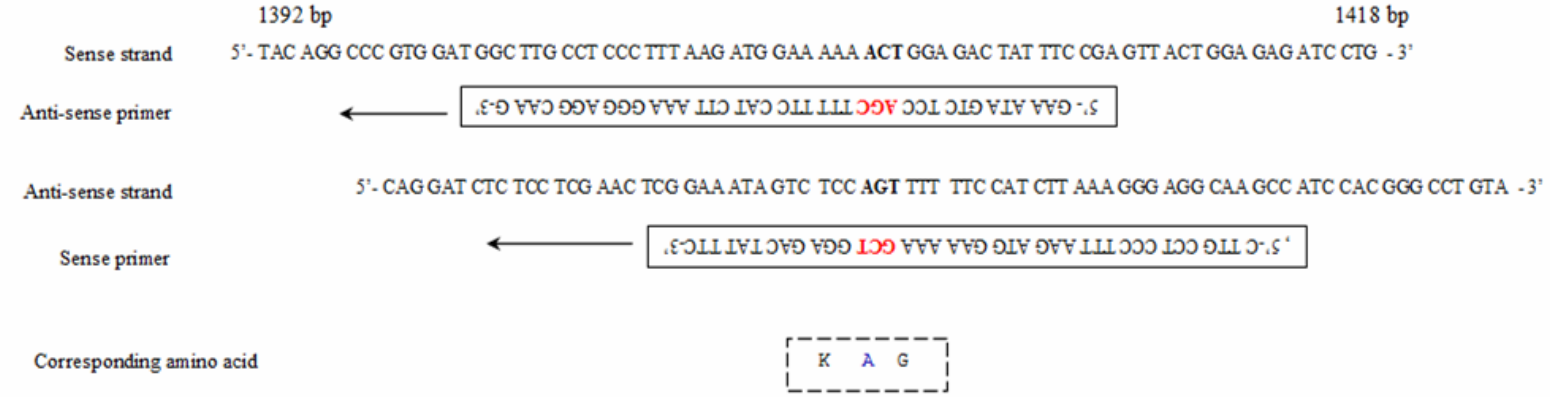

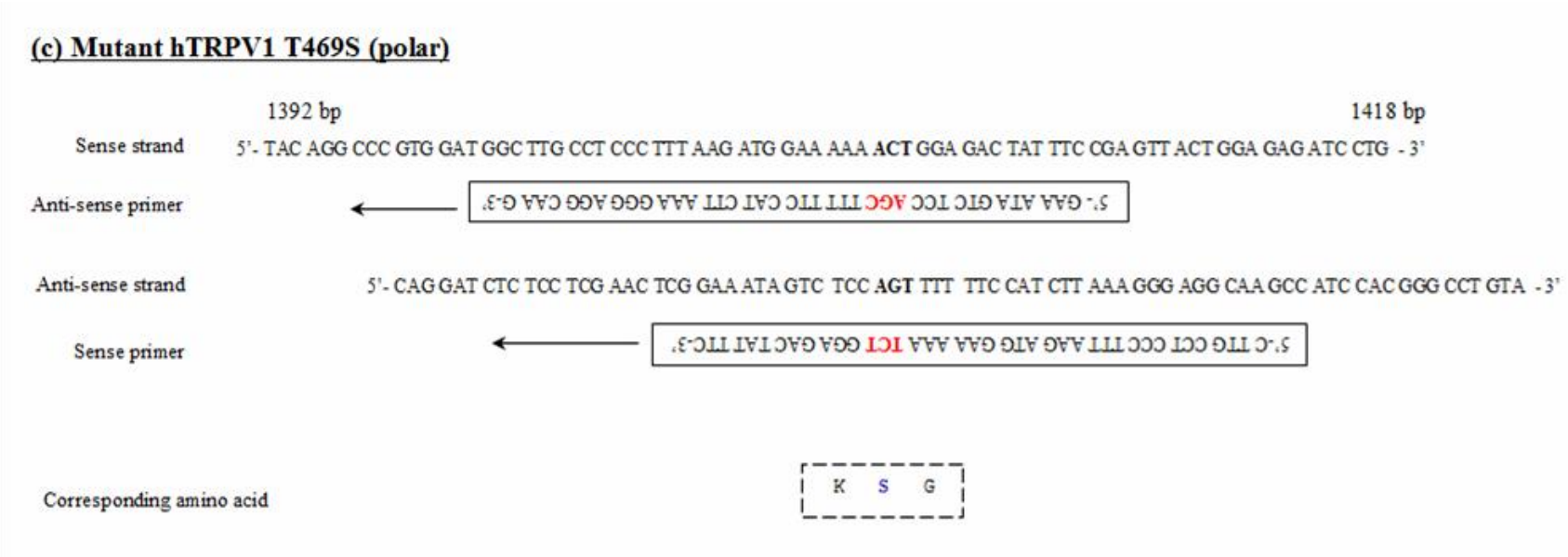

Figure 2.4. Location of mutagenic primers for site-directed mutagenesis of codon 469 on the hTRPV1 gene. (a) Wild-type hTRPV1. Sense and anti-sense cDNA sequences between bases 1392-1418 of the open reading frame of hTRPV1 gene and the corresponding in-frame translated amino acids are shown. Note: the anti-sense sequence is shown upside down, to illustrate how the sequences complement each other. Bases 1406-1408 which correspond to codon 469 are shown in bold. Codon 469 on the hTRPV1 gene, originally a polar threonine amino acid is altered using SDM to: (b) the non-polar amino acid, alanine (T469A); and (c) another polar amino acid, serine, (T469S). Sense and anti-sense strands are shown with the corresponding mutagenic sense and anti-sense primers (mutagenic bases are shown in red) to produce the desired mutant product resulting in a change of amino acid at codon 469 (shown in blue).Arrows indicate direction of amplification during PCR. Note: both primers contained the desired mutation and anneal to the same sequence on opposite strands. Also, the desired mutation on the nucleotide is situated in the middle of the primers with ~10-15 bases of the correct sequence on both sides.

Each mutagenesis reaction contained: QuikChange reaction buffer; QuikSolution; dsDNA template (10 ng); primer pair (125ng); dNTP mix; and *PfuTurbo* DNA polymerase (2.5 U/ul). The reaction mixture was placed in a thermal cycler (Gene Amp PCR System 9700, PE Applied Biosystems) producing mutated plasmid containing staggered nicks. The cycling parameters were as follows: an initial 1 minute incubation at 95°C for 30 seconds prior to the addition of polymerase to hot start the mixture. Then 18 cycles of each of the following steps were performed, namely: 95°C for 30 seconds; 60°C for 1 minute; and 65°C for 8 minutes (the plasmid DNA is ~7.7 kb). Dpn I digestion of the amplification products was then carried out using Dpn I restriction endonuclease (10 U/ul; Strategene, La Jolla, CA) at 37 ^{o}C for 1 hour to digest methylated non-mutated parental dsDNA template. The unmethylated mutated dsDNA was then transformed into XL1-Blue Supercompetent cells (Strategene, La Jolla, CA) by incubating the cells with Dpn I-treated DNA on ice for 30 minutes, and then heat pulsed at 42 ^{o}C for 45 sec. The mixture was further incubated on ice for a further two minutes. XL-1 blue competent cells were purchased pre-treated with calcium chloride, ready for transformation. The heat pulse enables uptake of DNA into competent cells. The length of the heat pulse and the temperature of the water bath are critical in obtaining optimal transformation as efficiency decreases sharply when cells are heat-pulsed for <45 seconds or for >60 seconds. LB broth was added to the reaction and incubated at 37 ^{o}C for 1 hour, with shaking, before plating of 10 µl, 100 µl, and 200 µl of the reaction medium onto agar plates containing ampicillin (100 ug/ml) which were left overnight (>16 hours) at 37 ^{o}C.

In order to increase the chances of identifying, and producing, the correct mutation, a total of 10 colonies from each reaction were picked from a selective plate and placed into 1.5 ml Terrific Broth containing ampicillin. The inoculated cultures were incubated for >12 hours with shaking. To isolate and purify sequencing grade plasmid DNA from bacterial cells QuickLyse Miniprep kit (Quigen) was used, as described by the manufacturer. The kit is optimised to isolated plasmid DNA from 1.5-3 ml of inoculated culture.

All site-directed mutated constructs were confirmed by DNA sequencing using 3.2 pmol/L of the following primers (MWG Biotech, Ebersberg, Germany) 5'-GCA GGA CAA GTG GGA CAG AT-3' (sense), and 5'-GCT GTC CAC AAA CAG GGT CT-3' (antisense; Fig 2.5). The primer set was designed to flank the DNA region of interest (between 1270-1531 bp of the hTRPV1 gene; see Fig), generating ~260 bp of PCR product. Sequencing was performed at the Sequencing Facility of the MRC-CSC Genetics Core Facility (Imperial College, Hammersmith Campus, London, United Kingdom).

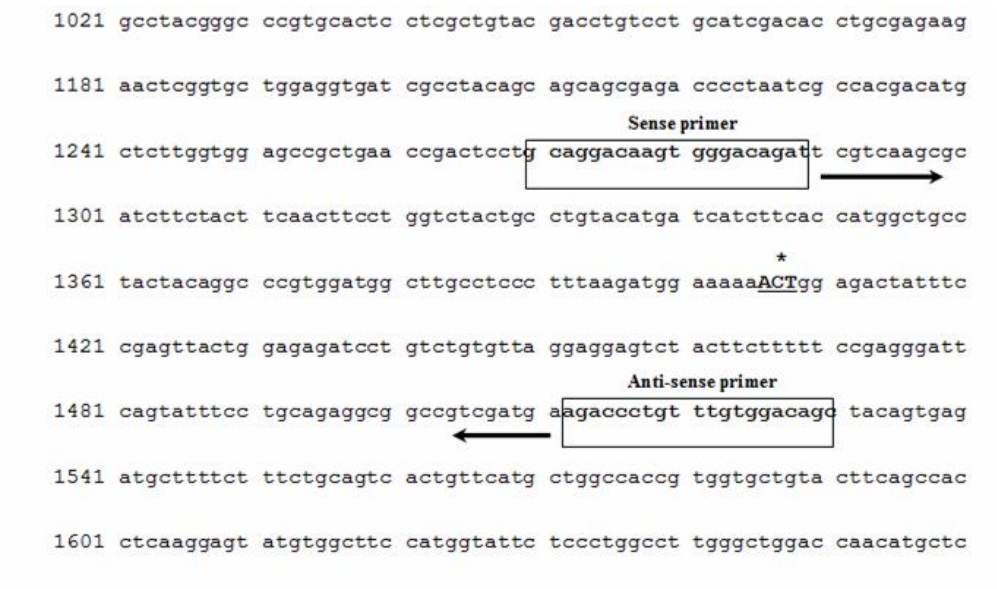

Figure 2.5. Complementary DNA sequence between bases 1021-1660 of the open reading frame of the human TRPV1 and the location of the primer pair flanking the region of site directed mutation. *Nucleotides ACT (bases 1406-1408, shown underlined) correspond to codon 469, which is the desired region of site-directed mutation. The sense primer and anti-sense primer were designed to flank bases 1406-1408. Arrows indicate direction of amplification.

After identifying the culture with the desired mutation, the DNA was re-transformed into DH5alpha competent cells and grown in 200 ml Terrific Broth containing ampicillin, thus allowing relatively large amounts to be obtained which were used for transient transfection. Quigen Plasmid Maxi Kit (Quigen) was used to purify plasmid from bacterial cells. The Maxi kit is able to isolate plasmid DNA from an inoculated culture volume of 100-500 mls. The plasmid DNA was then re-sequenced to confirm that the correct mutation had been achieved (Fig 2.6).

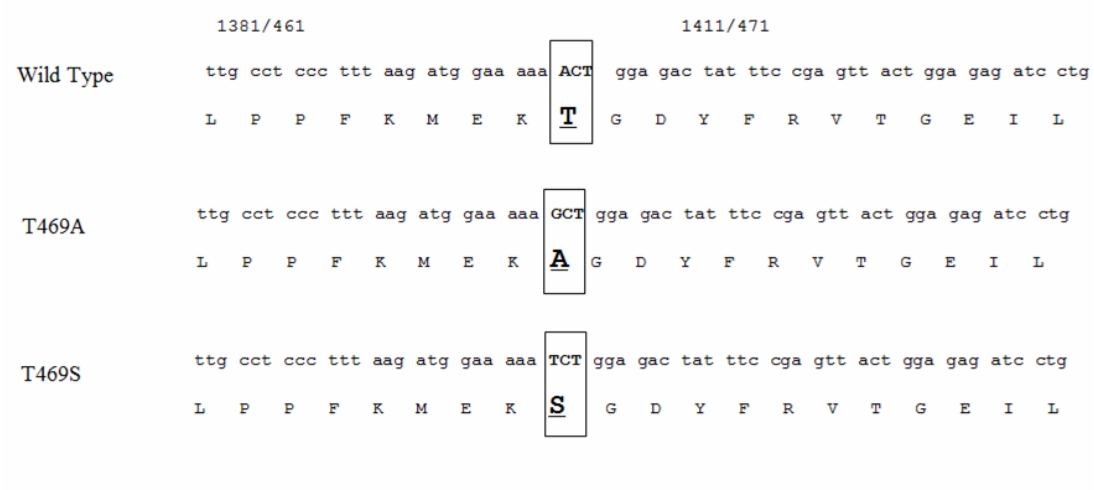

Figure 2.6. Sequencing data of site directed mutation of codon 469 of the human TRPV1 gene. Codon 469 (bases 1406-1408, shown in bold) of the open reading frame encoding the hTRPV1 gene was subjected to site directed mutagenesis. Two mutants were made, changing the wild-type codon encoding threonine, to either alanine (T469A), or serine (T469S). The numbering of nucleotides and codons shown above the wild-type sequence is taken from the open reading frame of the TRPV1 transcript and encompasses bases 1381-1441. The equivalent coding region for each of the two mutants, together with their in-frame translation products, is shown below this. Bases changed by site directed mutagenesis are shown in bold capitals and the resulting amino acid changes are underlined in bold.

Once the haplotypes were made, whole-cell patch-clamp recordings were carried out during applications of various TRPV1 activators to see whether the change in a single amino acid could result in change in agonist-evoked TRPV1-mediated activity.

2.4 Agonist-activated cobalt uptake

2.4.1 Theory of agonist-activated cobalt uptake

The agonist-activated cobalt uptake technique is a method of quantitatively analysing the extent of non-selective cation channel activation in neurons and other cells. The cells are placed in cobalt in solution with expectation, that their extracellular environment includes divalent cobalt cations (Co^{2+}). When the cobalt-permeable cation channels, are opened upon being stimulated by an agonist, these extracellular cobalt ions are drawn by their concentration and electrical gradients within the cell.

Intracellular Co^{2+} ions may be precipitated by exposure to sulphide ions to form cobalt sulphide (CoS) by application of ammonium polysulphide ((NH4)2S) or mercaptoethanol (HSCH2CH2OH) solution. The extent of the resulting intracellular staining offers a measure of the extent to which the ion channels in question have been activated by the agonist, or putative agonist. The intracellular staining can be assessed visually, using a microscope, which is adequate where the technique is employed only to determine whether there has been agonist activation of the channels under investigation. Hence, it can be used as a histology technique in whole cell tissue sections *in vitro* to localise cobalt-permeable ion channels (Anderson and Josephson, 1983; Pruss et al., 1991; Williams et al., 1992; Yin et al., 1994; Nagy et al. 1994; Zhou et al., 1995; Toomim and Millington, 1998; Borbély et al., 2009). However, such visual assessment is inadequate where one seeks to investigate the existence of gradations in staining, i.e., this method can not be used to quantify the level of response in individuals cell (all or nothing approach). Hence, the development of a computer programme which measures on an arbitrary scale the extent to which individual cells absorb light (i.e., are discoloured). While the scale is arbitrary, it is, nevertheless, relative which is all that is required since the enquiry relates to the extent of comparative, rather than absolute, staining by precipitated cobalt ions.

This technique was developed by Hogan then applied by Winter who showed the characterisation of capsaicin-sensitive neurones in the adult rat DRG cultures using cobalt-uptake staining (Hogan, 1983; Winter, 1987). The specificity of TRPV1-mediated cobalt-uptake is well established in DRG neurons (Winter, 1987; Wood et al., 1988; Nagy et al., 1993; Marin-Burgin et al., 2000; Sathianathan et al., 2003; Wach et al., 2003; Singh Tahim et al., 2005). The selective and specific TRPV1 antagonist, capsazepine (Bevan et al., 1992), has also been shown to completely block the number of capsaicin-mediated cobalt labelled cells, which suggest that the cobalt entry into the cells is mediated through TRPV1 (Mahmud et al., 2009; Sathianathan et al., 2003; Singh Tahim et al., 2005). Furthermore, DRG neurons obtained from TRPV1 knockout mice fail to show cobalt labelling in the presence of capsaicin application (unpublished data from our laboratory, see Chapter Four). Cobalt ions that enter DRG neurons do not occur via voltage-gated channels, as potassium-evoked depolarisation in these channels does not result in cobalt influx (Nagy et al., 1993; Reichling et al, 1997).

Subsequently, other cobalt permeable ion channels have also been identified. These include: the N-methyl-D-aspartate (NMDA) channel, some of the alpha-amino-3-hydroxy-5-methyl-4-isoxazolepropionic acid (AMPA) channel; and the non-NMDA kainate receptors of the ionotropic glutamate family (Chung et al., 2005; Malva et al., 2003; Kim et al., 2001; Smeraski et al., 2001; Zhou et al., 1997; Simmons et al., 1994; Pruss et al., 1991). Pruss and co-workers first showed that activation of kainate receptors causes Co^{2+} influx into neurons, type-2 astrocytes, and O-2A progenitor cells. Based on the pattern of responses to kainate, glutamate, and quisqualte, it was possible to discriminate between three functionally different kainate-activated ion channels using this cobalt-uptake technique (Pruss et al., 1991). In the presence of the competitive non-NMDA glutamate receptor antagonist CNQX, the number of cobalt-stained cells was significantly reduced in taste cells (Chung et al., 2005).

The TRPV1 ion channel is potently activated by capsaicin which is typically employed as an agonist to activate this channel. Therefore, the extent of capsaicin activation of these ion channels in the presence, and absence, of various substances

can be assessed using this technique. The standard protocol for cobalt labelling involves rinsing the cells twice for 2 minutes in a buffer without Co^{2+} followed by incubation for 5 minutes of the cells in buffer-containing cobalt, to which there has previously been added, sufficient capsaicin to allow for activation by capsaicin of TRPV1 expressed by the cells. The result is that the capsaicin activates these ion channels expressed in the cells in the presence of extracellular cobalt ions in solution. These cobalt ions thereby gain access to the cells, via the opened TRPV1 ion channel pores, where they discolour the cytoplasm when they are precipitated in the presence of sulphide ions. The cells most discoloured are usually referred to as having been "labelled" as TRPV1-activated cells. The precipitation is achieved after a brief rinsing of the cells in standard buffer followed by 1 minute incubation in ammonium polysulphide or mercaptoethanol solution.

The extent to which TRPV1 ion channels are activated when challenged with different concentrations of capsaicin can be determined by examining the uptake of cobalt by individual cells as evidenced by the discolouration of the cells when seen with by a light microscope attached to a charge coupled device (CCD) camera (Leica) and a PC running the QWin software package (Leitz, Wetzlar, Germany). A CCD camera is designed to convert optical brightness into electrical amplitude signals and then reproduce the image of a subject using the electric signals. Following background subtraction, the area of the cells and their optical density, measured on an arbitrary scale between 0 and 255, are measured in 100-150 randomly systematically chosen neurons on each coverslip. With these settings, greater optical intensity values represent light, labelled cells, while smaller optical intensity values represent dark, non-labelled cells.

Two buffers are necessary for cobalt-uptake. One buffer, named here as ‘Buffer A’ contains (in mM): 57.5 NaCl, 5 KCl, 2 $MgCl_2$, 10 HEPES, 12 glucose, 139 sucrose, buffered to pH 7.4. The second buffer, named here as ‘Buffer B’, consists of the same components as in Buffer A plus 5 mM of CoCl. The main concerns with the use of the cobalt uptake technique arise from the fact that the extracellular solution is not a physiological solution. In particular, it does not

comprise Ca^{2+}; and, moreover, the concentration of sucrose in the buffer creates a hypertonic extracellular solution.

The buffers first composed by Hogan (1983), which excluded Ca^{2+} ions to prevent these ions from competing with Co^{2+} for entry. Of course TRPV1 responses are affected by calcium, as calcium entry into the cell results in desensitisation/ tachyphlaxis (Koplas et al., 1997; Mohapatra et al., 2003). Therefore, in the absence of calcium no desensitisation/ tachyphlaxis occurs, hence during a 5 minute application of capsaicin in the absence of calcium, we assume no reduction of cobalt influx should occur. Furthermore, there is no known data on whether cobalt is able to induce any desensitisation or tachyphlaxis. Previous data show that cobalt used as a track tracer accumulates in the mitochondria (Székely et al., 1983). Similar mitochondria accumulation of cobalt could be observed after using cobalt uptake in neurons (Nagy, unpublished; Tanaka et al., 2004). This may suggest that cobalt may have significant effect of cell function/survival at longer incubation times. However within the five minutes of continuous application of cobalt-buffer to the cells, we assume no adverse effect occurs. In addition, it has been shown that cells activated by capsaicin for the first time in the absence of calcium, produce a larger current than in the presence of calcium (Docherty et al. 1996; Liu & Simon, 1996). This potentiation could not be explained purely to the lack of tachyphlaxis, because it needs time to develop (Schwarz et al., 2000). Therefore, the lack of competition from calcium could also contribute to an increased response. Docherty and co-workers studied the effect of capsaicin-induced Co^{2+} currents in DRG cells using whole-cell patch-clamp recordings. The experimental design consisted of a control I-V curve with Ca^{2+} in the solution, which was then replaced with Co^{2+}. Capsaicin was then applied in the presence of Co^{2+} to produce a test I-V curve. Their data showed that in Co^{2+} solution capsaicin produced an inward current at -90 mV and an outwardly rectifying increase in membrane conductance. When capsaicin was washed out and Co^{2+} was replaced with Ca^{2+}, there was no recovery of the calcium current. Moreover, when Co^{2+} was used to substitute for Ca^{2+} in control experiments and capsaicin was not applied, then the current recovered 70% (Docherty et al., 1991). However, the effect of Ca^{2+} and Co^{2+} in varying ratios to test the effect of Co^{2+}

current was not investigated. Hence, we cannot conclude whether there is any effect on calcium on cobalt entry. Nevertheless, since cobalt uptake here is used to find the proportion of responding cells, a putative increase in the cobalt entry in the absence of calcium, may be of benefit as it is easier to identify responding cells.

It has been found that this (139 mM) amount of sucrose employed is necessary to maintain the cells in the buffer in a healthy condition (Winter, 1987). However, the nature of the extracellular buffer may be such as to activate mechanoreceptors resulting in influx of Co^{2+} *via* these channels. However, when the cells are ultimately visualised under the microscope, there is no evidence of cell lysis – a finding which has been consistently made in all of the experiments performed in this and other laboratory (Lever et al., 2009; Baiou, et al; 2007; Santhianata et al, 2003; Singh et al., 2005; Sathianathan et al., 2003). Moreover, a 45 minute incubation of HEK cells in the Buffer A does not change the proportion of hTRPV1-expressing HEK cells responding to 10 nM-1 uM capsaicin (White et al., 2008). Furthermore, previous findings showed that the diameter of capsaicin-responding cultured DRG neurons measured by cobalt uptake is not different from that of TRPV1-expressing cultured and native DRG neurons (Lever et al., 2009; Baiou, et al; 2007; Santhianata et al, 2003). This suggests that the ionic composition of the cobalt buffers were within the isosmotic (pressure of the fluid is equal to cell) range as the cells did not show shrinkage or swelling.

If the buffers were indeed hypotonic or hypertonic the intracellular pressure may change and therefore might activate mechanoreceptors. While this is a possibility such activation does not affect my results because, when no capsaicin is added to the Buffer A which does not contain Co^{2+}, the proportion of labelled cells is negligible. However a low proportion of cells are seen in controlled experiments when no agonist is applied, (Fig 2.7). This could be due to several factors. First, the labelled cells could represent unhealthy cells with leaking membranes. Second, cobalt in these cells could enter through to TRPV1, due to an increase open probability with unknown reason. Finally, if mechanoreceptors are cobalt permeable these cells could

represent mechano-sensitive cells. However, cobalt staining is abolished in the presence of a capsaicin selective antagonist (Singh et al., 2005; Sathianathan et al., 2003) and no capsaicin-evoked cobalt-labelling occur in DRG cultures obtained from TRPV1-knock out mice (unpublished data, see Chapter Four).

Agonist-activated cobalt-uptake technique is cheap, efficient, and entirely suitable for the limited purpose for which it has been employed in our experiments. This technique is able to study the number, in terms of a percentage of responding cells to stimuli of the ion channel. This method can not be used to quantify the level of response in individual cells. Thus, cobalt-uptake technique is inferior to calcium imaging, where intracellular calcium status of a cell can be analysed in real time. Nevertheless, an advantage of using this technique over calcium imaging when studying cultured cells is that a large field of cells can be examined at once. The technique can also be applied to cells in culture or slices, or to tissue explants, and allows the use of additional pharmacological agents as controls (Lee et al., 1998). Furthermore, cobalt-uptake technique can be combined with immunocytochemistry to provide a powerful tool to study the morphology and distribution of cells expressing receptors with ligand-gated Ca^{2+} channels (Winter et al., 1987; Nagy et al., 1994; Carriedo et al., 1995; Yoshimura et al., 1998; Yoon et al., 1999; Chung et al., 2005; Ikenaga et al., 2006; Huesa et al., 2008).

2.4.2 Practical application of agonist-activated cobalt-uptake

Cobalt-uptake assay was used on hTRPV1.transfected HEK293 cells and DRG cultures to assess functional TRPV1 activity in those cells. Two buffers were, referred to here as *Buffer A* and *Buffer B.* Buffer A contained in mM: NaCl, 57.5; KCl, 5; $MgCl_2$, 2; HEPES, 10; glucose, 12; sucrose, 139; pH 7.4). Buffer B contained Buffer A components plus the addition of 5 mM $CoCl_2$. The standard protocol for cobalt-uptake assay involved rinsing the cells twice for two minutes at 37 ^{o}C in Buffer A, to remove growth medium and extracellular Ca^{2+} ions. The cells where then incubated the cells in cobalt-uptake Buffer B either alone, or in the

presence of a TRPV1 activator, for 5 minutes at 37^{o}C. TRPV1 expressed in the cells were activated upon addition of an agonist, thereby inducing channel opening. Cobalt ions in the buffer entered the cell *via* the open pore. Following one further brief washes for two minutes at 37^{o}C in Buffer A to wash out cobalt from the extracellular fluid, the water-soluble cobalt taken up by the cells was precipitated by 0.4 % mercaptoethanol (Sigma) dissolved in Buffer A for 1 minute (see Fig. 2.7). This resulted in the formation of dark, water-insoluble cobalt-sulphide in the cytoplasm of activated cells. The cells were then fixed in 70% ethanol and mounted on glass slides using glycerol for analysis.

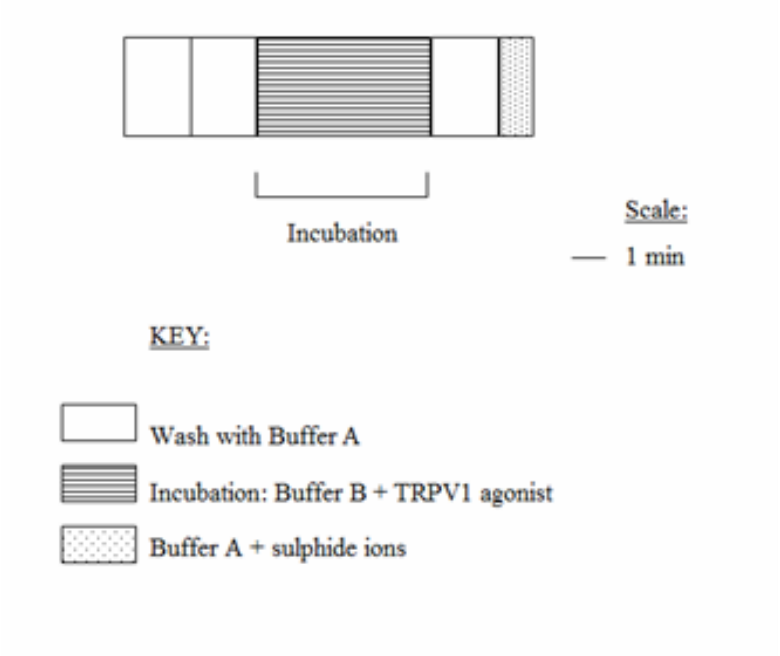

Figure 2.7 General procedure when carrying out cobalt-uptake assay to investigate functional TRPV1 activity in TRPV1-expressing cells.

2.4.2.1 Data analysis of agonist-activated cobalt-uptake

The analysis of cobalt-uptake was performed as described by Singh Tahim and colleagues (2005) using a Leica light microscope attached to a CCD camera (Hamamatsu, Japan) and a PC running the QWin software package (Leica, Wetzlar, Germany). A charge coupled device (CCD) camera is designed to convert optical

brightness into electrical amplitude signals and then reproduce the image of the subject using the electric signals. This analysis is based on measuring the optical density of defined pixels of digitised grey scale images and using a statistical approach to differentiate the sub-population with different optical intensity. Using this approach meant bias and error due to miss recognition of lightly labelled cells as cobalt-responding cells were avoided. Background subtraction must be performed to avoid errors due to differences in the illumination of various parts of the visual field produced by possible misalignment of the optical axis of the microscope. These differences due to misalignment could be as big as 5 arbitrary units on a 0-255 scale. This background subtraction results in an inverted image, with unlabelled cells having a dark appearance while labelled cells having a white appearance. The software package is able to measure the darkness and lightness (shade) of pixels on a 0-255 scale. In order to obtain quality inverted images, the light intensity of the visual field before the background subtraction was set around 200 arbitrary units. The condenser was lowered in order to see unlabelled cells. After the background subtraction, minor adjustments of the illumination were sometimes necessary to obtain a quality picture on the computer screen attached to the microscope. The setting of the illumination and position of the condenser was kept constant for the duration of analysis of each of the culture. Visual fields were randomly and systematically chosen and images were taken. Images were stored on the hard disk and analysed off line. In each coverslip the light intensity of at least 100 cells was measured.

The light intensity data were copied into Origin statistical software programme, where the frequency distribution of the light intensity values was computed. The agonist-activated cobalt-uptake assay was employed on hTRPV1-transfected cells and mouse DRG cultures neurons. Identical analyses were conducted, except cultured DRG neurons light intensity frequency distribution graph were fitted with three Gaussian curves when an agonist was present in cobalt-containing Buffer B, while hTRPV1-transfected cells were only fitted with two curves.

2.4.2.1.1 Data analysis for hTRPV1-transfected HEK293 cells

For each round of hTRPV1-transfected HEK293 cells, the frequency distribution of the optical intensities in the negative control (absence of TRPV1 activators) experiments was generated. The histogram of the HEK293 cells in these negative experiments were symmetrical bell-shaped with one peak, thereby suggesting that these cells have a normal distribution. This distribution could be fitted with one Gaussian curve (r^2>0.95) using the Origin software package (Fig. 2.8C), which confirmed that the distribution was normal. These were *unlabelled cells.* The histogram of the optical intensities of the cells incubated in the presence of a TRPV1 activator (capsaicin, proton or heat, i.e. positive control) showed a distinct bimodal distribution. I found that in the case of HEK293 cell the light intensity of labelled cell could be fitted with two Gaussian curves (Fig. 2.8D).

The cut off optical intensity value which distinguished between labelled and non-labelled cells was determined in experiments. In normally distributed variables the average ± 2 standard deviation of the population covers 95% of the total number of the population. Thus, this establishes the cut-off value between the labelled and unlabelled cells, with a 5% error. (For further detail, see Chapter Two: Statistical Analysis).The mean optical intensity values for cobalt-labelled cells were higher than the mean optical intensity values for unlabelled cells. After determining the percentage of cobalt-labelled cells in each treatment, the mean value for each protocol was calculated from experiments performed on at least 3 independent different cell passages.

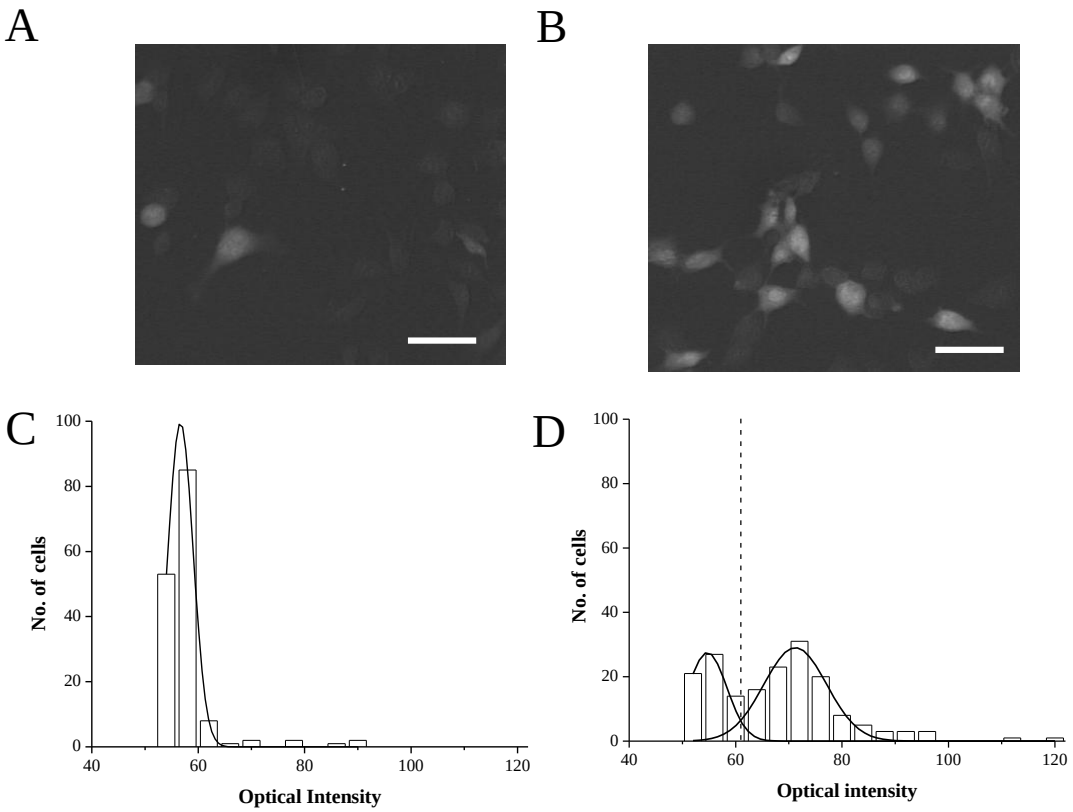

Figure 2.8. Analysis of cobalt-uptake assay on hTRPV1-transfected HEK293 cells. (A) Inverse image of cells incubated in the presence of $CoCl_2$ alone shows very few labelled cells. (B) Inverse image of cells incubated in the presence of 500 nM capsaicin and $CoCl_2$ shows cobalt-labelling in a large number of cells. (C) An example of the distribution of optical intensities on $hTRPV1_{111}$-transfected cells incubated with only $CoCl_2$ buffer. The graph is fitted with one Gaussian curve indicating the presence of only one population of cells with a normal distribution of optical intensities (r^2>0.95). (D) The distribution of optical intensities incubated in $CoCl_2$ buffer and 500 nM capsaicin. The frequency distribution of optical intensities is fitted with two Gaussian curves indicating the presence of 2 populations with a normal distribution of optical intensities (r^2>0.95). The dash line on (D) represents the cut-off optical intensity which discriminates between labelled and non-labelled cells. Scale bars represent 50 µm in figure (A) and (B).

2.4.2.1.2 Data analysis for mouse DRG culture

In each mouse DRG culture, the frequency distribution of the optical intensities in the negative control experiments (absence of TRPV1 activators) were created and fitted with two Gaussian curves, indicating the presence of two sub-populations of cells (Fig. 2.9A and B). The reason for the presence of these sub-populations regarding the optical intensity of the neurons is not clear. Histological staining of DRG cells differentiates light large and dark small cells in DRG sections (Lieberman 1976; Winter, 1987; Kitao et al., 1996). However, analysis of the cell size in the unlabelled subpopulation did not reveal a correlation between cell size and optical intensity (Sathianathan et al., 2003).

The distribution of the optical intensities of the positive control (capsaicin) could be fitted with three Gaussian curves, where the third population represented the cobalt-labelled cells (Fig. 2.9C and D). The mean optical intensity values for cells in the third subpopulation were higher than those for the two other subpopulations in both experiments and represented labelled cells. The cut-off optical intensity value which distinguished between labelled and unlabelled cells was determined on the positive control as the lower range of a 95% confidence interval for the third Gaussian curve (labelled cells). This value was employed in all coverslips from the respective cultures. The percentage of cobalt-labelled cells for each protocol was calculated from experiments performed on at least three different rodents.

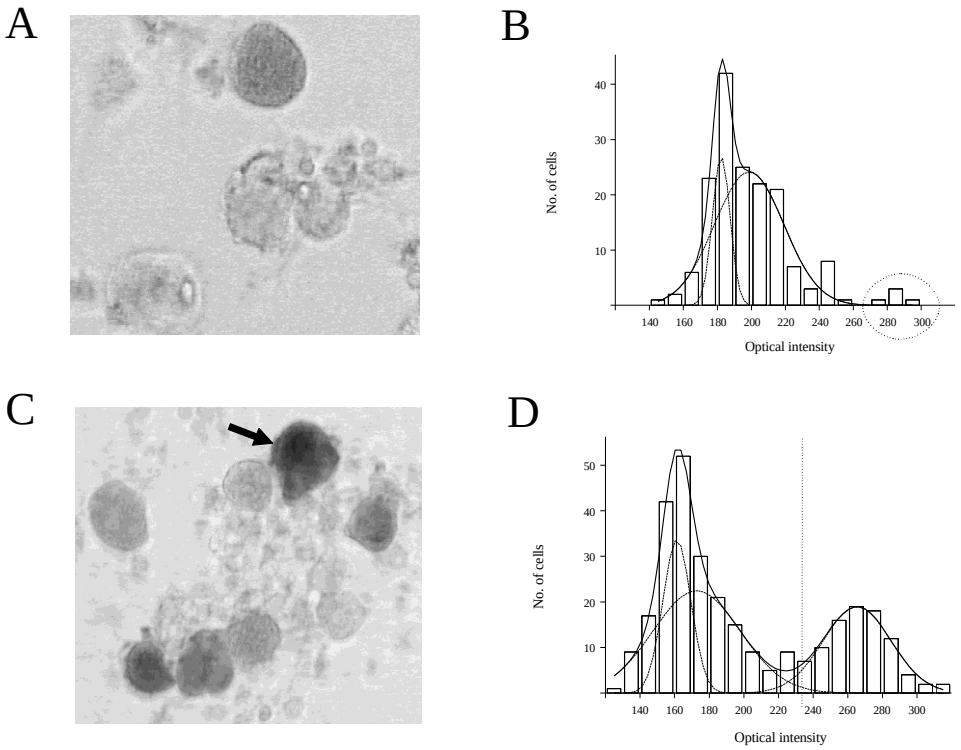

Figure 2.9 Analysis of cobalt-uptake assay on mouse DRG cells. (A) Incubation of cells in the presence of 5 mM $CoCl_2$ results in none or very few labelled cells. (B) The distribution of optical intensities of neurons incubated in the presence of 5 mM $CoCl_2$ shows the presence of two, largely overlapping, sub-populations of neurons, with only very few labelled cells (circled). (C) Image of neurons incubated with the addition of 500 nM capsaicin to the 5 mM $CoCl_2$-containing buffer results in dark cobalt-labelling in a proportion of cells. The arrow indicates a labelled cell. (D) The distribution of the optical intensities of cells incubated in the presence of 500 nM capsaicin and 5 mM $CoCl_2$ shows the presence of three populations; two, largely overlapping sub-populations, and a third, separate sub-population representing labelled cells. Dashed line on (D) indicates the cut-off optical intensity that differentiates between labelled and non-labelled neurons.

2.5 Whole-cell patch-clamp recordings

2.5.1 Introduction to whole-cell patch-clamp recording

Whole-cell patch-clamp recording is a technique which is routinely used by electrophysiologists to study the properties of ion channels in living cells. The patch clamping technique is a derived technique from the voltage-clamp configuration. During voltage-clamp recordings, currents necessary to maintain a defined membrane potential is measured. This current, if there are no leakage currents, is equal to the currents flowing through ion-permeable membrane pores. Since the membrane is maintained, this current is directly proportional to the membrane conductance of the channel. Gating of ion channels, whether through voltage- or ligand-dependence, results in changes in the membrane conductance.

The voltage-clamp technique was introduced initially by Cole in the late 1930's and was further developed by Hodgkin & Huxley (1952). They first described a two-electrode voltage-clamp set-up to study the ionic conductances of the giant squid axon. For this, one electrode functioned as a voltage sensor to record the transmembrane, whilst the second electrode served as a current source to pass current to the cell. Sharp electrodes (open tip diameter of 0.2-0.5 µm) are inserted into a cell and are connected through a feedback amplifier whereby any change in the membrane potential detected by the voltage electrode result in a current injection by the current electrode to maintain the voltage at a constant level (Fig. 2.10). In response the circuit produces a current injection equal and opposite to the ionic current. This can be measured. It is assumed that the current flow through the current electrode is the exclusive flow across the membrane.

A major disadvantage of this set-up is the requirement that two electrodes be placed within a cell, which often result in leakage of the intracellular fluid and a large electrical conductance across the plasma membrane. Furthermore, its application is limited to large cells of > 20 µm and to the study of cells embedded in tissue; therefore this technique is unfeasible (Sontheimer and Ransom, 2002).

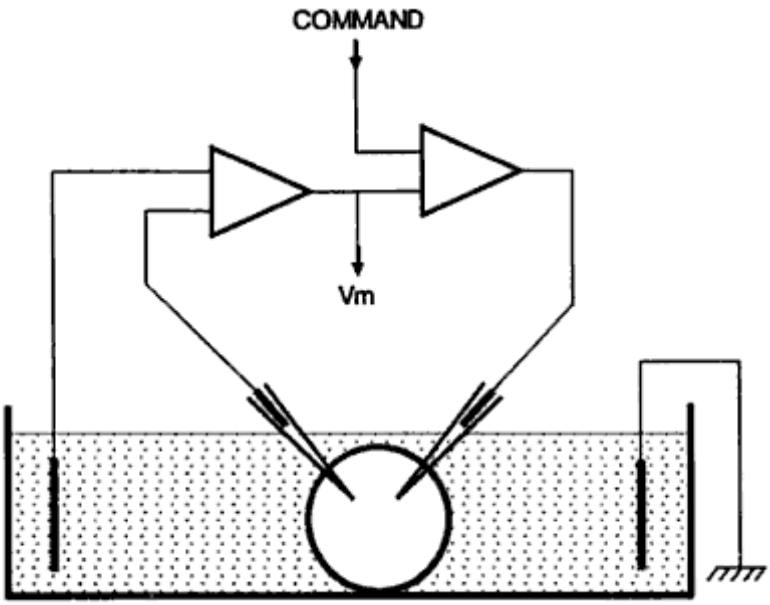

Figure 2.10 The main components of a two-electrode voltage-clamp set-up. The output of the left amplifier is the difference in potential between the bath and the cell electrodes (Taken from Stuhmer, 1997).

A single-electrode voltage-clamp was developed in an attempt to solve this problem. This allows the use of one sharp electrode to serve as the current and voltage electrode, in an alternating manner. However, this set-up is limited by time its time resolution as a result of the switching between the two modes (Sontheimer and Ransom, 2002).

The patch-clamp technique also uses one electrode to continuously measure the membrane potential and inject current to clamp the voltage at a constant level (Fig 2.11: Hamill et al., 1981; Neher and Sakmann, 1976). To measure small membrane currents using this technique requires a low-noise recording set-up. This is achieved by tightly sealing a glass electrode, referred to as patch electrode, on to the plasma membrane of an intact cell. Patch electrodes have relatively blunt but smooth ends (open tip diameter of 1-2 μm). The tip of the electrode is pressed against a plasma membrane and suction is applied to pull the membrane inside the tip of the electrode. The suction results in a tight seal between the patch electrode and the plasma membrane. These tight seals have an electrical resistance in the range of giga-ohms (10^9 ohms), and are referred to as either a *gigaseal* or a *gigaohmseal*.

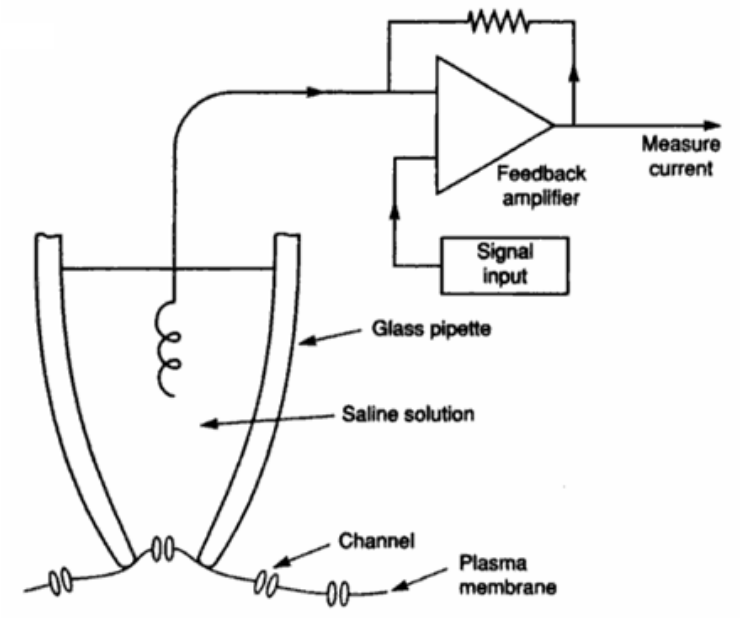

Figure 2.11 Diagram of the main components of a patch-clamp configuration using one electrode. The patch electrode is filled with saline (intracellular) solution and inserted over silver-chloride coated silver wire. The patch electrode forms a gigaseal with the plasma membrane of the cell, which not only prevents leak currents flowing between the patch electrode and the reference ground electrode, but also inhibits flooding of the cell with the bath solution. This configuration is referred to as cell-attached patch, where a single ion channel's membrane current can be recorded. The *signal input* refers to the ground electrode which is placed in the superfusing extracellular solution. The ground electrode is made from silver-chloride coated silver wire. Both the patch and ground electrode are connected to a feedback amplifier, which allow the small signal from the cell to be detected. The patch-clamp output of the amplifier is the difference in potential between the patch and the bath electrodes. (Taken from Aidley and Stanfield, 1996).

Ag/AgCl electrode

It is important to note that the patch electrode is not an electrode, per se. The electrode is a solid electric conductor, typically made from a silver-chloride coated silver (Ag/AgCl) wire, referred to as Ag/AgCl electrode. The patch electrode filled with intracellular solution covers the wire. The Ag/AgCl electrode enables electrical current to leave and enter the set-up (Fig 2.12).

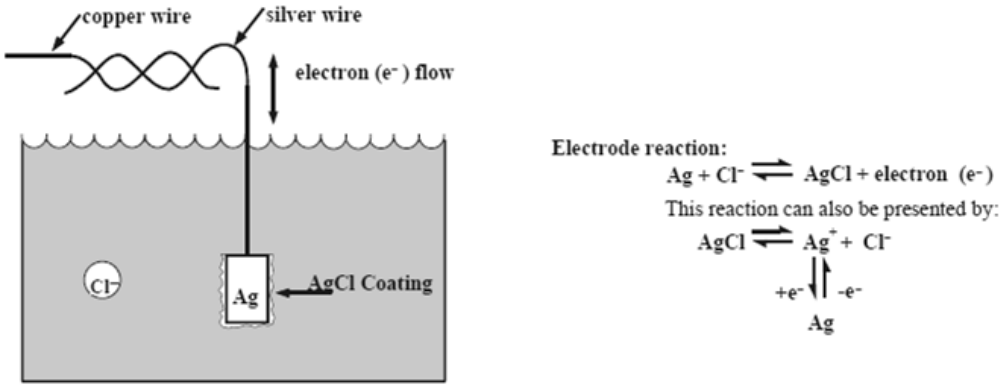

Figure 2.12 The Ag/AgCl electrode. Currents are able to flow in both direction of the electrode. (Taken from Axon Guide, 2008).

Due to the robust nature of a gigaseal, different configurations of the plasma membrane in relation to the patch electrode are achievable. These include: (i) cell-attached; (ii) inside-out; (iii) whole-cell patch-clamp; and (iv) outside-out configuration (Fig 2.13).

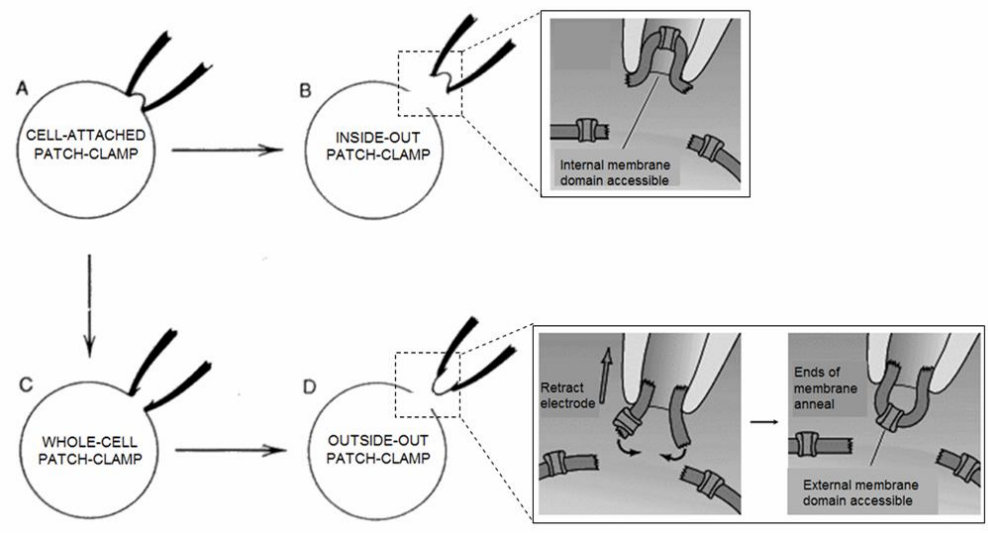

Figure 2.13 Four configurations of patch-clamp technique. (A) Cell-attached is a result of a tight seal between the patch electrode and the plasma membrane. (B) Inside-out patch is achieved by retracting the patch electrode in cell-attached mode, which causes a small piece of the membrane to remain attached to the electrode. The internal membrane surface is exposed to the extracellular bath solution, whilst the external membrane surface faces the intracellular pipette solution. This configuration is useful when studying channels that are activated by intracellular ligands. (C) Whole-cell patch configuration is obtained if the membrane patch within the patch electrode is ruptured in cell-attached mode by a brief suction (by mouth or with a syringe). This results in the interior solution of the patch electrode becoming continuous with the cytoplasm of the cell. (D) Outside-out patch is achieved by retracting the patch electrode in whole-cell mode. This causes a small piece of the membrane to remain attached to the electrode. The patch of membrane will be oriented with the internal membrane surface exposed to the intracellular pipette solution, the external membrane surface is submerged with extracellular bath solution. This set-up allows the study of ion channels isolated from the cell, which is particularly useful when investigating channel activity influenced by extracellular chemical signals. Taken and adapted from Fulton, 2000 and Purves et al., 2000.

Cell-attached patch-clamp configuration enables recordings of membrane currents flowing through a single ion channel, known as *single-channel recording*. Access to the cytoplasm of the cell is obtained as the membrane within the patch selected is perforated. This configuration allows the measurement of membrane currents from the entire cell and therefore is referred to as *whole-cell patch-clamp recording*. In my experiments whole-cell patch -clamp was used.

2.5.2 Biophysics of whole-cell patch-clamp technique

In order to understand the basis of whole-cell clamped membrane currents and data obtained by the whole-cell patch-clamp technique one must first understand the electrical properties of excitable cells and some principles of electricity. The electrical properties of an excitable cell are derived primarily from (i) the ion channels in the plasma membrane; (ii) the lipid bilayer of the plasma membrane; and (iii) the ionic composition of the intracellular and extracellular solution on either side of the plasma membrane.

2.5.2.1 Ion channels

Ion channels are large membrane proteins, with several subunits which contain amino acid chains that move back and forth across the membrane. Ion channels form transient pores which connect the interior and exterior side of the lipid membrane. The transient pore forming property of ion channels permit transit of ions across the plasma membrane according to theconcentration and electrochemical gradient. In many channels part of this protein forms a molecular *gate* that opens and closes the channel in response to stimuli. Hence these channels are referred to as *gated* channels. There are hundreds of different ion channels and they are distinguished on the basis of their sequence similarity, ion selectivity (Na^+ selective, K^+ selective, Ca^{2+} selective, Cl^- selective and non-selective), and gating mechanism. Ion channels

maybe gated by one or more, of the following, namely: voltage, ligand, pH, mechanical pressure, or temperature.

Since ion channels form transient pores which allow ions to cross the membrane when opened they can be regarded as conductors. Their conductance changes from 0 (in closed state) to a characteristic value (in open state). Conductors allow free movement of charged particles and therefore allow flow of ion currents. Charged particles, such as electrons, are moved along a conductor by the potential difference existing between the two ends of the conductor. The potential difference is created by the separation of the positive and negative charges.

The relationship between the current of the charged particles, the potential difference and the ability of the conductors to allow the current to flow is described by *Ohm's law* (Fig 2.14).

$$V = I \times R$$

where *I* is the electric current (the flow of electric charge measured in amperes); *V* is the voltage or the potential difference (the difference of electrical potential between two points of an electrical circuit measured in volts) and *R* is the resistance of the conductor (the property which restricts the flow of electric current measured in ohms).

Hence, R is inversely proportional to conductance *G* (the ease of flow of current between two points along an electrical circuit, measured in siemens).

Thus:

$$G = 1/R = I/V$$

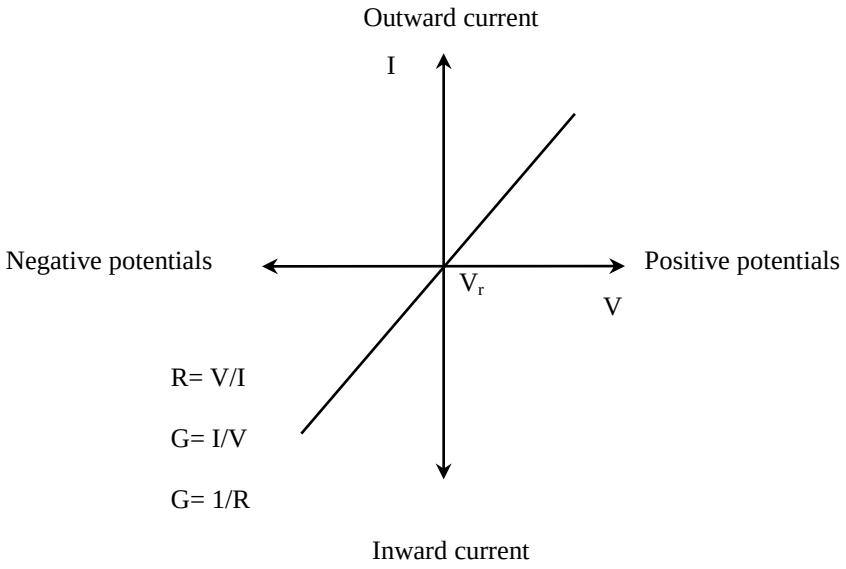

Figure 2.14 Ohm's law. Ohm's law states that there is a linear relationship between current *I* and voltage *V*. This law also specifies that the conductance *G* is constant. Hence the slope of the line yields the conductance. Conductance is the reciprocal of resistance *R*. When currents are measured across a membrane, by convention: an outward current is the flow of positive ions from the inside of the cell to the outside; and an inward current is the flow of positive ions from the outside of the cell to the inside. The reversal potential V_r is the membrane potential where there is no net current, the outward and inward are the same (Adapted from Golan et al., 2007).

As already mentioned ion channels can be regarded as conductors/ resistors and their resistance/conductance alters between two values. Ion channels are either (a) in a zero conductance and indefinite resistance state, called the 'closed state', or (b) in a maximal conductance and minimal resistance state, called the 'open state' (Fig 2.15). The probability of being in an open or close state is described by the open probability P_o. The P_o is 0 if the channel is in a closed state at all times and P_o is 1 if the channel is in open state at all times.

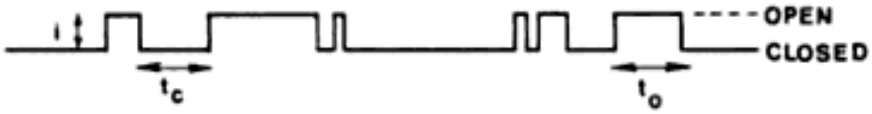

Figure 2.15 Schematic diagram of an idealised single channel recording. A channel opens and closes in a stochastic (random) manner. Each opening of the channel results in a current influx of the same amplitude. When the channel goes from a closed to an open state, a step change in the current indicates a single channel current (i). Taken from Levitan and Kaczmarek, 1986.

Furthermore, in whole-cell recording, when all the ion channels on a plasma membrane are activated or opened, the whole-cell total conductance G_{total} is the product of the number of ion channels N, and the single-channel conductance g, (see Fig 2.16).

$$G_{total} = N\,g$$

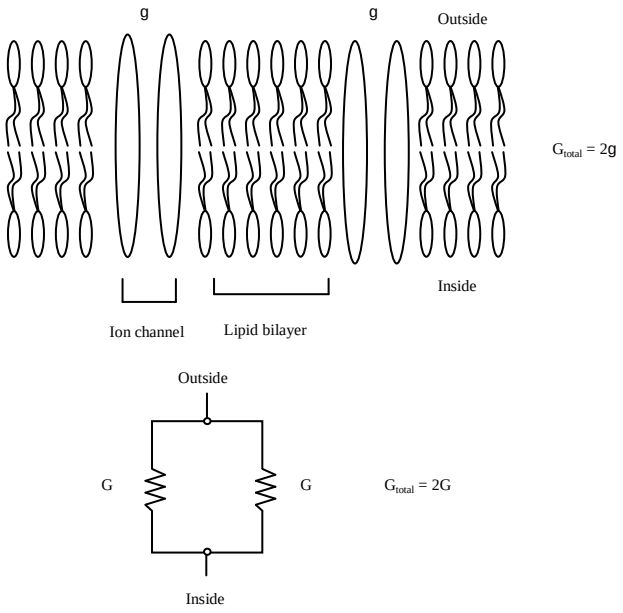

Figure 2.16 Ion channels as a parallel circuit. Ion channels on a membrane may act as parallel conductors hence the total conductance G_{total} of a cell can be calculated by adding all the single ion channel conductances g (Adapted from Axon guide, 2008).

A single-channel conductance is a measure of the current that flows through an open channel in response to a given electrochemical driving force. The electrochemical driving force, ΔV, is the electrical and chemical driving force that moves ions. The electrical driving force depends on the electrical potential difference across the membrane. The chemical driving force depends on the concentration gradients of specific ions across the membrane. The electrochemical driving force is defined as the difference between reversal potential V_r and the membrane potential V_m.

$$\Delta V = V_m - V_r$$

As ion channels open and close, the conductance changes and so does the current. The current that flows through all the open channels can further be defined as:

$$I = N\, g\, (E_m - V_r)$$

Therefore, the whole-cell current is proportional to the number of open channels at any given time and each open channel can be considered as an increase in conductance.

The plasma membrane expresses thousands of channels of the same type. While the open probability during activation is similar, their opening and closing is not synchronised. As a result, the whole-cell conductance or resistance produced by the activity of the same type of ion channel cannot be described by a two state model, i.e. open and close state.

$$I = pN\, g\, (E_m - V_r)$$

Since p is the open probability which follows Boltzmann distribution, the whole cell conductance must follow it.

The Boltzmann distribution function is defined as:

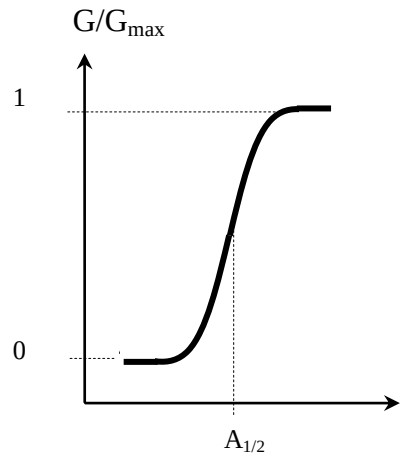

$$g = \frac{G_{max} - G_{min}}{1 + \exp((A_{1/2} - A)/\text{slope})} + G_{min}$$

where *G* is the whole-cell conductance which can be defined between two values: (i) the minimum value which is the result of P=0; and (ii) the maximum value which is the result of P=1. G_{max} is the maximum conductance with a minimal resistance; G_{min} is the minimum conductance with an indefinite resistance; and $A_{1/2}$ is the strength of activator which produces half maximal conductance which is in between $G_{min\ and}$ G_{max}; V_m is the membrane potential; and slope is the steepness of the curve.

2.5.2.2 Lipid bilayer

Ion channels are situated in the lipid bilayer. The lipid bilayer of the plasma membrane is not permeable to ions. Hence, it is a poor conductor of ionic current. The lipid bilayer behaves like an insulator which strongly resists the flow of ionic current.

2.5.2.2.1 Compensating the capacitive transients

It should be taken into account that during whole-cell patch-clamp recordings, whilst the cell is at rest, the electrical properties of the cell do not change with time. As long as the membrane potential remains constant, the lipid bilayer's capacitance is negligible. If the voltage changes as a result of ion channel opening, steady-state

currents in addition to transient capacitive currents, pass through the open channels. These capacitive currents must there for be compensated.

A capacitor is an electrical device able to store charge. Capacitance is a measure of a capacitor's ability to store charge in an electrical field. The amount of charge (measured in coulombs, symbol Q) stored by a capacitor is given by:

$$Q \text{ (coulombs)} = C \text{ (farads)} \times V \text{ (volts)}$$

The presence of capacitance at the amplifier input originates from several sources. These include: (i) the capacitance across the glass wall of the electrode immersed in solution; (ii) the stray capacitance from the rest of the electrode to nearby grounded surfaces; (iii) the stray capacitance from the electrode holder; and (iv) the capacitance to the ground at the input of the buffer (Axon Guide, 2008). The capacitance from these sources needs to be compensated for because otherwise the recording bandwidth is reduced. The bandwidth describes the difference between the highest and lowest frequency of the recording. The difference between the bandwidth and the frequency is referred to as the frequency of sampling. Reduced bandwidth therefore reduces the frequency of sampling, making it difficult to measure rapid currents during voltage steps or ramp protocols. Typically, during whole-cell recordings the capacitive current was compensated between 70 and 90 %.

2.5.2.3 Ionic distribution

An electrical potential difference ('membrane potential') exists between the interior and exterior of the plasma membrane, as no single ion species is distributed equally on both sides of the membrane of the cell. At rest, an excitable cell has an electrical charge as the outside of the membrane is positively charged, whilst the inside of the membrane is negatively charged. This is because the outside of the cell contains an excess of Na^+ and the inside of the cell contains excess of K^+ and A^-

(organic anions). Large organic anions are negatively charged proteins and nucleic acid molecules which inhabit the cell but are unable to permeate the cell membrane; hence the inside of the cell is more negative when compared to the outside. This separation of charges is maintained because of the properties of lipid bilayer of the membrane which prevents the diffusion of ions across the membrane and carrier molecules. Carrier molecules are essential, as without them the membrane potential would not be maintained.

The resting membrane potential describes a steady-state condition where there is no net flow of electrical currents across the membrane. The resting membrane potential is determined by the intracellular and extracellular concentration of ions to which the membrane is permeable and is also affected by the osmotic pressure and electrostatic forces.

The voltage/electrical potential of a cell membrane required to oppose the flow of any given ion X is called the equilibrium potential (E_X) and maybe calculated by the Nernst equation which is as follows:

$$E_X = {}^{RT}/_{zF} \ \mathrm{In} \ {}^{[X]o}/_{[X]i}$$

where *R* is the gas constant (8.3143 J/mol/K), *T* is the temperature in Kelvin, *z* is the valence of the ion, *F* is the Faraday constant (9.65 x 104 coulombs per mol) and $[X]_o$ and $[X]_i$ are the concentrations of ions outside and inside the cell.

The Nernst equation is applicable in situations where only one ionic species flows across the plasma membrane. However, many cells contain several different ion-selective channels all of which contribute to the overall resting membrane potential. The resting or equilibrium potential is influenced by each species of ions. The movement of each species of ions is governed by its concentration on the inside and outside of the cell and by the permeability of the membrane to that ion type. The

Goldman-Hodgkin-Katz equation describes this relationship between ion species and the cell membrane. The equation below refers only to monovalent ions

$$E_{rp} = {}^{RT}/_{F} \ln \frac{P_K [K^+]_o + P_{Na} [Na^+]_o + P_{Cl} [Cl^-]_i}{P_K [K^+]_i + P_{Na} [Na^+]_i + P_{Cl} [Cl^-]_o}$$

where E_{rp} is the resting membrane potential, R is the gas constant, T is the temperature in Kelvin, z is the valence of the ion, F is the Faraday constant, P_X is the membrane permeability of ion X, $[X]_o$ and $[X]_i$ are the concentrations of the ion outside and inside of the cell. This equation generally states that the higher the concentration of a specific ion type, the greater its membrane permeability, the greater its role in determining the membrane potential. Thus, when an ion-selective channel opens the membrane potential is driven toward the Nernst potential for that specific ion.

In practice, during electrophysiology recordings the ionic compositions of the intracellular and extracellular solution *in vitro* in which the cells are placed are controlled. The ionic compositions of *my normal* electrophysiology solutions used in this study were the following: extracellular solution consisted of (mM): NaCl, 130; KCl, 5; $CaCl_2$, 2; $MgCl_2$, 2, adjusted to pH 7.4. Intracellular solution consisted of (mM): NaCl, 5; KCl, 130; $MgCl_2$, 1.26. Using the Goldman-Hodgkin-Katz equation, the resting membrane potential for HEK293 cells maintained in these solutions was ~-60 mV.

In whole-cell voltage clamp experiments, the membrane potential of the cell was clamped or held at a pre-determined level. In these experiments the V_m was held at –60 mV and the transmembrane current required to maintaining this voltage was measured.

Due to the electrical properties of the plasma membrane of the cell, the plasma membrane can be modelled in terms of an electrical circuit containing resistors and capacitors, as shown in Fig 2.17.

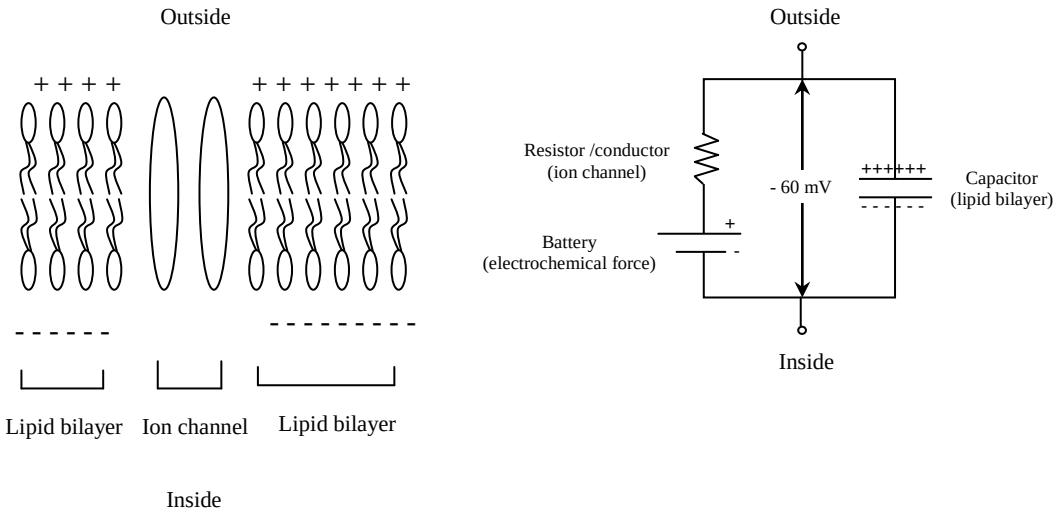

Figure 2.17 A single membrane ion channel as circuit. The cell membrane can be modelled as an electric circuit containing a resistor and a capacitor. Ion channels function as resistor (identical to conductors), through which ions flow down their electrochemical gradient. This RC (resistor-capacitor) circuit changes the timing between the flow of current and changes the voltage because of the lipid bilayer which acts as a capacitor as it stores some of the charge that passes across the membrane (Adapted from Axon guide, 2008).

2.5.2.3.1 Compensating for series resistance

Another issue that should be noted when using the whole-cell patch-clamp technique is the series-resistance of the configuration. That is, only one patch electrode is used for both voltage recording and current passing.

Series- resistance is the sum total of the resistance of the resistors in a series in an electrical circuit. The total resistance (R_{total}) of a series circuit where the electric current flows through a single path can be defined as the sum of each individual resistance (R) of each component in the circuit:

$$R_{total} = R_1 + R_2 + R_3 \ldots\ldots + Rn$$

In an ideal configuration, the resistance of the patch electrode in whole-cell recordings will equal 0 ohm. However, due to time resolution for measuring current and altering the membrane potential, to maintain resting holding potential is limited to the speed of the electronics in the configuration. Series-resistance compensation reduces the patch-clamp error due to the voltage drop across the resistance of the electrode, thus reducing the effect of the pipette resistance. However, compensation is never perfect due to practical applications (Axon Guide, 2008). Typically, during whole-cell recordings the series resistance was compensated between 70 and 90 %.

2.5.3 Practical components of whole-cell patch-clamp recordings

Briefly, TRPV1-mediated currents were measured using the conventional whole-cell patch-clamp technique with an Axopatch 200 B amplifier (Axon Intruments, Inc. Fig 2.18) and the pClampex 8 software package with a laboratory PC for storing and evaluating data. All experiments were performed at physiological temperature of 36-37 ^{o}C using a temperature controller (Wavelength Electronics). The membrane potential was held at - 60 mV. Data was collected using the pClampex 8 software package and analysed using the Clampfit data analysis programme (Axon Instruments Ltd). If the membrane current following the establishment of whole-cell configuration was more than -0.5 nA the cell was discarded.

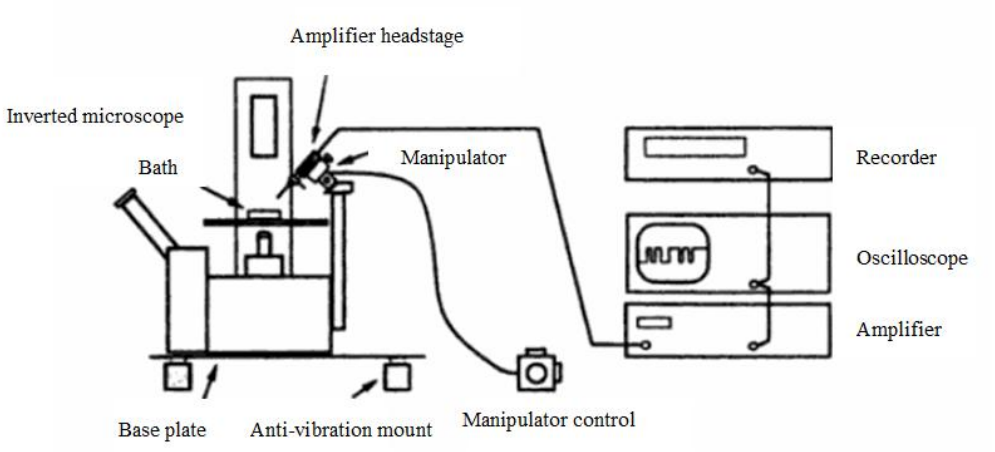

Figure 2.18 The main components of a patch-clamp set-up. The patch electrode is attached to the amplifier headstage. (Aidley and Stanfield, 1996)

2.5.3.1 Solutions

The normal extracellular buffer for patch clamp consisted of (mM): NaCl, 130; KCl, 5; $CaCl_2$, 2; $MgCl_2$, 2; glucose, 10; HEPES, 10; adjusted to pH 7.4.

Patch electrodes were filled with normal intracellular buffer for patch clamp which consisted of (mM): NaCl, 5; KCl, 130; $MgCl_2$, 1.26; HEPES, 10; adjusted to pH 7.4.

2.5.3.2 Patch Electrodes

Patch electrodes were pulled from borosilicate glass capillaries (1.5 mm outer diameter and 0.86 mm inner diameter: Harvard Apparatus Ltd, Kent, UK) by a two stage-puller using a DMZ-Universal 2-Stage Puller (DMZ, München, Germany; see Fig 2.19). For whole-cell patch-clamp recordings, the patch electrodes were pulled to have relatively blunt ends (1-2 µm: see figure e) with low-resistance of 4-6 Mohm in order to achieve and maintain mechanically stable electrode-membrane gigaseal (Sontheimer and Ransom, 2002).

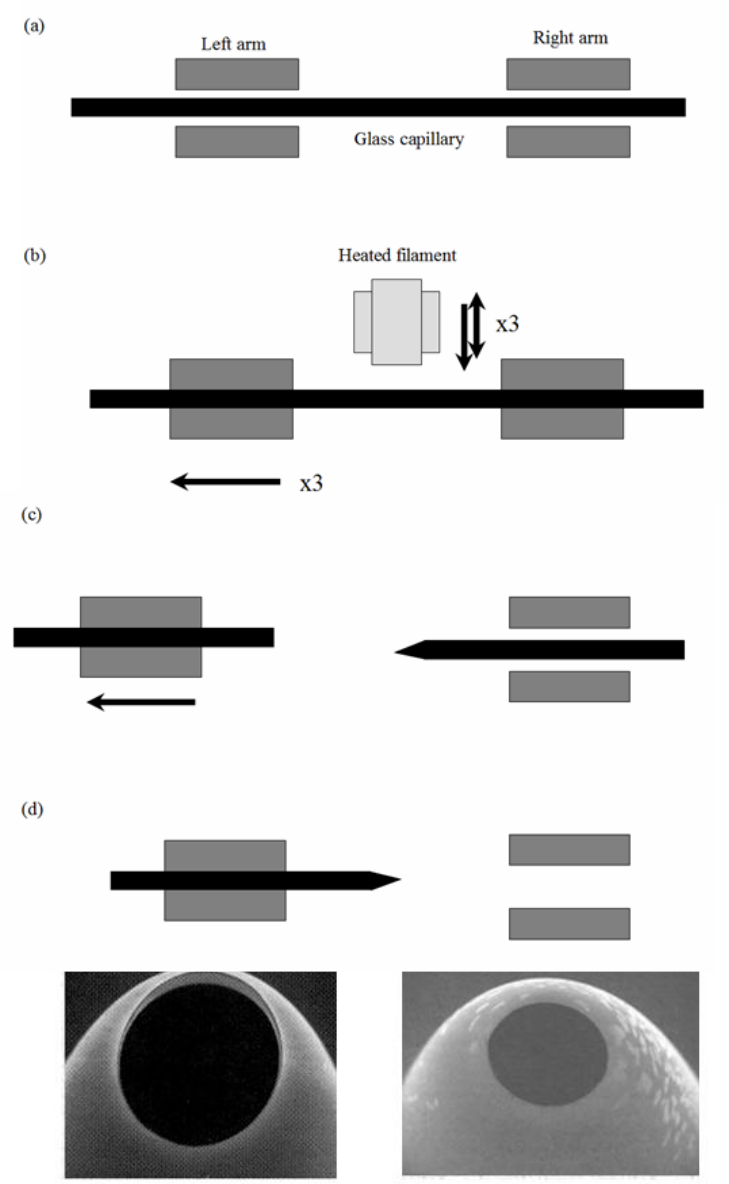

Figure 2.19 Schematic diagram of the fabrication of patch electrodes using a two-stage vertical puller. (a) A glass capillary is placed between the two clamps on the puller, so that it is roughly in the middle. (b) The pre-programmed automatic system is initiated. The right and left clamp closes, clamping the capillary into place. The puller pulls the capillary apart, as the heated metal filament starts to melt the glass. A two-stage puller mechanism is used. The first pull softens the glass and pulls it a short distance to thin the capillary, after which the second pull breaks the capillary, thus producing two patch electrodes (c) and (d) (Penner, 1995). Before each of the electrodes were removed from the puller and placed into a electrode holder, a final heat polishing step is used to smooth the edges of the tip. (e) An unpolished 27 µm giant patch electrode. (f) A polished patch electrode with smaller tip end. (Taken from www.dagan.com/puller.htm).

Prior to use, each electrode was filled, with standard intracellular buffer using a syringe and a fine needle (diameter less than 0.86 mm), making sure that no air bubbles were present. If air bubbles remain at the tip, the electrode resistance will be extremely high. The electrode was then inserted over the silver-chloride coated silver wire, into the electrode holder of the Axon headstage (Axon Instruments), making sure the wire is in contact with the solution inside electrode. The electrode was tightly screwed to fix into position, forming an air-tight seal. The electrode holder is attached to a tube connected to a syringe which is used as a suction line to aid in forming a gigaseal. The headstage sends the signal recorded by the electrode to the amplifier. The headstage unit is attached to 3D moveable platform (micro-manipulator) that can be controlled manually, for macro-movements and electronically, for micro-adjustments.

2.5.3.3 Perfusion system and drug application

For drug application, a system designed the enable to exchange of solutions, as well as to control the temperature of the superfusate, was used (Fig. 2.20). It consisted of a manifold, connected to the outlets of 6 solenoid valves. The perfusion system also contained a heat exchanger unit, which was able to heat, or cool, the superfusate to a specific temperature and was able to produce heat ramps at a desired range. The heat exchanger unit contained a semi-conductor thermoelectric device which works on the Peltier effect: when supplied with a suitable electric current, it pumps thermal energy from one side to the other which means that one side of the device is heated up, while the other is cooled down. One side of the thermal electric device was fitted with a silver heat exchanger block which contained a channel through which the superfusate flowed. The inlet of the heat exchanger block was connected to the outlet of the manifold. The outlet of the heat exchanger block was connected to a small delivery tube of 250 µm inner diameter. The end of this delivery tube was positioned at ~100 µm from the cell from which the recording was made. The valves were switched through a controller which was connected to the PC. The delivery tube contained a miniature thermocouple which was connected to an

electronic thermometer with an analogue output. The analogue output of the thermometer was connected to the PC through an AD interface, so that the temperature of the superfusate during the time of the recording can be traced. Each of the 6 tubes were connected to a reservoir containing solution separated from the tube by a valve that was closed under resting conditions. This arrangement allowed automated drug applications, and temperature-ramp applications, all of which was controlled by the Clampex 8 software package. The heat exchanger block was fitted with a thermocouple connected to the controller unit (Wavelength Electronics). A low-noise recording set-up was achieved by placing the parts of rig, particularly the microscope and the headstage, on top an anti-vibration table surrounded by a Faraday cage to minimise such interference from microscopic movements and vibrations, and to prevent environmental electromagnetic noise from entering the circuit. The anti-vibration table (Newport Corporation) works on the basis that pressurised gas has far superior vibration isolation properties compared to any sold material. Thus, the tabletop of the anti-vibration table is kept afloat by air cushions in the table legs from a pressurised gas source (Molleman, 2002).

A

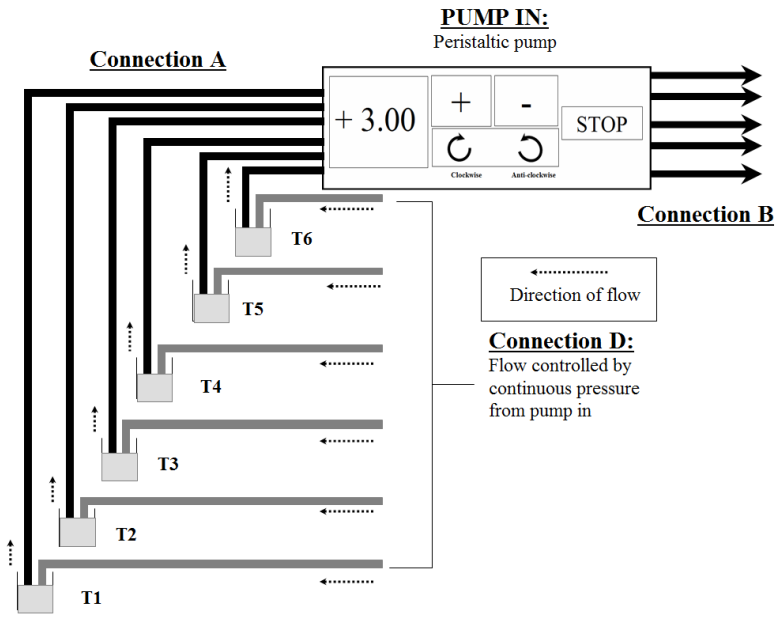

B

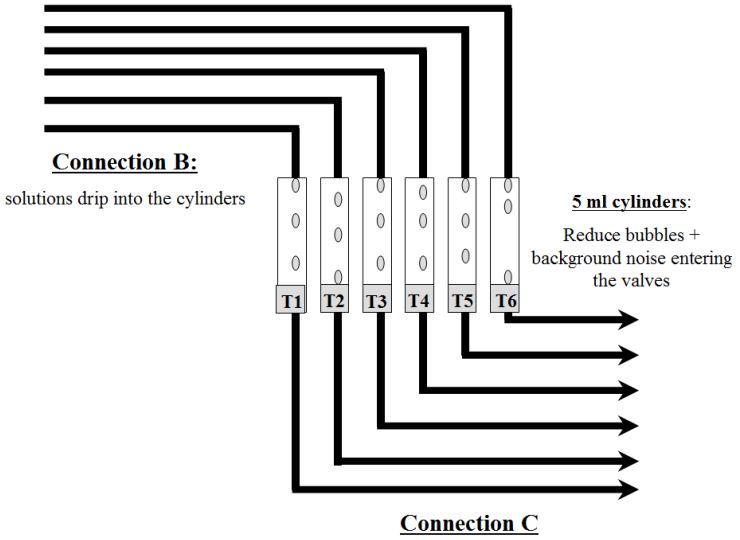
Connection B:
solutions drip into the cylinders
5 ml cylinders:
Reduce bubbles + background noise entering the valves
T1
T2
T3
T4
T5
T6
Connection C

C

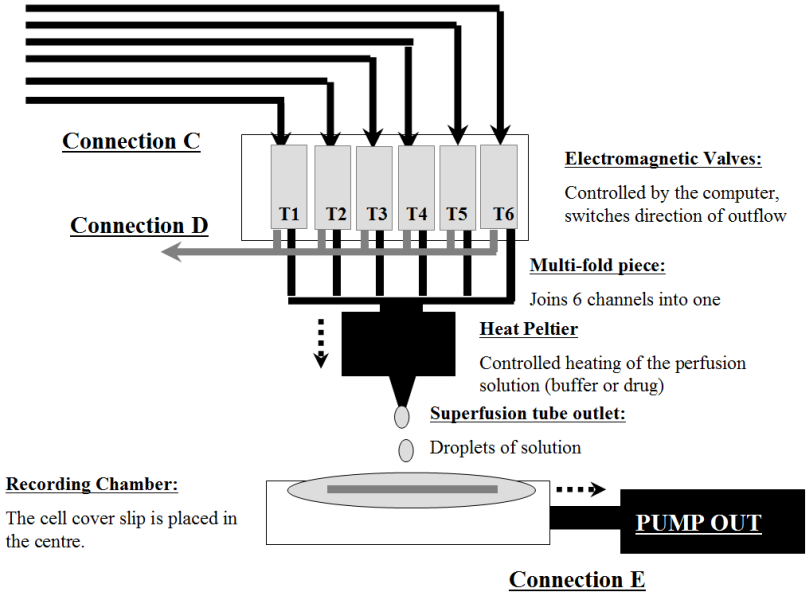
Connection C
Connection D
T1
T2
T3
T4
T5
T6
Electromagnetic Valves:
Controlled by the computer, switches direction of outflow
Multi-fold piece:
Joins 6 channels into one
Heat Peltier
Controlled heating of the perfusion solution (buffer or drug)
Superfusion tube outlet:
Droplets of solution
Recording Chamber:
The cell cover slip is placed in the centre.
PUMP OUT
Connection E

D

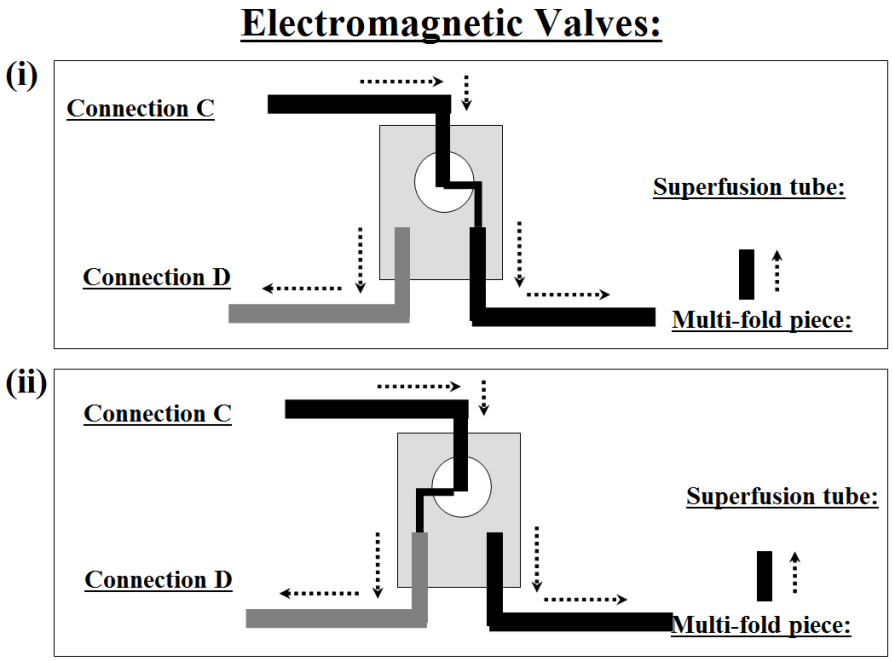

Figure 2.20 Perfusion system of the electrophysiology set-up. (A) The ends of tubes A are placed in test tubes containing buffer or drug solution. The tubes go through a peristaltic pump and are subsequently linked to connection B. The peristaltic pump controls the flow of the fluid circulating in the perfusion system at a smooth and constant flow at constant pressure. (B) Connection B is linked to 5 ml syringes reducing the bubbles entering the rest of the perfusion set-up. The cylinders are linked to connection C. (C) Connection C is connected to electromagnetic (solenoid) valves which control drug application automated by the PC. The end of the valves is linked to a manifold which connects 6 tubes to one tube which then enters the heat exchanger unit. The heat exchanger heats the buffer to the required temperature, before the superfusate enters the recording chamber. Waste is removed *via* connection E by another peristaltic pump. (D) The electromagnetic valves have two configurations: (i) The solution from connection C enters the manifold then the heat exchanger unit, before entering the recording chamber; (ii) The solution from connection C is linked to connection D which is placed back to the test tube containing buffer or drug solution, so unused fluids are recycled. Parts of the perfusion set up (figures (B) and (C)) are placed on top of an anti-vibration table surrounded by a Faraday cage which acts as a shield to prevent the environmental electromagnetic noise from entering the circuit.

2.5.3.4 Obtaining whole-cell patch-clamp configuration

A coverslip containing HEK293 cells transfected with hTRPV1 and GFP was removed from the tissue culture incubator and placed into the recording perfusion chamber fixed on top of the inverted fluorescent microscope. Positive cells were identified by GFP expression emission under the inverted fluorescent microscope (Nikon). With the use of the microscope, the superfusion tube outlet was positioned so as to be in the centre of visual field, a few micrometers above the cells. The patch electrode was inserted to the electrode holder of the headstage. The tip of the patch electrode was then gently placed into the extracellular buffer solution superfusing the recording chamber. Once this was achieved, the external command located in the "whole cell parameters" in the amplifier was turned turned off. The seal test in the computer usually read between 3-5 Mohm. The external command was then turned on. The external command was held at holding potential of –60 mV. A 5 mV test impulse was then applied; this evoked current steps as seen on the seal test window on the computer.

After compensating for the offsets of the amplifier, the patch electrode was further lowered onto the membrane of a GFP single cell membrane using the manipulator. Seal formation was monitored by observing the electrode current on an oscilloscope while applying 5 mV test pulses to the electrode. Before the electrode was placed into the bath solution, a flat current trace was observed. Upon entering the extracellular bath solution, the 5 mV test pulses resulted in current of 10-15 nA to flow in a 2-5 Mohm patch electrode. As the electrode approached the cell membrane, a slight decrease in current (2-5 nA) occurs reflecting an increase in the electrode resistance (10-15 Mohm), until the formation of a gigaseal For whole-cell configuration, the membrane patch was broken with additional suction. The additional suction was achieved via the suction line attached to a syringe, where 1-2 mls was adequate to break the membrane. Once the configuration of a whole-cell was obtained with the cell, the configuration was ready to record the responses of activator-induced membrane currents.

2.5.4 Recording protocols and data analysis

All data were recorded using the pClampex 8 software package. and analysed using the Clampfit data analysis programme (Axon Instruments Ltd). All experiments were performed at physiological temperature of 36-37 ^{o}C.

2.5.5 Capsaicin-evoked activation

To investigate the effect of capsaicin-evoked responses, stock solution of 50 mM (E)-capsaicin (Tocris) was prepared by dissolving the compound in 100% DMSO. Capsaicin was dissolved in standard extracellular buffer to various concentrations ranging between 10 nM and 100 µM. As a result of my finding that DMSO activates TRPV1 (see Chapter Three), capsaicin solutions were made to contain ≤ 0.05% DMSO content. The application of capsaicin for 10 seconds was controlled by the automated perfusion system controlled by the pClampex 8 software package, with only one application of capsaicin per cell. Normal extracellular and intracellular solutions were used. The membrane potential was held at - 60 mV

Capsaicin-evoked membrane currents were assessed using the Clampfit data analysis programme. In order to measure the peak amplitude of the current in response to agonist activation, two cursors were placed on the recording as responses were normalised to baseline current. The first cursor was placed over the baseline membrane current, which was defined as 1 second prior to application of the agonist. The second cursor was fitted over the peak of the current where the maximum amplitude was seen. The corresponding current amplitudes were then copied into an Excel spreadsheet. The maximum current amplitude was subtracted from the current seen at baseline.

To plot a capsaicin-concentration response curve, the data was placed into either Origin or Graphpad statistical analysis software. The data was then fitted with a sigmoidal dose-response curve (see Statistical Analysis section for further detail).

2.5.6 Anandamide-evoked activation

To investigate the effect of anandamide-evoked response, stock solution of 30 mM arachidonyl ethanolamide (anandamide; Tocris) supplied in a water soluble emulsion Tocrisolve (Tocris) was used. Anandamide was dissolved in standard extracellular buffer to various concentrations, namely: 1 µM, 3 µM and 10 µM. Since stock solution of anandamide was used, the percentage of Tocrisolve in these solutions were, namely: 0.03%, 0.01% and 0.003%, respectively. Application of anandamide for 50 seconds was controlled by the automated perfusion system controlled by the pClampex 8 software package. As a control, 0.03% Tocrisolve was also investigated. Normal extracellular and intracellular solutions were used. The membrane potential was held at -60 mV.

Anandamide-evoked membrane currents were assessed by subtracting the peak current of the response from the baseline current for each individual recording. This was done using Clampfit data analysis programme and Excel.

2.5.7 Proton-evoked activation

To investigate the effect of proton-evoked response, normal extracellular buffer was adjusted to a specific pH. Extracellular solutions were adjusted to specific pH, ranging from pH 4-7.

Solutions adjusted to pH 7.0, pH 6.5 and pH 6.0 were made by adjusting the pH of the normal extracellular buffer used in patch-clamp studies, using a pH meter. Normal extracellular buffer was used for this range of solutions because the

buffering agent HEPES buffering capacity was within this range. The buffering capacity of buffering salts is a measure of the resistance of a buffer solution to pH change on addition of H^+ ions. However, solutions adjusted to pH 4, pH 4.5, pH 5 and pH 5.5 were made by adjusting normal extracellular buffer containing 10 mM 2-(N-Morpholin) ethanesulfonic acid sodium (MES) buffering agent instead of HEPES, due to its lower range buffering capacity of pH $\leq$5.

Amiloride was added to these buffers to inhibit endogenous acid sensing ion channel in HEK293 cells. Stock solution of amiloride (Sigma) was made ddH20. 30 µM amiloride solution was added to the extracellular buffer. 30 µM amiloride solution was chosen as this concentration almost completely blocks the ASIC conductance in HEK293 cells (Gunthorpe et al., 2001).

Normal intracellular solutions were used. The membrane potential was held at -60 mV.

pH-evoked membrane currents were assessed by subtracting peak current of the response from the baseline current for each individual recording using Clampfit data analysis programme and Excel.

For pH-dose response curve, the data was placed into either Origin or Graphpad statistical analysis software. The data was then fitted with a sigmoidal dose-response curve.

2.5.8 Heat-evoked activation

To investigate the effect of temperature normal extracellular solution was passed through the heat exchanger unit. The heat exchanger unit is able to heat the passing solutions to a chosen constant temperature (37^{o}C), but could produce a rapid temperature-ramp at ~1.4 ^{o}C in 1 sec. Normal extracellular and intracellular solutions were used. The membrane potential was held at -60 mV.

2.5.8.1 Analysis of heat-sensitivity

2.5.8.2 Biophysics of heat-sensitivity

Detection of environmental temperatures is mediated by specialised molecules in the great majority of living organisms. In mammals, these molecules are ion channels which transduce thermal energy into electrical energy by temperature-induced transient changes in the permeability of the channels. Primary sensory neurons express a series of temperature-sensitive ion channels, suggesting that these cells, in addition to transmitting nociceptive information, can also detect various ranges of temperatures and transduce heat energy into electrical signals. The great majority of heat-sensitive ion channels belong to the transient receptor potential ion channel (TRP) family. These ion channels are referred to as thermo-TRP channels (see Fig 2.21). They include the "heat-sensitive" vanilloid type 1 (TRPV1), vanilloid type 2 (TRPV2), vanilloid type 3 (TRPV3), and vanilloid type 4 (TRPV4) and the "cold-sensitive" melastatin type 8 (TRPM8) and ankyrin type 1 (TRPA1) (Caterina et al., 1997; Caterina 1999, Xu et al., 2002; Guler et al., 2002McKemy, 2002; Story et al., 2003).

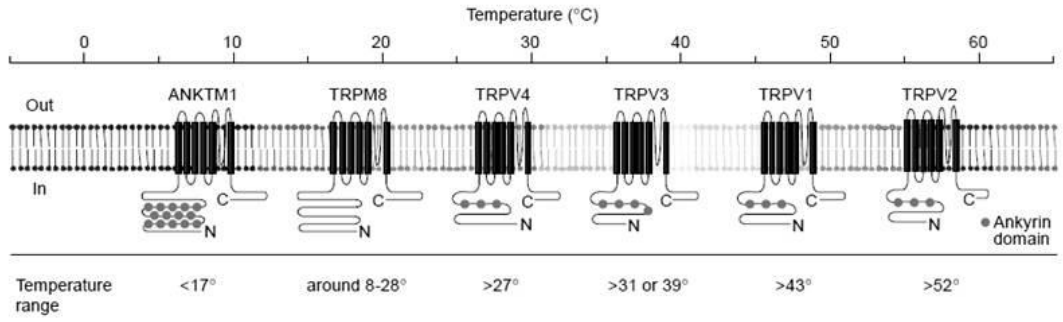

Figure 2.21 Thermo-TRP channels respond to a wide range of temperatures. The thermal threshold (below) and the range of temperatures to which they respond (above) are indicated for each channel. (Taken and adapted from Jordt et al., 2003)

Gating of thermo-TRP channels is controlled by temperature. As previously mentioned, gating of ion channels involves conformational changes of certain parts of the channel. The reaction rate constant between the transitions from open and close states are temperature-dependent. A reaction rate constant quantifies the speed of a chemical reaction. The temperature dependence of the rate constant can be defined by the Arrhenius relationship. The Arrhenius relationship is based on the collision theory which suggests the particles must collide with the correct orientation and with sufficient kinetic energy, in order for any physiological process to proceed. Furthermore, only a small proportion of particles have the ability to collide in the correct orientation and with sufficient kinetic energy to activate the physiological process, which is governed by the Boltzmann probability distribution:

$$-Ea/RT$$

where *Ea* is the activation energy, *R* is the gas constant and *T* is the absolute temperature in Kelvins.

Thus, the Arrhenius equation is:

$$k = A \exp^{-\frac{Ea}{RT}}$$

where *k* is the rate constant, *A* exp is the pre-exponential factor, and *-Ea/RT* is the Boltzmann probability distribution (Arrhenius, 1889). The pre-exponential factor is a temperature-independent factor and is defined as:

$$A = pZ$$

where *p* is steric factor and *Z* is the collision rate. The 'steric factor' represents the probability of molecules colliding in the correct orientation to activate the reaction.

Typically, the Arrhenius equation is written in logarithmic form which states that the logarithm of the rate constant is proportional to the reciprocal of the absolute temperature:

$$\ln k = \frac{Ea}{RT} + \ln A$$

Consequently an Arrhenius plot of the natural log of k *(lnk*) against the inverse of the absolute temperature (*1/T*) generates a linear relationship between the two variables (see Fig 2.22).

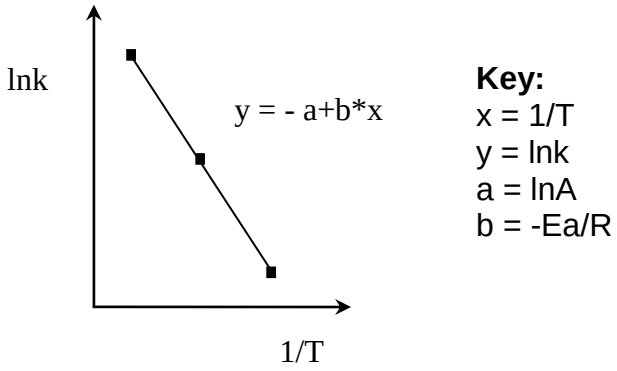

Figure 2.22 Schematic diagram of a typical Arrhenius plot. The Arrhenius plot shows the logarithm of a rate (lnk) against the reciprocal of the absolute temperature (1/T). Note: The activation energy (Ea) can be extrapolated from the gradient (b). Taken and adapted from Keusch, 2009).

Arrhenius plots have been used to identify temperature-induced changes in processes. A dramatic change in the slope, or a deviation from the straight line of an Arrhenius plot, suggests that the activation energy is different above and below the point of deviation. In thermo-TRP channels, a sudden deviation from the straight line can be defined as the thermal threshold of activation, where the channel's rate constant, i.e. the open probability, suddenly shows a great change. For example, the sudden appearance of a steeper slope means that the channel's rate constant at that temperature becomes greater; hence the open probability becomes higher.

Q_{10} is a measure used to describe the factor by which the rate (R) of reaction increases for every 10 ^{o}C rise in the temperature (T). R may represent any measure of the progress of a process. Typically, R is measured at two different temperatures, T_1 and T_2 (where $T_2 > T_1$), where the rate measurement R_1 (measured at T_1) and R_2 (measured at T_2), are obtained, respectively. The Q_{10} equation is then:

$$Q_{10} = \left(\frac{R_2}{R_1} \right)^{\left(\frac{10}{T2 - T1} \right)}$$

(Note that, the difference between T_1 and T_2 does not need to be exactly10 ^{o}C to permit the use this equation). A conductance of an open channel with a Q_{10} of 1.2-1.5 is considered to be relatively temperature insensitive, which can be accounted for by the temperature dependence of ionic diffusion and chemical reactions in general (Hille, 2001). Most ion channels and enzymes have a gating Q_{10} of 2-5 and are regarded as being highly temperature-dependent (Hille, 2001; Clapham, 2003). Thermo-sensing TRP channels are known to have high Q_{10} values (see Table 2.2).

Ion channel	Q10	Reference
TRPV1	27	Liu et al., 2003
	29.5	Ni et al., 2006
	25.6	Vlachova et al., 2003
	17.8	Vyklicky et al., 1999
	20.6	Welch et al., 2000
TRPV2	~100	Leffler et al., 2007
TRPV3	25	Xu et al., 2002
	6.6	Peier et al., 2002
TRPV4	9.9	Guler et al., 2002
	19.1	Benham et al., 2003
TRPM8	-23	Brauchi et al., 2004
	-35	Andersson et al., 2004
TRPA1		No published data

Table 2.2 TRP channels and their Q_{10} values as found in various studies. Note: Ion channels that are activated by heat or by an increase in temperature have a positive Q_{10} value, whereas channels that are activated by cold or a decrease in temperature have a negative Q_{10} value.

2.5.8.3 Analysis of heat-induced response

When analysing heat-induced response of hTRPV1, the current amplitude at a particular temperature, the Q10 value, the heat threshold of activation, and the activation energy are each calculated.

To determine the amplitude of the current at 48 ^{o}C two cursors were placed on the heat-induced membrane current using Clampfit 8.2 data analysis programme (Axon Instrument, Inc). The first cursor was placed over the baseline membrane current, which was defined as 1 second before the application of the heat ramp. The second cursor was fitted over the first instance that the temperature of the extracellular solution reached 48 ^{o}C. The corresponding current amplitudes were then copied into an Excel spreadsheet. The current amplitude detected at 48 ^{o}C was subtracted from the current amplitude obtained at baseline (37 ^{o}C).

To determine the Q_{10} of a heat-induced response, the Q_{10} equation was used (Saucr et al., 2001; Leffler et al., 2007):

$$Q_{10} = \left(\frac{I_2}{I_1} \right)^{\left(\frac{10}{T2 - T1} \right)}$$

where I_1 (measured at T_1) and I_2 (measured at T_2) represent the whole-cell currents conducted through the cell at two different temperatures T_1 and T_2 (where $T_2 > T_1$).

The first analysis of the heat-evoked currents in hTRPV1-transfected cells, the heat threshold of activation was determined by *manually* placing two lines at the two linear parts of the Arrhenius plot, as shown by the example in Fig 2.23 and published by Sutton (2005) and Vyklicky (1999). This was done by transferring the rising phase of the temperature ramp data from Clampfit 8.2 as a text file to *Excel*. Due to the high resolution of the data sampled during the whole-cell recording, the

data was reduced by calculating the average of every 5th data point to form an average data set. The common logarithm of normalised current at 37 ^{o}C and the reciprocal of the absolute temperature were calculated. The Arrhenius plot was then constructed using Origin statistical analysis software. Due to the nature of the heat-induced currents, the Arrhenius plot showed a curved line; in which (at least) two lines with different slopes are needed to adequately describe the relationship (Cesare and McNaughton, 1996; Vyklicky et al., 1999; Caterina et al., 1999). Two manual lines were then fitted on the plot. The first line was manually placed across the points between 37-42 ^{o}C. The second line was place across the steeper points on the plot, typically through 45-51 ^{o}C. From the intersection of these two lines, the threshold temperature for heat activation was established. However, the manual fit raised an issue relating to the reliability of the data. Therefore, a more valid and reliable approach was employed.

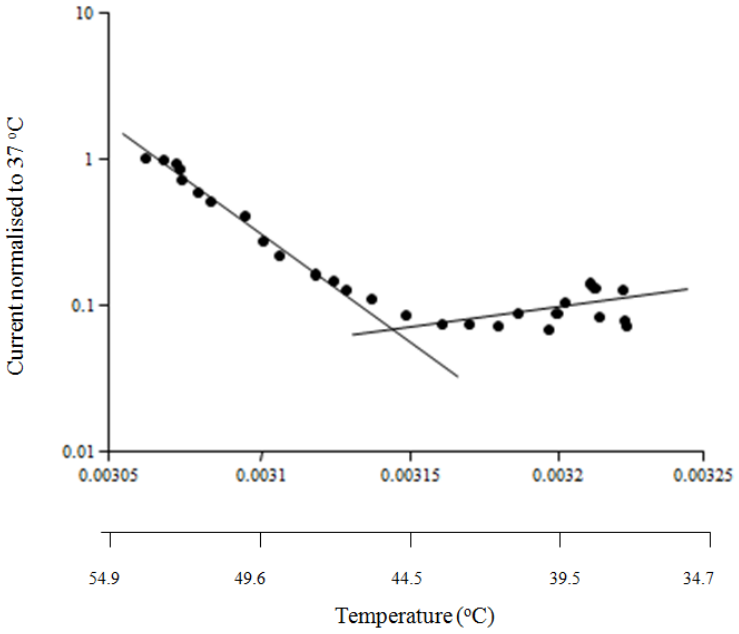

Figure 2.23 Arrhenius plot of heat-induced response in hTRPV1-transfected cells. The common logarithm of normalised current to 37 oC was plotted against the reciprocal of the absolute temperature (Arrhenius plot). The heat threshold was established from the intersection of these two lines fitted on the two linear parts of the graph. In this example the heat threshold was 44.6 ^{o}C (arrow).

During this analysis, recordings from untransfected HEK293 cells during application of a heat ramp were first analysed. Visual inspection showed no current increase with an increase in the temperature (see Fig. 1A). Consequently, the average amplitude at 48 ^{o}C was -63 ± 28 pA (n=7). This can be described as a non-specific heat-induced current. Current-temperature plots showed that there was only a moderate steady increase in membrane current with an increase in the temperature 37-51 ^{o}C (Fig. 2.24). Consequently, an Arrhenius plot was constructed and a linear regression was fitted across. All untransfected HEK293 cells showed a nearly horizontal line, indicating no linear relationship between the two variables (Fig. 2.24B). The Q_{10} for the rising phase of the temperature ramp (37-51 ^{o}C) was then calculated to be 1.12 ± 0.03 (n=7; Fig 2.24C), which corresponds to the non-specific effects of temperature on membrane properties. This suggests that untransfected cells showed no heat-evoked response.

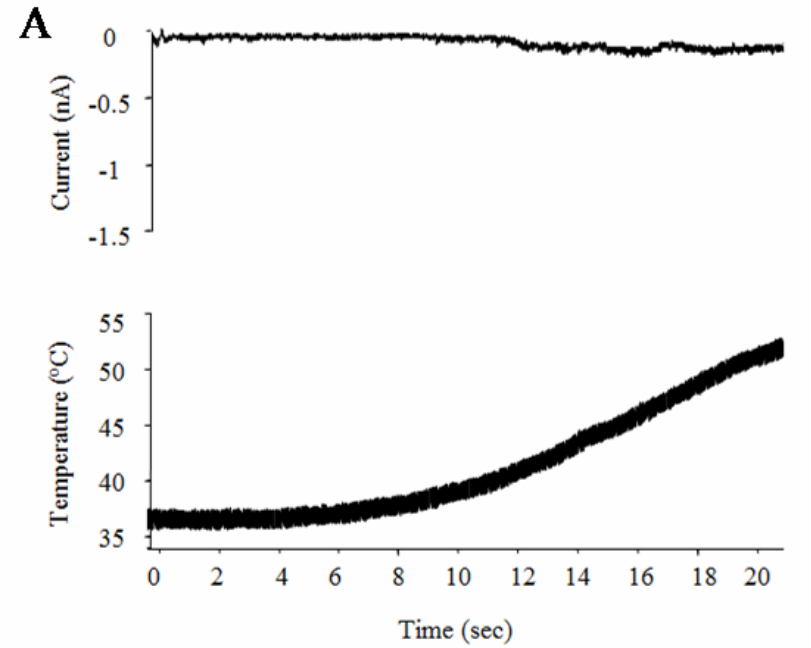
A
0
-0.5
-1
-1.5
Current (nA)
55
50
45
40
35
Temperature (°C)
0
2
4
6
8
10
12
14
16
18
20
Time (sec)

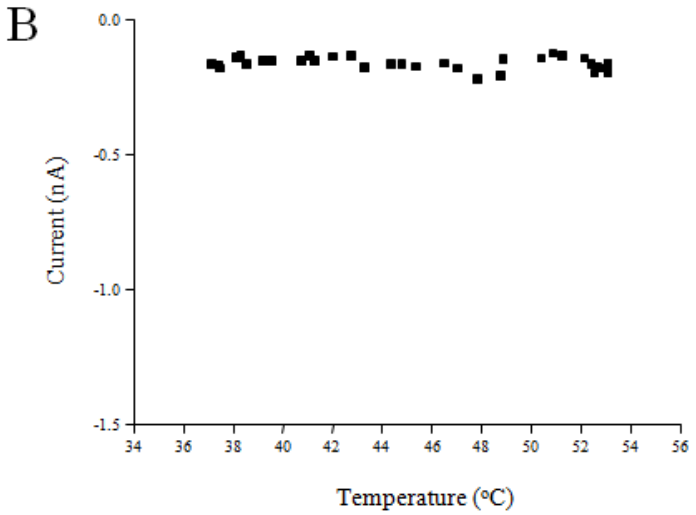
B
0.0
-0.5
-1.0
-1.5
Current (nA)
34
36
38
40
42
44
46
48
50
52
54
56
Temperature (°C)

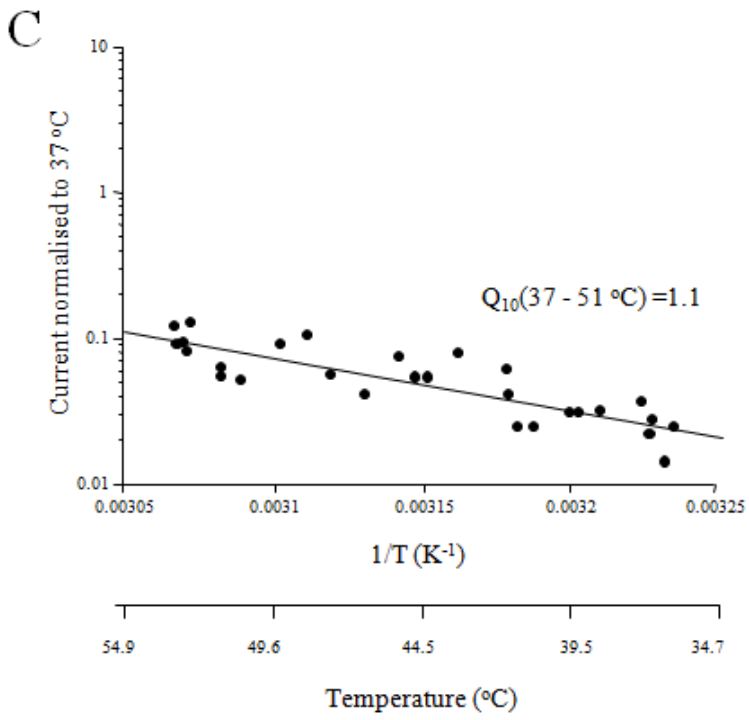

Figure 2.24 Whole-cell membrane current induced by heat ramp and its Q_{10} in an untransfected HEK293 cell. (A) A current trace at a membrane potential of -60 mV recorded using the whole-cell patch clamp technique. A heat ramp 37-51 ^{o}C was used to stimulate the cell. A very small heat-evoked response was seen in this cell. (B) Relationship between the membrane current and temperature using every 5th data value of the trace on A. A very small was seen with an increase in the temperature. (C) The common logarithm of normalised current to 37 ^{o}C was plotted against the reciprocal of the absolute temperature (Arrhenius plot). The temperature scale in degrees centigrade is shown below the scale of the reciprocal of the absolute temperature. The scatter plot was fitted with a linear regression. A linear regression was fitted, where the Q_{10} (37-51 ^{o}C) was calculated to be 1.1. This implies that the trace in A is temperature insensitive.

Recordings from TRPV1-transfected HEK293 cells during application of a heat ramp were then analysed. Inspection of a recording showed a large inward membrane current, as a result of an increase in the temperature of the solution superfusing the cell (for example see Fig 2.25A). By generating a current-temperature plot, the activation of the current was seen to be initiated at temperatures > 45 ^{o}C, which resulted in a distinct change in the gradient of the slope (Fig. 2.25B). The Arrhenius relationship was then constructed. Similar to the original analysis, two

lines were fitted on the plot, however, instead of a manual fit, the linear regression function in Origin software was used. The software produced a summary output detailing the equation of the linear regression and the correlation coefficient r value (see Chapter Two: Statistics for further detail). The linear regression was then extrapolated.The lines representing the Arrhenius plot can then be superimposed on to the graph and the temperature of the intersection of the two lines can be calculated as the heat threshold of activation (Fig 2.25C).

Often, the Arrhenius plot was not best represented with two lines at different slopes (for example Fig 2.25C). Original analysis of the temperature threshold of activation utilised only two lines at different slopes as, typically, a slow rising phase in the temperature range of ~37-42 ^{o}C was seen, followed by a fast rising phase between 46-51 ^{o}C. However, a third slope with a different gradient to the other two, could be fitted through 43-45 ^{o}C data points, which is the range of TRPV1 threshold of activation (Cesare and McNaughton, 1996; Vyklicky et al., 1999; Caterina et al., 1999; Sutton et al., 2005).

A

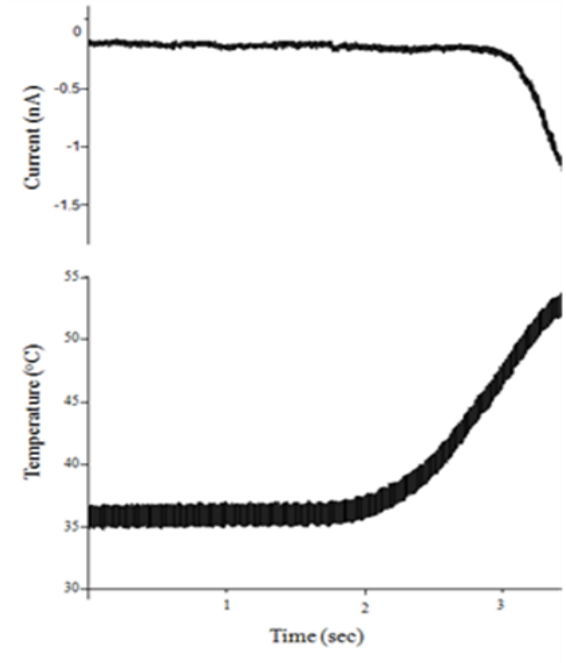
Current (nA)
0
-0.5
-1
-1.5
Temperature (°C)
55
50
45
40
35
30
1
2
3
Time (sec)

B

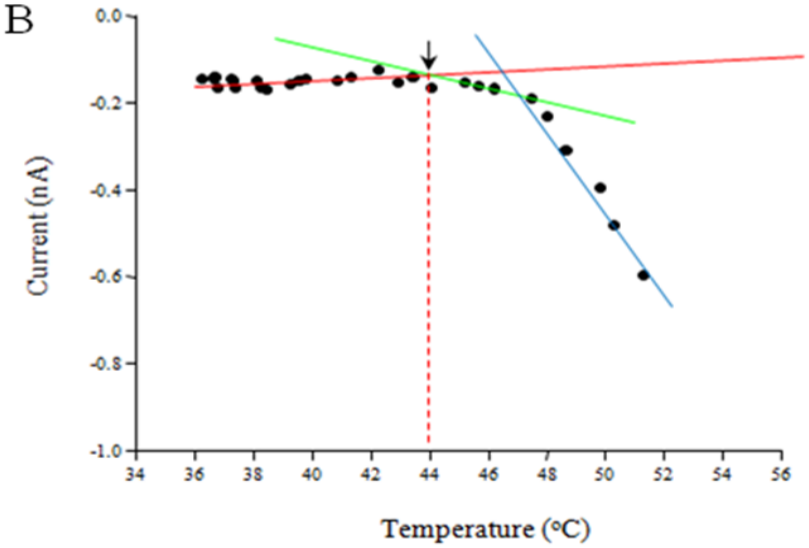
Current (nA)
0.0
-0.2
-0.4
-0.6
-0.8
-1.0
34
36
38
40
42
44
46
48
50
52
54
56
Temperature (°C)

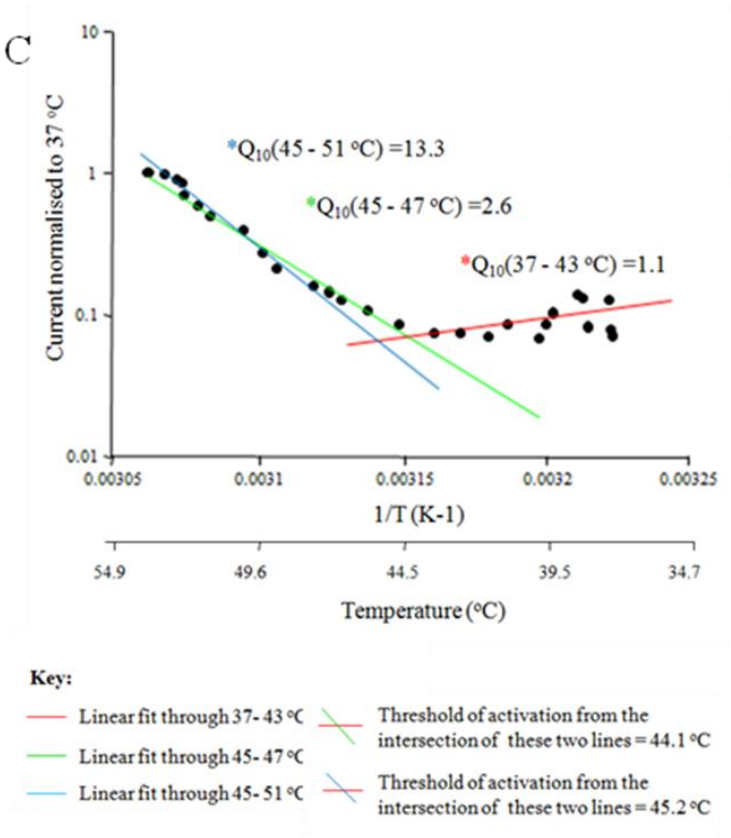

Figure 2.25 A whole-cell membrane current induced by a heat ramp and its Q_{10} in TRPV1-transfected HEK293 cell. (A) A current trace at a membrane potential of -60 mV recorded using the whole-cell patch clamp configuration. (B) Membrane current-temperature scatter plot using the mean of every 5th data value of the trace on A. To best represent the relationship of the trace, three manually fitted lines with different slopes were extrapolated on the plot. The current increased with temperature above 44 °C. Hence the estimated heat threshold for this example was 44 °C. (C) The common logarithm of normalised current to 37 ^{o}C was plotted against the reciprocal of the absolute temperature (Arrhenius plot). The temperature scale in degrees centigrade is shown below the scale of the reciprocal of the absolute temperature. The plot was fitted with three linear regressions using OriginLab 7 software. The first line was fitted across the points between 37-43 ^{o}C (red line, r = 0.2). The second line was fitted across the points between 45-47 ^{o}C (green line, r >0.95). The third line was fitted across the points between 45-51 ^{o}C (blue line, r >0.95). An r > 0.95 suggests a strong relationship between an increase in temperature and membrane current for the trace in A. The heat threshold was established from the intersection of the three lines fitted on the two linear sections of the plot. In this example, two heat thresholds of activation were calculated. The intersection between red line and green line showed a threshold of 44.1 ^{o}C whilst the intersection between red line and blue line exhibited a threshold of 45.2 ^{o}C. The temperature which was interpolated between the red and green line was accepted as the heat activation threshold, if the value was < 0.37 ^{o}C of the estimated value. The temperature which was interpolated between the red line and blue line illustrates that a linear fit between 45-51 ^{o}C was unreliable, as the value was > 0.37 ^{o}C of the estimated value.

Having a regard to the considerations stated above, each recording was subjected to a second analysis, in order to obtain a more reliable heat activation threshold of hTRPV1-transfected HEK293 cells. The protocol for the second analysis is as follows:

(i) Transfer the rising phase of the temperature ramp to a text file, which should include the membrane current of the cell be tested.

(ii) Calculate the current amplitude at 48 ^{o}C of the recording by subtracting the current at 48 ^{o}C from the current seen at 37 ^{o}C one second before the heat ramp (baseline) is initiated. Due to the non-specific heat-induced current in untransfected cells during application of the heat ramp, current traces with an amplitude of < 63 pA were excluded, whilst current amplitude > 63 pA, which was the amplitude of current at 48 ^{o}C in untransfected HEK293 cells, progressed to the next step.

(iii) Calculate the Q_{10} value for the rising phase of the temperature ramp (37-51 ^{o}C). Current traces with a Q_{10} of <1.1 were excluded while current values Q_{10} of >1.1 progressed to the next step, due to the characteristics of untransfected cells during a heat ramp.

(iv) Construct a current-temperature plot in Origin. Manually fit a line through the points at 37-40 ^{o}C, which is below the temperature range for wild-type TRPV1 activation. Estimate heat threshold of activation by placing a cursor at point which the current membrane deviates from the manually fitted line, for example ~44 ^{o}C. This was referred to as the estimated value.

(v) Construct the Arrhenius relationship. To be included in the next step, the plot must show a curved line which can be fitted with a least two lines. If the plot is best represented by one line, exclude data.

(vi) Compute a linear regression from 37 ^{o}C to the estimated threshold minus 1 ^{o}C, for example 44 - 1 = 43 ^{o}C. Compute another linear regression, this time from the estimated threshold plus 1 ^{o}C (i.e., 45 ^{o}C) to two degree centigrade from the estimated threshold (i.e., 45-47 ^{o}C). The latter linear

fit must have coefficient correlation of $r > 0.95$ to be included in the next step, while an $r < 0.95$ is excluded. The +1 ^{o}C or -1 ^{o}C from the estimated threshold were eliminated from the linear regression fit, to reduce the possibility of forcing the linear regression through these points. Thus, reducing biased heat activation threshold analysis.

(vii) Extrapolate the lines representing the equation for both of the linear regression. Work out the temperature threshold of activation at which the two lines intercept and compare this with the estimated threshold. Accept threshold if < 0.37 ^{o}C of the estimated value and reject if it is > 0.37 ^{o}C. A difference of 0.37 ^{o}C was chosen as the critical value because the lowest temperature threshold of activation cannot be lower than the baseline temperature of 37 ^{o}C. Thus, 1 % of 37 ^{o}C is 0.37 ^{o}C using 99 % confidence level (See Chapter 2: Statistical analysis for further detail on confidence level. A confidence level of 95 % was not chosen, as this relates to a critical value of 1.85 ^{o}C, which can consequently result in a huge error in estimating the temperature threshold of activation.

To determine the activation energy (Ea) for specific parts, that is, the slow rising phase and the fast rising phase, of the heat-induced response, the Arrhenius relationship is plotted in Origin and a linear regression is computed. As a result, values *a* and *b* from the linear regression equation (y = - a + b * x) are determined. The gradient of the line, represented as *b*, is equal to –Ea/R, where R is the gas constant (8.3145 J mol $^{-1}$ K^{-1}). Hence, the activation energy can be calculated (Lewis and Evans, 2006).

For example, the linear regression equation for the fast rising phase (between 46-51 ^{o}C), in Fig 2.25 C was determined to be:

$$y = 42.6 + -13564.8 * x$$

According to the equation, the slope is -13564.8 Kelvin. The minus sign of the slope is a mathematical convention, indicating that the graph slopes from right to left.

Thus,

$$-13564.8\ K = –Ea/R$$

Hence, the activation energy for this example is:

$$Ea = 13564.8\ K \times 8.3145\ J\ mol^{-1}\ K^{-1} = 112777.9\ J\ mol^{-1} \text{ or } 112.8\ kJ\ mol^{-1}$$

2.5.8.4 Comparison of analysing heat-induced responses by the two methods

In this section of my thesis I compare results obtained by analysing TRPV1-mediated heat-responses in hTRPV111-transfected HEK293 cells. Since the amino acid sequence of TRPV1 which was used to transfect cells has no importance, here I refere to this polymorph as TRPV1.

Increasing the temperature of the superfusing solution induced an increasing inward membrane current in hTRPV1-transfected cells in the range of 44-51 ^{o}C (Fig 2.25A). Untransfected HEK293 cells showed very small but visible heat-induced response during application of a heat ramp (Fig. 2.24A). Consequently, the amplitude at 48 ^{o}C of the hTRPV1-transfected cell was 419 ± 38 pA (n=8) which was significantly higher than that of the untransfected cells which was 63 ± 18 pA (n=7), (Fig 2.26).

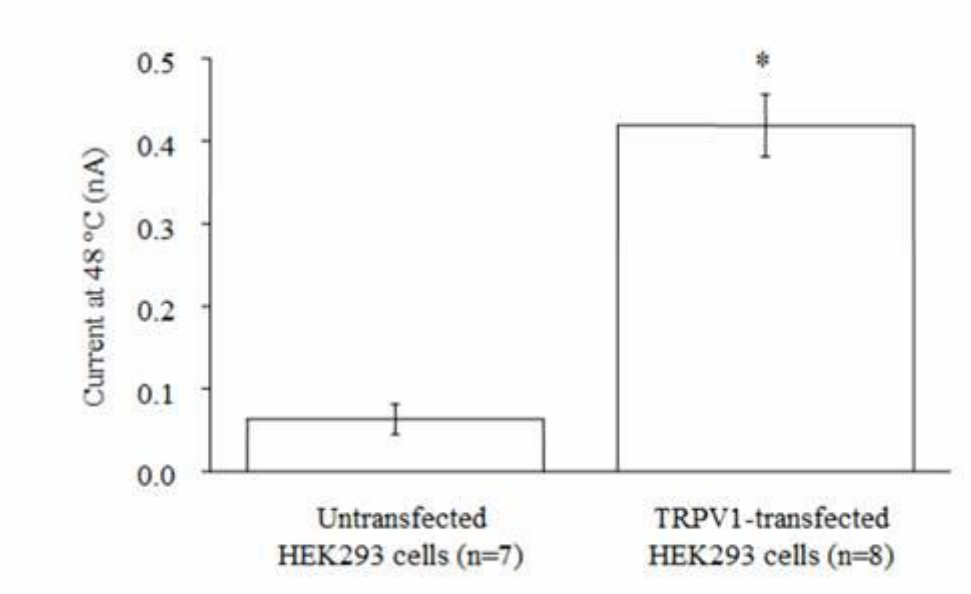

Figure 2.26 Current at 48 ^{o}C from untransfected HEK293 cells and hTRPV1-transfected HEK293 cells. Each data point represents the mean ± SEM. Both the f-test and the normality test showed a p-value of >0.05, High probability of equal variance and normal distribution. The statistical difference between the means was assessed using the Student t-test (two-tail distribution and two-sample equal variance). (*) Differences were regarded as being statistically significant at $p<0.05$. Note that comparisons between the means showed a significant difference.

Both the membrane current-temperature graph and the corresponding Arrhenius plot showed a notable change in the gradient in hTRPV1-transfected cells (Fig 2.25B-C). Untransfected cells showed a near horizontal line, when compared to that of the upper part (Fig 2.24B-C).

The Q_{10} of the rising phase of the temperature heat ramp (37-51 ^{o}C) for untransfected cells was 1.1 ± 0.04 pA (n=8), while the Q_{10} (37-51 ^{o}C) for hTRPV1-transfected cells was 3.75 ± 0. 28 pA (n=8), (see Fig 2.27). These values were significantly different from each other.

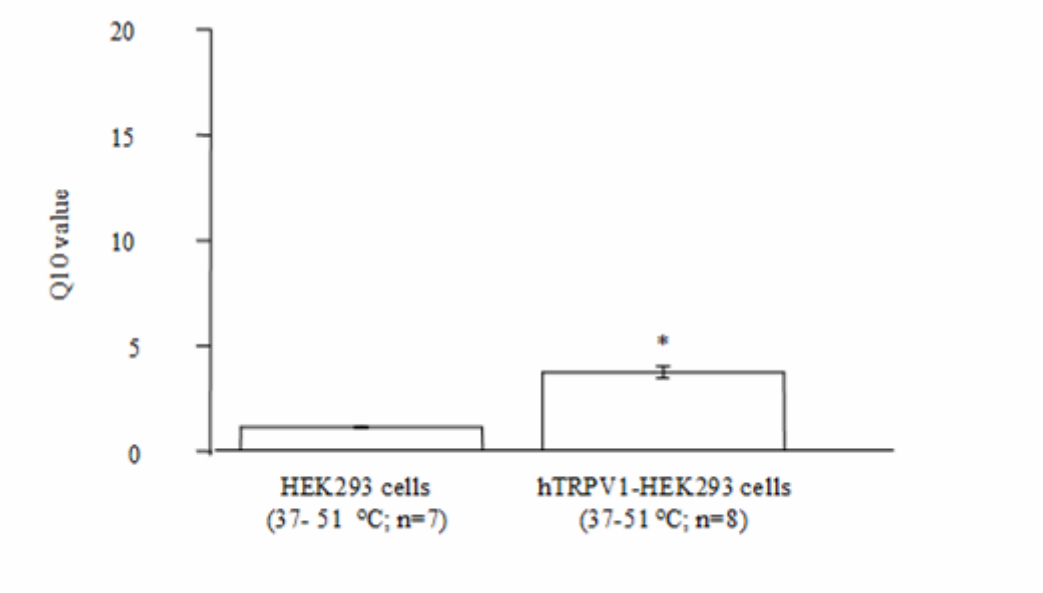

Figure 2.27 Q_{10} values of untransfected HEK293 cells and hTRPV1-transfected HEK293 cells between 37-51 ^{o}C. Each data point represents mean ± SEM. Both the f-test and the normality test (Shapiro-Wilk) showed p-values of >0.05, indicating high probability of equal variance and normal distribution. The statistical significance of the difference in the means was assessed using the Student t-test (two-tail distribution and two-sample equal variance). Differences were regarded as being statistically significant at *p<0.05. Note that comparisons between the means showed a significant difference.

In hTRPV1-transfected cells, two straight lines of different gradients could be distinguished in the Arrhenius plot, which were further characterised by their Q10 and their activation energy. The slow rising phase which was calculated in the range of 37-43 ^{o}C showed a Q_{10} of 1.5 ± 0. 12 pA (n=8), corresponding to Ea = 10.4 ± 2.1 kJ mol $^{-1}$ (n=8)). The fast rising slope in the range of ~46-51 ^{o}C had a Q_{10} of 14.1 ± 2.0 pA (n=8), relating to Ea = 10.4 ± 2.1 kJ mol $^{-1}$ (n=8)). Both the Q10 and the activation energy were significantly higher in the fast rising phase when compared to the slow rising phase of heat-induced membrane currents (see Fig 2.26). The Q_{10} for ~46-51 ^{o}C is slightly lower that the value of previously published data, which ranges from 18-30 (Liu et al., 2003, Ni et al., 2006; Vlachova et al., 2003; Vyklicky et al., 1999).

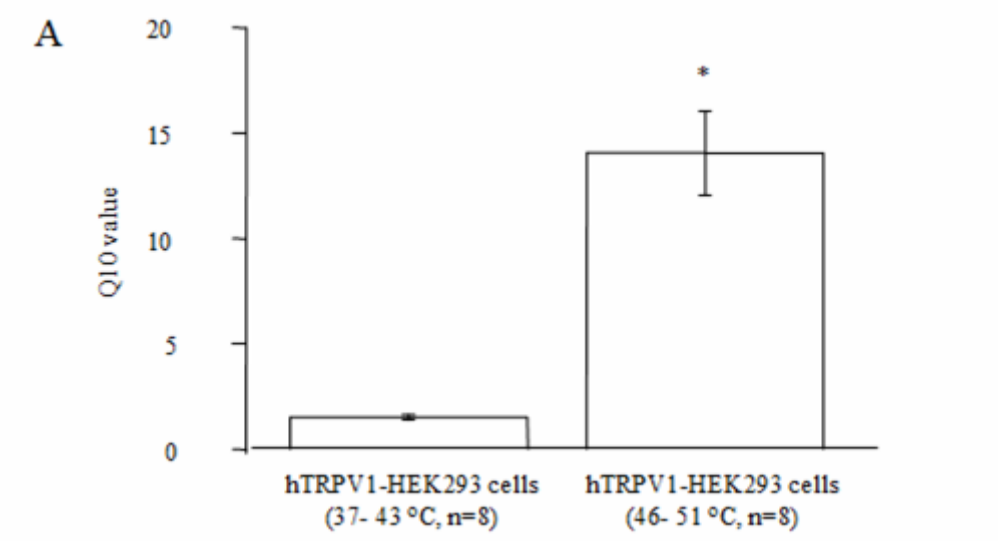

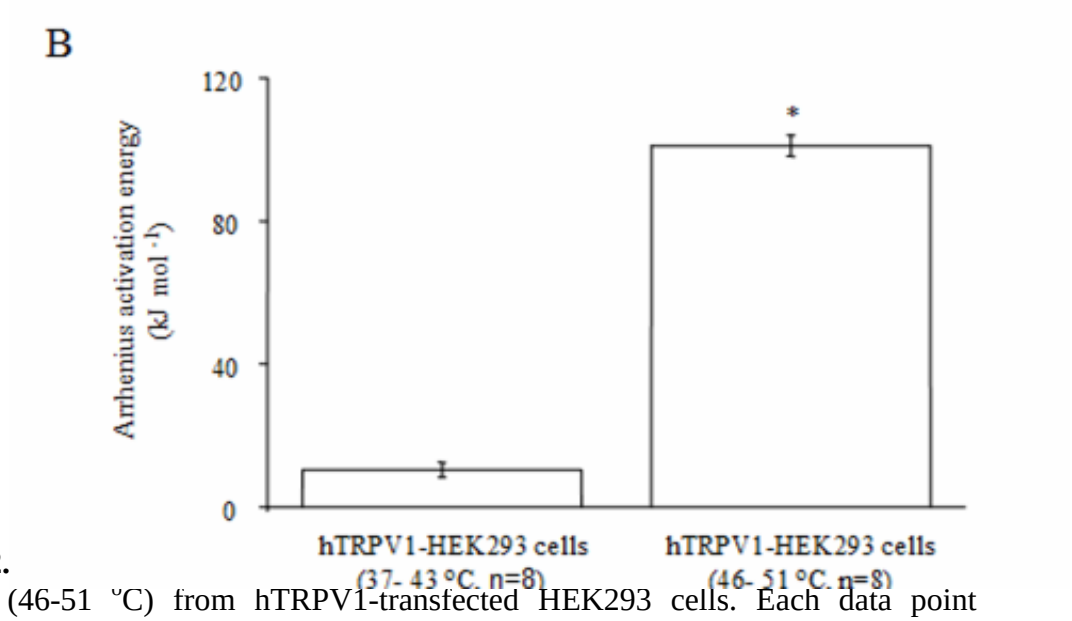

Figure 2.
the fast (46-51 ᵛC) from hTRPV1-transfected HEK293 cells. Each data point represents mean ± SEM. Both the f-test and the normality test (Shapiro-Wilk) showed p-values of >0.05, indicating equal variance and normal distribution. The statistical significance of the difference in the means was assessed using Student t-test (two-tail distribution and two-sample equal variance). (*) Differences were regarded as being statistically significant at $p<0.05$. Note that comparisons between the means showed a significant difference.

The heat threshold of activation of the first analysis of hTRPV1-transfected cells was 45.9 ± 0.45 ^{o}C (n=8). Two heat thresholds of activation were calculated from the second type of analysis of data which included analysis criteria and exclusion criteria. The first was obtained from the estimation of the temperature threshold of activation value from the deviation of the manually fitted line through data points 37-40 ^{o}C, which was 45.0 ± 0.36 ^{o}C (n=8). The second was constructed by intercept of the two linear lines extrapolated from the linear regressions, which was 44.8 ± 0.31 ^{o}C (n=8). Note that, there is less than 0.37 ^{o}C difference between the second analysis estimated value and second analysis value obtained from the intercepting the two lines, indicating that the estimation was of a good fit. Although the temperature threshold of activation obtained from the first analysis is higher than that of the second analysis, the difference was not statistically significant. Nevertheless, the second type of analysis was essential in order to obtain a more reliable heat activation threshold. Henceforth, all heat activation data presented were analysed using the second type of analysis.

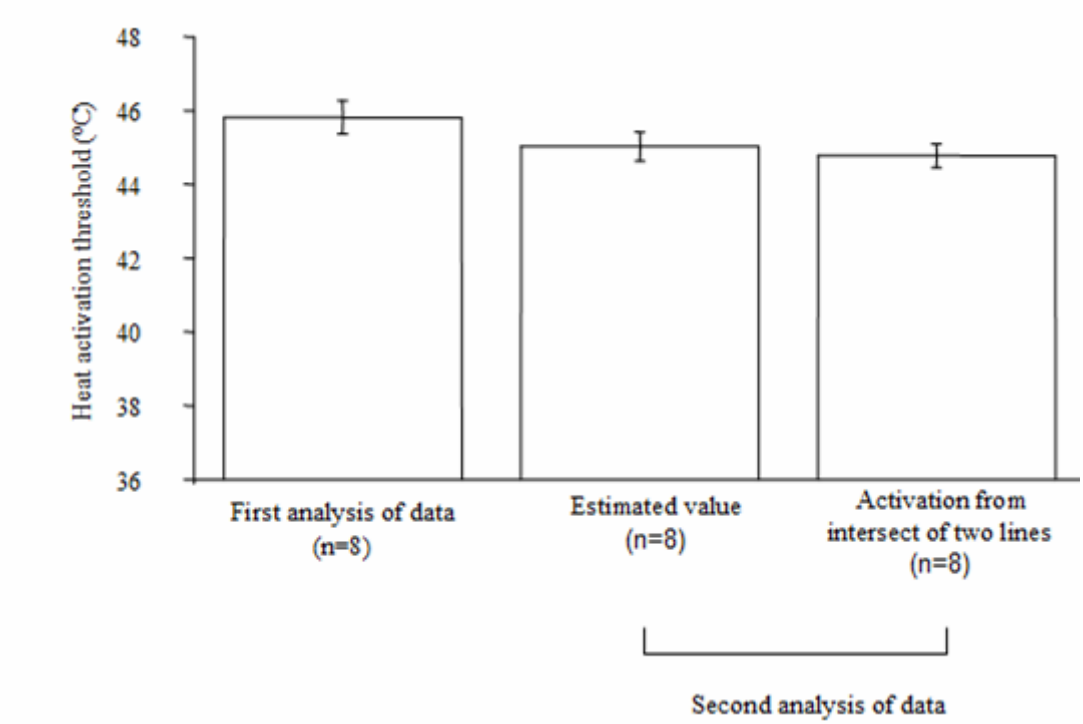

Figure 2.29 Heat activation threshold of first and second analysis of data. The difference between relevant groups was assessed by 1-ANOVA. Both the Bartlett's test for equal variance and the normality test (Shapiro-Wilk) showed p-values of >0.05, indicating equal variance and normal distribution. The statistical significance of the difference in the means was assessed using 1-ANOVA. A post hoc test was not computed as the overall p-value was >0.05. Note that comparisons between the means showed no significant difference.

2.5.9.1 Current-voltage relationship of the TRPV1 agonist-evoked responses

Ion channels, including TRPV1 frequently exhibit non-linear current-voltage relationship. This phenomenon is called rectification. TRPV1 shows outward rectification in both single channel and whole cell measurements (Nagy and Rang, 1999; Hayes et al., 2000). Regardless of the lack of linear relationship, TRPV1-mediated currents, like the great majority of other currents, show zero current at a certain membrane potential. This membrane potential is called the reversal potential. For TRPV1, at physiological ionic concentrations, the reversal potential is around 0 mV. The reversal potential measured in the presence of one permeable ion species gives an important clue to the ion selectivity of the ion channel (see Goldman-Hodgkin-Katz equation). For TRPV1 expressed in primary sensory neurons, the permeabilities of Na^+ and Ca^{2+} relative to the permeability of Cs^+ are between ~1-2 (Nagy and Rang, 1999).

Data in the literature showed that the capacitance of HEK293 cells is <50 pico Farad (Pelucci et al., 2006) while the membrane resistance is < 10 megaOhms (Zhu et al., 1998). Hence, the tau (τ) is 500 µsec. With time =5x τ (2.5 milliseconds), the desired voltage value is reached to 99.66%. Thus, in order to establish the current-voltage relationship of the TRPV1-mediated responses in HEK293 cells, a ramp was designed from -100 to +40 mV in 340 milliseconds (0.38 mV/ms). This value is comparable to previously reported (0.14 mv/ms: Hayes et al., 2004) when obtaining IV relationship in HEK cells expressing various channels including TRP channels.

To establish the I-V relationship of agonist-induced currents normal extracellular and intracellular solutions were used (extracellular buffer (mM): NaCl, 130; KCl, 5; CaCl2, 2; MgCl2, 2; glucose, 10; Hepes, 10; intracellular buffer NaCl, 5; KCl, 130; MgCl2, 1.26; Hepes, 10; adjusted to pH 7.4.). The membrane potential was held at -60 mV and the series resistance was compensated by 50-90 %. The residual uncompensated series resistance was 2.2 ± 0.2 MΩ (n = 55), which would

produce an expected error of 2.2 mV for an agonist-induced current of 1 nA at a holding potential of - 60 mV. The membrane patch was ruptured and a waiting period of at least 1 min was allowed for equilibration of the electrode solution with the contents of the cell. Agonists were applied to cells using the automated system. Only one recording was performed on any coverslip of cells to ensure that recordings were not made from cells which had been inadvertently exposed to any agonist. In order to study the current-voltage relationship of the agonist-evoked responses, a voltage ramp between -100mV to +40mV for 340 milliseconds was applied before (control curve) and during the 10 second agonist application (test curve) in hTRPV1-tranfected cells.

Current–voltage relationship was then established by subtracting the control curve from the test curve. The reversal potential was then interpolated from the zero current intercept of the fitted line of the current-voltage curve to 0 mV. Interpolation was achieved by plotting the two data points below and above the 0 nA and fitting them with a simple linear regression. The linear equation for the linear regression was noted and the reversal potential was then calculated.

2.5.10 Voltage-dependence

2.5.10.1 Biophysics of voltage-dependence

Voltage-gated ion channels open and close in response to changes in the membrane potential of the cell. The membrane potential is the voltage difference between the interior and exterior of the cell. Neurons contain voltage-gated ion channels and use changes in the membrane potential as a communication signal for receiving and sending information. A change in the membrane potential is caused by anything that alters the membrane permeability to any ion, or anything that alters the ion concentration on either side of the plasma membrane.

Hodgkin and Huxley suggested a simple model that could explain the voltage-dependence of ion channels. The model presumes that individual ion channels, each having a small ionic conductance, influences the activity of the whole membrane. As previously mentioned each ion channel has two conducting states: (i) an open state (O) where the gate is open allowing ions to travel across the membrane; and (ii) a closed state (C) where the gate is closed.

The transition from C to O is a conformational change that moves the gating charge of valence, z, from the inner membrane surface to the outer side. The symbols α and β are the rate constants for channel opening and closing, respectively. Both rate constants are highly temperature- and voltage- dependent (Hille, 2004; Sigworth. 1994). For voltage-gated ion channels, these rate constants reflect the response of the charge particles on the voltage sensor, to the electrical potential. Altering the membrane potential changes the probability that a channel is in the open conducting state, referred to as the open probability. Consequently, this increases the percentage of the total population of channels to be in the open state and hence increases the total membrane conductance. The maximum conductance is achieved when all the channels are open, where further depolarisation has negligible effect (Hodgkin and Huxley, 1952).

In order to calculate the overall open probability of voltage-dependent activation of an ion channel in a cell, a protocol was designed to obtain data on the amplitude of the current and the current's dependence on voltage. Typically, the membrane potential is stepped or changed from the holding potential to a range of potentials in a sequence, usually by 10-15 mV increments, at a given frequency. Maximum current at the beginning of each step and the current at the end of each step (steady-state current) can then be plotted to obtain the current-voltage curves (Guia et al., 2001). Tail current measurements are initiated with a membrane potential at which the channels have been fully active (open), and which is followed by successive voltage steps with potentials more negative and more positive of the reversal potential. Steady state current is the residual current that is seen after the channels have been fully activated or closed at the given the membrane potential.

The open probability can then be obtained by, first fitting the tail current amplitudes with a sigmoid Boltzmann distribution:

$$I_{tail} = I_{max} / (1+ \exp (- (V – V1/2) s))$$

where I_{tail} is the tail current, I_{max} is the maximum current amplitude, V is the membrane potential, $V_{1/2}$ is half-maximal activation potential, and s is RT/zF (R is the gas constant, and T is the temperature, z is the valence of the gating charge and F is the Faraday constant). Secondly, normalising the tail current to maximum current amplitude (Nilius et al., 2005):

$$Po = I_{tail} / I_{max} = 1 / (1+ \exp (- (V – V1/2) s))$$

The Boltzmann distribution determines the probability that a channel is open by voltage-dependent gating which is derived from the Boltzmann equilibrium. The Boltzmann equilibrium illustrates the ratio of the probability to be in one of the two conducting states, C and O, which is governed by free energy. The sigmoid relationship between the ionic conductance and the membrane potential is due to the physical principle for the movement of charged particles under an electrical field of

the plasma membrane. The steepness of the rise of the curve is governed by the valence of the gating charge: the larger the z becomes, the steeper the rise of the open probability in response to depolarisation (Matthews, 2000). Voltage-gated sodium and potassium ion channels are highly dependent on the membrane potential for activation which suggests that the gating charge has a large valence and activation which occurs in a relatively narrow range. For example, the potassium channel containing the shaker mutation has a z value of 12-13 (Schoppa et al., 1992; Aggarwal and Mackinnon, 1996) and the bacterial sodium channel, has gating charge of 15 (Kuzmenkin et al., 2004).

TRPV1 is a voltage-dependent ion channel which can be activated by depolarisation (Voets et al., 2004). The voltage dependence of TRPV1 can be established by studying the relationship between the membrane potential and the whole-cell conductance produced by TRPV1 normalised to the maximum whole-cell conductance due to TRPV1 activity. Maximum whole-cell current produced by TRPV1 could be achieved if the P_o of TRPV1 is at maximum. Since TRPV1 responds to various activators, in theory the maximum P_o ($P_{o\,max}$) could be produced in several ways. Previously, depolarisation was used in an attempt to achieve $P_{o\,max}$ (Voets et al., 2004). However, as mentioned before, depolarisation cannot achieve $P_{o\,max}$, as it is only a partial activator (Matta and Ahern, 2007). The other possibility mechanisms to achieve $P_{o\,max}$ includes activation by heat, pH, or capsaicin. However the application of heat affects the activity of multiple components of a cell and not just TRPV1. Again, the affect of pH are mediated also by acid sensing ion channels (ASICs) as well as TRPV1. Capsaicin is a specific and selective activator of TRPV1. Hence, capsaicin application to TRPV1 provides an appropriate mechanism for achieving $P_{o\,max}$. The capsaicin-concentration curve fitted with a sigmoidal curve for hTRPV1 based on my data (see chapter 5), together with the results of published work, justified the assumption that a saturating concentration of 10 uM induced Po max (Voets et al., 2004; Hayes et al., 2000; Matta and Ahern; 2007).

Establishing that TRPV1 is voltage-dependent in transfected HEK293 cells can be achieved provided these cells do not express any voltage-gated ion channels.

However, previous findings have shown that several voltage-gated ion channels are constitutively expressed in HEK293 cells. Several endogenous voltage-gated potassium (Yu and Kerchner, 1998; Perez-Garcia et al., 1999; Mohapatra and Trimmer, 2006) and calcium (Berjukow et al., 1996) channels are expressed in these cells. The presence of these endogenous channels results in the generation of small currents (several hundred picoamps) at various membrane potentials (Yu and Kerchner et al., 1998). Therefore, prior to studying TRPV1 voltage-dependence, I examined whether untransfected HEK293 cells respond to changes in whole-cell membrane potentials. If they were to respond, then the activity of these endogenous voltage-gated ion channels would effect the membrane potential, which would effect whole-cell currents in TRPV1-transfected cells, thus distort TRPV1-mediated currents.

2.5.10.2 Untransfected HEK293 cells and voltage-dependene

2.5.10.2.1 Study design and practical application

I used voltage steps in these experiments as this method is better suited for analysing time- and voltage-dependent features of ion channels (Nilius et al., 2005). The ionic compositions of the bath and pipette solutions to study voltage-dependent activation were designed so that the only permeable ion was Na^+.

Na^+ was chosen because TRPV1 is permeable to this ion (Caterina et al., 2001; Cesare and McNaughton 1996; Nagy and Rang 1999). In addition, while HEK293 cells express endogenous K^+ and Ca^+ channels, they are not known to express Na^+ channels (Thomas and Smart, 2005; Berjukow et al., 1996; Cummins et al., 2003; Yu & Kerchner, 1998). I used symmetrical Na^+ concentration in these experiments because any small deviation from the theoretical 0 mV reversal potential due to errors, such as error in offsetting, can easily be compensated for during analysis. Thus, in these experiments, both the bath and pipette solutions consisted of the following (mM): NaCl, 150; $MgCl_2$, 2; Hepes, 10; EGTA, 0.1; glucose, 10 (bath solution only); adjusted to pH 7.4. The voltage step protocol involved holding the membrane potential at 0 mV due to the symmetrical ionic composition followed by

voltage steps from +155 mV to -130 mV in 15 mV step intervals, of 100 milliseconds duration, before returning back to the holding potential of 0 mV (Fig. 2.30a). The ambient temperature of the recordings in these experiments was 37ºC. To improve voltage control during the voltage steps, the series resistance and capacitance were compensated between 50 and 70 %.

Conductance curves were then constructed by using the following description:

First, the current-voltage curve from each cell was generated by measuring the amplitude of the steady-state current at the end of the voltage-step (i.e. 1 millisecond before returning back to the holding potential of 0 mV), and analysed individually.

Due to the symmetrical ionic composition the reversal potential should be 0 mV. Therefore, in the second step, if the reversal potential was not at zero, it was interpolated to 0 mV. Interpolation was achieved by plotting the two data points below and above the 0 nA and fitting them with a simple linear regression. The linear equation for the linear regression was noted and the reversal potential was then calculated.

Thirdly, the conductance of the steady-state current from the untransfected cells was then calculated as follows:

$$G = \frac{I_{ss}}{(E_m - V_r)}$$

where G is conductance; I_{ss} is the steady-state current; E_m is the membrane potential; and V_r is the reversal potential. Finally, the conductance-voltage curve was constructed and fitted with the Boltzmann function and the half activation potential ($V_{1/2}$), was analysed.

2.5.10.2.2 Response of untransfected cell to changing the membrane potential

I examined the current-voltage relationship of changing the membrane potential by using voltage steps from + 155 mV to -130 mV in 15 mV step intervals with 100 milliseconds before returning back to the holding potential of 0 mV (Fig. 30a). The current-voltage curve for untransfected HEK293 cells showed a near linear relationship between -130 mV to +100 mV. However, from + 100 mV to +155 mV, the curve deviates from the linear part with a faster outward current. The reversal potential of untransfected cells was calculated individually and averaged to be - 0.33 ± 1.23 mV (n=14).

Figure 2.30d, shows a plot of average peak conductance versus membrane potential. The smooth curve is best fit to a Boltzmann function used to calculate minimal conductance G_{min}, maximal conductance $G_{max,}$ and voltage for half-maximal activation $V_{1/2}$ of the graph (r^2> 0.95). The G_{min} and G_{max} for untransfected cells were 28.17 ± 1.57 nS (n=14) and 78.87 ± 16.6 nS (n=14), respectively. The conductance-voltage curve for untransfected HEK293 cells showed a near constant conductance relationship between -130 mV to +100 mV. Furthermore, a constant conductance with a G_{min} of 28.17 ± 1.57 nS (n=14) is present at this range, which indicate that the current is flowing through the cell at all times. Conversely, from + 100 mV to +155 mV, the curve deviates from the near constants part with a larger conductance, and a G_{max} of 78.87 ± 16.6 nS (n=14). The $V_{1/2}$ was calculated to be 117.38 ± 16.0 mV (n=14).

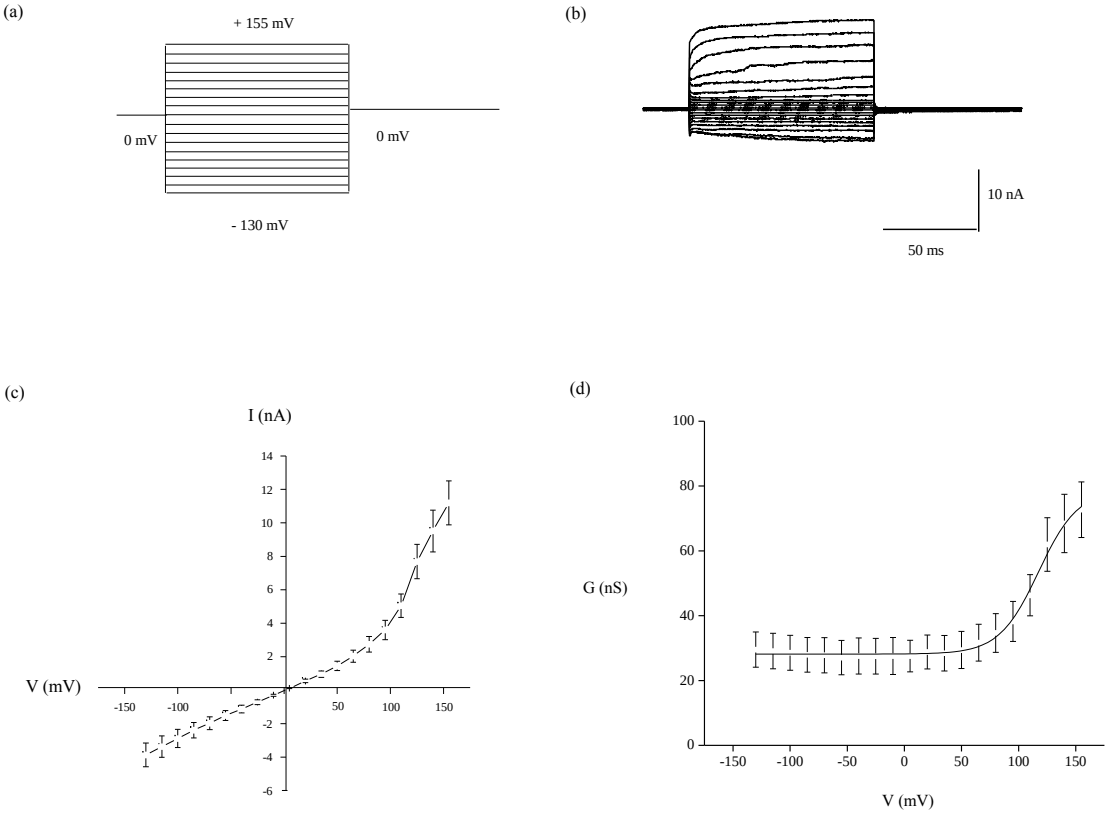

Figure 2.30 Response of untransfected cell to changing the membrane potential. (a) Voltage step protocol used in untransfected cells; (b) a typical trace measured using symmetrical Na^+ (150 mM); (c) current-voltage relationship; and (d) conductance-voltage relationship of the steady-state current of untransfected cells fitted with a Boltzmann function (OriginLab software analysis). Note that each data point represents mean ± SEM (n=14).

2.5.10.3 TRPV1-transfected HEK293 cells and voltage-dependent activity

2.5.10.3.1 Study design

Since untransfected HEK293 cells respond to changes in membrane potential with whole-cell currents (Fig. 2.30) voltage-dependence of TRPV1 could be only estimated. Therefore, I had to consider the most appropriate way to do that estimation. In order to do that I considered the following:

Any current recorded from the transfected cells contains both the HEK293 cell-generated non-specific background current and the TRPV1-mediated current, if there is any. Therefore, the total current (I_{total}) of HEK293 cells transfected with TRPV1 is

$$1. \qquad I_{total} = I_{TRPV1} + I_{non\text{-}specific}$$

where I_{TRPV1} is the voltage-activated current flowing through TRPV1 and $I_{non\text{-}specific}$ is the non-specific voltage-activated current produced by HEK293 cells.

The P_o can be determined as follows.

$$2. \quad P_o = G/G_{max}$$

G_{max} and Gcan be determined respectively, by measuring the current flowing through TRPV1 with a maximum open probability ($I_{TRPV1\ max}$) and with an open probability determined by the membrane potential ($I_{TRPV1\ Va}$). However, because of the presence of the non-specific current in HEK293 cells, any whole-cell recordings, in addition to the TRPV1-mediated maximum and variable current contain this non-specific current ($I_{non\text{-}specific}$).Therefore, the current flowing through the membrane of HEK293 cells transfected with TRPV1 which has a maximum open probability ($I_{total\ max}$) can be described as follows:

$$3. \qquad I_{total\ max} = I_{TRPV1\ max} + I_{non\text{-}specific}$$

Furthermore, the current flowing through the membrane of HEK293 cells transfected with TRPV1 which has an open probability between minimum (0) and maximum (1) determined by the membrane potential can be described as follows, where $I_{TRPV1\ Va}$ is the voltage-activated current flowing through TRPV1.

$$4. \qquad I_{total\ Va} = I_{TRPV1\ Va} + I_{non\text{-}specific\ Va}$$

In general, whole-cell current produced by one particular type of ion channels is:

$$5.\quad I = N\,g\,P_o\,\Delta V$$

where N is the total number of functional channels in the plasma membrane; g is the single channel conductance; P_o is the open probability of the channels; ΔV is the electrochemical driving force which is defined as

$$6.\quad \Delta V = V_m - V_r$$

where V_m is the membrane potential; and V_r is the reversal potential of the ionic current.

Therefore:

$$7.\quad I_{TRPV1\,max} = N\,g\,P_{o\,max}(V_m - V_r)$$

where $I_{TRPV1\,max}$ is the voltage-activated current flowing through TRPV1 at maximum open probability; and g is the single channel conductance.

$$8.\quad I_{TRPV1\,Va} = N\,g\,P_{o\,Va}(V_m - V_r)$$

where $I_{total\ Va}$ is the total voltage-activated current evoked by HEK293 cells transfected with TRPV1.

Therefore

$$9.\quad I_{total\,Va} = N\,gP_{o\,Va}(V_m - V_r) + I_{non\text{-}specific}$$

$$10.\quad I_{total\,max} = N\,gP_{o\,max}(V_m - V_r) + I_{non\text{-}specific}$$

Hence, the $P_{o\,Va}$ and $P_{o\,max}$ can be defined as:

$$11.\quad P_{o\,Va} = \frac{I_{Total\,Va} - I_{non\text{-}specific}}{N\,g\,(V_m - V_r)}$$

$$12.\quad P_{o\,max} = \frac{I_{Total\,max} - I_{non\text{-}specific}}{N\,g\,(V_m - V_r)}$$

The open probability can be defined as:

13.

$$\frac{P_{o\,Va}}{P_{o\,max}} = \frac{\dfrac{I_{Total\,Va} - I_{non\text{-}specific}}{N\,g\,(V_m - V_r)}}{\dfrac{I_{Total\,max} - I_{non\text{-}specific}}{N\,g\,(V_m - V_r)}}$$

Or

14.

$$\frac{P_{o\,Va}}{P_{o\,max}} = \frac{I_{Total\,Va} - I_{non\text{-}specific}}{I_{max} - I_{non\text{-}specific\,Va}}$$

Whole-cell current is defined as

15. $I = G\,\Delta V$

Based on these considerations, the total conductance of HEK293 cells transfected with TRPV1 is as follows:

16.

$$\frac{P_{o\,Va}}{P_{o\,max}} = \frac{(G_{total\,Va}\,\Delta V) - (G_{non\text{-}specific}\,\Delta V)}{(G_{total\,max}\,\Delta V) - (G_{non\text{-}specific}\,\Delta V)}$$

Therefore,

17.

$$\frac{P_{o\,Va}}{P_{o\,max}} = \frac{G_{total\,Va} - G_{non\text{-}specific}}{G_{total\,max} - G_{non\text{-}specific}}$$

Based on my finding that untransfected HEK cells do not respond to capsaicin, I considered the values of $G_{non\text{-}specific}$ in the numerator and in the dominator to be the same. Thus, any difference in the value $P_{o\,Va} / P_{o\,max}$ of the different clones must be due to the changes in the voltage dependence of TRPV1. Therefore, by

measuring whole-cell currents to which TRPV1 contributes with maximum open probability and whole-cell currents to which TRPV1 contributes with less than maximum open probability due to voltage-dependent activation, I can determine changes in TRPV1 voltage-dependence attributed to the differences in the haplotypes.

2.5.10.3.2 Practical application

In order to study voltage-sensitivity, compensation was made for the capacitance and series resistance between 50 and 70 %. A voltage protocol was then applied. In these experiments both the bath and pipette solutions consisted of the following (mM): NaCl, 150; $MgCl_2$, 2; Hepes, 10; EGTA, 0.1; glucose, 10 (bath solution only); adjusted to pH 7.4.

Two methods were initially considered to be capable of inducing $P_{o\,max}$. The first method was based on work done by Voets et al (2004), who showed that the channel reached $P_{o\,max}$ at + 155 mV. This involved depolarisation of the membrane by holding the cell at + 155 mV for 100 milliseconds to induce $P_{o\,max}$ (Fig. 2.31). This was then followed by voltage steps from +155 mV to -130 mV, in 15 mV step intervals, of 100 milliseconds duration, to evoke tail-currents followed by steady-state currents produced by voltage-dependent activation, before returning back to the holding potential of 0 mV (Fig. 2.31). There are two problems with this voltage step protocol: (i) due to fast gating, tail currents could be difficult to measure precisely; (ii) +155 mV may not open all the TRPV1 channels on the membrane (Matta and Ahern, 2007).

The second method involved application of 10 µM capsaicin to the cell to induce I_{max} at holding potential of + 60 mV to allow visual indication of whether the cell responded to capsaicin (i.e. produces an outward current, see capsaicin-concentration response curve for $hTRPV1_{111}$). The holding potential was then changed to 0 mV, which was followed by voltage steps + 155 mV to -130 mV, in 15 mV step intervals, of 100 milliseconds duration.

2.5.10.3.3 Response of TRPV1-transfected cell to voltage-dependence

In the majority of cells, both methods of inducing maximum TRPV1 open probability produced a linear I-V relationship ($r>0.95$). The I-V curves of the steady

state currents were different from the I-V curves of currents measured at maximum TRPV1 current. In each cell, the steady state current was smaller than the maximum TRPV1 current, produced by capsaicin at each membrane potential. This is in agreement with data published recently by Matta and Ahern (2007), that voltage is a partial activator of TRPV1. Due to reservations regarding the reliability of measuring tail currents, in the analysis, I decided to use the I-V relationship of the current flowing through the channel opened with 10 μM capsaicin to produce maximum TRPV1 current.

The V-G (voltage-conductance) and the G/Gmax curves were then constructed by using the following description. For each cell, two I-V curves were generated and analysed.

In the presence of 10 uM capsaicin, the I-V relationship of the current flowing through the channels was constructed by measuring the amplitude of the steady-state current at the end of the voltage-step (i.e. 1 millisecond before returning back to the holding potential of 0 mV). It was expected that the steady-state current produced during capsaicin application showed a linear I-V relationship because if the channel has an open probability which is not changed by the membrane potential, then the I-V curve should show ohmic relationship change not true. However, I-V curves of capsaicin-induced currents showed a small outward rectification below 0 mV. A reasonable explanation for the lack of linear I-V relationship could be that hyperpolarisation reduced the open probability slightly at 10 uM capsaicin.

In the absence of capsaicin, the I-V relationship of the current flowing through the channels with $P_{o\ Va}$ was constructed using the same steps, as mentioned above.

In theory, the voltage-activated current should be 0 nA, or near zero below certain negative membrane potentials. This is because at –60 mV membrane potential TRPV1 does not show single channel activity (Nagy and Rang., 1999;

Matta and Ahern., 2007; Raisinghani et al., 2005; Voets et al., 2004). On the other hand above a certain membrane potential, when TRPV1 reached $P_{o\ max}$, the I-V relationship should be linear.

In contrast to these expectations, I never managed to obtain a recording which had no current flowing through the cell at negative membrane potentials. This indicated that some current was present even if TRPV1 was closed at negative membrane potentials. This is in agreement with my findings made in untransfected HEK293 cells.

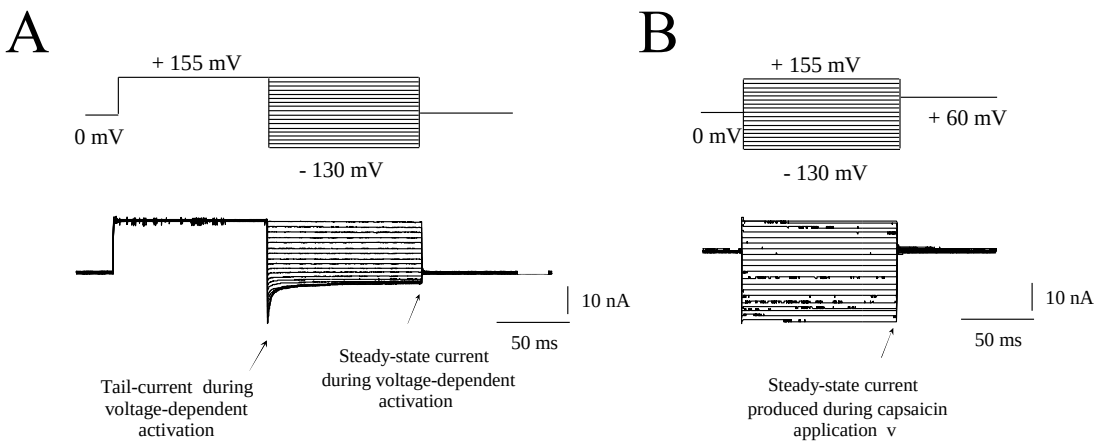

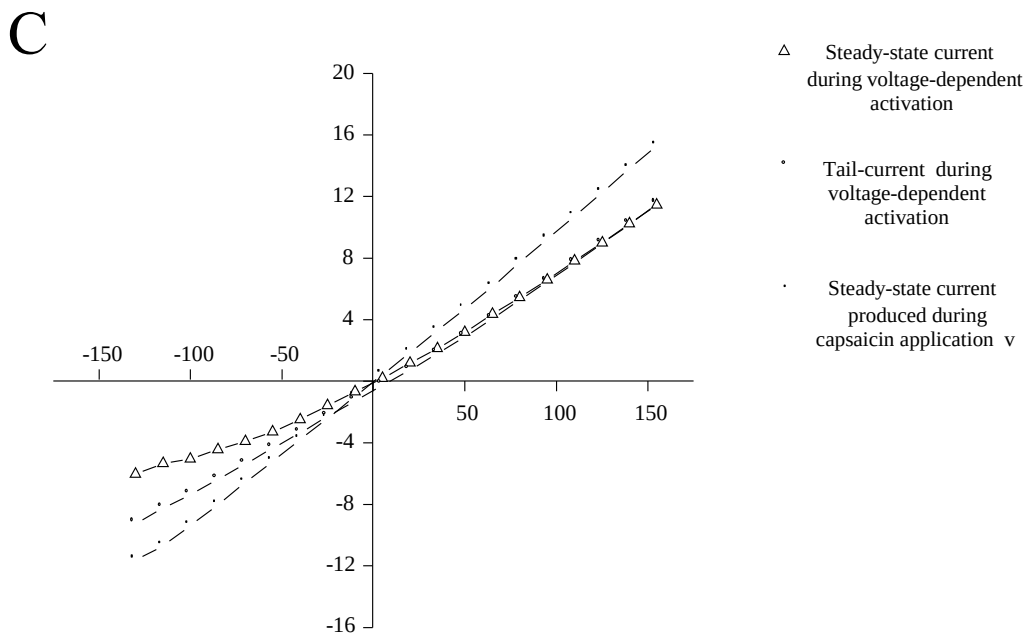

Figure 2.31. Data analysis of voltage-dependence of hTRPV1-mediated response. (A) Upper trace: Voltage protocol to evoke tail-currents and steady state currents. Lower trace: A typical recording using depolarisation to induce maximal opening probability measured at symmetrical Na+ (150 mM). (B) Upper trace: Current protocol during capsaicin-evoked activation. Lower trace: A typical recording using 10 µM capsaicin to induce maximal opening of the ion channel. (C) Current-voltage relationships of tail-current, steady-state current during voltage-dependent activation and steady-state current during capsaicin application.

The reversal potential was interpolated from the zero current intercept by plotting the two data points below and above 0 nA and fitting them with a simple linear regression. The linear equation for the linear regression was noted and the reversal potential was then calculated. The conductance G_{Va} of the steady-state current during voltage-dependent activation of the whole-cell $I_{ss\ Va}$ and maximum conductance G_{max} of the steady-state current during capsaicin application $I_{ss\ cap}$ of the whole-cell was calculated as follows:

1. $$G_{Va} = \frac{I_{ss\ Va}}{(E_m - V_r)}$$

2.

$$G_{max} = \frac{I_{ss\ cap}}{(E_m - V_r)}$$

An example of a corresponding conductance-voltage graph of the G_{va} and G_{max} can be seen in figure below (Fig. 2.32).

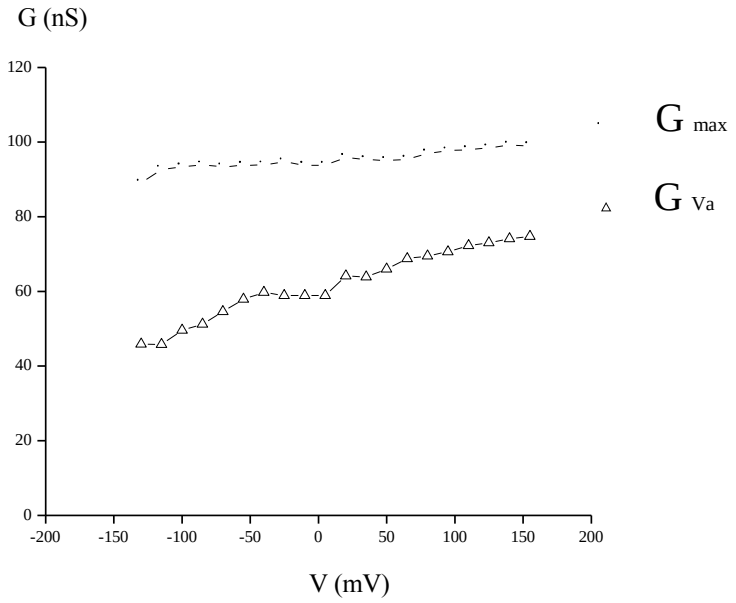

Figure 2.32 G_{Va} was calculated from the steady-state current during voltage-dependent activation whilst the G_{max} curve was constructed from the steady-state current during capsaicin application at the end of the voltage pulse. Note that Gmax is constant between ~0 and -130 mV. Above ~+60 mV it showed an increase. This increase corresponds with the voltage-dependence of non-specific current in untransfected cell (n=1). Note also that G_{va} showed increase between -120 mV and -40 mV and above 0 mV.

Then the G/G_{max} was analysed to obtain the open probability.

$$\frac{P_{o\ Va}}{P_{o\ max}} = \frac{G_{\text{total Va}} - G_{\text{non-specific}}}{G_{\text{total max}} - G_{\text{non-specific}}}$$

The points were fitted with the Boltzmann function. However, the result of the Boltzmann function showed a poor fit with an $r^2 < 0.95$ (Fig 2.33).

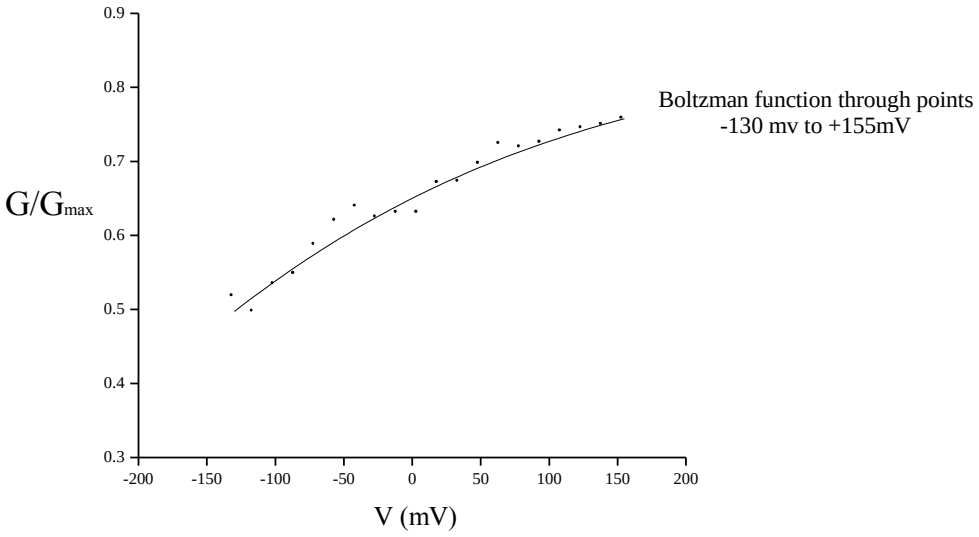

Figure 2.33 V-G/G_{max} relationship of conductances. The relationship was fitted with one Boltzmann function (r2<0.95) through all data points, from -130 to +155 mV (n=1). Note the poor fit.

A close inspection of the V-G/G_{max} relationship showed that two Boltzmann functions could be fitted instead of one, to best represent the data points (Fig 2.34).

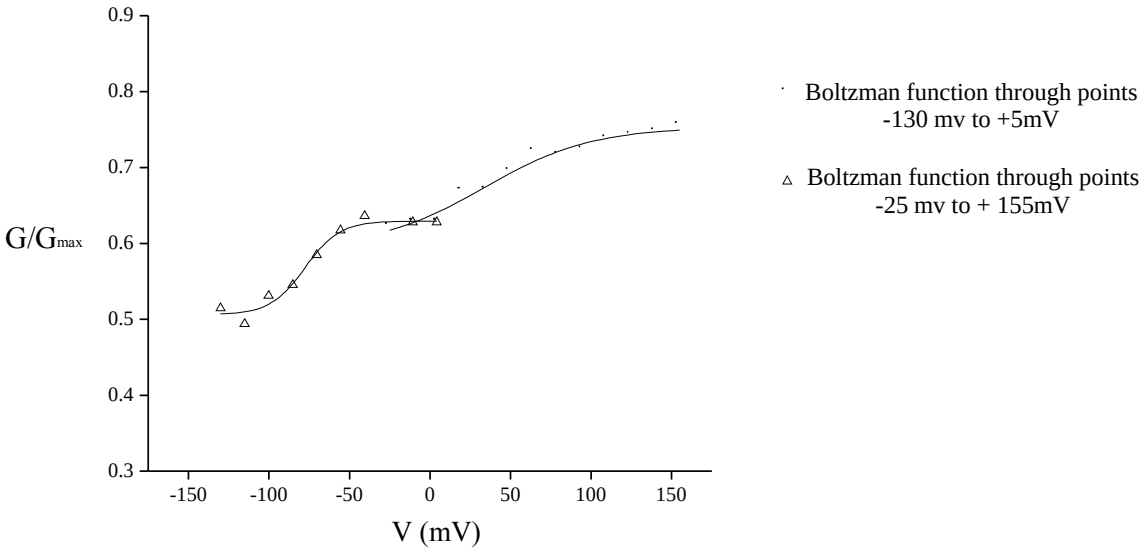

Figure 2.34 V-G/G_{max} relationship showed on fig 2.32, fitted with two Boltzmann functions. One sigmoid curve was fitted through data points from -130 mV to +5 mV (r^2>0.95), whilst another sigmoid curve was fitted through data points from -25 mV to +155 mV (r^2>0.95) (n=1). Note the high correlation coefficients of the fits.

The high correlation coefficients of the two fits, suggested the presence of two separate voltage-dependent currents in this cell: (i) between -25 mV and -130 mV; (ii) between -50 mV and +155 mV. Since untransfected cells exhibited only one voltage-dependent current, above ~0mV, these data suggest that the voltage-dependent current below 0 mV, in the transfected cells should be due to the presence and voltage-sensitivity of TRPV1.

Visual comparison of the average V-G relationships of voltage-activated currents in untransfected and hTRPV1 transfected cells (Fig. 2.35, and V-G/Gmax relationships of voltage-activated currents in hTRPV1 transfected cells confirmed that conductances in both $hTRPV1_{111}$- and $hTRPV1_{222}$- transfected had two components.

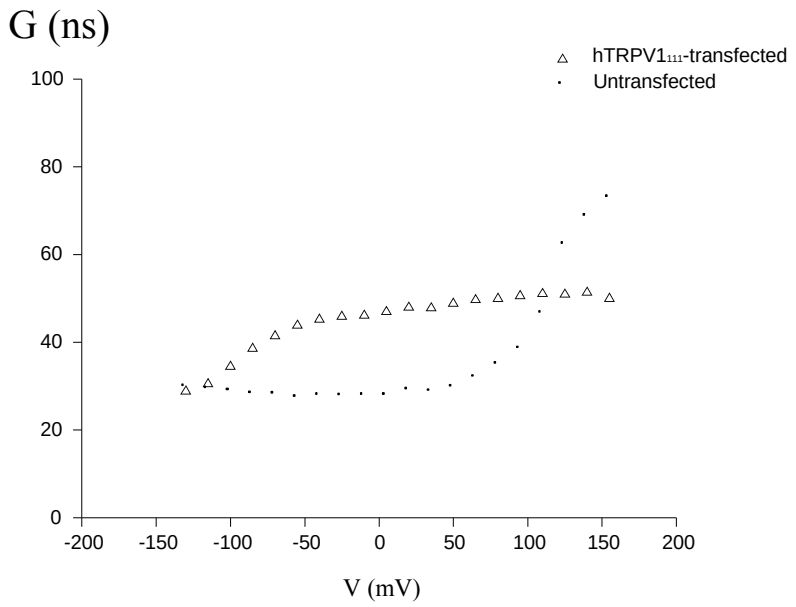

Figure 2.35 V-G relationship of voltage-activated current in untransfected cell and hTRPV1-transfected cell (n=1).

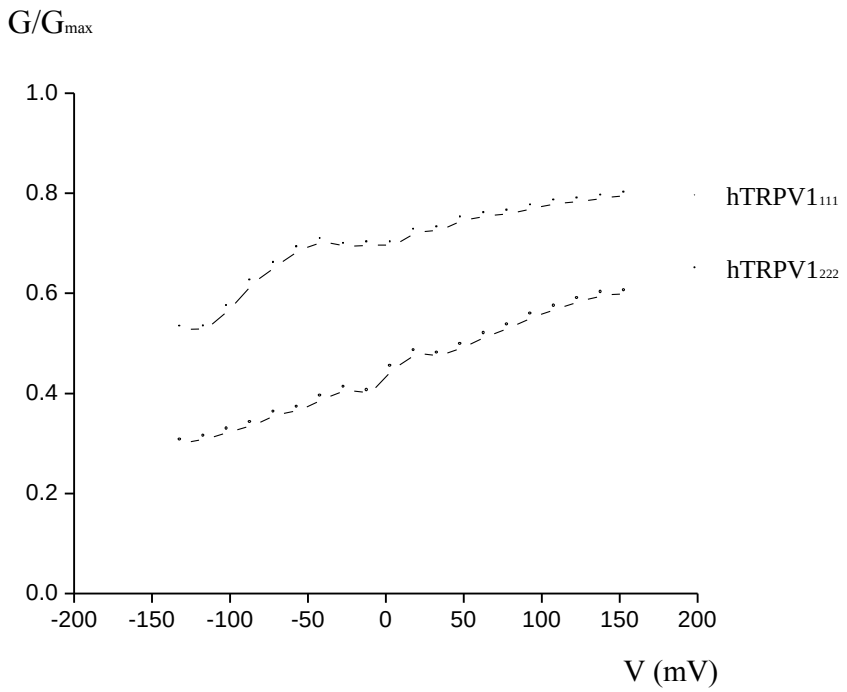

Figure 2.36 Average V-G/Gmax relationship of $hTRPV1_{111}$ and $hTRPV_{222}$. Capsaicin was used to induce maximum opening. Lines represent Boltzmann functions fitted to the data. Point represents n=1.

The transfection-associated appearance of a conductance at negative potentials together with the presence of a conductance at positive potentials both in untransfected and TRPV1-transfected cells suggested that while the conductance at negative potentials was very likely produced by voltage-dependent activation of TRPV1, the conductance at positive potentials was produced by an unidentified voltage-gated channel(s) expressed by HEK293 cells constitutively. However, comparison of the V-G relationship of the average conductance in untransfected cells to that of the TRPV1 transfected cells showed that the constitutive conductance could be affected by the transfection; in other words the two conductances might not be separated.

Therefore, proper characterisation of the voltage-dependence of TRPV1 could not be provided, i.e., the precise V1/2 of TRPV1 polymorphs alone could not be deteremined, it could only be estimated. Nevertheless, this estimation might reveal differences in voltage-dependence of the various polymoprhs if the differences are relatively large.

2.6 Statistical analysis

Statistical analysis is conveniently divided into two categories: (i) descriptive statistics; and (ii) inferential statistics.

2.6.1 Descriptive statistics

Descriptive statistics are used to quantitatively describe the basic features of the data sampled. Quantitative description is obtained by univariate analysis, which examines data from one group separately, in terms of central tendency, variability and distribution.

2.6.1.1 Central tendency

Central tendency is the value in a group of values which is the most *typical* for the group, or is a measure of the centre of distribution of values. There are three types of measures of central tendency: mean, median and mode. The description here is based on accounts given by Hinton (2004) and Coolican (2005).

The mean is the most commonly used measure of central tendency. The mean is the sum of observations divided by the number of observations. In most cases, the mean is not the same value as any values in the group. An advantage of using the mean is that all data values are used in the calculations and can be used in inferential statistics. However, the mean is more susceptible to extreme values in a data group. A single extreme value in one direction (an outlier) can distort the mean, whereas extreme values in both directions tend to cancel each other out (Coolican, 1995; Hinton, 2004).

The median is the value halfway through a range of numbers that are arranged in numerically order: ranked in ascending or descending order. If the data set has an odd number of values, the median is the central value of the ordered set. However, if

the data set has an even number of values the mean of the two central values is the median.

The mode is the value that occurs most often in a set of data. Data with one mode is referred to as unimodal distribution. However, there may be more than one mode from a set of data: hence, bi-modal (two modes) distribution or multimodal (several modes) distribution. An advantage of using the median and the mode is that they are not affected by extreme values in a set of data (Keeping, 1995).

For all data sets, the mean ($\underline{X}$) was computed as the sum of all scores ($\sum x$) divided by the total number of scores (N)

$$\overline{X} = \frac{\sum X}{N}$$

The mean of a group of data was calculated in *Excel*, where the function was performed by the formula where Array1 is the data set being analysed:

= AVERAGE(Array1)

2.6.1.2 Variability

Variability, or dispersion, of data refers to the spread of the values from the mean and can be expressed by the range, variance or standard deviation.

The range is the maximum value minus the minimum value from a group of data. The range is greatly affected by extreme values in one direction and does not include all values from a group.

Standard deviation refers to the relationship between the variability of the data from a group to the mean of the group. For example, the standard deviation is small if the values from a group are similar to the mean (standard deviation is zero when the data

are equal to the mean). The standard deviation is large if the values are distant from the mean. Standard deviation (s) is the root mean square deviation of values from the mean of a group.

$$S = \sqrt{\frac{\sum (X - \overline{X})^2}{N-1}}$$

where $\sum$ is the sum , X is the individual score, $\overline{X}$ is the mean of all scores, N is the sample size, and $\sqrt{}$ is the square root.

The variance is the sum of squared deviations from the mean divided by the number of observations. Hence, standard deviation is the square root of the variance or the variance is the standard deviation squared.

$$\text{Variance} = S^2$$

Standard deviation is easier to interpret in terms of the range of data from a group than the variance, thus it is the most common measure of variability. The main advantages of using standard deviation instead of the range are that: (i) standard deviation considers all data in a group; (ii) is able to illustrate variation above and below the mean; and (iii) is able to identify outliers from a group of values (Coolican, 1995; Hinton, 2004).

I calculated the standard deviation of a group of data was calculated in *Excel*, where the function was performed by the formula:

$$= \text{STDEV(Array1)}$$

where Array1 is the data set being analysed.

2.6.1.3 Distribution

The distribution is a summary of the frequency of individual values from a group of data, usually represented in a histogram or bar chart. There are three main characteristics to describe the frequency distribution histogram of a set of data: modality, skewness and kurtosis.

The *modality* describes the number of modes (distinct humps) in a distribution. The modality of distribution can be unimodal (one mode), biomodal (two modes), or multimodal (more than 2 modes).

The *skewness* is a measure of the asymmetry of the distribution, i.e., a symmetrical distribution exhibits no skewness and has a numerical value of zero. In a symmetrical unimodal distribution, all three central tendencies are located at the same point and hence, are equal to each other. An asymmetric frequency distribution can be either positively skewed or negatively skewed. A distribution is positively (right) skewed if the scores cluster around the lower end of the scale (i.e., smaller values), with progressively fewer scores at the upper end of the scale (i.e., larger values). In positively skewed distributions, the mean is larger than the median and has a numerical positive value. A distribution is negatively (left) skewed if the scores cluster around the upper end of the scale, with progressively fewer scores at the lower end of the scale. In negatively skewed distributions, the mean is smaller than the median and has a numerical negative value.

The *kurtosis* characterises the 'peakness' of a histogram, i.e., a normal distribution (see below) exhibits no kurtosis and exhibits a numerical value of zero. Kurtosis describes the extent to which the frequency distribution of scores is concentrated around the mode of the distribution. If a distribution is more peaked than a normal distribution, the kurtosis has a numerical negative value and is referred to as "leptokurtic". However, if a distribution is flatter than a normal distribution, the kurtosis has a numerical positive value and referred to as "platytkurtic".

In many natural processes, random variation conforms to a particular probability distribution known as the normal distribution. Normal distribution, also referred to as Gaussian distribution, is a theoretical frequency distribution for a set of variable data and can be explained by the Central Limit Theorem (CLT; Hinton, 2004). The CLT states, that regardless of the distribution of the data from a group, the distribution of the means of the random values approaches a normal distribution. Normal distribution is usually represented as a symmetrical bell-shaped density curve, with a single peak at the centre of the distribution. The single peak represents the mean, mode and median of the distribution. The spread of data or the girth of the bell curve represents the standard deviation.

Normal distribution can be transformed to *standard normal distribution,* by subtracting the mean of the group from the individual raw data and then dividing the difference by the standard deviation of the group. This conversion process will normalise data. Standard normal distribution, also referred to as *z distribution*, has a mean of zero and a standard deviation of 1, but the original symmetry or shape of the distribution remains unchanged. A z score indicates the number of standard deviation above or below the mean. All standard normal distributions satisfy the *Empirical Rule*, which provides that: (i) ~ 68% of all values fall within 1 standard deviation of the mean; (ii) ~ 95% of all values fall within 2 standard deviations of the mean; and (iii) ~ 99.7% of all values fall within 3 standard deviations of the mean (Fig 2.37).

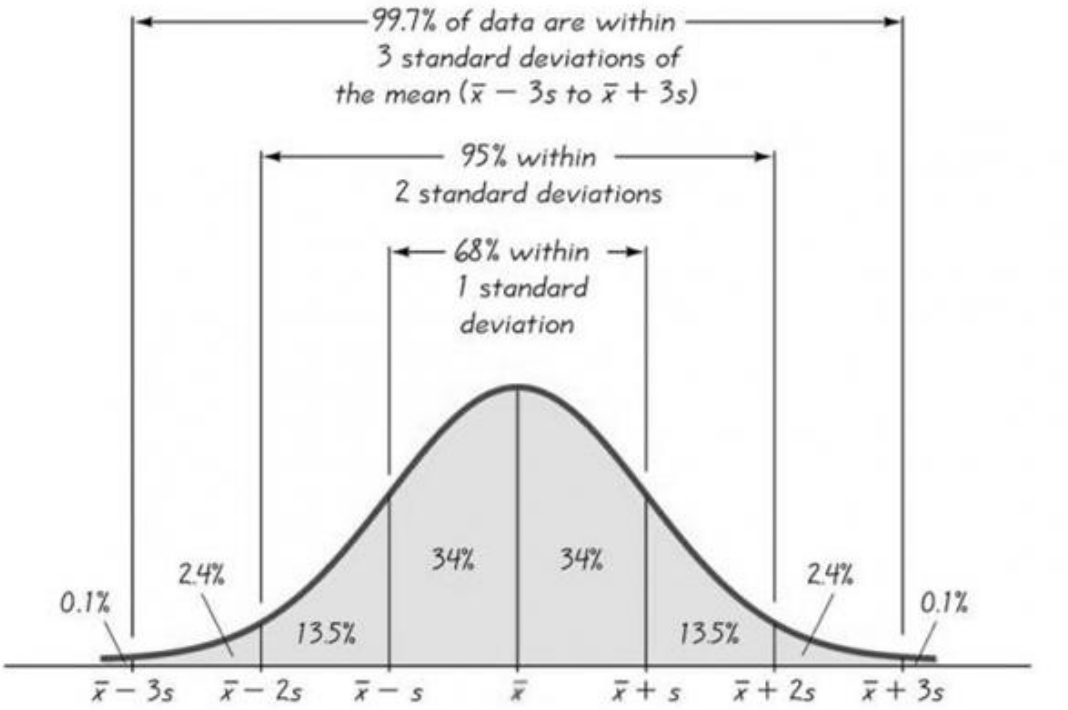

Figure 2.37 Normal distribution curve and the Empirical Rule. The curve is bell-shaped, where the mean, median, and mode are equal and are located at the centre of the distribution. The curve is symmetric to the mean (both sides of a vertical dashed line passing through the centre). The curve is continuous, that is, there are no gaps or holes. The curve never touches the x axis. The total area under a normal distribution curve is equal to 100%. The standard deviation (*s*) around the mean (*x*) is presented as the width. The Empirical Rule for normal distribution states that almost all data will fall within three standard deviations of the mean. (Taken and adapted from http://rchsbowman.wordpress.com/2009/09/08/statistics-notes-%E2%80%94-interpreting-standard-deviation-%E2%80%94-the-empirical-rule-68-95-997-rule/.)

2.6.1.4 Sampling distribution of the mean

The *sampling distribution* of the mean must also be considered as part of the descriptive analysis of data as it is used to construct confidence intervals and in significance testing (see later). The *sampling distribution* of the mean states that in a population with a mean and a standard deviation, the sampling distribution of the mean has mean and a standard deviation. The standard deviation of the sampling distribution of a mean is referred to as the standard error of the mean (SEM; Fig 2.38).

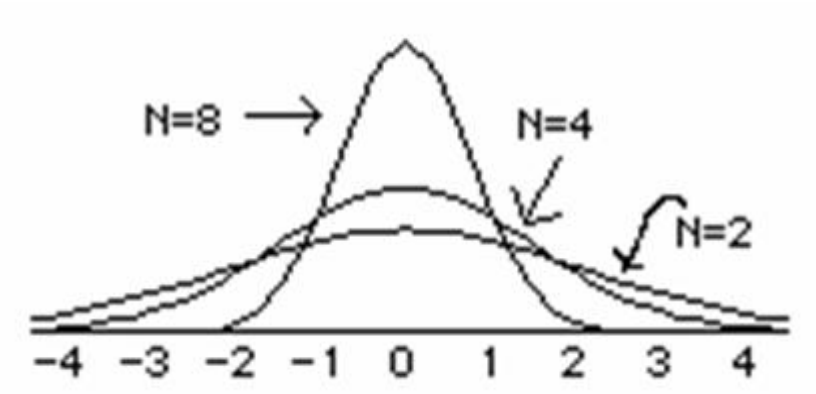

Figure 2.38 The spread of the sampling distribution of the mean. Note that as the number of sample sizes increases the spread of the sampling distribution decreases. However, the mean of the distribution is not affected by sample size. (Taken from Lane, 2009).

SEM is calculated by dividing the standard deviation by the square root of the number of samples (*n*) from a group. Hence, SEM is always smaller than standard deviation.

$$S_M = \frac{S}{\sqrt{N}}$$

where S_M is SEM, S is the standard deviation, √ is the square root, and N is sample size.

The main advantage of using SEM is that it takes into account, the standard deviation and the sample size of the group. SEM gets smaller as the number of samples increase.

I calculated the SEM of group of data was calculated in *Excel*, where the function was performed by the formula:

=STDEV(Array1)/SQRT(COUNT(Array1))

where Array1 is the data set being analysed:

2.6.2 Inferential statistics

Inferential statistics are used to make predictions about a population based on the data collected from small sample taken from that population. These statistics are dependent on the use of random sampling which ensures that a sample is representative of the population.

The two main methods used in inferential statistics: estimation statistics and hypothesis testing.

2.6.2.1 Estimation statistics

Estimation statistics are used to make estimates about the population based on the sampled data. In estimation statistics, the sample is used to estimate a parameter and a confidence interval about the estimate is calculated.

2.6.2.1.1 Parameter estimation

Parameter estimation statistics are used to determine the values of parameters based on the sampled data. Parameter estimation statistic tests include the linear regression model and the non-linear regression mode.

2.6.2.1.1.1 Linear regression model

A linear relationship between two variables (i.e., x and y, where y is a function of x) is usually first assessed by drawing a straight line through the points using a scatter plot. The line is drawn as near possible to the various points so as to best represent the trend and is referred to as the *line of best fit* or *trend line.* Linear regression line finds the best fit of a linear relationship between two variables and analyses these values with a correlation coefficient. The linear regression model was used by me when analysing the heat threshold of activation of hTRPV1-transfected cells during an application of a heat ramp (37-50 ^{o}C).

The linear regression equation is:

$$y = A + B * x$$

where y is the dependent variable, A is y intercept, B is the gradient of the slope and x is the independent variable

2.6.2.1.1.2a Correlation coefficient of a linear regression

Correlation analysis is a statistical test for measuring the relationship between data from two variables. Correlation coefficient (r) quantifies the strength of the *linear regression* between the variables and ranges from -1 to +1. (In comparison, r^2 quantifies the strength of the *nonlinear* regression *between the variables).* A positive coefficient indicates a direct relationship, where the variables change in the same direction, whilst a negative coefficient indicates an inverse relationship where one variable increases while the other decreases (Jones et al., 2007). A coefficient of zero implies that the two variables show no linear relationship; whilst an r value of -1 or +1 indicates that all points lie exactly on the line with no scatter. The Pearson's correlation coefficient is used, if the variables are normally distributed (parametric). If the data are not normally distributed (non-parametric), the Spearman's correlation coefficient is used (Sonnergaard, 2006).

Fitting a linear regression line

The simplest method of assessing linear regression is to plot the two variables, independent (x) and dependent (y) variable and fit a linear regression line to the points. All linear regression lines were done with the *fit linear* tool in Origin statistical analysis software; the r value and the values *A* and *B* from the linear regression equation were calculated.

2.6.2.1.1.2 Non-linear regression model

Non-linear regression models employed as part of my work included: the Gaussian distribution, the sigmoidal dose response and the Boltzmann sigmoidal

2.6.2.1.1.2a Gaussian distribution

The Gaussian distribution is a bell-shaped distribution of results from a normal sample population. Gaussian distribution was used when analysing agonist-evoked cobalt-labelling light intensity data.

The Gaussian equation is defined as:

$$Y=Amplitude*exp(-0.5*((X-Mean)/SD)^2$$

where *Amplitude* is the height of the centre of the distribution in Y units, *Mean* is the X value at the centre of the distribution. SD or standard deviation is a measure of the width of the distribution, in the same units as X (Motulsky, 2007).

Fitting a Gaussian curve to a histogram

The simplest method of assessing normal distribution or normality is to plot the frequency distribution histogram of the data and to fit a Gaussian curve to the histogram. All Gaussian curve fitting was performed by me with a curve fit tool in Origin statistical software analysis (OriginLab Corp).

First the raw data for a range of values was highlighted, and then under *Descriptive Statistics*, *frequency count* was selected. Frequency count is the number of events of a particular sort. This function opens the *Count* dialog box, in which the minimum and maximum values and the step size increments are specified. The programme then creates a set of bins, beginning at the minimum value and based on the step size

specified. The number of times a value is encountered which falls within the several bins is recorded. This function returns the result in the form of a worksheet: the first column shows the mid-point value in each bin and the second column displays the number of hits observed for each bin. A histogram can then be constructed with these values (OriginLab, 2007).

If the histogram appeared to visually display the presence of one bell-shaped curve with a single peak at the centre of the distribution, one normal distribution curve was fitted by selecting *Fit Gaussian*, under *Analysis* tab. If the histogram appeared to visually display the presence of two or more distinct peaks, multiple normal distribution curves were fitted by selecting *Fit Multiple-peaks* and *Gaussian*. This function opened a *Number of Peak* dialog box, in which the number can be entered. Using the cursor, the peak of each distribution was selected. The programme then fits a Gaussian curve or curves onto the histogram and a data dialog box appears with an r^2 value and confidence intervals which describes the relationship between the fitted curve and the histogram. The fitted parameters in terms of width, maximum amplitude, areas of the curve with SEM, are also computed.

2.6.2.1.1.2b Sigmoid curve

The sigmoid curve is an S-shaped curve, which is common curve in biological distributions as it describes the relationship between the amount of dose of a substance and the resulting response (Fig 2.39). Thus, it is referred to as the sigmoidal dose-response curve. Two assumptions are made when using this function: (i) that there is almost always a dose below where no response can be measured; and (ii) that once a maximum response is reached any further increases in the dose will not result in any increased effect. Sigmoidal dose-response curve was used to contract capsaicin- and pH-evoked hTRPV1-activated current

The equation for a dose-response curve is:

$$Y = \text{Bottom} + \frac{(\text{Top} - \text{Bottom})}{1 + 10^{\text{LogEC50}-X}}$$

where the variable *Bottom* is the *Y* value at the bottom region; *Top* is the *Y* value at the top region, and LogEC50 is the X value when the response is halfway between Bottom and Top. LogEC50 is the logarithm of the EC_{50} (effective concentration, 50%). This equation assumes a standard slope, where the response goes from 10% to 90% of maximal as X increases over about two log units. All sigmoidal dose-response curves were fitted using either Origin or Graphpad Prism statistical analysis software, were EC_{50} and maximal amplitude response, in this case current (I_{max}) response were computed with a SEM. r^2 value and confidence intervals were also shown (see later).

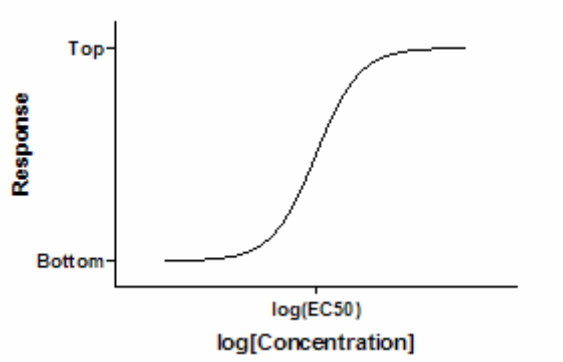

Figure 2.39 Sigmoidal dose response curve. The response is shown as a function of the logarithm of concentration. X is the logarithm of agonist concentration and Y is the response. (Taken from Graphpad Software Inc, 2007).

Statistical comparisons between two dose-response curves were analysed using Graphpad Prism statistical analysis software. EC_{50} and the I_{max} values were compared using Student t-test (two-tailed test, equal variance) to compare best fit variables of the non-linear regression used (see later).

2.6.2.1.1.2c Boltzmann curve

The Boltzmann curve can describe the voltage dependent activation of ion channels.

The equation for the Boltzmann fit

$$Y = Bottom + \frac{(Top - Bottom)}{1 + \exp\left(\frac{V50 - X}{Slope}\right)}$$

where the conductance varies from *Bottom* to *Top*. V_{50} is the potential at which conductance is halfway between *Bottom* and *Top* (Fig. 2.40). *Slope* describes the steepness of the curve, with a larger value denoting a shallow curve. Slope is expressed in units of potential, usually mV, and is positive for channels that activate upon depolarization. Under appropriate experimental conditions, the *Slope* is used to calculate the valence (charge) of the ion moving across the channel. *Slope* equals RT/zF where R is the universal gas constant, T is temperature in °K, F is the Faraday constant, and z is the valence. Since RT/F » -26 mV at 25°C, z = -26/SLOPE. *Bottom* is commonly made a constant equal to 0.0. If the *Top* is a constant equal to 1.0, then Y can be viewed as the fraction of channels that are activated (Graphpad Software Inc, 2007). All Boltzmann curves were fitted with Graphpad Prism statistical analysis software (Graphpad Software, Inc).

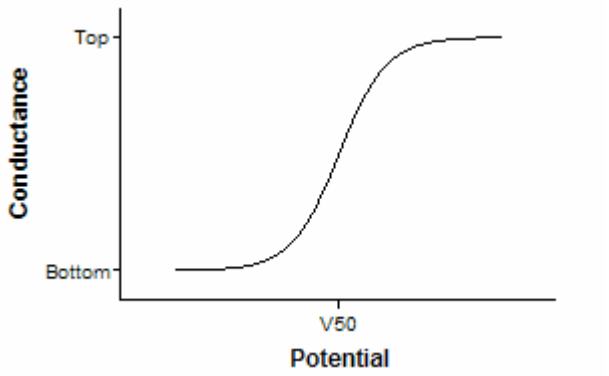

Figure 2.40 Boltzmann curve. The fit describes voltage dependent activation of ion channels. It describes conductance (Y) as a function of the membrane potential (X). (Taken from Graphpad Software Inc, 2007).

Statistical comparisons between two Boltzmann curves were analysed using Graphpad Prism statistical analysis software. V_{50} of the two curves were compared using Student t-test (two-tailed test, equal variance) to compare best fit variables of the non-linear regression used (see later).

2.6.2.1.1.3 The goodness of fit of nonlinear regression

The goodness of fit of nonlinear regression or r^2 quantifies the strength of the nonlinear regression between the variable and ranges from 0 to 1. An r^2 value of zero implies that the two variables show no relationship, whilst an r^2 value of 1 indicates that all points lie exactly on the curve with no scatter. r^2 is computed from the sum of the squared values of the distances of the points from the best-fit curve determined by nonlinear regression.

2.6.2.1.1.4 Confidence intervals

Confidence interval is a measure of the accuracy of an estimated value. The interval represents a range of values, consistent with data that has a generally high probability of capturing the true population value. Confidence level, expressed as a percentage or a probability, is the likelihood that the confidence interval will contain the true population parameter. Confidence intervals are therefore defined in terms of confidence levels. Confidence intervals can be constructed from any level of confidence level. The most common levels are 90 %, 95 % and 99 %.

For example, selecting 95 % confidence level means that there is a 0.95 probability - that the specified interval will include the true population parameter.

2.6.2.2 Hypothesis testing

Hypothesis testing uses statistical data analysis to make statistical conclusions about whether or not the sample data supports a particular hypothesis. Thus, in statistics, a hypothesis is a predication of a relationship between data to be measured. Hypothesis testing uses statistics to determine if the hypothesis is not true with a high probability. Hypothesis testing consists of the following steps:

(i) Formulation of hypotheses: Two hypotheses are initially stated. The null hypothesis (H_0) states that one group of data is not different from another group of data.

$$H_0 : \mu 1 = \mu 2$$

where μ1 is population l mean, and μ2 is a population 2 mean. The alternative hypothesis (H_A) is a statement which is true if the null hypothesis false, that is the refusal of H_0.

$$H_A : \mu 1 \neq \mu 2$$

where ≠ is not equal. Furthermore, the H_A can either one-tailed or two-tailed. One-tailed alternative hypothesis includes the direction of the effect according to the null hypothesis.

$$H_0 : \mu 1 = \mu 2$$

$$H_A : \mu 1 < \mu 2 \quad \text{or} \quad H_A : \mu 1 > \mu 2$$

A two-tailed alternative hypothesis predicts no direction of the result corresponding to the null hypothesis.

$$H_0 : \mu 1 = \mu 2$$

$$H_A : \mu 1 \neq \mu 2$$

(ii) Setting the critical p-value or statistical significance level: The probability value, also referred to as the p-value, is the probability that the value obtained in a statistical test is due to chance, rather than a true relationship between the groups being compared.

A critical value is the value that a statistical test must exceed in order for the null hypothesis to be rejected. Thus, significance level is the fixed critical p-value, to determine whether or not the null hypothesis is rejected. The most universally accepted level of statistical significance is 0.05 or 5%, also written as p = 0.05. This means that there is 5% chance that the null hypothesis is rejected, even though it is true.

(iii) Identify the appropriate statistical test to calculate critical value: To assess the truth of the null hypothesis a suitable statistic test is used to calculate the p-value. The critical value is compared with the set significance level of the statistical test used. The critical value is always calculated assuming the null hypothesis is true.

2.6.2.2a Statistical errors: type I and type II error

In any hypothesis statistical test one can never be 100% certain that one has to reject (or accept) the null hypothesis. There is, therefore, the possibility of making an error. There are two types of statistical errors associated with hypothesis testing: Type I error and Type II error (Fig 2.41).

Type I error relates to the incidence of a false positive result. It refers to the situation where the null hypothesis is incorrectly rejected, when it should be accepted. To reduce the possibility of making a type I error, one must assign small p-values ($p \leq 0.05$) (Columb and Stevens, 2008).

Type II error relates to the incidence of a false negative result. It refers to the situation when the null hypothesis is accepted incorrectly. The "power" of a

statistical test refers to the probability of detecting a true positive result, That is, it rejects the null hypothesis when it is true. Thus the power of the hypothesis test is the probability of not committing a type II error and is estimated by subtracting the probability of making a type II error from 1 (Columb and Stevens, 2008). The most universally accepted power of an experimental study is 0.8 or greater i.e. there is at least an 80% chance of correctly detecting a difference. Power analysis can be used to reduce the risk for Type II errors by estimating in advance how big a sample is needed (Hinton, 2004).

		NULL HYPOTHESIS:	
		True:	False:
Decision:	Reject	Type I error	Correct
	Accept	Correct	Type II error

Figure 2.41 Types of statistical errors associated with hypothesis testing. (Taken from http://www.microbiologybytes.com/maths/1011-20.html).

2.6.2.2b Power analysis

Power analysis estimates in advance how big a sample is needed prior to the study to obtain a significant result. There are four components in a power analysis:

1. *The significance criterion*: The more stringent this criterion is, the lower the power.
2. *The sample size*. As the sample size increase, the power increases.
3. *The effect size*: The effect size is an estimate of how wrong the null hypothesis is, i.e, how the strength of the relationship between the variables is in the population

4. *Power*. This is the probability of falsely rejecting the null hypothesis, when in fact its true.
5. Typically, the critical value of power is equal 0.8, that is there is a 20% risk of committing a type II error. Although this percentage is high, a value of >0.8 requires much larger sample size, which is economically unaffordable (Polit and Beck, 2008).

A number of assumptions must be made when using power analysis. An estimation of what is relatively important difference may not always be clear and in studies where small differences are important, inaccuracies may be magnified. Standard deviation estimations from pilot studies may not be representative of the population as the samples are often small. Nevertheless, the power analysis provides at least some guidance with a scientific basis (Columb and Stevens, 2008). A power analysis was not calculated prior to my investigations. It was taken that value of 3, was the minimum size for each data point, as this was the minimum sample size required to calculate a standard deviation. However, when a means comparison test showed significant difference between the two groups or more in the Student t-test or 1-ANOVA, respectively (see later), where n=3, the power was calculated in conjunction with the parametric test employed. A critical value was set to 0.8. If the power calculated was >0.8, the null hypothesis for the means comparison test, was rejected.

2.6.2.2.1 Parametric tests

Prior to using a parametric test, the normality of the distribution of data must be assessed, using a normality test. Furthermore, the standard deviation between the groups of data must also be assessed for variance, as parametric tests assume equal variance between the samples being compared.

2.6.2.2.1a Test for normality of the distribution

A normality test is a statistical test used to determine whether the data sampled are from a population which is normally distributed. A normality test is useful because other statistical tests, such as t-test and ANOVA, assume that the data is from a normally distributed population. There are several tests available to analyse the homogeneity of variance, one of which is the *Shapiro-Wilk W test*.

The Shapiro-Wilk W test is used to test for normality. It tests whether the null hypothesis (i.e., that the data are normally distributed) is true. The Shapiro-Wilk W test is the preferred the test for normality because it possesses good power properties when compared to alternative tests, such as the Kolmogorov-Smirnov test and the Lilliefors Test (StatSoft, Inc. 2001). The null hypothesis for all normality tests is that the data set is similar to the normal distribution. Therefore, a sufficiently small p-value indicates non-normal data.

Performing a normality test

The normality test was used to investigate the probability of accepting the null hypothesis, that the distribution is normal and was performed using an Origin statistical analysis programme. In the Origin statistical analysis programme, the data being analysed was highlighted and under *Descriptive Statistics*, the *Normality Test (Shapiro-Wilk)* was selected. The function returns the result of the normality test under the assumption that the null hypothesis is true. The function calculates the W-value, the p-value and the decision whether the data is normal at 0.05 level. If the resulting p-value is smaller than or equal to the pre-determined significance level ($p \leq 0.05$), this suggests that the data is not normally distributed. However, if the p-value value is *larger than* the significance level ($p > 0.05$), this indicates that the data distribution is normal.

2.6.2.2.1b Test for equal variance

Equal variance across groups, or homogeneity of variance, is assumed when using parametric tests. There are several tests available to analyse the homogeneity of variance: the F-test; the Bartlett's test; and the Levene's test.

The F-test or Fisher test is used to investigate whether the variances of two groups are equal by comparing the ratio of two variances. Since variance is the standard deviation squared, the F-test formula is calculated by dividing the variance of the first sample by the variance of the second sample

$$F = S_1^2 / S_2^2$$

where S_1^2 is standard deviation squared of Group 1 and S_2^2 is standard deviation squared of Group 2. The larger of the two variances was placed as the numerator, in order for the F-value to exceed 1. If the variances are exactly the same between the two groups, the ratio of the variances has an F-value of 1. The F-test for significance indicates whether, given the sample sizes of the groups, the F-value is significant (Dever, 1991).

The Bartlett's test and the Levene's test are equal variance tests used to investigate the homogeneity of variances of three or more groups. The Bartlett's test analyses the equality of variance in populations having normal distributions. Thus, this test is sensitive to departures from normality. If the samples obtained are not normally distributed, the Bartlett's test may be used to test for non-normality. Levene's test is an alternative to the Bartlett's test as it is less sensitive to departures from normality and should be used if the data are not normally distributed (e-Handbook of Statistical Methods). For this reason, Levene's test was the preferred equal of variance test for three or more groups.

The null hypothesis for the variance test states that there are no differences between the variances of two groups or more, i.e., the variances are equal between the groups tested. Whilst, the alternative hypothesis for the variance test states that there are differences between the variances of two or more groups. Furthermore, the H_A can be either one-tailed or two-tailed: one-tailed test states the direction of the variance of the groups being compared to be less than, or more than, each other, whilst the two-tailed test does not state the direction of the variance.

Performing a test for equal variance

The F-test was used to investigate the probability of accepting the null hypothesis, that the variances of two groups are equal. An F-test was performed using an Origin statistical analysis programme. In the Origin statistical analysis programme, the data being analysed was highlighted and under *Statistics, Hypothesis Testing* was selected. Under *Hypothesis Testing, Fit Comparison was* selected. This function compares two data sets by fitting the same function to the data. The value of 0.05 was selected for significance level for comparison with the p-value for F-test. As a result, a *decision rule* was shown as a statement whether or not the population means were significantly different at a 0.05 level

Levene's equal variance test was used to assess the equality of variance of three or more groups, in terms of probability. A Levene's test was carried out in conjunctions with the analysis of variance test (see later) using the Origin statistical analysis programme (see 1-ANOVA).

2.6.2.2.1.1 Comparing the means of data

The Student's t-test and analysis of variance (ANOVA) are widely used statistical tools used to compare the means of data.

2.6.2.2.1.1 (a) Student t-test

Student's t-test is used to compare the means of two groups and assess whether the means of the two groups are statistically different from each other. The t-test assumes that the data analysed within each group are normally distributed and that the variances are equal.

The t-test is a comparison between two group means, which takes into considerations the difference in group variation and group size of the two samples.

The t-test formula states:

$$t = \frac{\bar{x}_1 - \bar{x}_2}{\sqrt{\frac{s_1^2}{n_1} + \frac{s_2^2}{n_2}}} \quad \mapsto \quad \frac{\text{difference between means}}{\frac{\text{variance}}{\text{sample size}}}$$

where $\bar{x}_1$ = mean of sample 1

$\bar{x}_2$ = mean of sample 2

n_1 = number of subjects in sample 1

n_2 = number of subjects in sample 2

s_1^2 = variance of sample 1 = $\frac{\Sigma(x_1 - \bar{x}_1)^2}{n_1}$

s_2^2 = variance of sample 2 = $\frac{\Sigma(x_2 - \bar{x}_2)^2}{n_2}$

The numerator is the difference between the means. The t-value gets larger as the means of the groups get further apart. The denominator is the standard error of the difference between the means. The probability of getting the t-value under the null hypothesis is calculated using the t-distribution. The t-distribution is a probability distribution that arises in the problem of estimating the mean of a normally distributed population when the sample size is small. Thus the t-test function returns the probability value that the t-value equals a desired value, assuming a t-distribution (McDonald, 2009).

Performing a Student t-test

The Student t-test was used to find the probability of rejecting the null hypothesis, that the means of two groups are statistically different from each other. A t-test was performed using an Origin statistical analysis programme. In the Origin statistical analysis programme, the data being analysed was highlighted and under *Statistics, Descriptive Statistics was* selected. Under *Statistics was* selected *two sample t-test*. This function opened a two sample t-test dialog box, where certain parameterswere chosen, such as the *type of test, hypothesis and power analysis.*

In t*ypes of test* two could be selected: (i) *paired test*; or (ii) *independent test*. A paired t-test was applied when the two sets of data were from the same sample and had the same sample size. Independent t-test was used when the two sets of date were from independent samples. This test may also be used even if the sample sizes are not equal. The appropriate type of test was selected.

In *hypothesis*, under the *null hypothesis*, the value of 0 was entered as the estimated difference of the sample mean, indicating no mean difference between the groups. In *hypothesis,* under *alternate hypotheses* two different types of tails could be selected: two-tailed test or one tailed test. A two-tailed test was used for all Student t-tests as no assumption was made prior to the treatment used. The value of 0.05 was selected

for significance level for comparison with the p-value for t-test. The power analysis function was also selected.

Once all the parameters were chosen, the *Compute* button was selected. The function returned the result of the t-test which was shown in the *Results Log Table* where the t-value, the p-value and a decision whether the data was normal at 0.05 levels, was shown. A *decision rule* was shown as a statement whether or not the population means were significantly different at a 0.05 level. The result of power analysis was also shown.

2.6.2.2.11(b) ANOVA

Analysis of variance (ANOVA) is used to simultaneously compare the means of more than two groups of data and assess whether the means of the groups are statistically different from each other. The name is derived from that fact that in order to assess statistical significance between the mean values of data, the variances between groups are analysed. There are lots of different experimental designs that can be analyzed with different kinds of ANOVA.

One-way ANOVA is used to test for differences among two or more independent groups with dependent variable. The independent variable is the variable being manipulated or changed. The dependent variable is the observed result of the independent variable being manipulated. 1-ANOVA for repeated measures is used when the groups are subjected to repeated measures. Factorial ANOVA is used when the experimental design studies the effects of two or more treatment variables. Multivariate analysis of variance (MANOVA) is used when there is more than one dependent variable (Hinton, 2004).

Due to the experimental design of my studies, only 1-ANOVA was used to compare the mean of more than two groups.

1-ANOVA

Before using 1-ANOVA, there are three criteria which must be met: (i) the population from which the samples are obtained must be normally distributed; (ii) the samples must be independent of each other; and (iii) the variances of the population must be equal. The null hypothesis will be that all population means are equal. Thus, the alternative hypothesis is that at least one mean is different.

1-ANOVA, calculates the mean of each group being tested and then compares the variance among these means to the average variance within each group. Thus, 1-ANOVA is expressed as a ratio, referred to as the F-ratio: the variance determined between-group differences divided by the variance determined within-group differences, also referred to as *error term.* The error term provides a measure of the variance due to chance. When the null hypothesis is true, the error term measures the same value of variance as the numerator of the F-ratioso that, as the means get further apart, the variance among the means increases (McDonald, 2009).

The F ratio is calculated under the assumption of equal population variance (f-distribution), as variation within each of the groups can be combined to form one estimate of the variation due to error. The F-distribution is a continuous probability distribution which is used to calculate the probability of getting a ratio which equals a desired value. Thus, when the probability is $p \leq 0.05$, the ratio is considered to be statistically significant.

1-ANOVA calculates the average difference between the group means. As a consequence of comparing the means of three or more groups, a relatively large mean difference between these group means may be determined even if two of the three or more group means are identical. Thus, a statistically significant F-ratio indicates that there is a statistical difference between the mean of at least two of the groups being compared. It does not indicate which groups differ from each other significantly. Therefore, a post hoc test is required to indicate where the differences lie (Urden, 2005).

2.6.2.2.1.1(c) Post hoc tests

Post-hoc tests are used at the second stage of ANOVA, if the null hypothesis is rejected, i.e., if there is a statistical significance between the means of at least two groups. There are a wide variety of post hoc tests available to analyse data. Each of these tests has advantages and disadvantages. However, all post-hoc tests use the same basic principle of comparing the differences between two means (pair-wise) against the critical difference (similar to critical value) required for significance. If the differences between two means are more than or equal to the critical difference, the difference is significant. If the differences between two means are less than the critical difference, there is no significant difference between the pairs being compared. The critical difference required to call a pair of means significantly different, is what differentiates all pair-wise tests from each other.

The *Fisher's least significant difference* (LSD), *Tukey's honestly significant difference (HSD)* and *Scheffe's* test are the most widely used tests employed to find where the differences between means lie when the Analysis of Variance indicates the means are not all equal. The Fisher's LSD test explores all possible pair-wise comparisons of means using the equivalent of multiple Student t-tests. Tukey's HSD test computes a single value which determines the minimum difference between the two means that is necessary for significance. If the mean difference is more than Tukey's HSD, the difference is considered to be statistically significant. The Tukey test is generally used when the sample sizes are all the same (McDonald, 2009; Kau and Green, 2008). Scheffe's test uses the F-ratio obtained from 1-ANOVA to test for a significant difference between any two means. The critical value for the Scheffe's test is the same as the F-ratio from the overall ANOVA. The Scheffe's' test is generally used when the sample sizes are different (McDonald, 2009; Kau and Green, 2008).

As there are substantial differences among these post hoc tests, there are advantages and disadvantages to each. Thus careful consideration as to the appropriate test

should be given in each experimental investigation. Fisher's LSD test is the *least rigorous* of post hoc tests and is most likely to result in a type I error. Tukey's HSD is similar to Fisher's LSD but is less likely to result in a type I error. Scheffe's test is one of the *safest* or *conservative* post hoc tests, as it uses an extremely cautious method for reducing the risk of a type I error. In many experimental investigations, different post-hoc tests may lead to the same conclusions and which of the above tests is actually used is often a matter of fashion or personal taste (Hilton and Armstrong, 2006).

An acceptable way of deciding which post hoc test to use is to consider the purpose of the experimental investigation. If the purpose of the investigation is to decide which of a group of treatments is likely to have an effect, it is justifiable to use the more liberal Fisher's LSD test. This is because it is better not to overlook a possible effect. In comparison, if the purpose of the investigation is to establish that a particular treatment does have an effect; it is better to use the more conservative Scheffe's and Tukey's HSD test (Hilton and Armstrong, 2006).

Performing 1-ANOVA

1-ANOVA was used to investigate whether the mean data of three or more groups were statistically different from each other was carried out using Origin statistical analysis programme. In Origin, the data being analysed was highlighted, where each column presented raw data of one group. Under *Statistics*, *1-ANOVA* was selected. This function opened the 1-ANOVA dialog box, where certain parameters were chosen, such as the *significance level*, *means comparison test* and *equal variance test*. The value of 0.05 was selected for significance level for comparison with the p-value when making the statistical decision. The means comparison test was chosen on the basis of the experimental design. If the purpose of the investigation was to decide which of a group of treatments was likely to have an effect, the Fisher's LSD test was used. If the purpose of the investigation was to establish that a particular treatment did have an effect, the Scheffe's of Tukey's HSD test were used. Furthermore, if the sample size were different from each other, the Scheffe's' test

was selected. However, if the sample sizes were equal to each other, the Tukey's test was selected. Levene's test was selected to test for equal variance of the data. Once all the parameters were chosen, the *Compute* button was selected. The function returned the results of the 1-ANOVA under the assumption that the null hypothesis is true. Summary Statistics dialog box (including the Null and Alternative hypotheses), an ANOVA table, and a decision rule were shown in the Results Log. Similar results for Levene's test for equal variance were also disclosed.

Chapter 3

DMSO ACTIVATES TRPV1

3.1 Introduction

In order to ascertain that the dimethyl sulfoxide (DMSO) employed to dissolve capsaicin did not activate or inhibit TRPV1, the DMSO-evoked effects both in untransfected and hTRPV1-transfected cells were studied. In addition, the DMSO-evoked effect was also investigated in cultured DRG neurons prepared from wild-type mice and TRPV1 knock-out mice.

3.2 Methods

The following techniques were employed in this section, namely: cell culture of HEK293 cells; primary culture of DRG neurons, transient transfection, cobalt-uptake and whole-cell patch clamp-technique. For further detail, see Chapter Two: Materials and Methods. The wild-type $hTRPV1_{111}$ haplotype was used in this investigation to assess the effect of DMSO in TRPV1-transfected HEK293 cells. For, simplicity this haplotype will be referred to as hTRPV1.

3.2.1 Whole-cell patch-clamp recordings

Whole-cell patch-clamp recordings were taken from hTRPV1-transfected and untransfected HEK293 cells in order to assess whether DMSO is able to induce currents. For further details on whole-cell patch-clamp technique, see Chapter Two.

Briefly, DMSO-mediated currents were measured using the conventional whole-cell patch-clamp technique with an Axopatch 200 B amplifier (Axon Intruments, Inc.) and the pClampex 8 software package with a laboratory PC for storing and evaluating data. All experiments were performed at a physiological temperature of 36-37 ^{o}C using a temperature controller (Wavelength Electronics). The membrane potential was held at -60 mV. Data was collected using the pClampex 8.2 data analysis programme (Axon Instruments, Inc). The cell was discarded if the membrane current following the establishment of whole-cell configuration was below -0.5 nA.

Solutions

Normal extracellular buffer consisted of (mM): NaCl, 130; KCl, 5; $CaCl_2$, 2; $MgCl_2$, 2; glucose, 10; HEPES, 10; adjusted to pH 7.4.

Patch electrodes were filled with normal intracellular buffer (mM): NaCl, 5; KCl, 130; $MgCl_2$, 1.26; HEPES, 10; adjusted to pH 7.4.

A stock solution of capsaicin (Tocris, UK) and capsazepine (Tocris Bioscience, Avonmouth, UK) was dissolved in 100 % DMSO (Sigma). All further capsaicin and DMSO dilutions were made using normal extracellular buffer. In these experiments 100 nM, 500 nM capsaicin and 5 μM capsazepine solutions containing 0.006% DMSO were used. A stock solution of allyl isothiocyanate (Aldrich) was dissolved in 100% mineral oil (Aldrich Chemical, Tokyo).

Dimethylsulfoxide (DMSO) is routinely used in laboratories to dissolve lipophilic compounds and it is totally soluble in water. DMSO has a molecular weight of 78.12 g/mol, density of 1.101 g/ml and a purity of 99.7%. The DMSO concentration and percentage in solution was calculated by reference to the dilution factor used in the experiments (Table 3.1).

DMSO dilution factor	DMSO % in solution	DMSO concentration
1 in 200	0.5%	70 mM
1 in 500	0.2 %	28 mM
1 in 1000	0.1 %	14 mM
1 in 2000	0.05 %	7 mM
1 in 4000	0.025	3.5 mM
1 in 16,000	0.006	0.9 mM

Table 3.1 DMSO in terms of dilution factor, percentage in solution and concentration.

3.2.1.1 Application of 0.2% DMSO

To investigate the effect of DMSO in transfected and untransfected cells, DMSO was dissolved in normal extracellular buffer in the following percentages, namely: 0.2%, 0. 1 %, 0.05 %, 0.025 % and 0.006 % (see Table 5.1). Application of DMSO for 10 seconds was controlled by an automated system which was itself controlled by pClampex 8 software. As a control the effect of 500 nM capsaicin was also investigated. 500 nM capsaicin was made so that the DMSO in solution was 0.006%. A concentration of 500 nM was chosen to investigate TRPV1-mediated response because it is approximately the EC50 value of capsaicin to TRPV1-expressing cells (Caterina et al., 1997; Welch et al., 2000; Hayes et al., 2000; Ahern et al., 2006).

Data were then analysed by measuring the maximum amplitude of the responses using the pClampfit 8.2 software. The maximum amplitude of both the capsaicin- and DMSO-evoked responses were established.

3.2.1.2 Application of 0.2% DMSO in the presence of capsazepine

Whole-cell recordings were also used to investigate the effect of the competitive TRPV1 antagonist capsazepine on the DMSO-evoked currents in hTRPV1-transfected HEK293 cells. In these experiments cells were continuously perfused (minimum period of 2 minutes) with 5 µM capsazepine (DMSO content 0.006%) before applying 0.2 % DMSO for 10 seconds. As a control for the antagonistic effect of capsazepine, the effect of 500 nM capsaicin (0.006%) was also investigated in this condition. The maximum amplitudes of the responses were also established.

The effect of 0.006% and 0.012% DMSO, which was the percentage of DMSO in capsaicin and capsazepine alone, and when applied at the same time, respectively, was not investigated (Table 4.2). This is because; whole-cell patch-clamp experiments showed no membrane current when 0.05 % DMSO was applied on to

hTRPV1-transfected cells (see results). Hence, we assumed that DMSO of *less than* 0.05% in solution will not evoke TRPV1-mediated membrane current. The effect of 0.206 % DMSO when 0.2% DMSO was simultaneously applied with capsazepine was not investigated as we assume that an increase of 0.006% DMSO was undetectable due to the sensitivity of the whole-cell patch-clamp configuration (noise of the set-up contributed ~15-20 pA).

3.2.2 Cobalt-uptake of hTRPV1-transfected HEK293 cells

Cobalt-uptake assay was performed on TRPV1-transfected and on untransfected HEK293 cells in order to assess the effect of DMSO.

Solutions

Buffer A contained (in mM): 57.5 NaCl, 5 KCl, 2 MgCl2, 10 HEPES, 12 glucose, 139 sucrose, adjusted to pH 7.4. Cobalt-containing Buffer B consisted of Buffer A plus the addition of 5 mM of CoCl.

In these experiments 500 nM capsaicin and 5 µM capsazepine solutions containing 0.006% DMSO were used.

3.2.2.1 0.2% DMSO application

The cobalt-uptake assay was carried out in: (i) hTRPV1-transfected HEK293 cells; and (ii) untransfected cultures, to assess whether DMSO is able to induce cobalt-labelling.

Cells were washed in Buffer A twice and then incubated for 5 minutes at 37^{o}C in either: (i) drug-free cobalt-containing Buffer B; (ii) cobalt-containing Buffer B plus 500 nM capsaicin (DMSO content 0.006 %); or (iii) cobalt-containing Buffer B plus 0.2 % DMSO. The cells were then briefly washed before precipitating the cobalt with

0.4 % mercaptoethanol for 1 minute. Cells were fixed in 70% ethanol, mounted in glycerol on slides and analysed. This was carried out in at least three independent cultures of HEK293 cells.

3.2.2.2 0.2% DMSO application in the presence of capsazepine

In order to investigate the effect of the competitive TRPV1 antagonist, capsazepine, on the DMSO-evoked cobalt-labelling of hTRPV1-transfected HEK293 cells the following protocols steps were carried out, see table 3.1.

Six cover-slips containing transfected cells were washed twice in Buffer A. They were then pre-incubated for 5 minutes at 37^{o}C in the respective treatment group indicated in table 3.1 under the heading of "pre-incubation for 5 minutes" containing either drug-free Buffer A or Buffer A containing 5 uM capsazepine (DMSO content of 0.006 %). A pre-incubation step was used to allow the antagonist to occupy the binding sites of the receptor without interference from the agonist. The cells were then incubated in cobalt buffer for a further 5 minutes at 37^{o}C in shown in Table 4.2, under the heading of "incubation for 5 minutes" in Buffer B containing cobalt ions, where 0.2 % DMSO and 500 nM capsaicin (DMSO content 0.006 %) were used. The cells were then briefly washed before precipitating the cobalt with 0.4% mercaptoethanol for 1 minute. Cells were then fixed in 70% ethanol, mounted in glycerol on slides and analysed. This was carried out in at least three independent cultures of HEK293 cells.

We have been using capsazepine in our laboratory as a capsaicin receptor antagonist for studying TRPV1-mediated responses. Although at first capsazepine was shown to be a selective and specific inhibitor of capsaicin-evoked currents in primary sensory neurons (Bevan et al., 1991, 1992; Dickenson and Dray, 1991; Dray et al., 1991), later it was found to inhibit patch-gated calcium currents with an IC50 of 7.7 uM (Docherty et al., 1997). Therefore, we have been using 5µM capsazepine routinely in our laboratory. We used the same concentration of capsazepine in these

experiments, although using higher capsazepine concentration in studying TRPV1-mediated responses either by whole-cell patch-clamp recordings or cobalt uptake should not have any non-specific effect. During whole-cell recordings the membrane potential is kept at -60 mV constantly therefore we do not activate patch-gated calcium channels. Due to the low Na+ concentration in the cobalt uptake buffer it is very unlikely that patch-gated Ca2+ channels are activated. Further, cobalt cannot pass through voltage-gated calcium channels (Llinás and Sugimori, 1980; Toomim et al., 1992; Shen, 2006; Nagy et al., 1993).

Protocol	Pre-incubation treatment for 5 mins	Incubation treatment for 5 mins	% DMSO in incubation treatment
A	Buffer A	Buffer B	0
B	Buffer A	Buffer B + Capsaicin 500 nM	0.05
C	Buffer A	Buffer B + 0.002% DMSO	0.20
D	Buffer A + Cpz 5 µM	Buffer B + Cpz 5 µM	0.05
E	Buffer A + Cpz 5 µM	Buffer B + Cpz 5 µM + Capsaicin 500 nM	0.10
F	Buffer A + Cpz 5 µM	Buffer B + Cpz 5 µM + 0.002% DMSO	0.206

Table 3.2. Protocols of cobalt-uptake assay to investigate the effect of capsazepine (Cpz) on capsaicin-evoked and DMSO-evoked cobalt-labelling. The percentages of DMSO in the incubation treatment step were calculated.

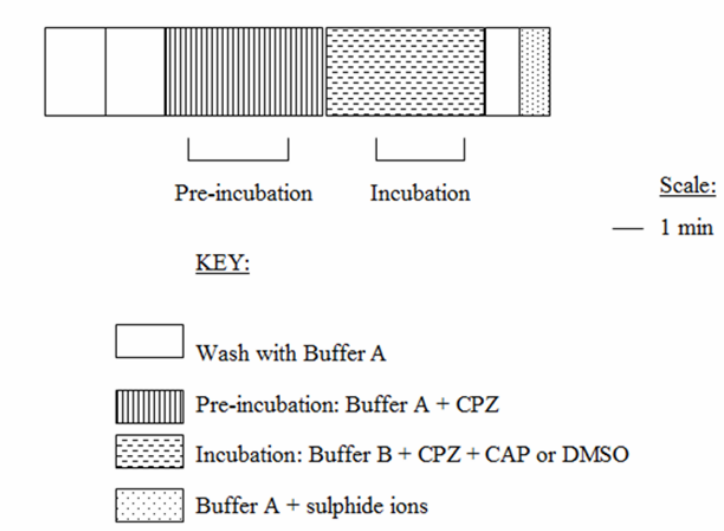

Figure 3.1 Sequence of treatment steps performed to investigate capsazepine on capsaicin-evoked and DMSO-evoked capsaicin-evoked cobalt-labelling.

3.2.2.3 Repeated applications of capsaicin and DMSO in the presence and absence of calcium ions.

Cobalt-uptake was also used to investigate the effect of repeated applications of capsaicin and DMSO in the absence and presence of calcium ions as desensitisation is calcium-dependent (Koplas et al., 1997; Mohapatra et al., 2003).

Buffer A and Buffer B was first composed by Hogan 1983, which excluded Ca^{2+} ions, to prevent these ions from competing with cobalt ions for entry. Of course, TRPV1 responses are affected by calcium, as calcium entry into the cell results in desensitisation/ tachyphlaxis (Koplas et al., 1997; Mohapatra et al., 2003). Therefore, in the absence of calcium, no desensitisation/ tachyphlaxis occurs. Furthermore, during successive application of capsaicin in the absence of calcium no reduction of cobalt influx should occur (Mandadi et al., 2003). The effect of two successive applications of capsaicin and DMSO in the presence and absence of 2 mM $CaCl_2$ were investigated. This was carried out on at least three independent cultures of mice DRG.

Since the original solutions used in the cobalt-uptake technique were made without $CaCl_2$ the effect of repeated application in the absence of Ca^{2+} was first investigated. Nine cover-slips containing hTRPV1-transfected cells were washed twice in Buffer A and then pre-incubated for 5 minutes at 37 ^{o}C as indicated in the table below (Table 3.3) under the heading, "pre-incubation for 5 minutes". The cells were washed again twice with Buffer A. The cells were then incubated in a cobalt-buffer for a further 5 minutes at 37 ^{o}C as described in the table below under the heading, "incubation for 5 minutes". The cells were then briefly washed once before precipitating the cobalt with 0.4 % mercaptoethanol (Fig. 3.2). Cells were fixed in 70% ethanol, mounted in glycerol on slides and analysed.

Next the effect of repeated application in the presence of Ca^{2+} was investigated. Since the original solutions used in the cobalt-uptake technique were made without $CaCl_2$, two additional buffers were made: Buffer A containing 2 mM CaCl; and Buffer B containing 2 mM CaCl. This was carried out in at least three independent cultures of HEK293 cells.

Protocol	Pre-incubation for 5 mins	Incubation for 5 mins
A	Buffer A	Buffer B
B	Buffer A	Buffer B + Capsaicin 500 nM
C	Buffer A	Buffer B + 0.2 % DMSO
D	Buffer A + Capsaicin 500 nM	Buffer B
E	Buffer A + Capsaicin 500 nM	Buffer B + Capsaicin 500 nM
F	Buffer A + Capsaicin 500 nM	Buffer B + 0.2 % DMSO
G	Buffer A + 0.2 % DMSO	Buffer B
H	Buffer A + 0.2% DMSO	Buffer B + Capsaicin 500 nM
I	Buffer A + 0.2% DMSO	Buffer B + 0.2 % DMSO

Table 3.3 Protocols of cobalt-uptake assay to investigate the effect of repeated applications of capsaicin and DMSO.

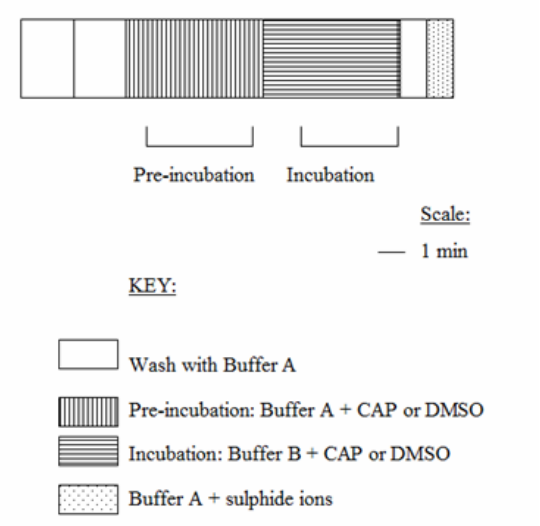

Figure 3.2 Sequence of treatments steps investigates the effect of successive applications of capsaicin and DMSO.

3.2.2.4 Application of capsaicin dissolved in varying percentages of DMSO

I also used the cobalt-uptake assay in order to assess whether the DMSO content in a capsaicin solution had any effect in mediating the responses of hTRPV1 activation to the capsaicin.

Six cover-slips containing transfected cells were washed twice in Buffer A. The cells were then incubated in Buffer B containing 100 nM capsaicin dissolved in various percentages of DMSO, namely: 0.1 %, 0.05 %, 0.012%, 0.025 % and 0.006 % for 5 minutes at 37^{o}C (refer to Table 3.1). As a control, the sixth coverslip was only incubated in drug-free cobalt-containing Buffer B. The cells were then briefly washed before precipitating the cobalt with 0.4 % mercaptoethanol. Cells were fixed in 70% ethanol, mounted in glycerol on slides and analysed. This was carried out in at least three independent cultures of HEK293 cells.

3.2.2.5 Cobalt-uptake on cultured DRG neurons

The cobalt-uptake assay was also used in DRG cultures obtained from wild-type and TRPV1-knock-out mice to assess whether DMSO is able to induce cobalt-labelling through native TRPV1 ion channels. See "Chapter Two: Cell culture of DRG neurons" for further details.

In these experiments cells were washed in buffer A twice and then incubated for 5 minutes at 37 ^{o}C in either: (i) drug-free cobalt-containing Buffer B; (ii) Buffer B containing 500 nM capsaicin (DMSO content 0.006%); (iii) Buffer B containing 0.2 % DMSO; and (iv) cobalt buffer containing 60 µM mustard oil (positive control for cobalt-uptake on DRG neurons obtained from TRPV1 knock-out mice). The cells were then briefly washed before precipitating the cobalt with 0.4% mercaptoethanol. Cells were then fixed in 70% ethanol, mounted with glycerol on slides and analysed. This was carried out in at least three independent DRG neuronal cultures.

Mustard powder was dissolved in 100 % mineral oil so that the solution contained 0.05 % mineral oil. Although the effect of 60 μM mustard oil cobalt-labelling may be due to either the mustard oil alone or the mineral oil which the mustard oil was dissolved in or a combination of the two, the effect of 0.05% mineral oil was not investigated. This is because the purpose of using mustard oil was used to investigate whether the DRG neurons obtained from knock-out mice were healthy and could respond to agonist-evoked cobalt-labelling other than capsaicin-evoked labelling.

3.2.3 Statistical analysis

Differences between the variances were analysed by the F-test or the Levene's test, as appropriate. The normality test (Shapiro-Wilk) was used to investigate whether the data was normally distributed. Differences between the averaged values were analysed by 1-ANOVA or an independent two-sample t-test, as appropriate. Following ANOVA, Fisher's LSD test was used to establish the statistical significance of the differences. Differences were regarded as being statistically significant at $p<0.05$.

In whole-cell recordings, the data are presented as mean ± standard error of means of the maximum amplitude of the current from different cell and *n* refers to the number of cells on which a given treatment was repeated. In cobalt uptake studies, the data are presented as mean ± standard error of means is the number of cobalt-labelled cells. In cobalt uptake studies, n refers to the number of independent cultures on which a given treatment was repeated.

3.3 Results

3.3.1 Properties of DMSO-evoked hTRPV1-mediated currents

As part of my control studies I investigated whether DMSO used to dissolve capsaicin could alone activate TRPV1 in transfected cells during whole-cell patch clamp recordings. I investigated the following DMSO percentage, namely: 0.5%, 0.2%, 0.1%, and 0.05%. These were the percentages of DMSO routinely used in my laboratory to dissolve lipophilic compounds. I used 500 nM capsaicin (0.006% DMSO) application to activate hTRPV1 as a positive control in order to check whether the cells responded to TRPV1 activation.

Application of 500 nM capsaicin to hTRPV1-transfected cells produced an inward current (-1.43±0.3 nA, n=7; Fig 3.3). Application of 0.5% DMSO to transfected cells caused the cells to initially swell and then rupture resulting in loss of the whole-cell configuration (n=5). Application of 0.2 % DMSO produced an inward current in the hTRPV1-transfected cells (-261 ± 5.1 pA, n=10; Fig 3.3). Application of 0.1% DMSO produced an inward current (-189 ± 24.4 pA, n=13; Fig 3.3). Decreasing the percentage of DMSO to 0.05% failed to produce any response (-20 ± 10 pA, n=4; Fig 3.3) as the noise of the whole-cell patch-clamp configuration contributed to ~15-20 pA; Fig 3.3).

In comparison, I found that application of capsaicin to untransfected HEK293 cells failed to produce any currents (not shown) and that 0.2% DMSO also failed to elicit any response in these cells (-21 ± 6.3 pA, n=7; noise of the set-up contributed ~15-20 pA; Fig 3.3). However, application of 0.5% DMSO also resulted in the loss of whole-cell configuration (n=5; data not shown).

0.006% DMSO was not tested; it was assumed that DMSO of *less than* 0.05% in solution will not evoke TRPV1-mediated membrane current.

A hTRPV1-transfected HEK293 cells

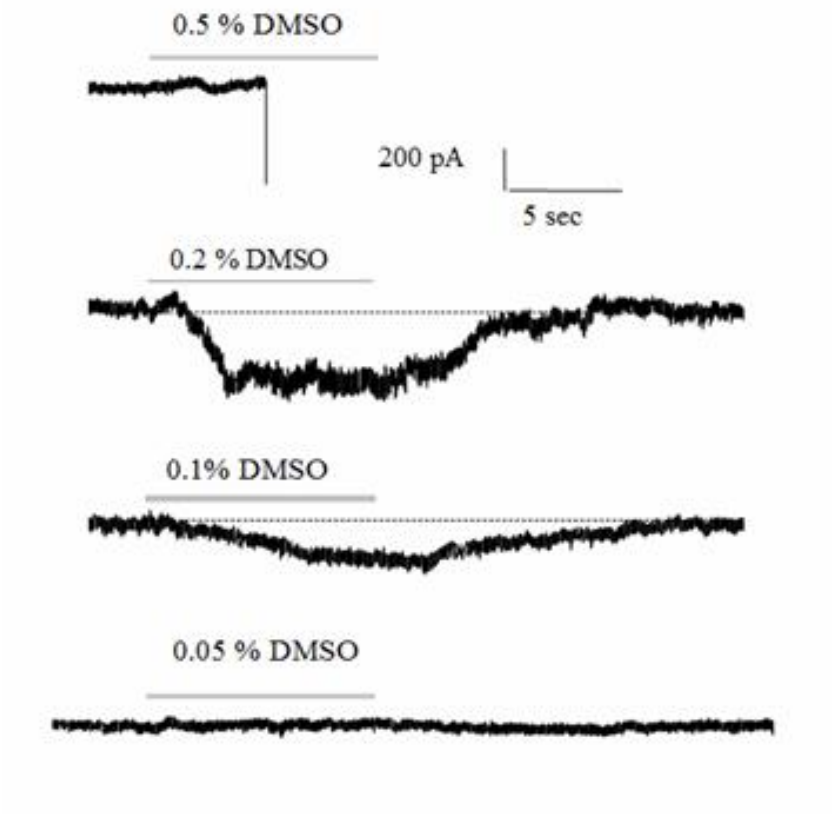

B Untransfected HEK293 cells

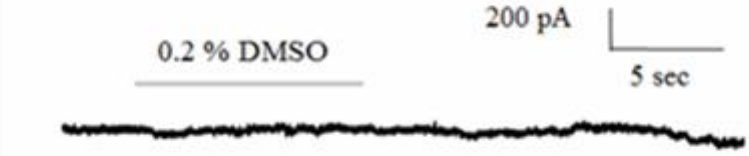

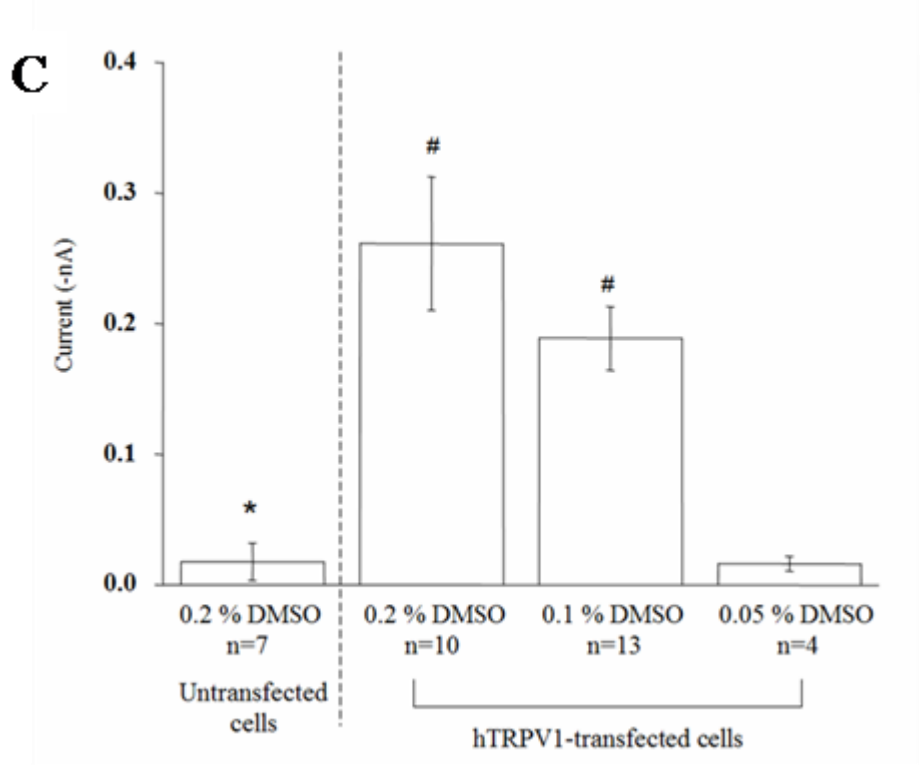

Figure 3.3. DMSO-evoked responses in untransfected cells and hTRPV1-transfected cells using whole-cell patch-clamp recordings. (A) Currents produced by hTRPV1 during application of DMSO at varying percentages. The whole-cell configuration could not be maintained during the application of 0.5% DMSO, as the cell lyses. However, 0.2% DMSO and 0.1% DMSO elicited a small inward current. No response was seen during the application 0.05% DMSO. (B) No inward current was seen during an application of 0.2% DMSO to untransfected cells. (C) Average amplitudes of DMSO-evoked currents in untransfected cells and hTRPV1-transfected cells. Each data point represents the mean ± SEM of the maximum amplitude of the current from different cells. The n represents the number of cells on which a given treatment was repeated. Both the Levene's test for equal variance and the Shapiro-Wilk normality test showed p-values of >0.05, indicating equal variance and normal distribution. The statistical significance of the difference in the means between untransfected and transfected cells was assessed using Student's t-test (two-tail distribution and two-sample equal variance). The statistical difference between the means with varying percentages of DMSO for transfected cells was assessed using 1-ANOVA. Whether the differences found were significant was established using Fisher LSD post-hoc. (* and $^{\#}$) Differences were regarded as being statistically significant at $p<0.05$. (*) A statistical significance was seen between the untransfected and hTRPV1-transfected cells. ($^{\#}$) 0.2 % and 0.1 % DMSO were statistical different from 0.05 % DMSO in TRPV1-transfected cells.

To investigate this DMSO-evoked TRPV1 activation, I then studied the effect of capsazepine, a selective TRPV1 antagonist (Bevan et al., 1991, 1992; Dickenson and Dray, 1991; Dray et al., 1991; Walpole et al, 1994). Here I studied the effect of this TRPV1 antagonist on 0.2% DMSO-evoked current. The effect of this antagonist on capsaicin-evoked response was also investigated.

I found in this study that continuous perfusion of capsazepine significantly reduced the capsaicin-mediated currents from – 1.43 ± 0.31 nA (n=7; Fig 3.4A and C) to - 0.44 ± 0.21 nA (n=7; Fig 3.4B and C), a reduction of ~ 70 %. Consequently, capsazepine significantly reduced the DMSO-mediated currents from - 261 ± 51 pA (n=10; Fig 3.5A and C) to - 48 ± 0.21 nA (n=6; Fig 3.5B and C), a reduction of ~ 80%.

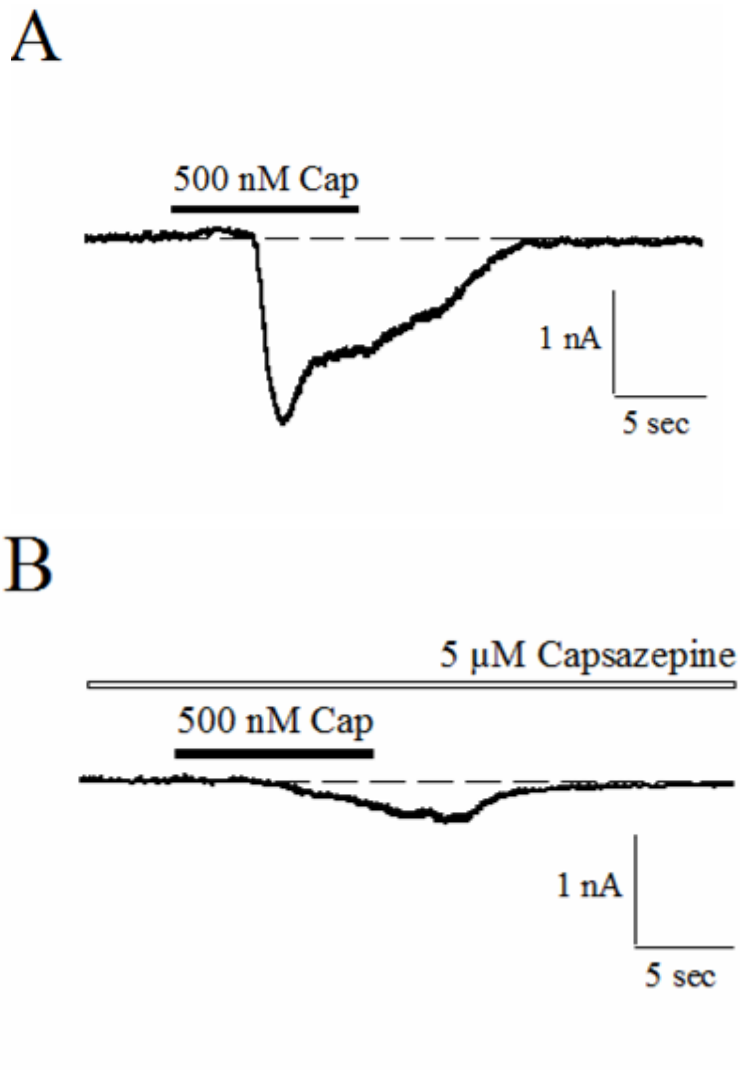

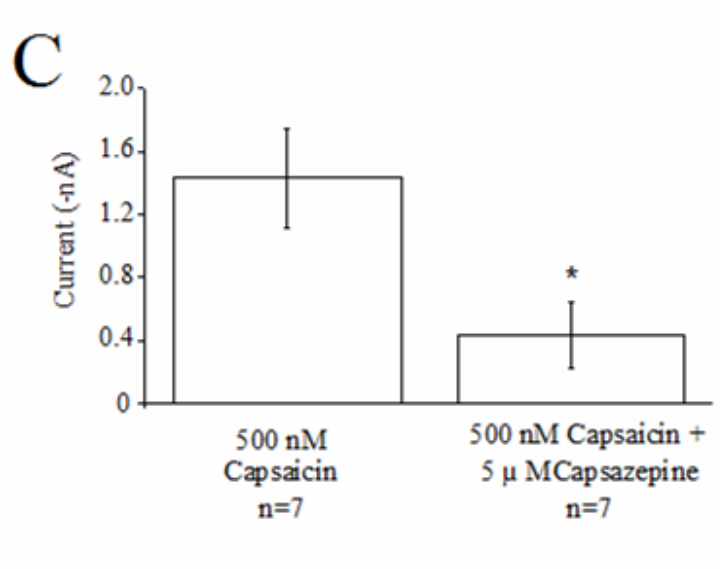

Figure 3.4 The effect of capsazepine on capsaicin-evoked activation of hTRPV1-transfected cells using whole-cell recordings. Whole-cell currents during application of: (A) 500 nM capsaicin; and (B) continuous perfusion (minimum period of 2 minutes) of 5 µM capsazepine and 500 nM capsaicin in hTRPV1-transfected cells. (C) Capsazepine significantly reduced capsaicin-induced current. Each data point represents the mean ± SEM of the maximum amplitude of the current from different cells. The *n* represents the number of cells on which a given treatment was repeated. Both the f-test and the normality test (Shapiro-Wilk) showed p-values of >0.05 indicating equal variance and normal distribution. The statistical difference between the means was assessed using Student's t-test (two-tail distribution and two-sample equal variance). (*) Differences were regarded as being statistically significant at $p<0.05$.

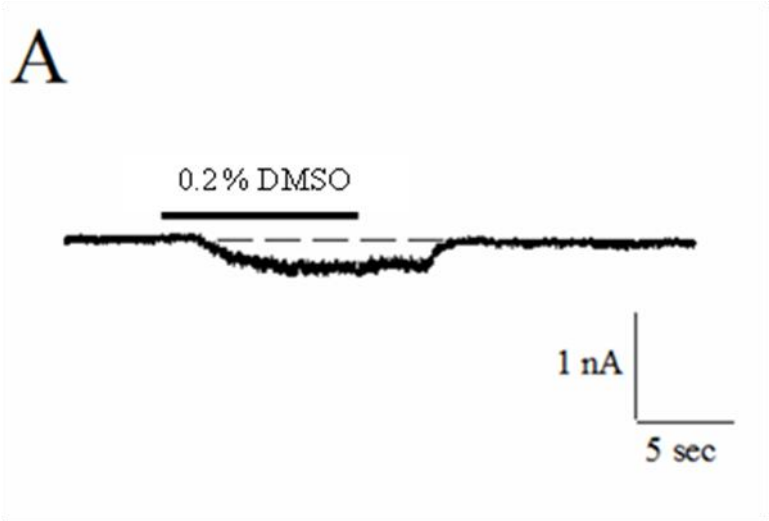

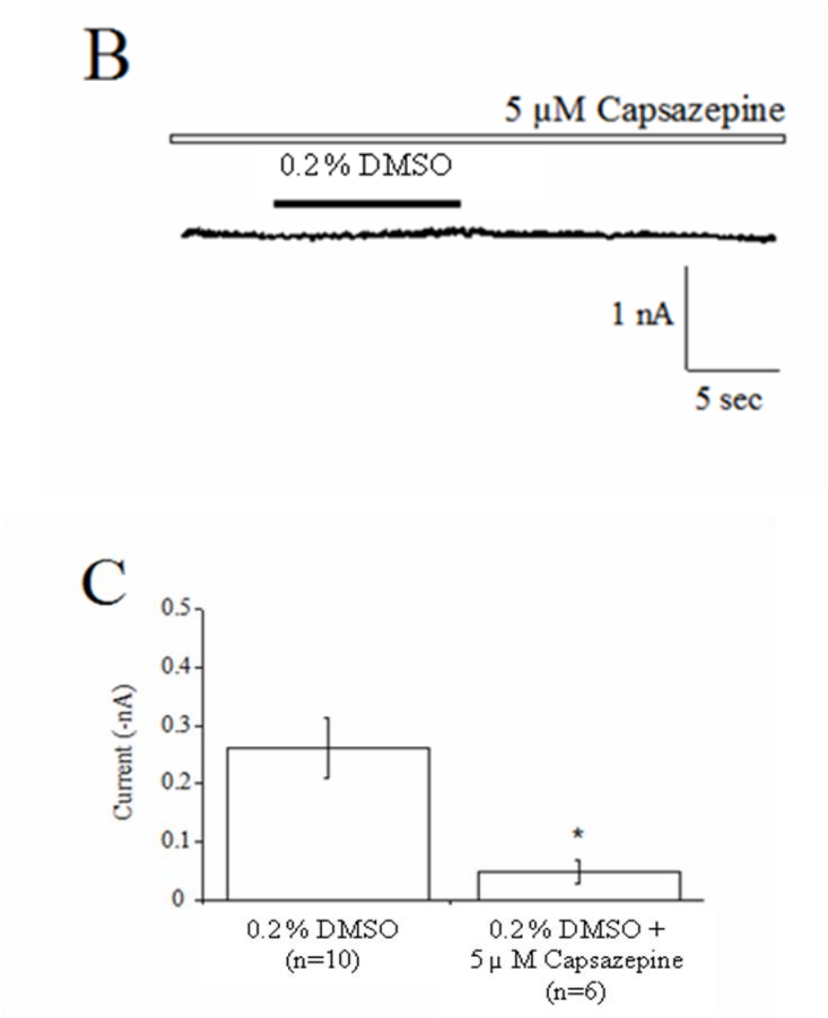

Figure 3.5 The effect of capsazepine on 0.2% DMSO-evoked currents in hTRPV1-transfected cells using whole-cell recordings. Whole-cell currents during application of (A) DMSO in 1:500, and (B) continuous perfusion of 5 µM capsazepine and DMSO in 1:500 in hTRPV1-transfected cells. (C) Capsazepine significantly reduces DMSO-induced currents. Each data point represents the mean ± SEM of the maximum amplitude of the current from different cells. The *n* represent the number of number of cells on which a given treatment was repeated. . The f-test showed unequal variance of the data, while, the normality test (Shapiro-Wilk) showed a normal distribution. The statistical difference between the means was assessed using the Student's t-test (two-tail distribution and two-sample unequal variance). (*) Differences were regarded as being statistically significant at $p<0.05$.

3.3.2 The effect of DMSO on cobalt-uptake

Next, I studied DMSO-evoked effects on hTRPV1. The cobalt-uptake technique was used on hTRPV1-transfected HEK293 cells and untransfected HEK293 cells.

I found in these experiments that untransfected cells did not respond to drug-free cBuffer B, 500 nM capsaicin or to 0.2 % DMSO (Fig 3.6).

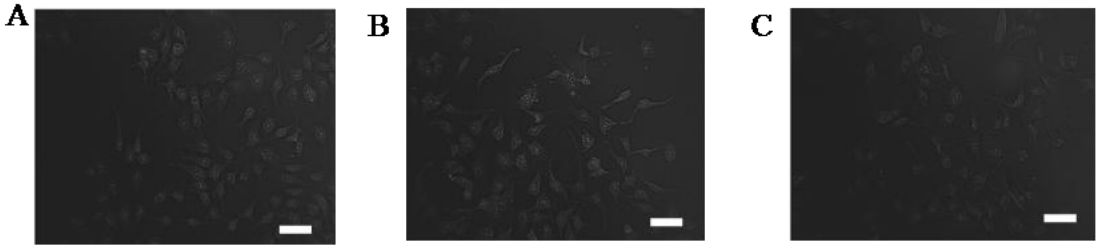

Figure 3.6 Grey scale images of cells following cobalt-uptake assay of untransfected cells in response to 500 nM capsaicin and 0.2% DMSO application. (A) drug-free cobalt-containing Buffer B, (B) Buffer B with 500 nM capsaicin and (C) Buffer B with 0.2% DMSO showed no cobalt-labelling. Bar indicates 50 µM..

In comparison, 500 nM capsaicin induced cobalt labelling in 59.9 ± 2.3 % (n=3) of the hTRPV1-transfected cells. This proportion of labelled cells was significantly greater than that produced by the drug-free cobalt-containing buffer in the hTRPV1-transfected cells (4.4 ± 1.4 %, n=3). Surprisingly, application of DMSO in 0.2% (30µM) produced cobalt labelling in 24.2 ± 5.2 % (n=3) of the transfected cells. This proportion of labelled hTRPV1-transfected cells by DMSO was significantly greater than that produced by drug-free cobalt-containing buffer (4.4 ± 1.4 %, n=3), and was significantly less than that produced by 500 nM capsaicin.

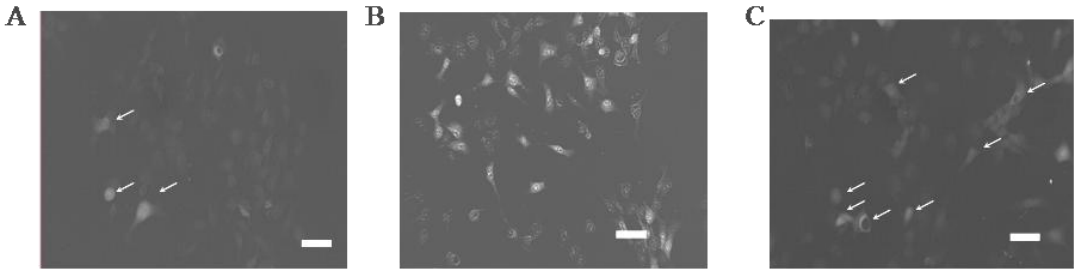

Figure 3.7 Grey scale images of cells following cobalt-uptake assay Cobalt-uptake images of hTRPV1-transfected cells in response to 500 nM capsaicin and 0.2% DMSO application. (A) Inverse image of cells incubated in the presence of drug-free cobalt-containing buffer shows very few labelled cells (arrows). (B) Inverse image of cells incubated in the presence of 500 nM capsaicin and $CoCl_2$ shows cobalt-labelling in a large number of cells. (C) Inverse image of cells incubated in the presence of 0.2% DMSO and $CoCl_2$ shows more cobalt-labelled cells than in image A. Bar indicates 50 µM..

To investigate whether DMSO indeed induced the cobalt-uptake through TRPV1, I next studied the effect of the TRPV1 antagonist capsazepine on the DMSO-evoked cobalt-uptake. I found that 5 µM capsazepine (DMSO content 0.006%) alone did not produce cobalt-entry in a significantly higher proportion of hTRPV1 transfected cells (5.1± 1.4 %, n=3) than that produced by drug-free cobalt-containing buffer (4.0 ± 0.7 %, n=6). I also found that capsazepine (0.006% DMSO) significantly reduced the percentage of labelled cells produced by capsaicin from 58.9 ± 3.5 % (n=6) to 32.5 ± 2.3 % (n=3), a reduction of 55%. Capsazepine had a similar inhibitory effect on DMSO-evoked cobalt-uptake. It reduced the labelling from 14.3 ± 1.7 % (n=6) to 8.5 ± 1.6% (n=3), a reduction of ~ 65 %, which indicated that the capsaicin-evoked responses are indeed mediated through TRPV1 (Fig 3.8).

These findings together indicated that DMSO can activate hTRPV1 in a heterologous system. In subsequent experiments, DMSO-evoked TRPV1 activation was characterised and its characteristics were compared to the characteristics of capsaicin-evoked TRPV1 activation.

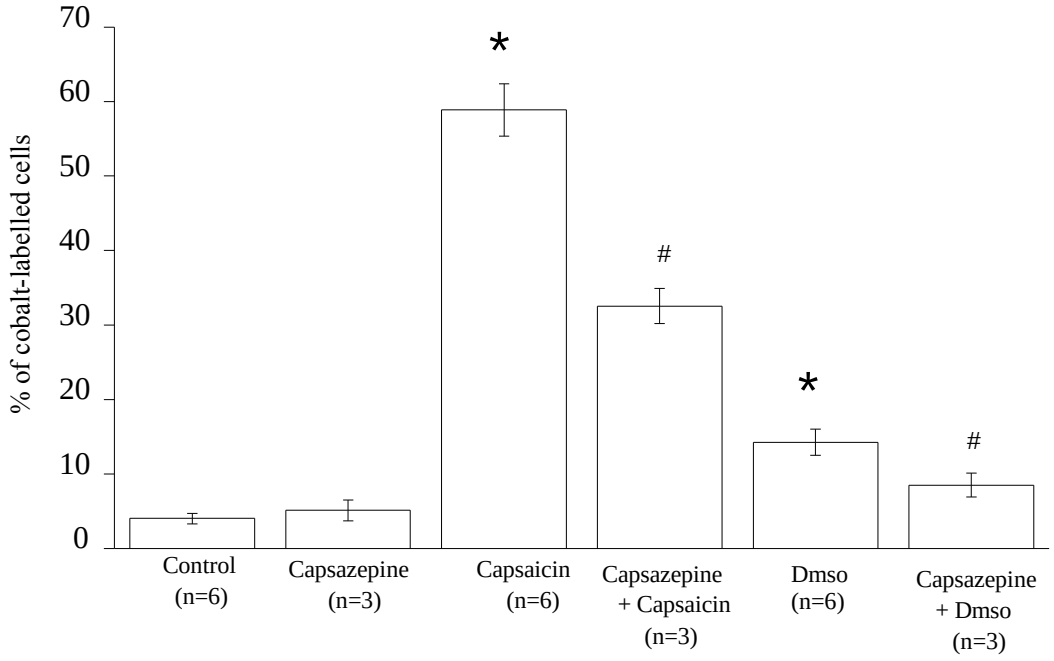

Figure 3.8 The effect of capsaicin (500nM), capsazepine (5µM) and DMSO (0.2 %) on hTRPV1-transfected cells using cobalt-uptake. Data show that both applications of capsaicin and DMSO in the presence $CoCl_2$ significantly increased the number of labelled cells when compared to control (*). Labelling is significantly reduced ($^{\#}$) in the presence of capsazepine. Each data point represents the mean ± SEM of the number of cobalt-labelled cells. *n* represent the number of independent cultures on which a given treatment was repeated. Both the Levene's test for equal variance and the normality test (Shapiro-Wilk) showed p-values of >0.05, indicating equal variance and normal distribution. The statistical significance of the difference in the means was assessed using 1-ANOVA. Comparisons of means were computed using Fisher's LSD post-hoc test. Power test showed a value of >0.95. (* and $^{\#}$) Differences were regarded as being statistically significant at $p<0.05$.

3.3.3 DMSO-evoked desensitisation in the presence of calcium ions.

Repeated activation of TRPV1 by many of its ligands, including capsaicin, results in the characteristic of desensitisation. Cobalt-uptake was used to investigate the effect of repeated applications of capsaicin and DMSO. Also, I wanted to compare the effect of repeated application of capsaicin and DMSO in the absence and presence of Ca^{2+} to find out how the presence of Ca^{2+} affects desensitisation. (Koplas *et al*, 1997; Mohapatra *et al*, 2003; Mandadi *et al*., 2003).

Responses in absence of Ca^{2+}

In control experiments, cells were pre-incubated in drug-free buffer A for 5 minutes, followed by incubation in drug-free or drug-containing Buffer B. Incubation of cells in the drug-free Buffer produced labelling in 3.8 ± 1.8% (n=3) of the cells. Addition of capsaicin to Buffer B resulted in labelling in 58.4 ± 6.7 % (n=3) of the cells. Addition of DMSO to Buffer B resulted in labelling of 28.4 ±3.6 % (n=3). The proportion of the cells produced by capsaicin and DMSO was statistically different from the control (Fig 3.9B).

Next, I studied the effect of pre-incubating the cells in capsaicin for 5 minutes in Buffer A on drug-free capsaicin-evoked cobalt uptake. Unexpectedly, incubation of cells in drug-free cobalt-containing buffer after pre-incubation in capsaicin resulted in labelling of 41.7 ± 3.9% (n=3) of the cells. Buffer B in the presence of capsaicin produced labelling in 53.0 ± 4.0 % (n=3) of the cells. Statistical analysis showed that pre-incubation of the cells in capsaicin for 5 minutes significantly increased the number of cobalt labelled cells produced by drug-free Buffer B. However, it had no significant effect on the capsaicin-induced cobalt labelling (Fig 3.9B).

In addition, I studied the effect of pre-incubating the cells in DMSO for 5 minutes in Buffer A before incubating the cells in drug-free, DMSO-containing Buffer B. Here, the drug-free Buffer B produced labelling in 11.0 ± 1.2 % (n=3) of the cells, while addition of DMSO to Buffer B produced labelling in 13.4 ± 0.2 % (n=3) of the cells. Statistical analysis revealed that the pre-incubation of cells in DMSO did not significantly increase the number of cells produced by drug-free buffer B. In addition, it had no significant effect on the DMSO-induced cobalt labelling (Fig 3.9B).

Responses in the presence of Ca^{2+}

In control experiments, cells were pre-incubated in drug-free Buffer A for 5 minutes, followed by incubation in drug free or drug-containing buffer B. Incubation of cells in the drug-free Buffer B produced labelling in 2.8 ± 0.9% (n=3) of the cells. Addition of capsaicin to Buffer B resulted in labelling in 44.3 ± 3.5 % (n=3) of the cells. Addition of DMSO to Buffer B resulted in labelling of 17.1 ± 1.3 % (n=3). The proportion of the cells produced by capsaicin and DMSO was statistically different from the control (Fig 3.9C).

Next, I studied the effect of pre-incubating the cells in capsaicin for 5 minutes in Buffer A on drug-free- capsaicin-evoked cobalt uptake. Incubation of cells in drug-free Buffer B after pre-incubation in capsaicin resulted in labelling of 11.4 ± 2.4% (n=3) of the cells. Capsaicin application to the Buffer B produced labelling in 15.4 ± 2.2 % (n=3) of the cells. Statistical analysis showed that pre-incubation of the cells in capsaicin for 5 minutes had no significant effect on the number of cobalt labelled cells produced by drug-free buffer B. In addition, it had no significant effect on the capsaicin-induced cobalt labelling (Fig 3.9C).

Subsequently, I studied the effect of pre-incubating the cells in DMSO for 5 minutes in buffer A before incubating the cells in drug-free or DMSO-containing Buffer B. Here, the drug-free Buffer B produced labelling in 15.3 ± 1.1 % (n=3) of the cells. Addition of DMSO to Buffer B produced labelling in 3.7 ± 3.1 % (n=3) of

the cells. Statistical analysis revealed that the difference in the number of labelled-cells found with or without pre-incubating the cells in DMSO was significantly different. However, pre-incubating cells in DMSO had no significant effect on the DMSO-induced cobalt labelling (Fig 3.9C).

I then analysed the effect between the respective treatment groups of the absence and presence of Ca^{2+}. I found that while, the percentage of cobalt-labelling obtained in the absence of Ca^{2+} were somewhat lower than in presence of Ca^{2+} the differences were not significant, with the exceptions of three treatment groups. I found that repeated application of capsaicin and DMSO was significantly lower in the presence of Ca^{2+}. Furthermore pre-incubation of capsaicin, followed by incubation of drug free Buffer B was significantly lower in the presence of Ca^{2+} (Fig 3.9D).

In summary, I found that, in the absence of Ca^{2+}, repeated application of either DMSO or capsaicin did not result in a reduction of cobalt-labelled cells. Instead, pre-incubation with capsaicin, but not DMSO, had a sensitising effect in the absence of Ca^{2+}. However, in the presence of Ca^{2+}, DMSO, like capsaicin, produced desensitisation.

A

Protocol	Pre-incubation	Incubation
A	Buffer A	Buffer B
B	Buffer A	Buffer B + Cap 500 nM
C	Buffer A	Buffer B + 0.2% DMSO
D	Buffer A + Cap 500 nM	Buffer B
E	Buffer A + Cap 500 nM	Buffer B + Cap 500 nM
F	Buffer A + 0.2% DMSO	Buffer B
G	Buffer A + 0.2% DMSO	Buffer B + 0.2 % DMSO

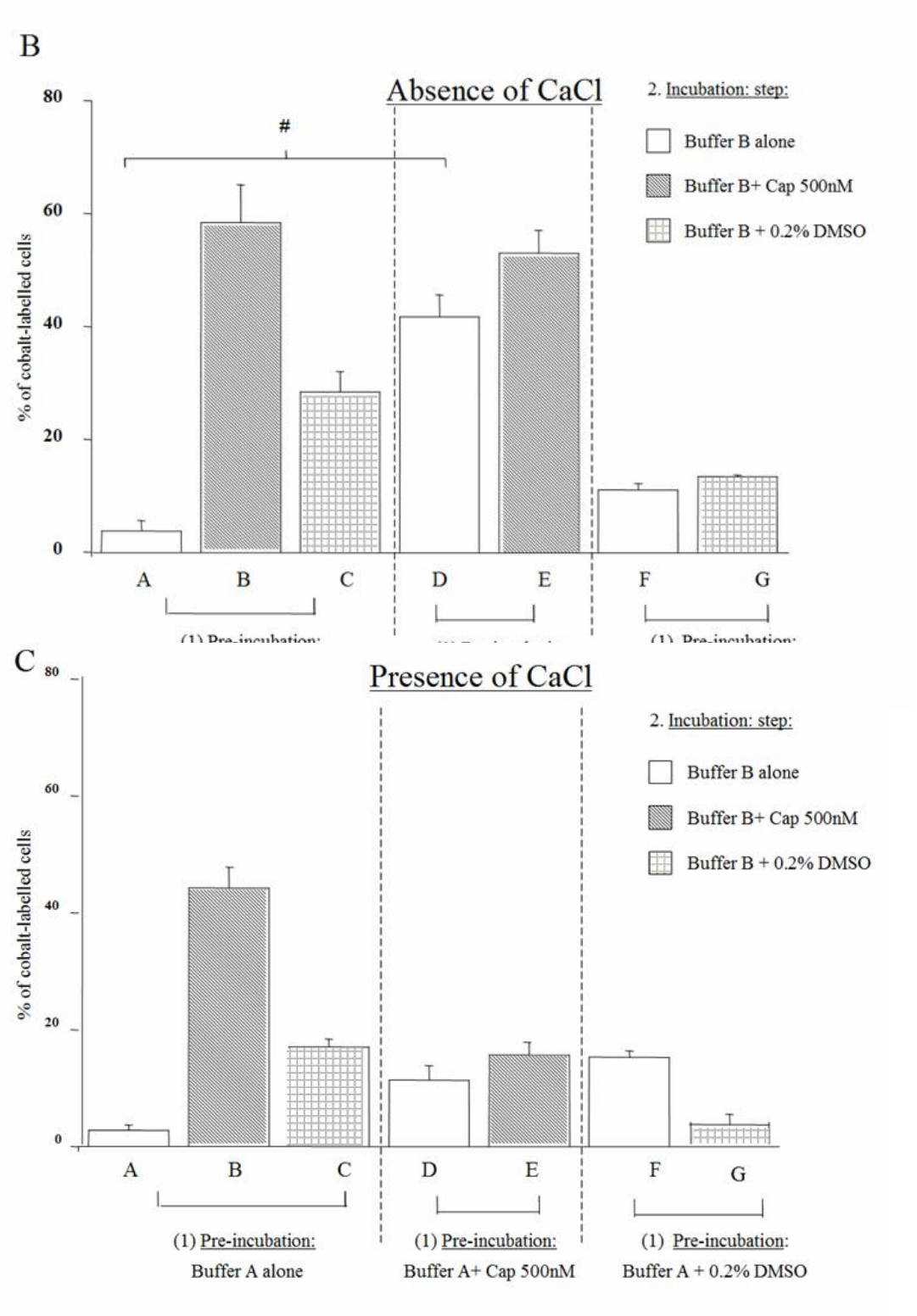
B
Absence of CaCl
2. Incubation: step:
Buffer B alone
Buffer B+ Cap 500nM
Buffer B + 0.2% DMSO
% of cobalt-labelled cells
80
60
40
20
0
#
A
B
C
D
E
F
G
C
Presence of CaCl
2. Incubation: step:
Buffer B alone
Buffer B+ Cap 500nM
Buffer B + 0.2% DMSO
% of cobalt-labelled cells
(1) Pre-incubation:
Buffer A alone
(1) Pre-incubation:
Buffer A+ Cap 500nM
(1) Pre-incubation:
Buffer A + 0.2% DMSO

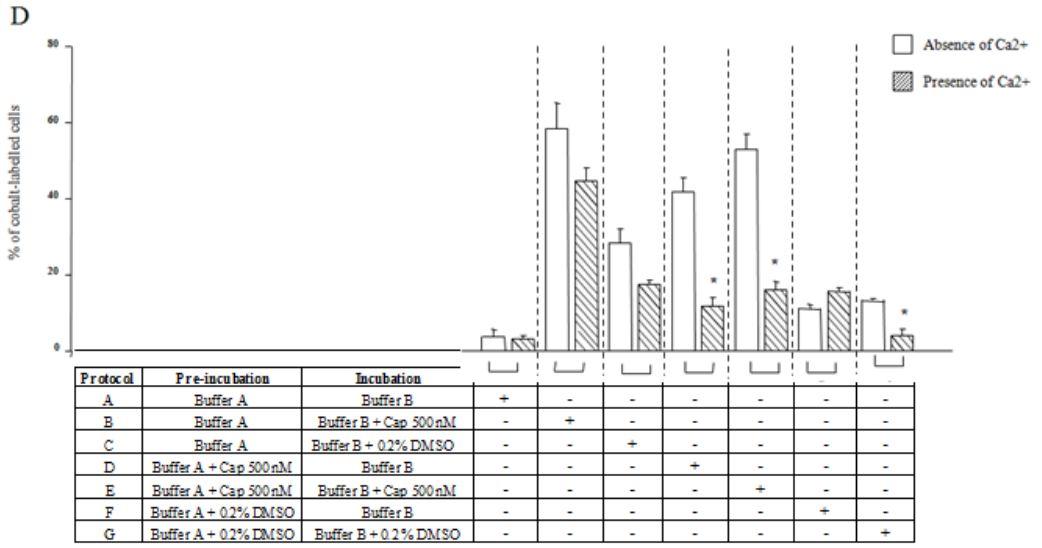

Protocol	Pre-incubation	Incubation							
A	Buffer A	Buffer B	+	-	-	-	-	-	-
B	Buffer A	Buffer B + Cap 500 nM	-	+	-	-	-	-	-
C	Buffer A	Buffer B + 0.2% DMSO	-	-	+	-	-	-	-
D	Buffer A + Cap 500 nM	Buffer B	-	-	-	+	-	-	-
E	Buffer A + Cap 500 nM	Buffer B + Cap 500 nM	-	-	-	-	+	-	-
F	Buffer A + 0.2% DMSO	Buffer B	-	-	-	-	-	+	-
G	Buffer A + 0.2% DMSO	Buffer B + 0.2% DMSO	-	-	-	-	-	-	+

Figure 3.9 Repeated application of capsaicin and DMSO in hTRPV1-transfected cells in the presence, and absence, of 2 mM $CaCl_2$ using the cobalt-uptake assay. (A) Protocols of cobalt-uptake assay to investigate the effect of repeated applications of capsaicin and DMSO. (B) Cobalt-labelling in the absence of Ca^{2+}. (C) Cobalt-labelling in the presence of Ca^{2+}. (D) Cobalt-labelling in the absence and presence of Ca^{2+} in their respective treatment groups. Each data point represents mean ± SEM (n= 3). Both the Levene's test for equal variance and the Shapiro-Wilk normality test showed p-values of >0.05, equal variance and normal distribution. The statistical difference between the means of the various treatments within a group was assessed using 1-ANOVA. Whether the differences found were significant was established using Fisher LSD post-hoc. The statistical difference between the means in the respective treatment groups was assessed using Student's t-test (two-tail distribution and two-sample equal variance; data not shown). Differences were regarded as being statistically significant at $p<0.05$. ($^{\#}$) Significant increase was seen in drug-free pre-incubation and pre-incubation with capsaicin in the absence of CaCl (Fig 3.9 B). (*****) Repeated application in the presence of $Ca^{2+,}$ were significant different higher than in the absence of Ca^{2+} (Fig 3.9 D).

3.3.4 Effect of DMSO on the capsaicin-evoked hTRPV1 activation

The data obtained so far clearly showed that 0.2% DMSO, like capsaicin, activates TRPV1. Since TRPV1 is a stimulus integrator (Tominaga *et al.*, 1998) it could be that the amount of DMSO used to dissolve capsaicin, above 0.1% DMSO, may modify the effect of capsaicin. Therefore, it was also necessary to assess whether the DMSO content in a capsaicin solution has any effect on hTRPV1-mediated responses.

Using the cobalt-uptake technique, I found that 100 nM capsaicin dissolved in various percentage of DMSO, namely: 0.1 %; 0.05 %; 0.025 %; and 0.006 %, produced labelling in a similar number of cells (48.1 ± 8.0%, n=3; 41.3 ± 5.7%, n=3; 42.3 ± 1.6%, n=3; 47.6 ± 3.6%, n=3; and 40.0 ± 2.2%, n=3; respectively; Fig 3.10). Furthermore, there were no statistical differences between the means of values. These relative numbers of labelled cells were all significantly different from control where no DMSO was added to the solution (3.1 ± 1.0%, n=3).

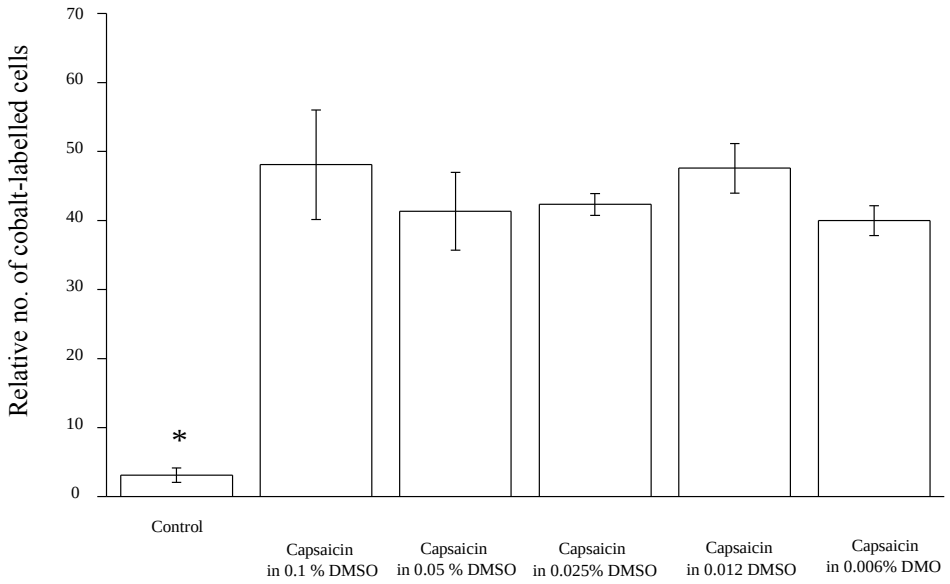

Figure 3.10 The effect of the percentage of DMSO content in capsaicin on hTRPV1-mediated capsaicin responses assessed by the cobalt-uptake assay. The relative number of cobalt-labelled cells induced by 100 nM capsaicin was similar in all tested DMSO contents. Each data point represents the mean proportion of labelled cells ± SEM (n= 3). Both the Levene's test for equal variance and the Shapiro-Wilk normality test showed p-values of >0.05, indicating equal variance and normal distribution. The statistical difference between the means was assessed using 1-ANOVA. Whether the differences found were significant was established using Fisher's LSD post-hoc test. (*) Differences were regarded as being statistically significant at $p<0.05$. Note that comparisons between the means showed no significant difference.

3.3.5 DMSO-evoked responses in DRG cultures

The data obtained on hTRPV1-transfected HEK293 cells showed that DMSO activates hTRPV1. Although that activation resembles that produced by capsaicin, it is possible that this effect can be observed only in heterologous systems, or that other TRP channels are also activated by DMSO. In order to study these possibilities, I next studied DMSO-evoked cobalt-uptake in DRG neurons taken from wild-type, and TRPV1 knock-out, mice.

I found that application of drug-free Buffer B produced none, or very few, labelled cells in prepared from wild-type, and TRPV1 knock-out mice (1.9 ± 0.4 % (n=3), 1.2 ± 0.4 % (n=3), respectively; Fig 3.9). Addition of 0.2% DMSO into Buffer B resulted in a significant increase of cobalt-labelled neurons to 8.6 ± 1.0 % (n=3; Fig 3.9) in DRG cultures prepared from wild-type animals. However, in cultures prepared from TRPV1 knock-out mice there was no significant increase in the proportion of cobalt-labelled cells by the addition of 0.2% DMSO to the cobalt-containing buffer (0.9 ± 0.6 %, n=3; Fig 3.9). In addition, this value was not significantly different from drug-free Buffer B in TRPV1 knock-out mice (Fig 3.11).

To confirm that the mice used were from TRPV1 knock-out mice, I incubated these cells in the presence of TRPV1 agonists, 500 nM capsaicin and Buffer B. Both wild-type and TRPV1 knock-out mice were investigated. In these experiments, I found that capsaicin significantly increased the proportion of cobalt-labelled cells in wild-type mice in comparison to TRPV1 knock-out mice (from 1.2 ± 0.6 % (n=3) to 14.6 ± 1.5 %, n=3; Fig 3.11). In addition, there was no significant difference between drug-free Buffer B and Buffer B containing capsaicin, in TRPV1 knock-out mice.

As the TRPV1 knock-out mice did not respond to capsaicin-evoked cobalt-labelling, this confirmed that the mice used were knock-out animals. To confirm that the failure of DMSO to produce cobalt-uptake in cells collected from TRPV1 knock out mice was not due to a general unresponsiveness of the cells, I incubated these cells in the presence of the TRPA1 agonist (Jordt et al., 2004), mustard oil (60 μM), and

cobalt-containing Buffer B. In these experiments, I found that mustard oil significantly increased the proportion of cobalt-labelled cells in comparison to drug-free cobalt-containing Buffer B (14.6 ± 3.5 %, n=3; Fig 3.11).

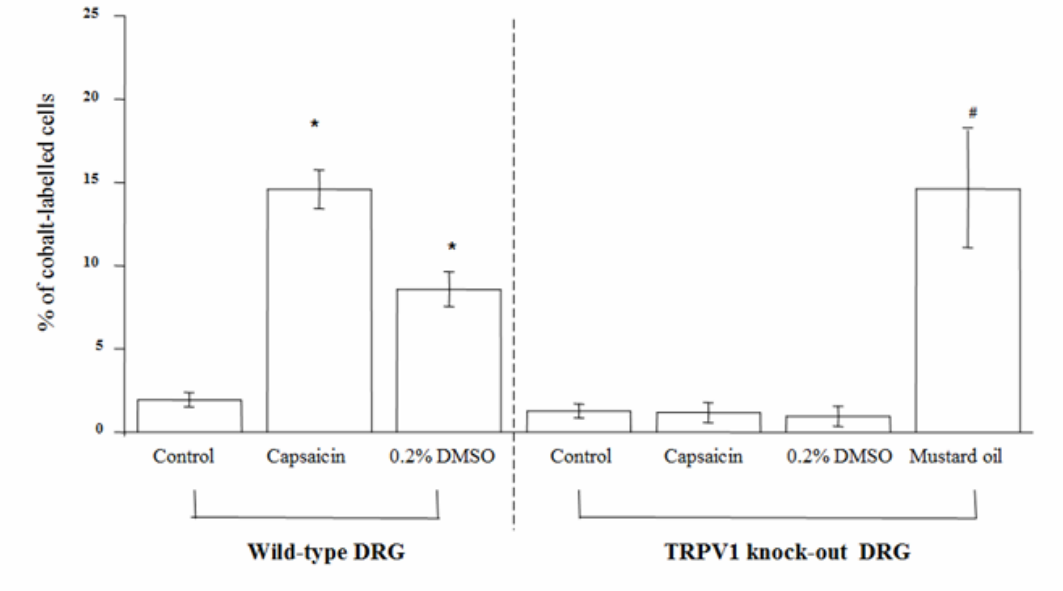

Figure 3.11 The effect of 0.2% DMSO in DRG cultures prepared from wild-type, and TRPV1 knock-out mice using the cobalt-uptake technique. (*) In the presence of DMSO, the relative number of cobalt-labelled cells obtained from wild-type mice was significantly higher those neurons prepared from TRPV1 knock-out mice. Similar effect was seen for capsaicin-evoked labelling. ($^{\#}$) 60 µM mustard oil induced labelling in a significant number of cells when compared to control, from neurons obtained from knock-out mice. Each data point represents the mean proportion of labelled cells ± SEM (n=3). Both the Levene's test for equal variance and the Shapiro-Wilk normality test showed p-values of >0.05, indicating equal variance and normal distribution. The statistical difference between the means of a group was assessed using 1-ANOVA. Whether the differences found were significant was established using Fisher LSD post-hoc. Differences were regarded as being statistically significant at $p<0.05$.

In summary, these data confirmed that DMSO indeed produced cationic influx into hTRPV1-transfected HEK293 cells through hTRPV1, and that the DMSO-evoked effect is concentration-dependent between 28 mM and 14 mM, which were 0.2% and 0.1%, respectively. In addition, the effect of 0.2% DMSO was inhibited by capsazepine, both in whole-cell patch-clamp recording (Fig 3.5) and in cobalt-uptake assay (Fig 3.8). A further finding showed that in the presence of calcium, DMSO is able to desensitise TRPV1.

3.4 Discussion

Data from these experiments indicate that DMSO concentration-dependently activates TRPV1. To the best of my knowledge, this is the first time that this effect of DMSO on this specific ion channel has been demonstrated. I found that, while untransfected cells did not, hTRPV1-tranfected cells did, respond to DMSO, and that this response was reduced by capsazepine.

A comparison of DMSO-evoked responses obtained in cobalt-uptake assay and whole-cell recordings to those evoked by capsaicin showed that, DMSO has a lower potency and efficacy as an activator than capsaicin. The finding that 5 μM capsazepine, a competitive TRPV1 antagonist, reduced the DMSO-evoked responses may suggest that DMSO may interact with the capsaicin binding site. However, results from a recent study by Matta and Ahern (2007) indicate that capsazepine might act as an inverse agonist because capsazepine is capable of reducing TRPV1 activity induced by activators other than capsaicin. To expand on this, in addition to capsazepine and other competitive inhibitors of capsaicin, these compounds are able, with varying degrees, to inhibit heat, protons, cations (Tominaga et al., 1998; Ahern et al., 2005. Therefore, DMSO may interact with TRPV1 at a site different from the capsaicin binding site.

I also found in these experiments that, while application of DMSO to neurons collected from wild-type animals produced cobalt-labelling, a similar application did not evoke a similar response in neurons collected from TRPV1 knock-out mice. These data indicate that, in addition to heterologous TRPV1, native TRPV1 expressed in primary sensory neurons also respond to DMSO.

While DMSO did not produce responses from TRPV1 knock-out mice, I found that mustard oil induced cobalt-labelling in these cells. Mustard oil selectively activates another TRP channel, the cold-sensitive transient receptor potential ankyrin type 1 (TRPA1; Jordt et al., 2004; Macpherson et al., 2005; Bautista et al., 2005). TRPA1

has been shown to be co-expressed with TRPV1 on a subset of sensory neurons in DRG (Story et al., 2003; Kobayashi et al., 2005). The mustard oil-evoked cobalt-uptake on primary sensory neurons confirms that the absence of DMSO-evoked cobalt labelling in neurons collected from knock-out animals was not due to unresponsiveness of cells. Furthermore, these data also indicate that, in addition to TRPV1, other temperature sensitive ion channels, such as TRPA1, are also permeable to Co^{2+}.

Having confirmed the excitatory effect of DMSO on TRPV1 in both heterologous and native systems, I compared various other aspects of the DMSO-evoked response to the response evoked by the archetypical TRPV1 activator, capsaicin. Sensitisation and desensitisation are two of the main characteristics of TRPV1. TRPV1 is essential for the development of inflammatory heat hyperalgesia (Davis et al., 2000; Caterina et al., 2000). During inflammation, TRPV1 mediated responses are increased due to a process, called sensitisation. Sensitisation involves phosphorylation of the receptor by multiple pathways involving PKA and PKC (Premkumar and Ahern, 2000; Numazaki et al., 2002; Ahern et al., 2005; Morenill-Palao et al., 2004; Lee et al., 2005). For example, PKA is able to phosphorylate TRPV1, which results in decreased desensitisation and increased sensitivity to each of anandamide, capsaicin, protons and heat (Di Marzo et al., 2002). Increased protein kinase activities are induced by various inflammatory mediators, including nerve growth factor, prostaglandin, and bradykinin (Cesare et al., 1996; Chuang et al., 2001; Zhuang et al., 2004; Moriyama et al., 2005; Rukwied et al.,2007; Fischer and Reeh, 2007).

Desensitisation of TRPV1 is a calcium dependent process (Koplas et al., 1997; Mohapatra et al., 2003). In the presence of an inhibitor of calcineurin, a Ca^{2+}-and calmodulin-dependent protein phosphatase 2B, the desensitisation effect of capsaicin is reduced (Docherty et al., 1996). Moreover, Ca^{2+}-dependent phosphorylation, and dephosphorylation, of PKA and of PKC have been shown to also modulate desensitisation of TRPV1 (Liu et al., 2004; Mohapatra and Nau, 2003; Mohapatra and Nau, 2005; Mandadi et al., 2004). It is well documented that

repeated, or prolonged, application of capsaicin induces profound desensitisation of TRPV1 (Jancsó and Jancsó-Gabor, 1949; Jancsó, 1968).

Thus, in order to investigate this effect, I repeated applications of capsaicin and DMSO, in the presence and absence of CaCl, and used cobalt-uptake assay. As the standard cobalt-uptake buffer does not contain Ca^{2+}, the first experiments were done in the absence of extracellular Ca^{2+}. In this condition, I found that pre-incubation with capsaicin but not DSMO, sensitised hTRPV1, as the number of labelled cells induced by agonist-free cobalt-buffer was increased. This effect could not be due to capsaicin remaining in the buffer, as the cells were washed once with 300 µl of buffer, which should have removed all traces of capsaicin. A plausible explanation of this sensitising effect is that pre-incubation of the cells with capsaicin reduce the heat threshold from ~44 ^{o}C to below 37 ^{o}C for a duration that was long enough to allow the 5 minute incubation in drug-free cobalt-containing buffer to produce labelling.

Repeated application of DMSO treatments did not have any significant effects on the number of labelled cells. Similar findings were seen for successive application of capsaicin. The failure of DMSO to induce sensitisation may be due to differences in cellular responses evoked by capsaicin and by DMSO. The absence of sensitisation to successive application of capsaicin may be due to the saturation of cobalt-labelling by capsaicin. Capsaicin, at a concentration of 500 nM, may have induced maximal cobalt-labelling rendering additional exposure to capsaicin redundant. It may be that efficacy of the transfection was approximately the same as the number of cobalt-labelled cells evoked by 500 nM capsaicin.

In the presence of Ca^{2+}, the experimental paradigms described above produced desensitisation. Both successive application of capsaicin or DMSO resulted in the reduction of cobalt-labelled cells. The same protocol, *in the presence of* Ca^{2+}, failed to increase the number of labelled cells, in contrast to the increase in the number of cobalt-labelled cells following pre-incubation of cells in capsaicin or DMSO followed by incubation of the cells in drug-free cobalt-uptake *in the absence*

of Ca^{2+}. The number of cobalt-labelled cells induced in the Ca^{2+}-containing cobalt-buffer in the presence of capsaicin, or DMSO, without pre-incubation, was slightly lower than the number of cobalt-labelled cells in the absence of Ca^{2+} in the comparable experiments. This could be explained by the presence of Ca^{2+}. Both Co^{2+} ions and Ca^{2+} ions are capable of permeating certain non-selective, ligand-gated ion channels, including TRPV1. Thus, Co^{2+} ions may have competed with Ca^{2+} ions for entry into the cell, when TRPV1 was activated. As Ca^{2+} is likely to have a higher permeability than Co^{2+} through TRPV1, due to calcium's smaller size, more Ca^{2+} could have entered than Co^{2+}, thereby reducing the number of cobalt-labelled cells.

Collectively, this finding suggests that, although there are differences in the characteristics of DMSO-evoked, and capsaicin-evoked, responses, DMSO behave like a typical TRPV1 ligand, and is capable of inducing desensitisation. Moreover, in agreement with previously published data, these findings confirmed that TRPV1 desensitisation indeed depends on calcium (Koplas et al, 1997; Mohapatra et al, 2003).

It has been demonstrated that TRPV1 activators, such as heat, protons, and post-translational modification, respectively, potentiate the responses of other TRPV1 agonists (Caterina et al., 1997; Tominaga et al., 1998, Tominaga et al., 2005, Cesare et al., 1996; Chuang et al., 2001; Baumann & Martenson, 2000; McLatchie & Bevan, 2001; Ryu et al., 2003). Thus, it may be that concentrations of DMSO, which could not open the channel on their own, may modify the effect of other agonists e.g. capsaicin dissolved in DMSO. Thus, DMSO may be able to potentiate the response of TRPV1 to an agonist. The effect of 100 nM capsaicin dissolved in various dilutions of DMSO on TRPV1 was next studied, using the cobalt-uptake assay. A capsaicin concentration of 100 nM was chosen instead of the typical 500 nM on the basis of the latter being able to induce maximal cobalt-labelling, hence precluding the DMSO-induced potentiation. Data from these experiments showed that 100 nM capsaicin dissolved varying percentages of DMSO, namely: 0.1 %, 0.05 %, 0.025 %; 0.012% and 0.006 %. DMSO resulted in similar, but varying, relative numbers of cobalt-labelled cells. These findings were unexpected as 0.1% DMSO activated

TRPV1 on it own. Hence, a combination of 0.1% DMSO and 100 nM capsaicin was expected to produce higher labelling than 100 nM capsaicin in combination with DMSO in lower percentages. The reason for the absence of this expected effect may reside in the limited sensitivity of the cobalt-uptake assay. While the amount of cobalt that entered the cells during incubation of the culture in various DMSO contents in the capsaicin solutions might have varied, the analysis of the labelling could not have reliably recognised that variability. Only whole-cell recordings could determine whether the content of DMSO has any effect on the capsaicin-evoked responses. Another plausible explanation is that DMSO may be a partial agonist. Nevertheless, results of these experiments suggest that DMSO dilution in solutions intended to be used on TRPV1-expressing cells should be kept below 0.05 % because DMSO is able to activate TRPV1 and may potentiate the effect of other TRPV1-activators. It is also important that the DMSO concentration should be kept constant in order to avoid the possible variability of the responses due to the possible interference of DMSO in some other TRPV1 activator-induced response.

In conclusion, these data show that the DMSO content of solutions must be taken into consideration. Consequently, as a result of these findings, the DMSO content of capsaicin when used by me in subsequent experiments was ≤0.05% DMSO.

Chapter 4

CONSTITUTIVE ACID SENSITIVITY OF HEK293 CELLS

4.1 Introduction

HEK293 cell lines are routinely used in laboratories as an expression system for recombinant proteins including ion channels. Their popularity is due to their ability to produce highly reliable and efficient transfection and protein production. However, HEK293 cells express their own receptors and ion channels on their plasma membranes which may compromise studies on heterologously expressed membrane molecules. HEK293 cells, specifically, have been reported to express acid-sensing ion channels (ASIC; Hayes et al., 2000; Gunthorpe et al., 2001). ASIC channels belong to the degenerin type of sodium channels (Waldmann et a., 1997) and, like TRPV1, they can be activated by acids. In order to determine how these endogenously expressed, proton-responding ion channels effect the proton-evoked responses of hTRPV1, I have studied pH-activated whole-cell currents on untransfected cells.

4.2 Methods

Cell culture of HEK293 cells, cultured DRG neurons, transient transfection, cobalt-uptake and whole-cell patch clamp technique were used in this section. For further detail, see Chapter Two: Materials and Methods. The wild-type $hTRPV1_{111}$ haplotype was used in this investigation to assess the effect of DMSO in TRPV1-transfected HEK293 cells. For, simplicity this haplotypes will be referred to as hTRPV1.

4.2.1 Whole-cell patch-clamp recordings of hTRPV1-transfected HEK293 cells

Whole-cell patch-clamp recordings were performed on hTRPV1-transfected and on untransfected HEK293 cells in order to assess the effect of endogenously expressed acid-sensing ion channels (Hayes et al., 2000; Gunthorpe et al., 2001) on TRPV1-mediated responses induced by protons, capsaicin and heat application.

Briefly, TRPV1-mediated responses were measured using the conventional whole-cell patch-clamp technique with an Axopatch 200 B amplifier (Axon Intruments, Inc.) and the pClampex 8 software package with a laboratory PC for storing and evaluating data. All experiments were performed at physiological temperature of 36-37 ^{o}C using a temperature controller (Wavelength Electronics). The membrane potential was held at -60 mV. Data were collected using the pClampex 8.2 data analysis programme (Axon Instruments). If the membrane current following the establishment of whole-cell configuration was more than -0.5 nA the cell was discarded.

Solutions

The normal extracellular buffer consisted of (mM): NaCl, 130; KCl, 5; $CaCl_2$, 2; $MgCl_2$, 2; glucose, 10; Hepes, 10; adjusted to pH 7.4.

Patch electrodes were filled with normal intracellular buffer (mM): NaCl, 5; KCl, 130; $MgCl_2$, 1.26; Hepes, 10; adjusted to pH 7.4.

Solution adjusted to pH 7.0, pH 6.5 and pH 6.0 were made by adjusting the pH of the normal extracellular buffer used in patch-clamp studies, using a pH meter. Normal extracellular buffer was used for this range of solutions because the buffering agent HEPES buffering capacity was within this range. The buffering capacity of buffering salts is a measure of the resistance of a buffer solution to pH change on addition H^+ ions. However, solutions adjusted to pH 4, pH 4.5, pH 5 pH 5.5 were made by adjusting normal extracellular buffer containing 10 mM 2-(N-Morpholin) ethanesulfonic acid sodium (MES) buffering agent instead of HEPES due to its lower buffering capacity of pH $\leq$5.

Amiloride-containing extracellular buffer was made from normal extracellular buffer used for patch clamp with the addition of 30 µM amiloride solutions. A stock solution of amiloride (Sigma) was made is dd$H_2$0. 30 µM amiloride solution was

chosen as this concentration almost completely blocks the ASIC conductance in HEK293 cells (Gunthorpe et al., 2001).

Stock solution of capsaicin (Tocris, UK) was dissolved in 100 % DMSO (Sigma). All further capsaicin and DMSO dilutions were made with normal extracellular buffer. In these experiments capsaicin within the concentration ranges between 10 nM and 10 µM were used. As a result of my previous finding (Chapter Four: DMSO activates TRPV1), where feasible, capsaicin solutions were made to contain 0.006%. However, due to the stock solution of capsaicin, higher concentrations of capsaicin (3-10 µM) were made to contain ≤ 0.05% DMSO content, as 0.006% DMSO was unachievable.

4.2.1.1 Proton application in the absence and presence of amiloride

To investigate the effect of proton application (pH 5) in untransfected cells, the pH of 10 mM 2 MES salt containing standard buffer was adjusted to pH 5 and applied for 10 seconds. The application was controlled by an automated system driven by the pClampex 8 package.

To investigate the effect of 30 µM amiloride on proton application (pH 5) in untransfected cells, the cells were continuously perfused (minimum period of 2 minutes) with 30 µM amiloride before applying pH 5 bath solution for 10 seconds. Data were analysed by measuring the maximum amplitudes of the responses using the pClampfit 8.2 software package.

These experiments were repeated on hTRPV1-transfected cells to investigate the effect of amiloride on hTRPV1-mediated responses evoked by pH 5. In addition to establishing the maximum amplitude, the activation time (10-90%) and inactivation time (90-10%) of proton-evoked responses in the absence or presence of amiloride were also calculated.

The kinetics of proton-evoked currents in the absence or presence of amiloride were analysed by measuring the activation and deactivation time for the inward current. Activation time was measured as the time taken for the response to activate from 10 % to 90% of its maximum amplitude. Deactivation time was measured as the time taken for the response to deactivate from 90 % to 10% of its maximum amplitude.

The effect of 30 µM amiloride on the proton response relationship of hTRPV1-transfected cells was also assessed by applying protons between the range of pH 5 to pH 7.4 for 10 seconds, in the presence or absence of this agent. Cells were continuously perfused for a minimum period of 2 minutes with amiloride before each proton application. Buffering salts in the bath solution consisted of 10 mM HEPES (pH 7.0, pH 6.5 and pH 6.0) or 10 mM MES (pH 5.5 and pH 5.0). Data were analysed by measuring the maximum amplitudes of the responses using the pClampfit 8.2 software package.

4.2.1.2 Capsaicin application in the absence and presence of amiloride

I investigated the effect of 30 µM amiloride on the capsaicin-response relationship using 10 seconds application of capsaicin within the concentration range 10 nM to 10 µM on hTRPV1-transfected cells. This was carried out in the absence and presence of amiloride. DMSO content ≤0.05 %. Cells were continuously perfused for a minimum period of 2 minutes with amiloride before each capsaicin application. The maximum amplitude was then established for each recording.

4.2.1.3 Heat application in the absence and presence of amiloride

The effect of 30 µM amiloride on heat-evoked responses in hTRPV1-transfected cells was assessed by applying a heat ramp between 37-50 ^{o}C. This was done in the absence and presence of this agent. Cells were continuously perfused for a minimum period of 2 minutes with amiloride. The heat activation threshold and the amplitude of the current produced at 48 ^{o}C were both established. For further details on determining the heat activation threshold, see section 2.2.9.2.

4.2.2 Statistical analysis

The mean and standard error of the mean (SEM) of corresponding data were calculated. The f-test and the normality test (Shapiro-Wilk) were also used to analyse variance and normality of data. The significance of difference between two groups was established by the Student's t-test (2-tailed distribution, two-sample equal). Statistical comparisons between two concentration-response curves were analysed using Student's t-test (two-tailed test, equal variance) to compare best fit variables (EC50 and Imax). Differences were regarded as being statistically significant at $p<0.05$. Data are presented as mean ± standard error of means of the maximum amplitude of the current from different cells. *n* refers to the number of cells recorded.

4.3 Results

4.3.1 Proton-evoked responses in untransfected HEK293 cells

In agreement with a previous report (Gunthorpe et al., 2001), application of an acidic extracellular solution (pH 5.0) to untransfected cells produced an inward current. Responses of all cells had two components, namely, a fast activating and inactivating response followed by a slowly activating and inactivating current. A fundamental characteristic of ASICs is their marked sensitivity to amiloride, a sodium channel blocker diuretic agent. The effect of amiloride on proton-evoked responses on untransfected HEK293 cells was therefore explored. In agreement with published data 30 µM amiloride significantly reduced the fast activating and inactivating current (from -1.18 ± 0.36 nA (n=4) to -0.22 ± 0.09 nA (n=3); an 82 % reduction: Fig 4.1) as well as the slower component (from -1.78 ± 0.46 nA (n=4) to -0.20 ± 0.16 nA (n=3); an 88 % reduction: Fig. 4.1) of the proton-activated responses (Gunthorpe et al., 2001). These findings confirmed that ASIC channels are constitutively expressed on HEK293 cells and suggested that, in order to assess the proton-evoked responses of hTRPV1, the superfusate should contain 30µM amiloride.

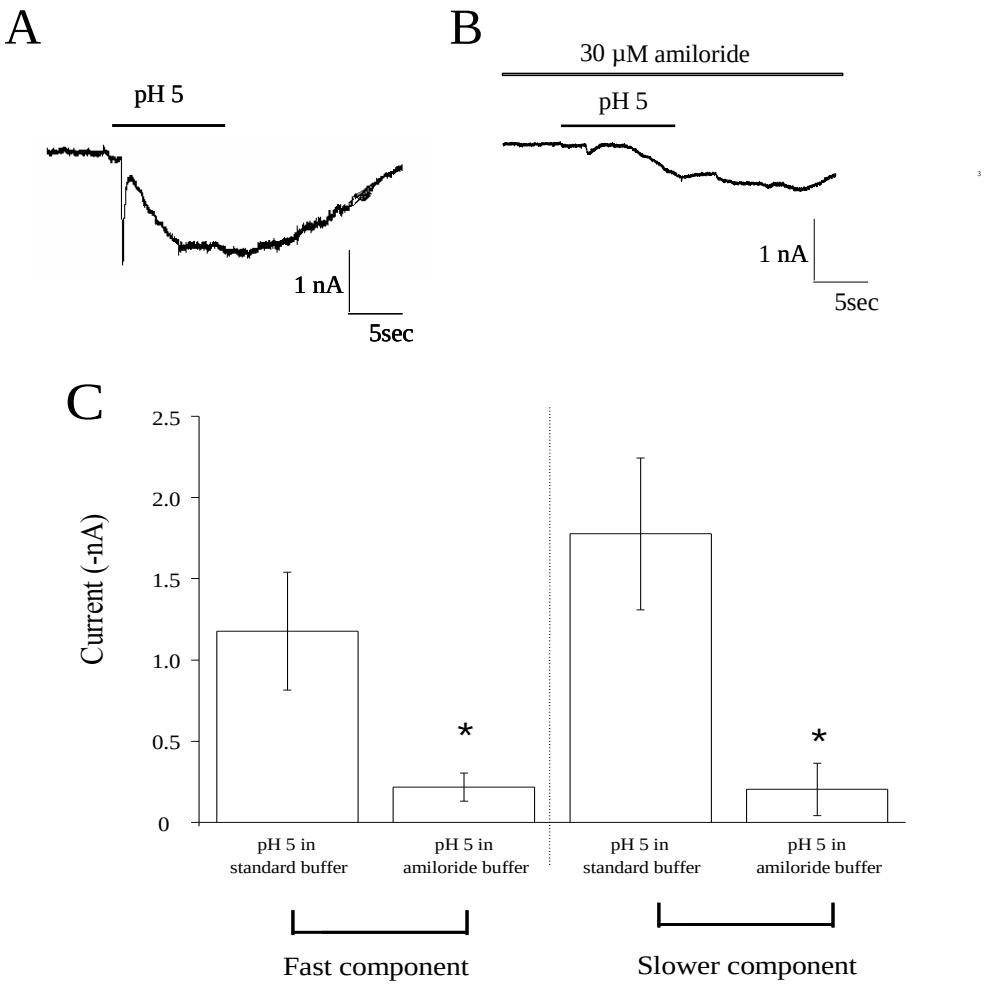

Figure 4.1 Untransfected HEK293 cells constitutively express proton-responding ion channels. Whole-cell patch-clamp recordings from untransfected HEK293 cells reveal proton-activated responses. (A) A typical inward current activated with a superfusate of pH5. The response has fast and slowly activating and inactivating components. (B) Pre-incubation of cells in 30µM amiloride for a minimum period of 2 minutes reduces both components of the proton-activated current. (C) Average maximum amplitude of proton-evoked responses with and without 30µM amiloride. Note that amiloride significantly reduces the maximum amplitudes of both components. Each data point represents the mean ± SEM (n=3). Significance was $p < 0.05$. Both the f-test and the normality test (Shapiro-Wilk) showed p-values of >0.05, indicating equal variance and normal distribution. The statistical significance of the difference in the means was assessed using Student's t-test (two-tail distribution and two-sample equal variance). (*) Differences were regarded as being statistically significant at $p<0.05$.

4.3.2 The effect of amiloride on hTRPV1-mediated responses in hTRPV1-transfected cells

Since amiloride may not only affect the ASICs but also TRPV1, it was necessary to study the affect of amiloride on TRPV1. Therefore, I studied the effect of 30 µM amiloride on TRPV1-evoked responses.

4.3.2.1 The effect of amiloride on proton-evoked responses

First, I compared the proton-evoked responses in hTRPV1-transfected cells in the absence and presence of 30µM amiloride. hTRPV1-transfected cells responded to application of an acidic extracellular solution (pH 4.0). Application of pH 4 in the presence of amiloride elicited smaller currents than in standard buffer (- 4.20 ± 0.60 nA (n=6) and - 2.47 ± 0.59 nA (n=5) (Fig. 4.2). These values were significantly different from each other. Interestingly, the proton concentration–response curves in standard buffer, or in the presence of 30 µM amiloride, showed that the half-maximal pH ($pH_{0.5}$) for channel activation was pH 6.03 ± 0.2.18, and pH 5.8 ± 0.25, respectively (Fig 4.3). These values were not significantly different from each other. However, the I_{max} for pH evoked activation was significantly lower in the presence of 30 µM amiloride than in standard buffer (2.54 ± 0.30 nA and 4.0 ± 0.28 nA, respectively) (Fig. 4.3).

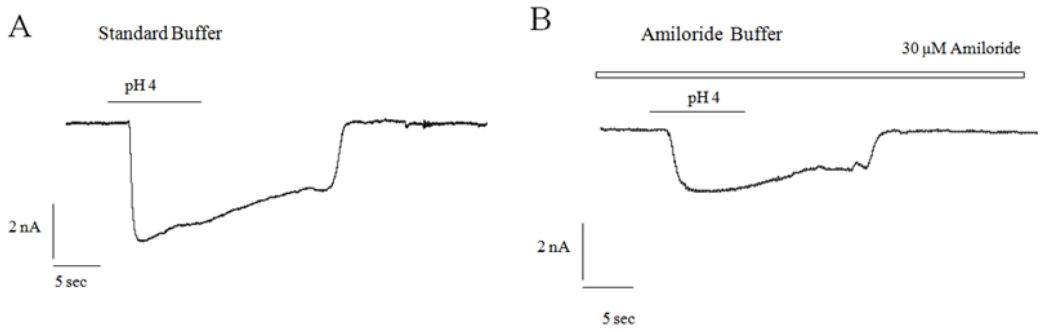

Figure 4.2

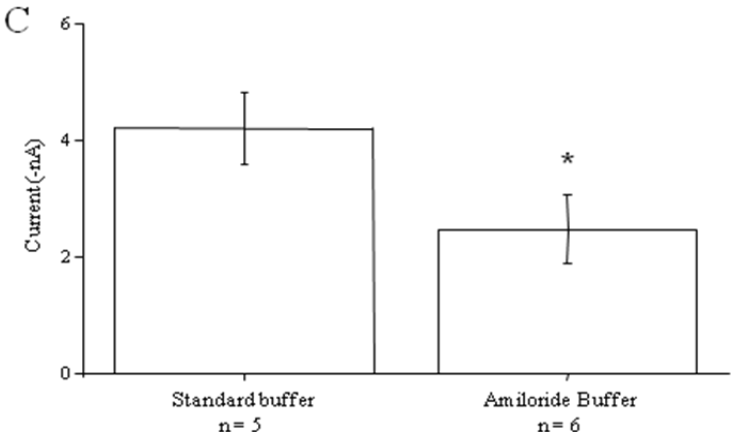

Figure 4.2 Whole-cell patch-clamp recordings of hTRPV1-mediated response to protons (pH 4.0) in the absence and presence of amiloride. (A) Current trace in standard buffer. (B) Current trace in amiloride buffer. (C) Bar chart showing mean peak amplitudes in the presence and absence of amiloride. Both the f-test and the normality test (Shapiro-Wilk) showed p-values of >0.05, indicating equal variance and normal distribution. The statistical significance of the difference in the means was assessed using Student's t-test (two-tail distribution and two-sample equal variance). (*) Differences were regarded as being statistically significant at $p<0.05$. Note that comparisons between the means showed a significant difference.

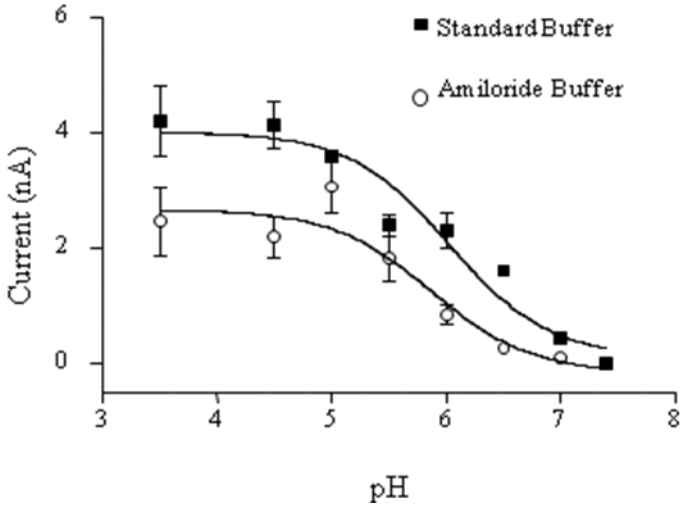

Figure 4.3 Proton concentration–response curve of hTRPV1-transfected HEK293 cells in the absence and presence of amiloride. Note that Imax is higher in the presence of amiloride. Each data point represents mean ± SEM ($n\geq5$). Both the Levene's test for equal variance and the normality test (Shapiro-Wilk) showed p-values of >0.05, indicating equal variance and normal distribution. The pH-response was fitted with a sigmoidal dose-response curve (Graphpad Prism, r2 ≥0.95). Statistical comparisons between two dose-response curves were analysed using Student t-test (two-tailed test, equal variance). There was a significant difference between the I_{max}s but not the EC_{50}s of the two solutions.

4.3.2.2 The effect of amiloride on capsaicin-evoked responses

Next, I studied the effect of amiloride on capsaicin-evoked responses. The capsaicin concentration-response curves were established both in the absence and presence of 30 µM amiloride. Application of 10 µM capsaicin in the presence of amiloride elicited larger currents than in standard buffer (-7.54 ± 0.86 nA (n=6) and -5.81 ± 0.32 nA (n=5) indicating that amiloride sensitises TRPV1. However, these values were not significantly different from each other (Fig. 4.4). Interestingly, the EC_{50} of capsaicin in the presence of amiloride was somewhat higher (817.61 ± 148 nM) than in the absence of this blocker (734 ± 255 nM) (Fig. 4.5). However, this difference was not significant. The curve fitting also revealed that the I_{max} for the capsaicin evoked TRPV1-activation in the standard buffer, or in the presence of 30 µM amiloride were 5.39 ± 0.34 nA or 6.36 ± 0.45 nA, respectively (Fig 4.5). These values were not significantly different from each other.

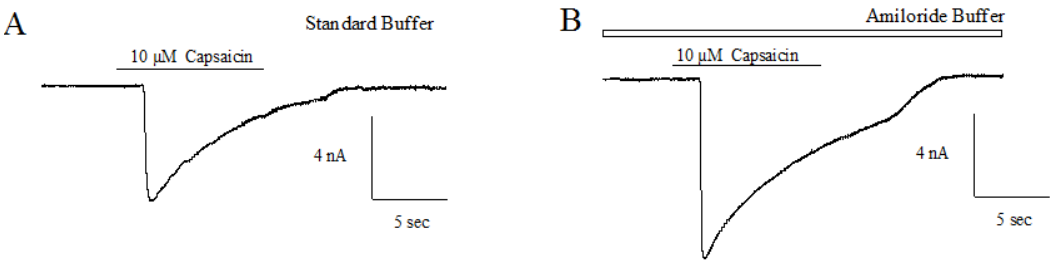

Figure 4.4

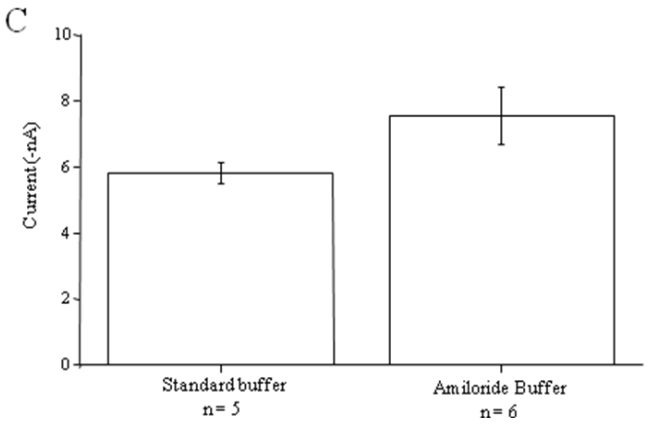

Figure 4.4 Whole-cell patch-clamp recordings of hTRPV1-mediated responses to 10 µM capsaicin in the absence and presence of amiloride buffer. (A) Current trace in standard buffer. (B) Current trace in amiloride buffer. (C) Bar chart showing mean peak amplitudes. Each data point represents mean ± SEM (n≥5). Both the f-test and the normality test (Shapiro-Wilk) showed p-values of >0.05, indicating equal variance and normal distribution. The statistical significance of the difference in the means was assessed using Student's t-test (two-tail distribution and two-sample equal variance). Note that comparisons between the means showed no significant difference.

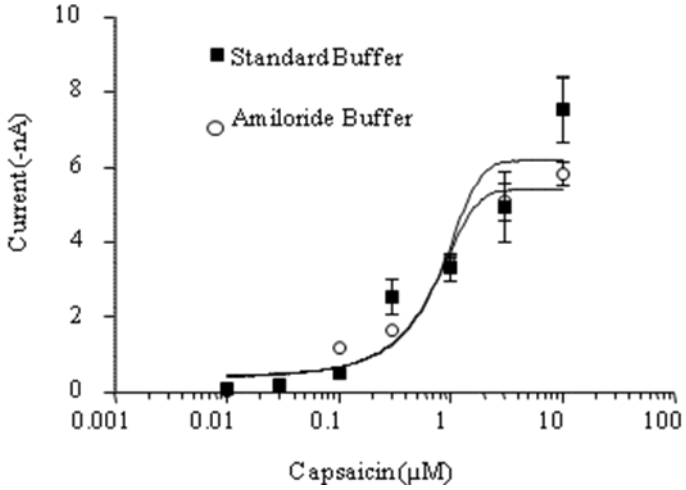

Figure 4.5 Concentration response curves of hTRPV1 to capsaicin in the absence and presence of 30 µM amiloride. Each data point represents mean ± SEM (n≥5). Both the Levene's test for equal variance and the normality test (Shapiro-Wilk) showed p-values of >0.05, indicating equal variance and normal distribution. The capsaicin-response was fitted with a sigmoidal dose-response curve (Graphpad Prism, r2 ≥0.95). Statistical comparisons between the two dose-response curves were done using Student's t-test (two-tailed test, equal variance). There was no significant difference between the EC_{50}s and the I_{max}s of the two solutions.

4.3.2.3 The effect of amiloride on heat-evoked responses

Finally, I also compared the heat evoked responses in the absence and presence of amiloride. Increasing the temperature of the superfusing solution induced an increasing inward membrane current in hTRPV1-transfected cells in the range of 44-51 ^{o}C both in absence and presence of amiloride buffer (Fig 4.6A+B). The inward current elicited at 48 ^{o}C in the presence of amiloride was significantly higher when compared to that measured in the standard buffer (-957 ± 159 pA, (n=5) and - 419 ± 38 pA (n=8), respectively (Fig. 4.6 and Fig. 4.7 A). However, there was no significant difference between the heat thresholds of activation in standard and amiloride buffer (44.8 ± 0.31 ^{o}C (n=8) and 45.20 ± 0.74 ^{o}C (n=5), respectively: Fig. 4.5 and Fig. 4.6 B).

Recordings from untransfected HEK293 cells during application of a heat ramp in standard buffer were also analysed. Untransfected HEK293 cells showed very small but visible heat-induced response during application of a heat ramp (Fig. 4.6). The average amplitude of untransfected cells at 48 ^{o}C was -63 ± 28 pA (n=7), which was significantly lower than that of the TRPV1-transfected cells (Fig. 4.7A). Consequently, untransfected cells in amiloride buffer during application of a heat ramp were not investigated, as the responses of these cells in standard buffer were non-specific heat-induced currents.

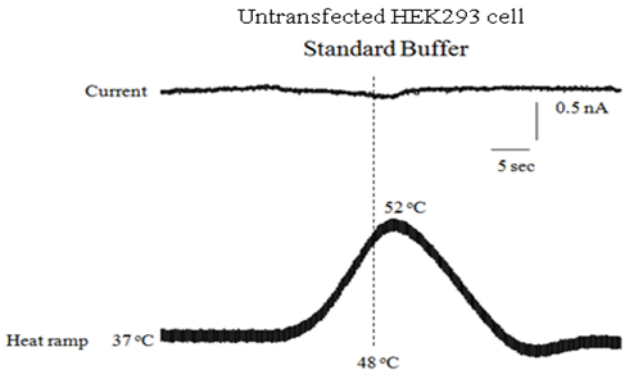

Figure 4.6 Heat-evoked response of untransfected cell in standard buffer. Upper trace: Whole-cell patch-clamp recording of untransfected cell in response to heat ramp (37 to 52 ^{o}C) in standard buffer. Lower trace: temperature of the superfusate from ~100µm from the cell from which the recording was done.

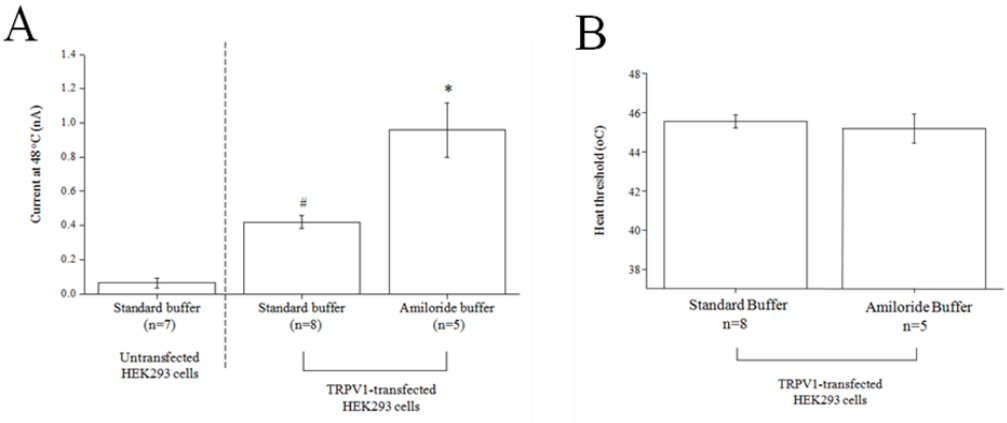

Figure 4.7 Heat-evoked responses of hTRPV1-transfected and untransfected cells in the absence and presence of amiloride (Part II). (A) Amiloride buffer significantly increases the amplitude of currents seen at 48 ^{o}C when compared to the response measured in the standard buffer (*). Transfecting HEK293 cells with TRPV1 significantly increases the current seen at 48 ^{o}C when compared to the response of untransfected cells in standard buffer (#). (B) Amiloride does not affect the heat activation threshold of hTRPV1. Each data point represents the mean ± SEM. Both the f-test and the normality (Shapiro-Wilk) test showed p-value of >0.05, indicating equal variance and normal distribution. The statistical significance of the difference in the means was assessed using the Student's t-test (two-tail distribution and two-sample equal variance). (* and #) Differences were regarded as being statistically significant at $p<0.05$.

Taken together, the results of these experiments showed that amiloride reduced the proton-activated current mediated through the constitutively expressed ASIC channels, and has a sensitising effect on TRPV1-mediated heat-evoked responses. However, amiloride does not affect TRPV1-mediated capsaicin -evoked responses.

4.4 Discussion

ASICs and TRPV1 are ion channels which are gated by protons. The presence of proton-responding ASIC channels in untransfected HEK293 cells suggests that these constitutively expressed ASICs should be taken into account in experimental design of subsequent experiments relating to TRPV1 (Hayes et al., 2000; Tominaga et al., 1998; Gunthorpe et al., 2001). My findings are in agreement with previously published data showing functional expression of hASIC in HEK293 cells, and a reduction of sensitivity to protons in the presence of amiloride, a sodium channel blocker. Interestingly, in addition to reducing ASIC-mediated responses, amiloride increased the TRPV1-mediated capsaicin-, and heat-evoked responses.

Whole-cell patch-clamp recordings of untransfected HEK293 cells showed that proton-evoked (pH 5.0) responses exhibited a fast activating and inactivating component followed by a slow activating and inactivating component. The fast activating and inactivating component of the response is similar to the rapidly desensitising ASIC-mediated response identified previously (Waldmann et al., 1997; Gunthorpe et al., 2001). However, the slow activating and inactivating component has not been reported by previous authors. One possible explanation for this difference may be that proton application was longer in this study than in previous studies. Application of protons for a longer period seems to activate an unidentified response which may even be mediated by a receptor other than hASIC. Interestingly, amiloride was also able to reduce the slow activating and inactivating component of the response, as well as the fast component. Further studies are required in order to elucidate the molecular basis of this response. Nevertheless, these data show that constitutive expression of hASIC contributes to proton-evoked currents in TRPV1-transfected HEK293 cells.

Initial inspection of the recordings during application of pH 4.0 in the presence and absence of amiloride to hTRPV1-transfected HEK293 cells showed a noticeable difference. In the presence of amiloride a larger current was seen. Initial

inspection of the recordings during application of pH 4.0 in the presence and absence of amiloride to hTRPV1-transfected HEK293 cells showed a noticeable difference. In the presence of amiloride a larger current was seen. Interestingly, the currents produced by TRPV1-transfected HEK293 cells in the absence of amiloride in this study are different from those found in previous reports. Hayes and colleagues (2000) reported a clearly visible, fast proton-gated current elicited by endogenous ASICs, which was shortly followed by a slower proton-gated current mediated by TRPV1. In the present study I did not find these two distinct currents. The reason for this difference could be that all the present recordings were made at 37^{o}C, while Hayes and colleagues recorded at room temperature. Due to the heat-sensitivity of TRPV1 (Caterina et al., 1997; Tominaga et al., 1998; Davis et al., 2000), the TRPV1-mediated component of the proton-induced response in these cells could appear earlier. Thus, the TRPV1-mediated response to protons may be merged with the response mediated by the activity of endogenously expressed receptors. The proton concentration–response curve of hTRPV1-transfected HEK293 cells in the presence of amiloride showed $pH_{0.5}$ response at pH 5.6 which is close to that reported for both human and rat TRPV1 (Hayes et al., 2000; Tominaga et al., 1998). In the absence of amiloride, the $pH_{0.5}$ was at pH 6.2, which reflects the combination of the ASIC and TRPV1 receptors found in hTRPV1-transfected HEK293 cells. These data therefore suggest that in order to distinguish the difference between ASIC- and TRPV1-mediated proton-evoked current, it is essential to inhibit the endogenously expressed ASIC when studying heterologously expressed TRPV1 in HEK293 cells, at least at 37 ^{o}C.

There are no data available on the possible effect of amiloride on TRPV1-mediated responses evoked by heat and capsaicin. Accordingly, I investigated the effect of amiloride on TRPV1-mediated capsaicin-evoked, and heat-evoked, responses in hTRPV1-transfected HEK293 cells.

Although 10 μM capsaicin produced a larger response in the presence of amiloride, this difference was not significant. Furthermore, I found that the capsaicin concentration response curve in the presence of amiloride was not different from that

found in the absence of the sodium channel blocker. These data suggest that amiloride does not affect TRPV1 responses to capsaicin-induced activation.

Interestingly, the heat evoked responses in the presence and absence of amiloride were different. Although the heat threshold of activation in the presence of amiloride was not significantly different from that measured in the standard buffer, the amplitude of the current elicited at 48^{o}C, in the presence of amiloride, was significantly larger than that found in absence of this agent. These data indicated that heat-induced currents were affected by amiloride but not capsaicin-induced currents. The underlying mechanism of this effect is not clear and requires further investigation. However, given the complex effect of amiloride on the TRPV1-evoked responses, it may be that amiloride affects the integration mechanism of the channel.

Chapter 5

NATURALLY OCCURRING POLYMORPHISM IN HUMAN TRPV1 GENE ALTERS THE SENSITIVITY OF THE ION CHANNEL.

5.1 Introduction

The human TRPV1 ion channel exhibits several naturally occurring polymorphisms To investigate whether the ethnic differences in heat-sensitivity are due to mutations in TRPV1 five haplotypes were made containing SNP. $hTRPV1_{111}$ and $hTRPV1_{222}$ were chosen for the first comparison as, if there were any differences in the responses, it would be apparent in these two haplotypes, because they show the greatest genetic variability. To elucidate whether these mutations produce any functional differences, whole-cell patch-clamp recordings were done during application of each of capsaicin, anandamide, protons and heat, and voltage activation.

	Amino Acid		
Code name.	**Position 315**	**Position 469**	**Position 585**
$hTRPV1_{111}$	I	T	V
$hTRPV1_{211}$	M	T	V
$hTRPV1_{121}$	I	I	V
$hTRPV1_{112}$	I	T	I
$hTRPV1_{222}$	M	I	I

Table 5.1. Table showing 5 haplotypes of hTRPV1, where isoleucine (I), threonine (T) and valine (V) are substituted by a different amino acid within a specified position.

5.2 Methods

Cell culture of HEK293 cells, transient transfection, and whole-cell patch clamp technique were used in this section. For further detail, see Chapter Two: Materials and Methods.

5.3 Results

5.3.1 Comparative analysis of $hTRPV1_{111}$-, and $hTRPV1_{222}$ - mediated responses to various activators

I studied the issue of whether naturally occurring mutations in hTRPV1 have functional effects by analysing the differences in whole-cell currents produced by $hTRPV1_{111}$ and mutant hTRPV1s to various TRPV1 agonists. Responses were elicited by application of: capsaicin; anandamide; protons; and heat; or alterations in the membrane potential.

Four different mutants were available for comparative analysis. One of these mutants ($hTRPV1_{222}$) possessed all of the mutations found individually in the other three mutants. Therefore, I decided to use this mutant ($hTRPV1_{222}$) for the initial comparative analysis with $hTRPV1_{111}$.

5.3.1.1 Comparison of responses to capsaicin

Capsaicin is the archetypical activator of TRPV1. Therefore, first I compared capsaicin-activated currents produced by $hTRPV1_{111}$ and $hTRPV1_{222}$ using normal electrophysiology bath and pipette solutions. The membrane potential was held at -60 mV. All experiments were performed at physiological temperature of 36-37 ^{o}C.

I found in this experiment that capsaicin evoked concentration-dependent responses in cells transfected by either of the clones (Fig. 5.1 A and B). The EC_{50}s of capsaicin in $hTRPV1_{111}$-transfected, and $TRPV1_{222}$-transfected cells were 817.61 ± 148 nM and 89.64 ± 64 nM, respectively, which were significantly different from each other (Fig. 5.1C). There was no significant difference between I_{max} of capsaicin in $hTRPV1_{111}$-transfected, and $TRPV1_{222}$-transfected cells (6.36 ± 0.45 nA and 5.84 ±

0.89 nA, respectively) (Fig. 5.1D). Untransfected HEK293 cells failed to elicit responses, during application of 10 µM capsaicin (not shown).

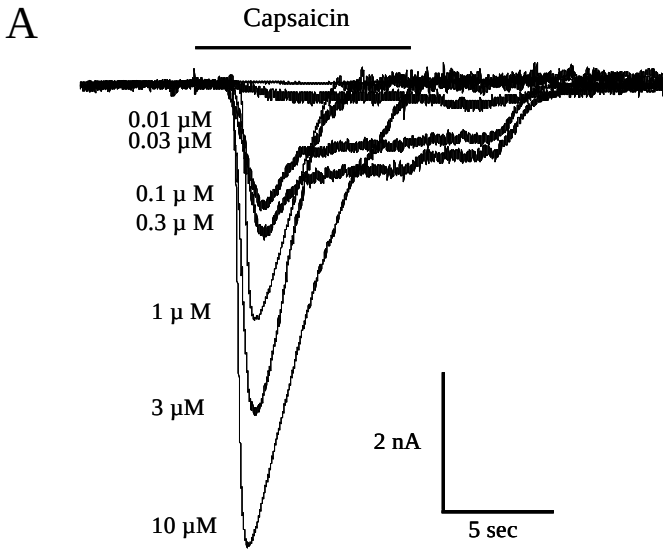

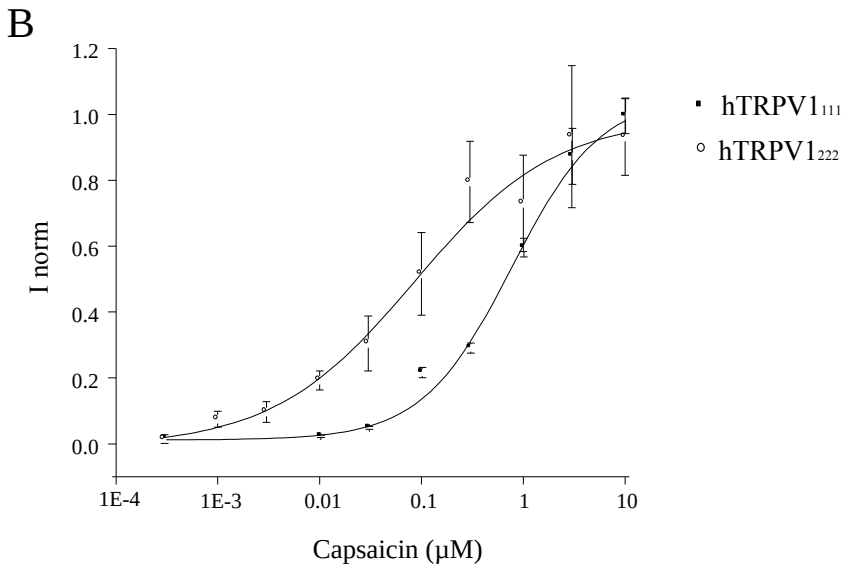

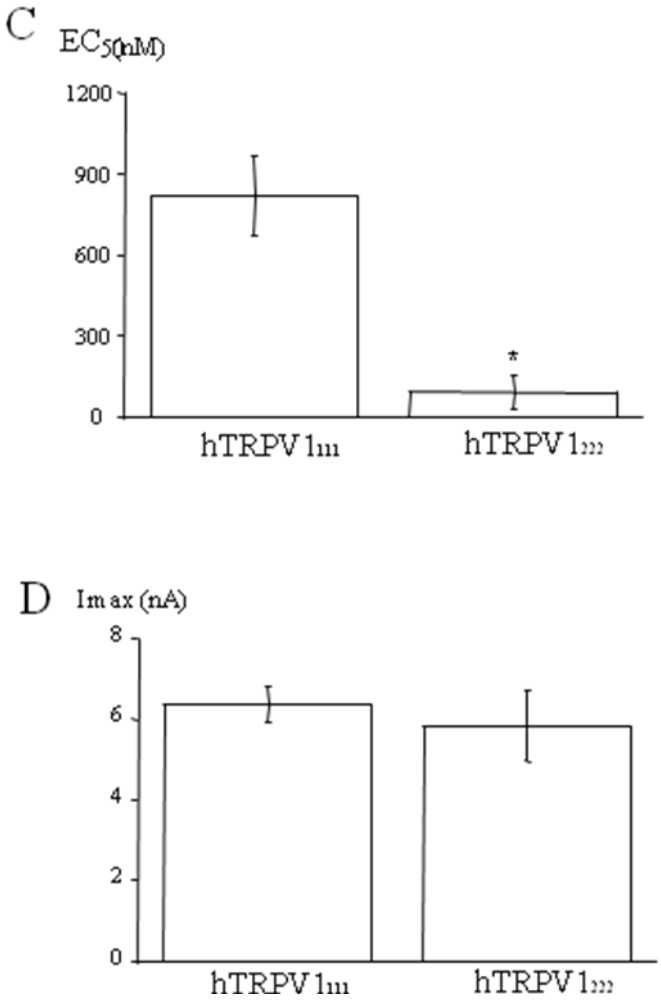

Figure 5.1. Capsaicin-evoked responses of $hTRPV1_{111}$-transfected, and $hTRPV1_{222}$-transfected, HEK293 cells. Normal extracellular and intracellular solutions were used. (A) Whole-cell patch-clamp recordings of $hTRPV1_{111}$-mediated responses evoked. Note the concentration-dependence of the peak amplitudes. (B) Pooled normalised concentration response curves of $hTRPV1_{111}$ and $hTRPV1_{222}$ to capsaicin. (C) E_{50} of capsaicin in $hTRPV1_{111}$-transfected and $hTRPV1_{222}$-transfected, cells. (D) I_{max} of capsaicin in $hTRPV1_{111}$-transfected and $hTRPV1_{222}$-transfected, cells. Data obtained from each cell were normalised to the cell's response of $hTRPV1_{111}$ at 10 µM capsaicin. Each data point represents mean ± SEM ($n \geq 5$). Both the Levene's test for equal variance and the normality test (Shapiro-Wilk) showed p-values of >0.05, indicating equal variance and normal distribution. The capsaicin-response was fitted with a sigmoidal dose-response curve (Graphpad Prism, r2 ≥0.95). Statistical comparisons between two dose-response curves were analysed using Student's t-test (two-tailed test, equal variance). Note that comparisons between the EC_{50}s showed a significant difference but not I_{max}s of the two clones.

I next studied the current-voltage relationship of the 1 μM capsaicin-evoked currents in standard electrophysiology bath and pipette solutions, using voltage ramps between -100mV and +40mV (340 milliseconds). The current-voltage curves for both $hTRPV1_{111}$ and $hTRPV1_{222}$ showed similar outward rectification (Fig. 5.4). The reversal potential of $hTRPV1_{111}$ and $hTRPV1_{222}$ were 10.1 ± 6.1 mV (n=5) and 5.3 ± 4.2 mV (n=5), respectively. These data showed that the mutations in $hTRPV1_{222}$ did not have any effect on the efficacy of capsaicin or on the ion selectivity of the channel.

A

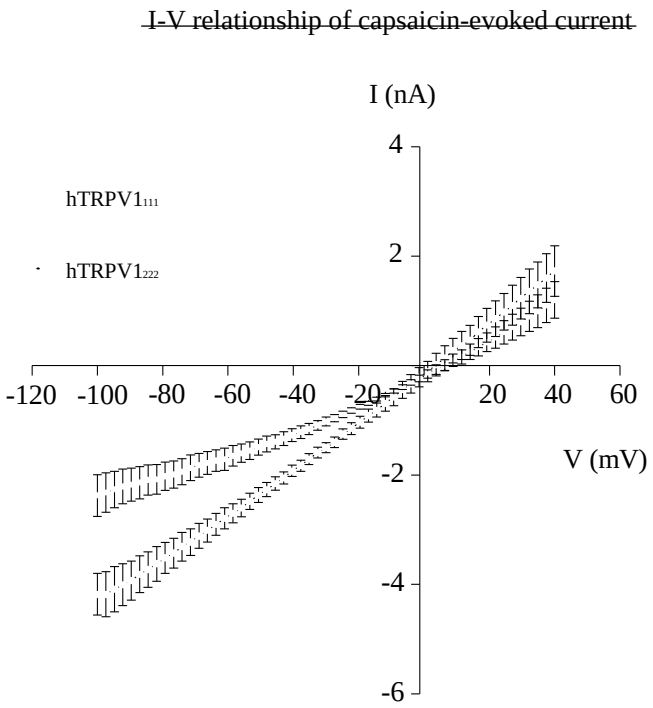

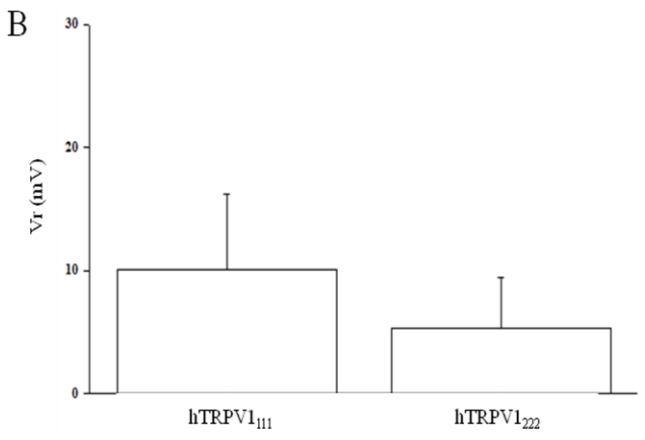

Figure 5.4. Current-voltage relationship of 1 μM capsaicin-evoked current of $hTRPV1_{111}$ and $hTRPV1_{222}$. Normal extracellular and intracellular solution was used. (A) I-V relationship of capsaicin-evoked currents. (B) Reversal potential of capsaicin-evoked currents. Note that currents produced by either clones show similar outward rectification and reversal potentials. Each data point represents mean ± SEM ($n \geq 5$). Each data point represents mean ± SEM. Both the f-test and the normality test (Shapiro-Wilk) showed p-values of >0.05, indicating high probability of equal variance and normal distribution. The statistical difference in the means was assessed using the Student t-test (two-tail distribution and two-sample equal variance). Note that there were no statistical differences between the reversal potentials of the two clones.

5.3.1.2 Comparison of responses to anandamide

Previous findings indicated that the endogenous lipid, anandamide, may be one of the most important endogenous TRPV1 activators under certain conditions (Zygmunt et al., 1999; Smart et al., 2000; Dinis et al., 2004; Olah et al., 2001; Singh Tahim et al., 2005). In order to find out whether the $hTRPV1_{111}$ and $hTRPV1_{222}$ clones respond to anandamide differently, I compared the anandamide–evoked response of $hTRPV1_{111}$-transfected and $hTRPV1_{222}$-transfected cells, using normal electrophysiology bath and pipette solutions. The membrane potential was held at -60 mV. All experiments were performed at physiological temperature of 36-37 ^{o}C.

I found that anandamide in Tocrisolve produced concentration-dependent responses in both clones (Fig. 5.3 A and B). The mean peak current during 1 µM, 3 µM and 10 µM anandamide during 50 seconds application to $hTRPV1_{111}$ were 83.13 ± 48.92 pA (n=5), 166.25 ± 28.12 pA (n=5), 181.30 ± 71.90 pA (n=5), respectively, and $hTRPV1_{222}$ were 117.15 ± 27.77 pA (n=5), 160.75 ± 53.24 pA (n=5), 183.17 ± 36.23 (n=5), respectively. Moreover, 0.03 % Tocrisolve failed to evoke a response when applied to $hTRPV1_{111}$-transfected cells (data not shown). There were no significant differences between both clones from any of the three concentrations of anandamide tested. These data indicated that those mutations in $hTRPV1_{222}$ did not have any effect on the anandamide-mediated current when compared to $hTRPV1_{111}$.

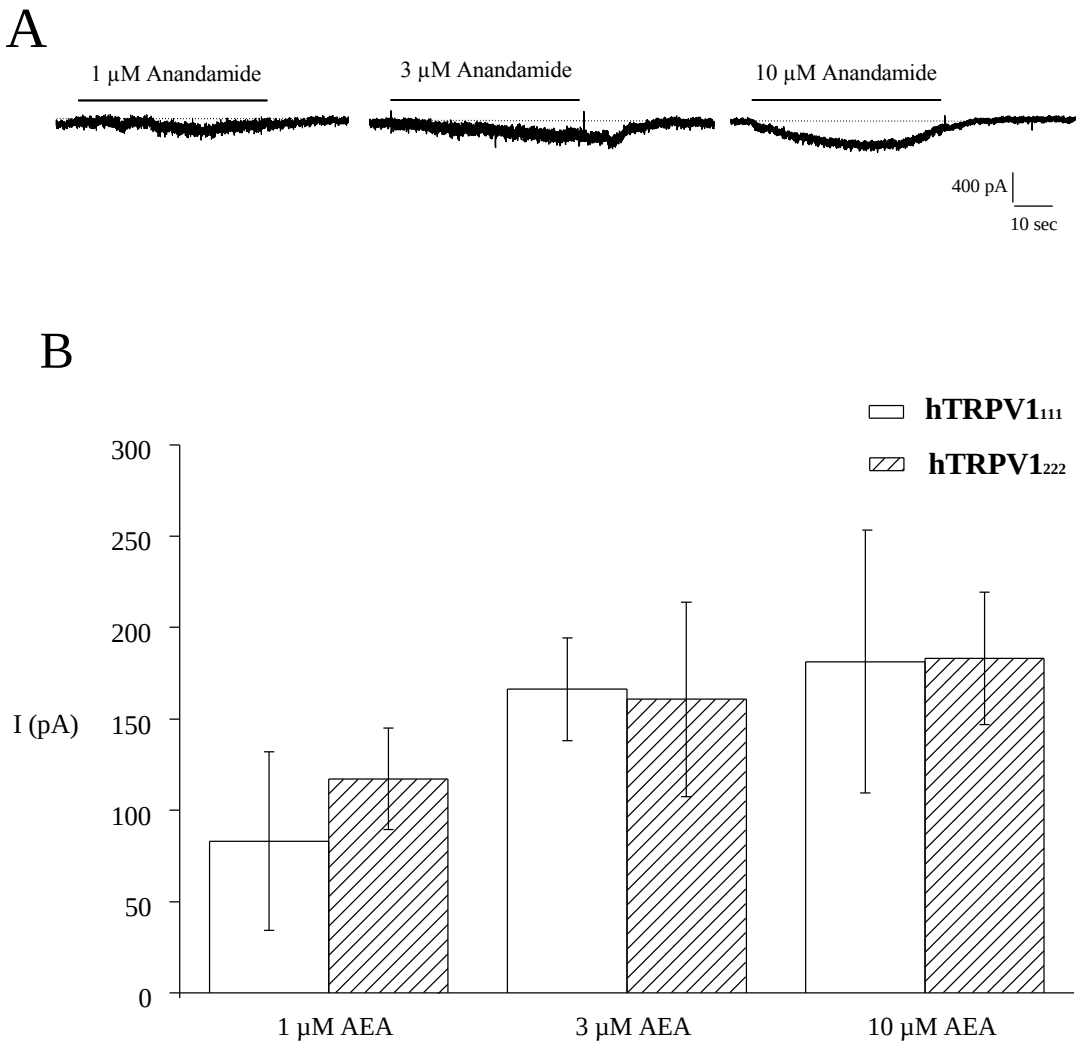

Figure 5.3. Anandamide-evoked responses in $hTRPV1_{111}$-transfected, and $hTRPV1_{222}$-transfected, HEK293 cells. Normal extracellular and intracellular solutions were used. (A) Whole-cell patch-clamp recordings of $hTRPV1_{111}$-mediated responses to anandamide using normal extracellular and intracellular solution. (B) Pooled normalised concentration response curves of $hTRPV1_{111}$ and $hTRPV1_{222}$ to anandamide. Each data point represents mean ± SEM (n = 5). Both the Levene's test for equal variance and the Shapiro-Wilk normality test showed p-values of >0.05, equal variance and normal distribution. The statistical difference between the means of the various treatments within a group was assessed using 1-ANOVA. Whether the differences found were significant was established using Fisher LSD post-hoc test. The statistical difference between the means in the respective treatment groups was assessed using Student's t-test (two-tail distribution and two-sample equal variance). A post hoc test was not computed as the overall p-value was >0.05. Note: the means of each group were not statistically different from each other.

5.3.1.3 Comparison of responses to protons

Protons are potent activators of the TRPV1 (Caterina et al., 1998; Jordt et al., 2000; Ryu et al., 2003). Therefore, I next studied proton-activated currents in $hTRPV1_{111}$-transfected and $hTRPV1_{222}$-transfected, cells. Having regard to previous reports (Jordt et al., 2000; Ryu et al., 2003) and my finding that HEK293 cells constitutively express proton-responding ion channels, the superfusate contained 30 µM amiloride (see chapter 4).

In these experiments, I found that protons produced concentration-dependent responses in both clones (Fig. 5.4 A and B). The half-maximal pH (pH_{50}) for channel activation for $hTRPV1_{111}$ and $hTRPV1_{222}$ were pH 5.80 ± 0.14 and pH 5.77 ± 0.19, respectively (Fig. 5.4 C). The maximal effect of pH (pH_{max}) for channel activation for $hTRPV1_{111}$ and $hTRPV1_{222}$ were 2.54 ± 0.30 nA and 1.80 ± 0.125, respectively (Fig. 5.4 D).

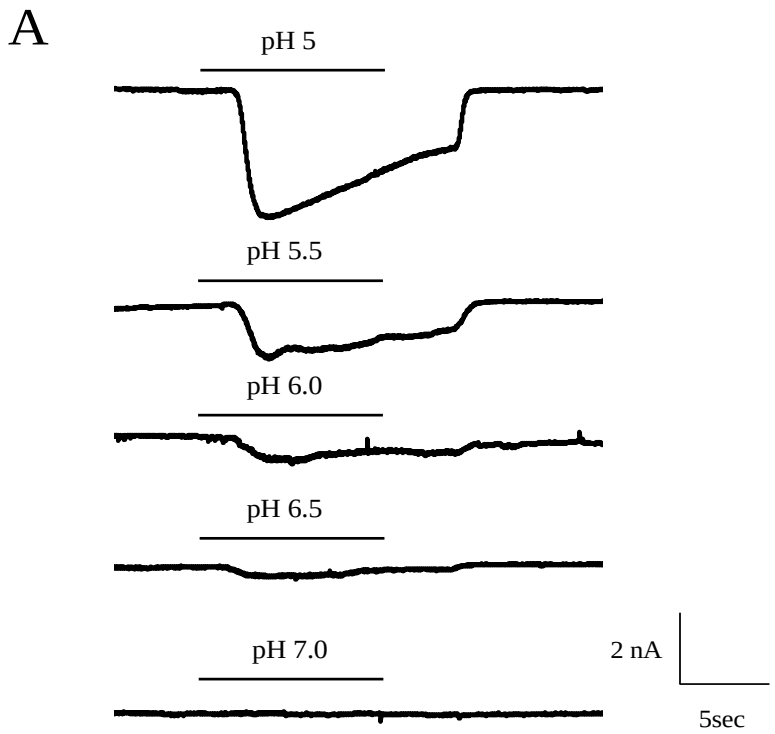

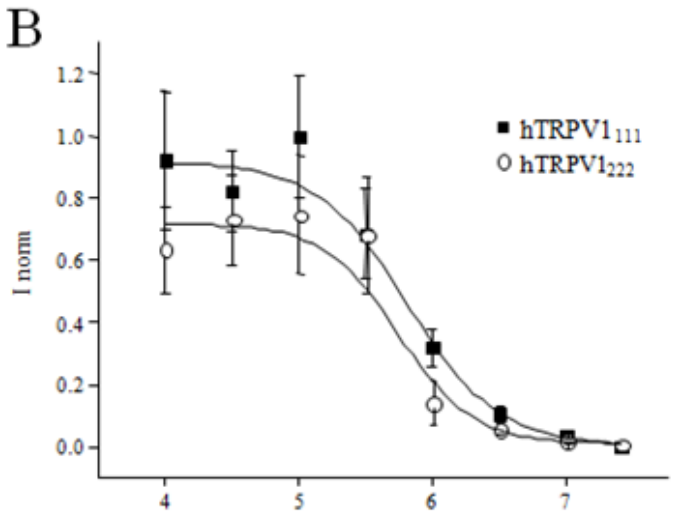
B
I norm
1.2
1.0
0.8
0.6
0.4
0.2
0.0
4
5
6
7
hTRPV1 111
hTRPV1222

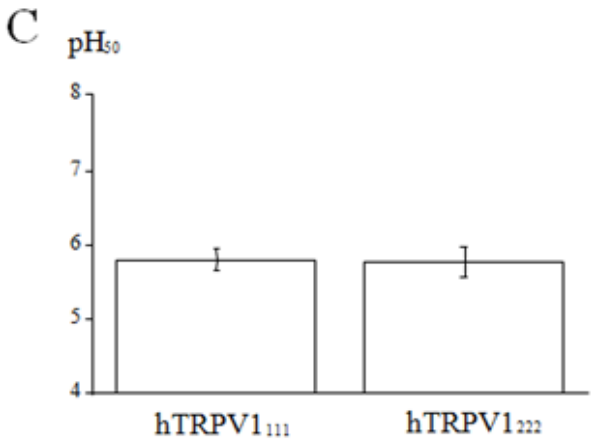
C
pH50
8
7
6
5
4
hTRPV1 111
hTRPV1 222

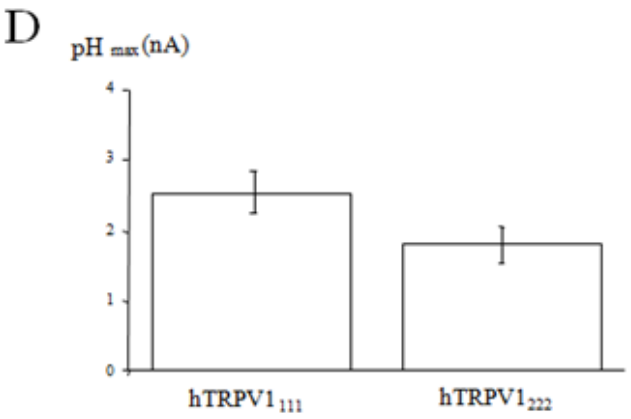
D
pH max (nA)
4
3
2
1
0
hTRPV1 111
hTRPV1222

Figure 5.4. Proton-evoked responses of $hTRPV1_{111}$-transfected and $hTRPV1_{222}$-transfected, HEK293 cells. Extracellular solution containing amiloride and normal intracellular solutions were used. (A) Whole-cell patch-clamp recordings of $hTRPV1_{111}$-evoked response to protons using extracellular solution containing amiloride and normal intracellular solution. (B) Pooled normalised concentration response curves of $hTRPV1_{111}$ and $hTRPV1_{222}$ to protons. Data obtained from each cell were normalised to the cell's response of $hTRPV1_{111}$ to pH 5. Each data point represents mean ± SEM ($n \geq 5$). Data points fitted with sigmoidal curve function (Graphpad Prism statistical analysis programme). (C) pH_{50} of protons in $hTRPV1_{111}$-transfected and $hTRPV1_{222}$-transfected, cells. (D) pH_{max} of protons in $hTRPV1_{111}$-transfected and $hTRPV1_{222}$-transfected, cells. Both the Levene's test for equal variance and the normality test (Shapiro-Wilk) showed p-values of >0.05, indicating equal variance and normal distribution. The pH-response was fitted with a sigmoidal dose-response curve (Graphpad Prism, $r2 \geq 0.95$). Statistical comparisons between two dose-response curves were analysed using Student t-test (two-tailed test, equal variance). Note, there was no statistical difference between pH_{50} and $pH_{max.}$ The current was normalised to pH5-mediated $hTRPV1_{111}$-activation.

I next examined the current-voltage relationship of pH 5-evoked currents in standard electrophysiology bath and pipette solutions using voltage ramps between -100 mV and +40mV (340 milliseconds). The current-voltage curve for $hTRPV1_{111}$ and $hTRPV1_{222}$ showed similar outward rectification (Fig. 5.7). The reversal potential of $hTRPV1_{111}$ and $hTRPV1_{222}$ using physiological bath and pipette solutions were 18.7 ± 7.1 mV (n=5) and 22.18 ± 2.5 mV (n=4), respectively. These values were not significantly different from each other. These data indicated that either those mutations in $hTRPV1_{222}$ did not have any effect on the potency and efficacy of protons on $hTRPV1_{111}$, and the ion selectivity of the channel or, alternatively, the change produced by the mutations compensated for each other's effects.

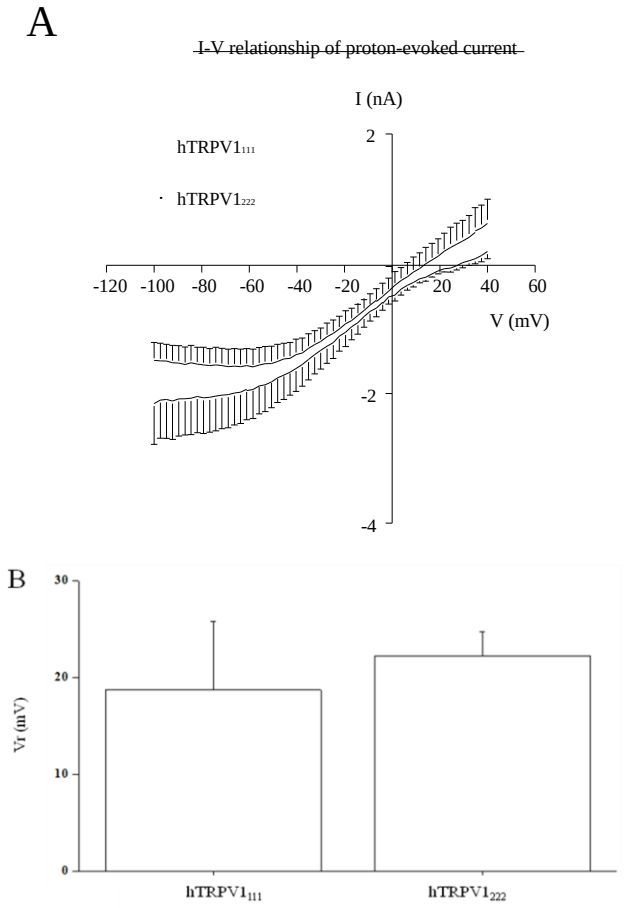

Figure 5.7. Current-voltage relationship of pH 5-evoked currents of $hTRPV1_{111}$ and $hTRPV1_{222}$ using normal extracellular and intracellular solution. (A) I-V relationship of pH 5-evoked currents. Both clones show similar outward rectification and reversal potentials (B) Reversal potential of of pH 5-evoked currents. Each data point represents mean ± SEM ($n \geq 5$). The statistical difference in the means was assessed using the Student t-test (two-tail distribution and two-sample equal variance). Note that there were no statistical differences between the reversal potentials of the two clones.

5.3.1.4 Comparison of responses to heat

One of the most characteristic features of TRPV1 is its sensitivity to heat. TRPV1 at negative membrane potentials produces an inward current when activated by heat above ~ 44 ^{o}C (Caterina et al., 1998; Hayes et al., 2000; Smart et al., 2003). Hence, I next compared heat-activated currents in hTRPV1$_{111}$-transfected, and hTRPV1$_{222}$-transfected, cells by applying heat *via* a temperature ramp between 37-50 ^{o}C using standard electrophysiology bath and pipette solutions.

Using the Arhenius plots (Vyklicky et al, 1999), I found that hTRPV1$_{111}$ and hTRPV1$_{222}$ show a mean threshold of activation of 44.49 ± 0.31 ^{o}C (n=8), and 42.43 ± 0.44 oC (n=8), respectively (Fig. 5.6 A and B). These threshold values were significantly different from each other. The amplitude of the responses at 48 ^{o}C were also calculated and found to be -429 ± 34.6 pA (n=8) and -991 ± 226 pA (n=5), respectively (Fig. 5.6 A and B). These values were also significantly different from each other.

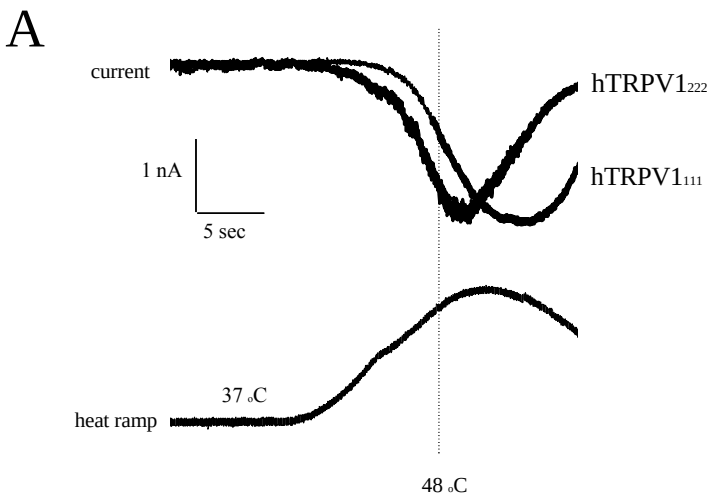

Figure 5.6

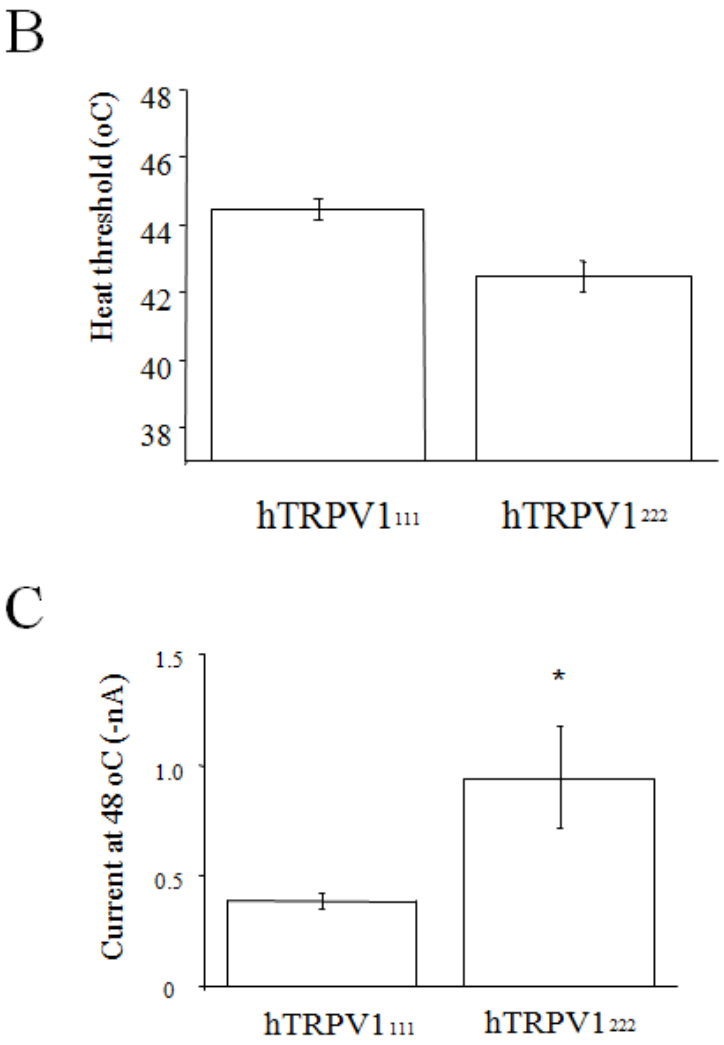

Figure 5.6 Heat-evoked responses of $hTRPV1_{111}$-transfected and $hTRPV1_{222}$-transfected, HEK293 cells. Normal extracellular and intracellular solutions were used. (A) Upper trace: $hTRPV1_{111}$-mediated, and $hTRPV1_{222}$-mediated, currents evoked by heat ramp (37 - 50^{o}C). Lower trace: temperature of the superfusate from ~100µm from the cell from which the recording was done. (B) Heat threshold of, and (C) amplitude of current at 48ºC mediated by, $hTRPV1_{111}$ and $hTRPV1_{222}$. Note that while the heat threshold is lower, the current measured at 48ºC is higher for the $hTRPV1_{222}$-mediated current than for the $hTRPV1_{111}$ mediated current. Each data point represents mean ± SEM (n ≥). The statistical difference in the means was assessed using the Student t-test (two-tail distribution and two-sample equal variance). (*) Differences were regarded as being statistically significant at $p<0.05$.

I then examined the current-voltage relationship of heat-evoked currents in the standard bath and pipette solutions using voltage ramps between -100mV and +40mV (340 milliseconds). The current-voltage curves for $hTRPV1_{111}$ and $hTRPV1_{222}$ in this experiment also showed similar outward rectification (Fig. 5.9). The reversal potentials of $hTRPV1_{111}$ and $hTRPV1_{222}$ were 9.15 ± 4.60 mV (n=10) and 19.26 ± 3.84 mV (n=5), respectively. The difference in the reversal potentials of $hTRPV1_{222}$ and $hTRPV1_{111}$ was not significant.

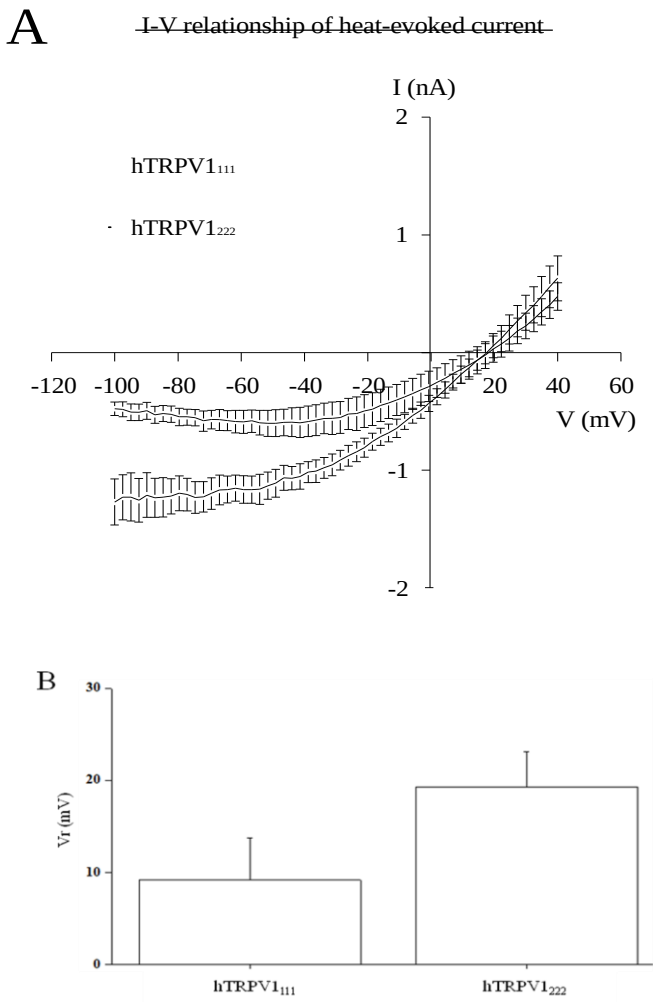

Figure 5.9 Current-voltage relationships of heat-evoked currents of $hTRPV1_{111}$ and $hTRPV1_{222}$. Normal extracellular and intracellular solutions were used. (A) I-V relationship of heat-evoked currents. Note that both currents show similar outward rectification and reversal potentials. (B) Reversal potential of heat-evoked currents. Each data point represents mean ± SEM (n ≥5). The statistical difference in the means was assessed using the Student t-test (two-tail distribution and two-sample equal variance). Note that there were no statistical differences between the reversal potentials of the two clones.

5.3.1.5 Comparison of responses to voltage-dependent activation

TRPV1, in addition to being a ligand-, and temperature-, gated ion channel, is also a voltage-gated ion channel (Piper et al., 1999; Gunthorpe et al., 2000; Voets et al., 2004; Matta and Ahern, 2007). Therefore, I next, with limitations discussed in Chapter 2, investigated $hTRPV1_{111}$-mediated, and $hTRPV1_{222}$-mediated, responses to changes in membrane potentials. The voltage-dependent activation of the clones was established from the differential current of the current-voltage relationships of currents of the voltage-activated steady-state current and the current flowing through TRPV1 at maximum open probability. The maximum open probability was produced by the application 10 μM capsaicin. The currents were measured at symmetrical Na+ concentrations (130 mM).

Since re-analysis of the conductances in $hTRPV1_{111}$ and $hTRPV1_{222}$ transfected cells showed the presence of two voltage-dependent conductances, the half activation potentials of these two conductances were established for each haplotype. In $hTRPV1_{111}$ the lower and upper $V_{1/2s}$ were: -87.2 ± 2.2 mV and 42.3 ± 10 mV, respectively (Fig. 5.8). In $hTRPV1_{222}$ the lower and upper $V_{1/2}$s were: -1.5 ± 5.9 mV and 83.3 ± 10 mV, respectively (Fig. 5.8).

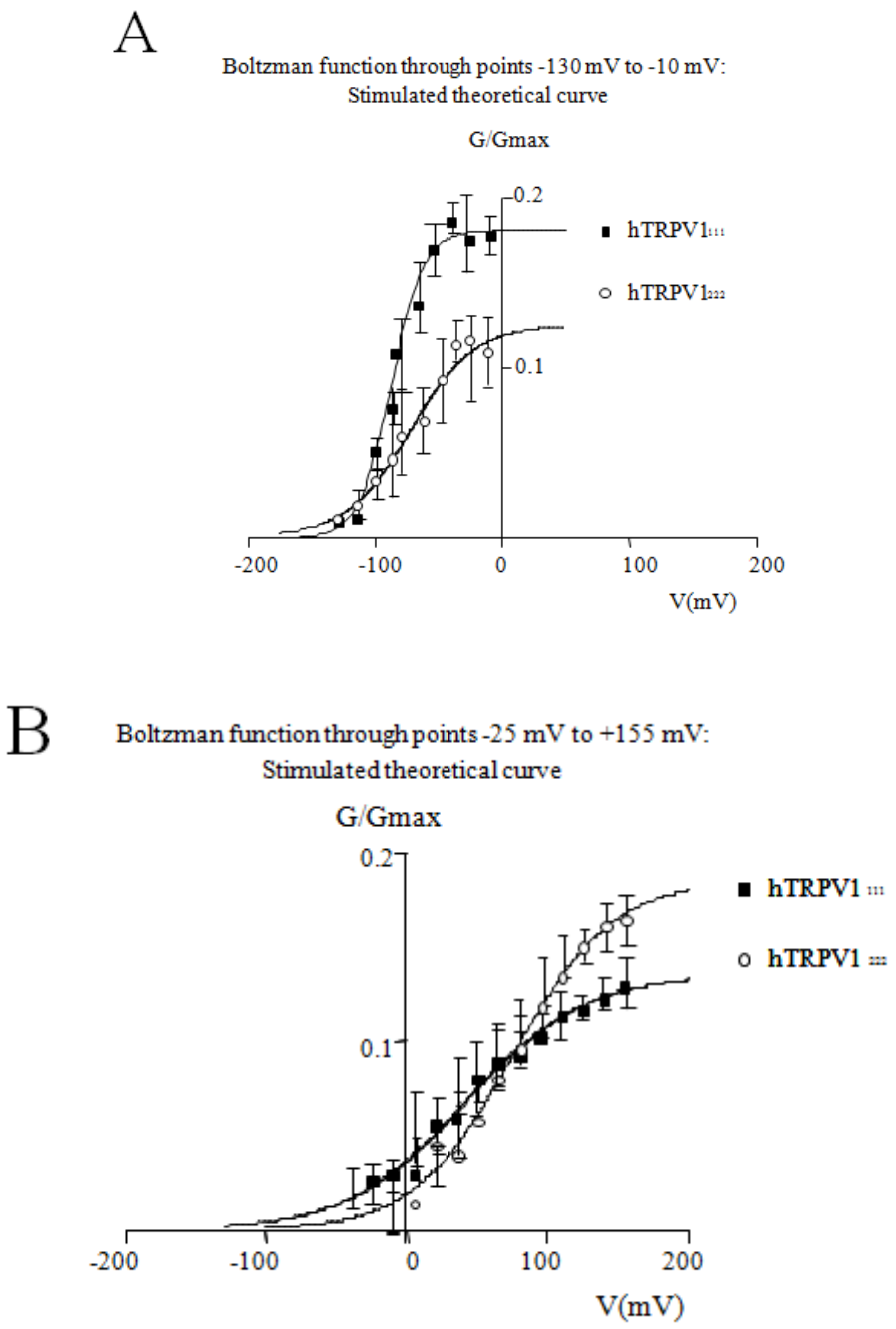
A
Boltzman function through points -130 mV to -10 mV:
Stimulated theoretical curve
G/Gmax
0.2
0.1
hTRPV1111
hTRPV1222
-200
-100
0
100
200
V(mV)
B
Boltzman function through points -25 mV to +155 mV:
Stimulated theoretical curve
G/Gmax
0.2
0.1
hTRPV1 111
hTRPV1 222
-200
-100
0
100
200
V(mV)

Figure 5.8

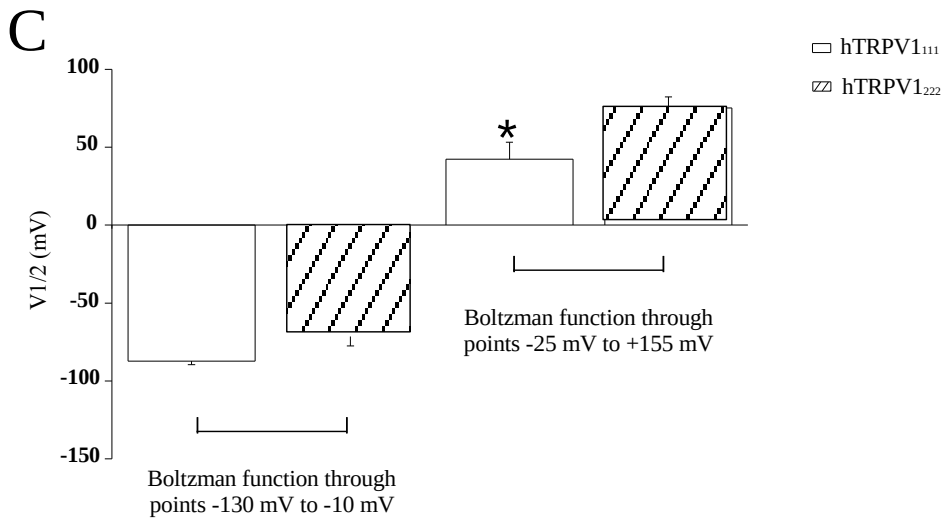

Figure 5.8 Voltage-evoked response of hTRPV1$_{111}$-transfected, and hTRPV1$_{222}$-transfected HEK293 cells using symmetrical Na+ concentrations (130 mM). (A) Data points are fitted with a Boltzmann function through data points 130 mV to -10 mV. (C) $V_{1/2}$ of the corresponding Boltzmann function curves. Each data point represents mean ± SEM (n=5). Statistical comparisons of two dose-response curves were performed using Student t-test (two-tailed test, equal variance). (*) Differences were regarded as being statistically significant at $p<0.05$. Note that comparison between the $V_{1/2}$s through points -25 mV to +155 mV showed a significant difference.

5.3.1.6 Summary of comparisons of responses of hTRPV1$_{111}$ and hTRPV1$_{222}$ to various to TRPV1 activators

The comparison of responses to various activators produced by hTRPV1$_{111}$ and hTRPV1$_{222}$, respectively, demonstrated substantial differences (Table 5.2). The mutations in positions I315M, T469I and V585I, found in hTRPV1$_{222}$ resulted in increased potency for capsaicin without affecting the efficacy of hTRPV1$_{111}$. The mutations also increased the heat-sensitivity of the channel and reduced voltage-sensitivity. However, I found that the mutations did not change the proton-sensitivity, anandamide-sensitivity or the reversal potential obtained from current-response curves evoked by various TRPV1 activators (Fig. 5.9).

The mutations at positions I315M and V585I involved changes of neutral amino acids to other neutral amino acids. However, the mutation at position 469 involved a change of a polar amino acid to a neutral, non-polar, amino acid. Therefore, I hypothesised that the mutation which may be responsible for the changes may be the one at position 469.

	hTRPV1$_{111}$	hTRPV1$_{222}$	Sig. Diff
Capsaicin EC_{50}	817 ± 148 nM	89.6 ± 64.7 nM	yes
Capsaicin I_{max}	6.36 ± 0.45 nA	5.84 ± 0.89 nA	no
Anandamide	no difference	no difference	n/a
pH_{50}	pH 5.80 ± 0.14	pH 5.77 ± 0.19	no
pH_{max}	2.54 ± 0.30 nA	1.80 ± 0.25 nA	no
Heat threshold at -60 mV	44.5 ± 0.31ºC	42.3 ± 0.45 ºC	yes
Heat current at 48 ^{o}C	429 ± 34 pA	991 ± 229 pA	yes
$V_{1/2\ lower}$	-87.2 ± 2.2 mV	-71.5 ± 5.9 mV	no
$V_{1/2\ upper}$	42.3 ± 10 mV,	83.3 ± 10 mV	yes

Table 5.2. Summary of responses of hTRPV1$_{111}$-transfected and hTRPV1$_{222}$-transfected, HEK293 cells evoked by various TRPV1 activators. Normal extracellular and intracellular solution was used, with the exception of $V_{1/2}$ where recorded using symmetrical Na^{+} (150 mM).

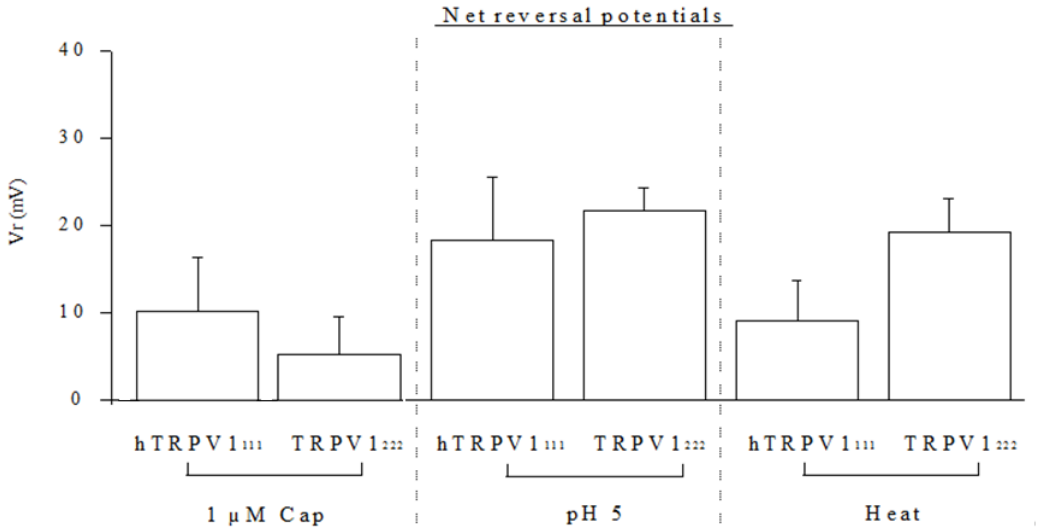

Figure 5.9. Summary of reversal potential obtained from current-response curves of $hTRPV1_{111}$-transfected and $hTRPV1_{222}$-transfected, HEK293 cells evoked by various TRPV1 activators. Normal extracellular and intracellular solutions were used. The statistical difference between the means of the various agonists within a group was assessed using 1-ANOVA. Whether the differences found were significant was established using Fisher LSD post-hoc test. The statistical difference between the means in the respective haplotype was assessed using Student's t-test (two-tail distribution and two-sample equal variance shown). Note that there is no statistical difference between the reversal potentials.

5.3.2 The relationship between heat and voltage for $hTRPV1_{111}$ and $hTRPV1_{222}$

It has been shown that TRPV1 is a stimulus integrator (Tominaga et al., 1998; Davis et al., 2000; Caterina et a., 2000; Cortright et al., 2004; Tominaga et al., 2005). While the mechanism of stimulus integration has not been elucidated, currently there are two hypotheses regarding this mechanism. According to the first hypothesis, the heat sensor may play a central role in stimulus integration and channel gating because other activators, including capsaicin, protons, and post-translational modifications, all reduce the heat threshold of the receptor (Jordt et al., 2000; Liang et al., 2001; Babes et al., 2002; Sugiura et al., 2002; Petho et al., 2001; Chuang et al., 2001; Prescott and Julius, 2003 Premkumar and Ahern, 2000; Tominaga et al., 2001). According to the second hypothesis, however, the ultimate activator of TRPV1 is depolarization, i.e., a shift of the activation threshold towards the resting membrane potential (Voets et al., 2004; Nilius et al., 2005). This latter hypothesis also postulates that the temperature sensitivity is tightly linked to voltage-dependent gating of TRPV1. This assumption is based on the findings that: (i) increasing the ambient temperature reduces the threshold of voltage-dependent gating of TRPV1; and (ii) depolarising the membrane reduces the heat threshold of TRPV1 (Voets et al., 2004). Therefore, I next studied the link between heat-sensitivity and voltage-sensitivity in both $hTPRV1_{111}$ and $hTRPV1_{222.}$

5.3.2.1 The heat threshold depends on the holding potential

In the first experiment I measured heat-activated responses at different holding potentials. The heat activation threshold for $hTRPV1_{111}$ at holding potentials of: -20 mV, -40 mV, -60 mV and -80 mV were 43.42 ± 0.67 ºC (n=5), 44.49 ± 0.31°C (n=8), 40.78 ± 0.88°C (n=5), and 40.01 ± 1.25 °C (n=5), respectively (Fig. 5.11). The respective values for $hTRPV1_{222}$ were as follows: 42.04 ± 0.80 °C (n=5), 42.43 ± 0.44 °C (n=8), 38.00 ± 0.23 °C (n=5) and 39.44 ± 0.90 °C (n=5), (Fig. 5.11).

Overall, these data show that depolarising the membrane potential decreases the heat activation threshold (Fig. 5.10). The heat activation threshold for $hTRPV1_{222}$ at -20 mV and -40 mV were not significantly different from each other either. However, the heat activation threshold measured at -20 mV was significantly different from the threshold measured at -60 mV. In addition, the heat activation thresholds measured at both -20 mV and -40 mV were significantly different from that measured at -80 mV. The heat activation thresholds measured at holding potentials of - 60 mV and - 40 mV, were significantly lower for $hTRPV1_{222}$ than $hTRPV1_{111}$.

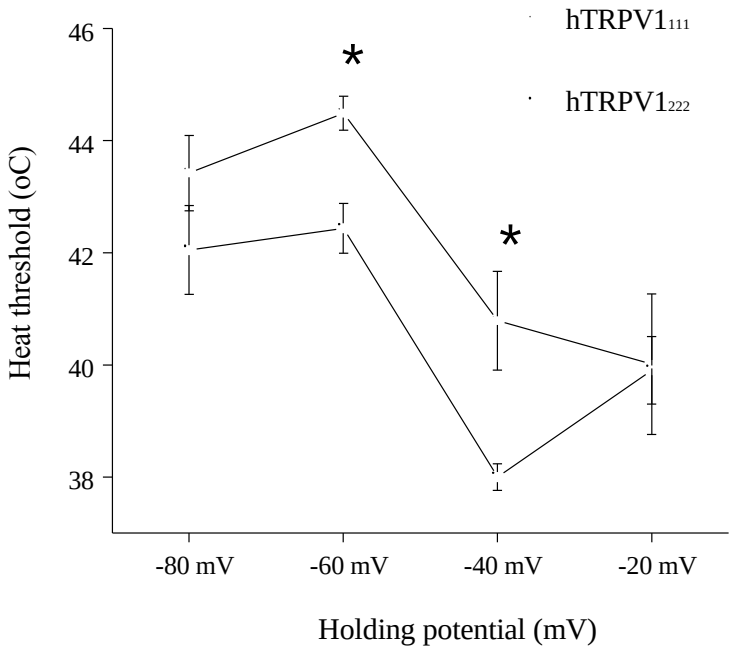

Figure 5.10. Heat activation threshold of $hTRPV1_{111}$ and $hTRPV1_{222}$ at four different holding potentials. Normal extracellular and intracellular solutions were used. Note that depolarization reduces the heat threshold for both clones. Note also that the heat activation threshold of $hTRPV1_{222}$ is significantly lower that that of $hTRPV1_{111}$ at each membrane potential. Each data point represents mean ± SEM (n= 5 or more). The statistical difference between the means of the various membrane potential within a group was assessed using 1-ANOVA. Whether the differences found were significant was established using Fisher LSD post-hoc. The statistical difference between the means in the respective membrane potential was assessed using Student's t-test (two-tail distribution and two-sample equal variance; data not shown). (*) Differences were regarded as being statistically significant at $p<0.05$

5.3.3 Comparative analysis of $hTRPV1_{211}$-, $hTRPV1_{121}$- and $hTRPV1_{112}$-, mediated responses

Given that the mutation at T469I ($hTRPV1_{121}$) was the only mutation involving a change in the polarity of an amino acid in $TRPV1_{222}$, it was considered that this mutation was the most likely to be responsible for the differences in responses to various activators found in $hTRPV1_{111}$ and $hTRPV1_{222}$. Thus, I examined the response of $hTRPV1_{121}$ to heat and to voltage-dependent activation. To eliminate the involvement of the other SNPs found in $hTRPV1_{222}$, namely, I315M ($hTRPV1_{211}$) and V585I ($hTRPV1_{112}$), both of these clones were also tested. I used heat and voltage-dependent activation as the activators in these experiments because only heat-, capsaicin-, and voltage-sensitivities were altered by the mutation. Furthermore, previous studies report that capsaicin and other ligands activate TRPV1 either by reducing the heat-threshold or the $V_{1/2.}$ In addition, I also examined the affect of heat activation thresholds during alterations in membrane potentials for all three clones.

5.3.3.1 Responses of $TRPV1_{211,}$ $hTRPV1_{121,}$ and $hTRPV1_{112}$ to heat

Firstly, I studied heat-evoked currents in $hTRPV1_{211-,}$ $hTRPV1_{121-,}$ and $hTRPV1_{112}$-, transfected cells at a holding potential of -60 mV. Heat stimulation was done by the usual temperature ramp between 37 – 50 ^{o}C.

Here, I found that the heat threshold of $hTRPV1_{211,}$ $hTRPV1_{121}$ and $hTRPV1_{112}$ were 44.47 ± 0.82 ^{o}C (n=4), 41.56 ± 0.56 ^{o}C (n=6) and 44.19 ± 0.47 ^{o}C (n=5), respectively, (Fig. 5.11 A). Moreover, I found that the currents evoked at 48 ^{o}C were: - 422 ± 146 pA (n=5), - 941 ± 221 pA (n=7) and - 240 ± 80 pA (n=6), respectively, (Fig. 5.11 B). Both the threshold and the amplitude of the $hTRPV1_{121}$-mediated heat-evoked responses were significantly different from those of $hTRPV1_{111}$, $hTRPV1_{211}$ and $hTRPV1_{112}$, but were similar to the values obtained from $hTRPV1_{222}$. These results confirmed the hypothesis that the mutation at position 469 altered the heat-sensitivity and heat-evoked responses of $hTRPV1_{111}$.

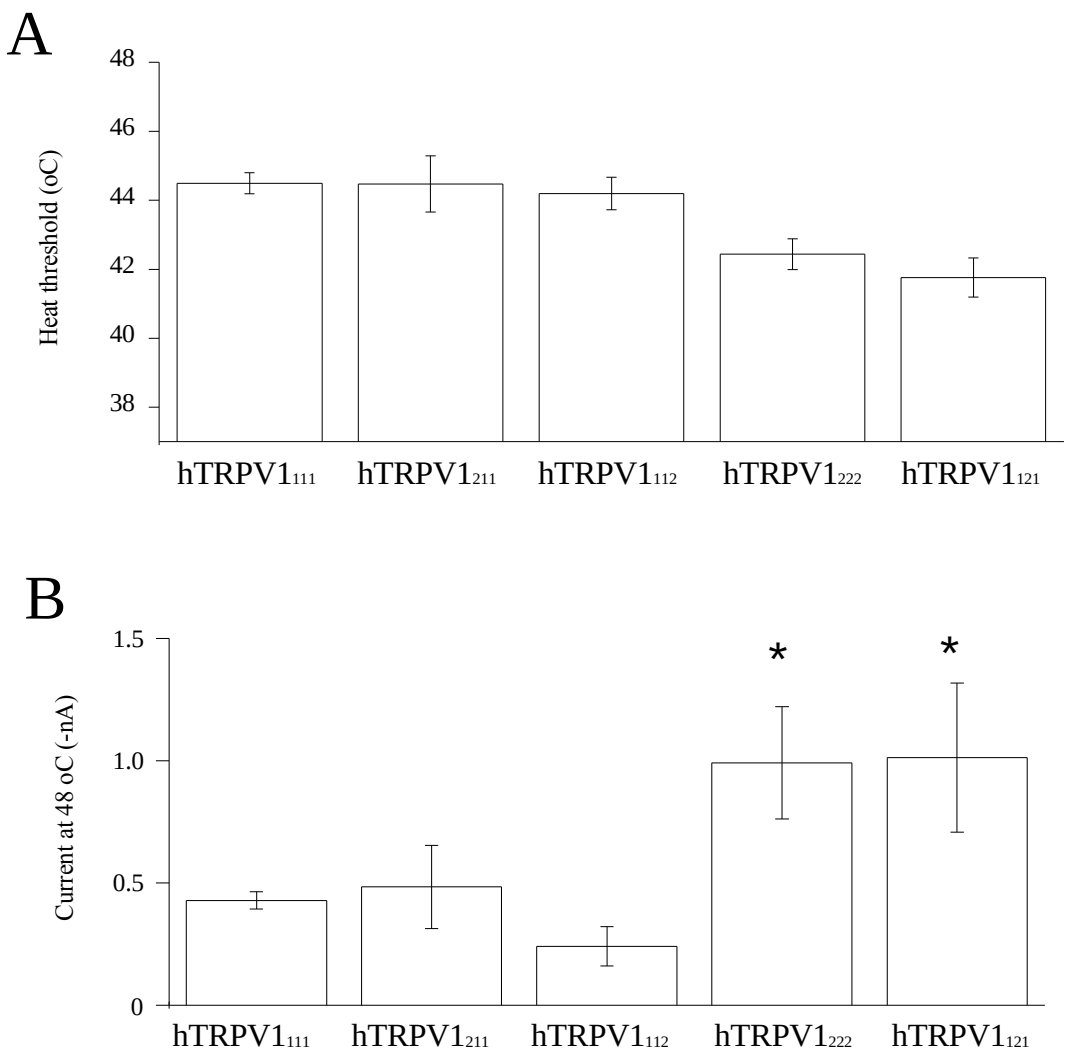

Figure 5.11. Heat responses of $hTRPV1_{111,}$ $hTRPV1_{222,}$ $hTRPV1_{121,}$ $hTRPV1_{211}$ and $hTRPV1_{112}$. Normal extracellular and intracellular solutions were used. (A) Heat threshold, and (B) amplitude, of current at 48 ^{o}C all clones. Note that the heat activation threshold and current at 48 ^{o}C of $hTRPV1_{222}$ and $hTRPV1_{121}$ is significantly different than those of $hTRPV1_{111,}$ $hTRPV1_{211}$ and $hTRPV1_{112}$. Each data point represents mean ± SEM (n= 5 or more). The statistical difference between the means of the various membrane potential within a group was assessed using 1-ANOVA. Whether the differences found were significant was established using Fisher LSD post-hoc test. (*) Differences were regarded as being statistically significant at $p<0.05$.

5.3.3.2 Response of hTRPV1$_{121}$ to voltage-dependent activation

To further assess the validity of my hypothesis that the mutation which produced the alteration in hTRPV1 responsiveness was that found in hTRPV1$_{121}$, I investigated the effect of alteration in membrane potential on the activation of hTRPV1$_{121}$. The data were then compared to those obtained previously from hTRPV1$_{111}$ and hTRPV1$_{222}$.

I found that the $V_{1/2}$ of hTRPV1$_{121}$, using depolarisation to achieve maximal open probability at 37 ^{o}C, was 85.38 ± 1.78 mV (n=5), which was similar to that of hTRPV1$_{222}$ and significantly different from that of hTRPV1$_{111}$ (Fig. 5.12 A and B).

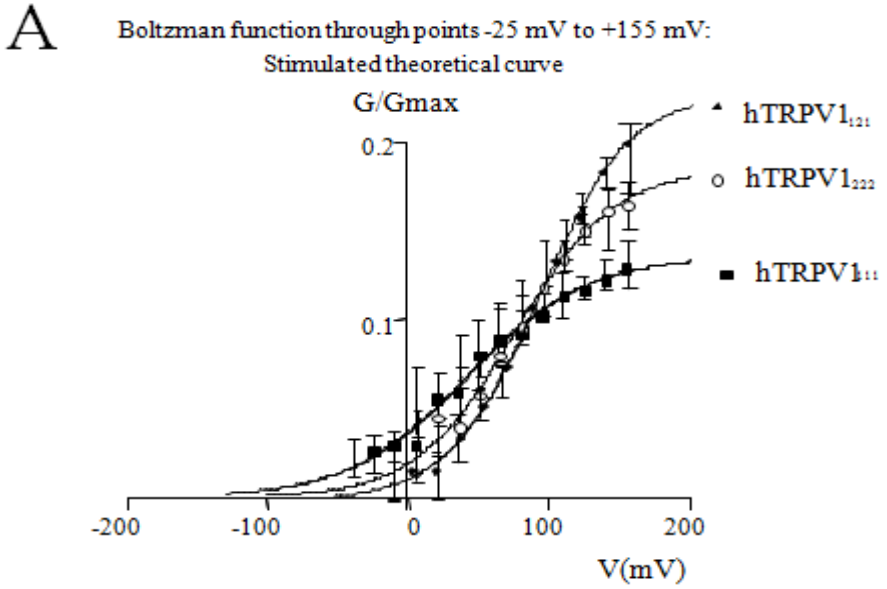

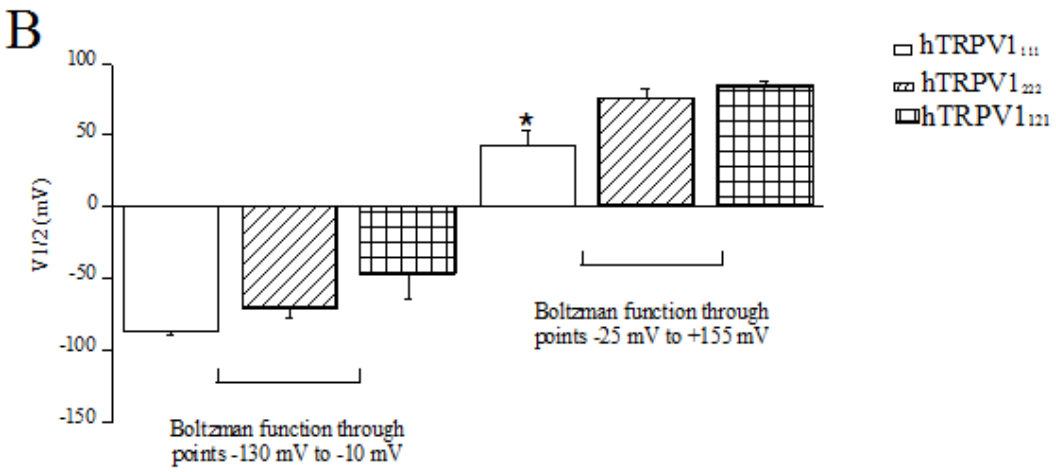

Figure 5.12. Voltage-dependent activity of $hTRPV1_{111,}$ $hTRPV1_{222}$, and $hTRPV1_{121}$. (A) Voltage-dependent activation curves at 37 ^{o}C using depolarisation to open the channel with maximum open probability. Lines represent Boltzman functions fitted to the data. (B) $V_{1/2}$ at 37 ^{o}C of $hTRPV1_{111}$, $hTRPV1_{222}$ and $hTRPV1_{121}$ using depolarisation. Each data point represents mean ± SEM ($n \geq 3$). Statistical comparisons between three Boltzmann curves were analysed using ANOVA (Graphpad Prism). Whether the differences found were significant was established using Fisher LSD post-hoc test. (*) Differences were regarded as being statistically significant at $p<0.05$.

5.3.4 Comparative analysis of hTRPV1 $_{121\text{-}S}$ and hTRPV1$_{121\text{-}A}$ mediated responses

I have shown that the mutation at position 469 of TRPV1 involving the change from the polar amino acid, threonine, to the non-polar amino acid, isoleucine, found in hTRPV1$_{121}$, is responsible for the difference in sensitivity in heat and voltage-dependent activation. I made twonon-natural mutants by site directed mutagenesis. This involved changing the wild-type amino acid encoding a polar threonine at position 469 in twofurther mutants. These were: a charge-conserving polar serine mutation (hTRPV1$_{121\text{-}S}$ mutant); and a charge-neutralising non-polar alanine mutation (hTRPV1$_{121\text{-}A}$ mutant). I then tested the sensitivity of these mutants to heat. The data obtained were then compared to the previous results from hTRPV1$_{111,}$ hTRPV1$_{222}$ and hTRPV1$_{121}$.

5.3.4.1 Responses of mutants to heat

Recordings were made on HEK293 cells transfected with one, or other, of these mutants while heating the bath solution from 37^{o}C to 50^{o}C. All mutants formed functional channels upon expression in HEK293 cells in response to heat. The heat activation thresholds for hTRPV1$_{121\text{-}S}$, and hTRPV1$_{121\text{-}A,}$ transfected cells were: 44.91 ± 0.77 ^{o}C (n=5); and 42.65 ± 0.23 ^{o}C (n=5), respectively, (Fig. 5.13 A). The currents evoked at 48 ^{o}C were: -688 ± 266 pA (n=5); and-1037 ± 253 pA (n=5), respectively (Fig. 5.13 A). Voltage-dependence could not be analysed because of quality issues.

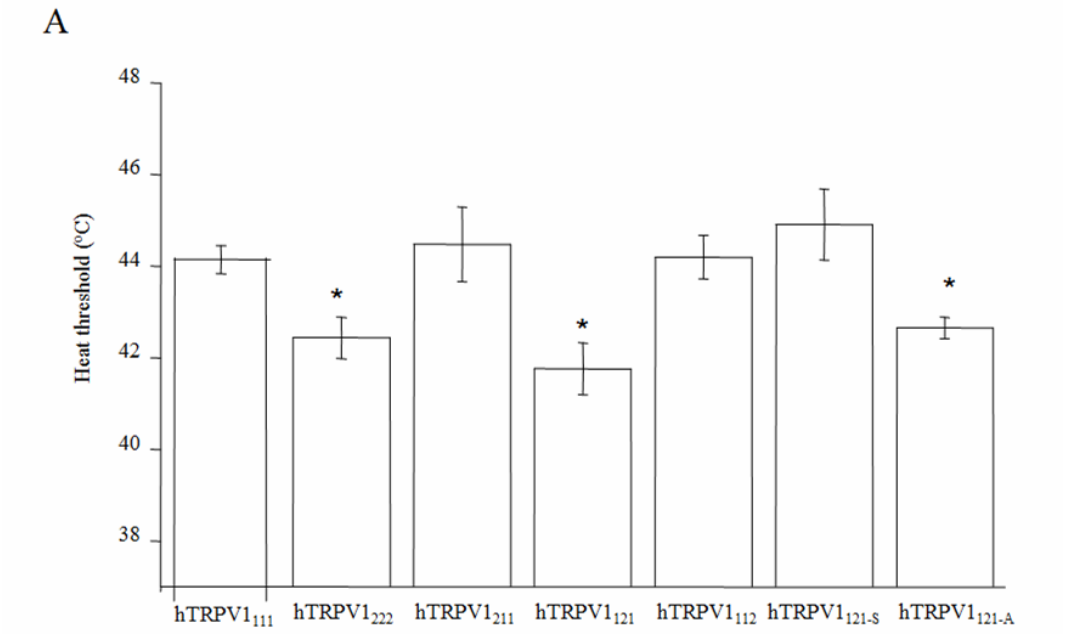

Figure 5.13. Heat-activation thresholds of $hTRPV1_{111}$, $hTRPV1_{222}$, $hTRPV1_{121}$, $hTRPV1_{121\text{-}S}$, and $hTRPV1_{121\text{-}A}$. Normal extracellular and intracellular solutions were used. Each data point represents mean ± SEM (n ≥5). * P < 0.05 from $hTRPV1_{111}$. The statistical difference between the means of the various membrane potential within a group was assessed using 1-ANOVA. Whether the differences found were significant was established using Fisher LSD post-hoc test. (*) Differences were regarded as being statistically significant from $hTRPV1_{111}$ at $p<0.05$.

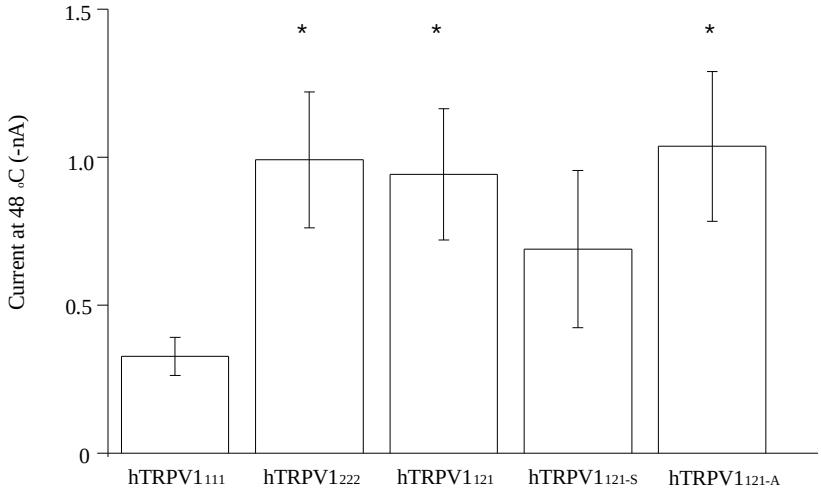

Figure 5.14. Amplitude of currents at 48°C of $hTRPV1_{111}$, $hTRPV1_{222}$, $hTRPV1_{121}$, $hTRPV1_{121\text{-}S}$, and $hTRPV1_{121\text{-}A}$. Normal extracellular and intracellular solutions were used. (A) Amplitude of currents at 48°C, and (Each data point represents mean ± SEM (n ≥5). The statistical difference between the means of the various membrane potential within a group was assessed using 1-ANOVA. Whether the differences found were significant was established using Fisher LSD post-hoc test. (*) Differences were regarded as being statistically significant at $p<0.05$ from $hTRPV1_{111}$.

5.4 Discussion

Several SNPs were found while cloning the hTRPV1 receptor. Davis and colleagues therefore searched for hTRPV1 missense SNPs in three ethnic groups (Caucasians, African-Americans and Asians) to investigate whether the previously reported ethnic differences in heat-sensitivity in these groups were due to mutations in their TRPV1 (Campbell et al., 2005). In total, only three non-synonymous SNPs in the hTRPV1 gene in Caucasians and African Americans were found to produce a frequency of more than 20%. Five clones were made; three clones contained single missense SNPs. These were $hTRPV1_{211}$ (I315M), $hTRPV1_{121}$ (T469I) and $hTRPV1_{112}$ (V585I). Clone $hTRPV1_{111}$ (I315/T469/V585) represented "wild-type" $hTRPV1_{111}$, whereas $hTRPV1_{222}$ (I315M/T469I/ V585I) had the combination of all three missense SNPs of hTRPV1 in one clone.

A recent study by Campbell and colleagues compared the noxious heat-evoked responses in Caucasians and in African-Americans and showed that, although the threshold of heat pain did not differ in these two groups, African-Americans exhibited significantly lower tolerance to heat-induced pain. Moreover, the intensity and unpleasantness of suprathreshold heat pain were rated higher in African-Americans than in Caucasians (Campbell et al., 2005). It is well established that individual phenotypic variations, due to underlying genetic variations, are inherited (Morely et al., 2004; Schadt et al., 2003; Spielman et al., 2007). Consequently, it is reasonable to suggest that phenotypic variations in pain perception among individuals are controlled by gene expression and the level of gene products. Here, I postulate that the three non-synonymous SNPs in the hTRPV1 gene may explain these variations in sensitivity to noxious heat. They may also explain the variations found in TRPV1-dependent functional characteristics and in pathological conditions, such as visceral hyperreflexia and heat hyperalgesia following inflammation (Charrua et al., 2007; Dinis et al., 2004; Davis et al., 2000; Caterina et al., 2000)

Therefore, I aimed to investigate whether any of the three SNPs in hTRPV1 would produce functional differences upon application of "classical" TRPV1 activators (capsaicin, heat and protons) and voltage in hTRPV1 heterologously expressed in HEK293 cells. $hTRPV1_{111}$-mediated and $hTRPV1_{222}$-mediated responses were initially tested and compared to capsaicin, heat and protons. SNPs found in $hTRPV1_{222}$ resulted in *increased sensitivity* to capsaicin (~ 10 fold) and heat (~ 2 ^{o}C lower threshold). However, no difference was seen in proton-evoked responses or in the ion selectivity of the receptors.

Due to the existence of voltage-dependent conductances in native HEK293 cells, establishing the voltage-dependent properties of hTRPV1 polymorphs properly was not possible. Nevertheless, here I was able to show: first, that transfecting HEK293 cells with hTRPV1 modified the voltage-dependent activation curve of the HEK293 cells, indicating that TRPV1 can indeed be activated by changing the membrane potential. Second, I was also able to show that different polymorphs could have different voltage-dependency because transfecting HEK293 cells with various polymorphs modified the voltage-dependent activation curves differently. Results of these experiments suggest that $TRPV1_{111}$ might be more significantly sensitive to depolarisation than $TRPV1_{222}$. These data together suggested that SNPs found in hTRPV1 could indeed result in altered sensitivity of the molecule to some of the activators.

The outward rectification of the I-V curve of TRPV1 seen at negative membrane potentials (Caterina et al., 1997) could be interpreted, by some, as a sign of voltage-dependent reduction in the open probability of TRPV1. However, there is no apparent voltage-dependent change in the open probability in single channel recordings shown by Nagy and Rang (1999). Furthermore, the I-V curve of the single channel TRPV1-mediated currents showed outward rectification (Nagy and Rang, 1999). These together indicate the existence of voltage-dependent change in the conductance of the ion channel. Therefore, the outward rectification shown in whole cell recordings could also be due to the voltage-dependence of channel conductance and not due to voltage-dependent change in the open probability.

It has also been reported that TRPV1 can be activated by depolarisation (Voets et al., 2004; Matta and Ahern, 2007). Therefore our data do agree with these previous findings. However, while we found that voltage-activated currents are different in TRPV1-transfected and untransfected cells, the presence of voltage-activated currents in untransfected cells makes proper analysis of TRPV1 voltage-dependence impossible. The reasons for the difference in relation to constitutively expressed voltage-activated currents in HEK293 cells by the present and previous studies are not known (Thomas and Smart, 2005). Since the solutions used in the present study and by other previously are essentially identical, the only possibility could be in the HEK cells.

Although voltage-sensitivity of TRPV1 has been shown by several groups (Voets et al., 2004; Matta and Ahern, 2007) still it may be regarded as a controversial issue. As discussed before, the current-voltage relationship of non-voltage-sensitive ion channels should follow Ohm's law, i.e., it should show a linear relationship. However, the I-V relationship of the majority of ion channels deviates from the linear regression at certain potential ranges. This indicates that the conductance of the channel is altered by the change of the membrane potential. The conductance of a channel is changed if its permeability is reduced or increased. There are at least two possibilities to change the conductance of an otherwise open ion channel: (i) a charged particle, an ion occupies the channel which cannot pass the pore; (ii) the pore exhibits a voltage-dependent change in its shape, diameter or properties of ion selectivity, which may result in an overall change in conductance. There are several examples for non-permeable ions occupying the pore including inward rectifier potassium channels and N-methyl-D-aspartate (NMDA) type of glutamate receptor channels (Tanaka and Tokimasa, 1999). Both of these channels have magnesium binding sites within their pore and depending on the membrane potential, magnesium ions enter the pore and block permeation of other ions. However, no such TRPV1 ion channel-occupying charged particle has been reported so far. On the contrary, Caterina and co-workers have shown recently that properties of the selectivity filter of TRPV1 depend on concentration and type of agonists (Caterina et al., 2008). The presence of outward rectification in the single channel I-V curve of TRPV1 suggests

that the membrane potential may also affect the selectivity filter. Taken together the currently available data indicate that membrane potential may have a complex effect on TRPV1. On the one hand, findings from Voets and co-workers (2004) and Matta and Ahern (2007) suggest that changes in membrane potential directly regulate the probability of channel opening; while on the other hand, changes in membrane potential may also affect ion selectivity of TRPV1. Elucidation of both of these possibilities requires further studies.

Data obtained from $hTRPV1_{111}$ were substantially similar to previously published data from 'wild-type' hTRPV1. The EC_{50} of capsaicin for $hTRPV1_{111}$-tranfected HEK293 cells was ~ 861 nM, which is slightly higher than that of 640 nM reported by Hayes and colleagues (2000). The heat activation threshold for $hTRPV1_{111}$ was ~ 45.6 ^{o}C which is higher than that reported at ~ 42^{o}C by Smith and colleagues (2002). If we accept the assumption that the conductance at negative membrane potentials represents the majority of the conductance of TRPV1, and that the constitutive HEK293 cell conductance does not produce any major effect on that, then the $V_{1/2}$s of both $TRPV1_{111}$ and $TRPV1_{222}$ established at 37^{o}C were much more negative than that reported by Voets and co-workers (2004) where the $V_{1/2}$ obtained at 35 ^{o}C was ~ +10 mV. The normalised G/Gmax values were also different. In my experiments they were between 0.1-and 0.2. While Voets and colleagues reported up to 1, Matta and Ahern (2007) found it to be 0.6. Thus, a comparison of the characteristics of $hTRPV1_{111}$ to data previously reported on wild-type hTRPV1 reveals differences in heat sensitivity and possibly voltage sensitivity.

The difference between the heat threshold of $hTRPV1_{111}$ in the present study and that found in previous studies on wild-type hTRPV1 may have been due to differences involved in measuring the temperature of the superfusate and establishing the threshold. Smith and colleagues (2002) activated the cells by superfusing the bath solution set to specific temperatures instead of using a heat ramp. In their report, they failed to mention measuring the temperature of the superfusate near the cells. Moreover, they established the heat threshold from simple current-temperature plots taken at every 2- 3 ^{o}C by finding the deviation of the plot of the hTRPV1 transfected cells from that of the untransfected cells. This method is obviously much less

accurate than the method used in this study, which involved applying a heat ramp and establishing the Arrhenius plot. In addition, the hTRPV1 used by Smith's group and the $hTRPV1_{111}$ used in this study may have been different and this difference may well have resulted in different characteristics of the two channels.

The difference in the $V_{1/2}$ values could clearly be due to the presence of the constitutive voltage-activated currents in HEK293 cells. Since we do not know how this constitutive conductance affected TRPV1 conductance any discussion on the possible reasons for the differences would be mere speculation.

The differences found between the functional characteristics of $hTRPV1_{111}$ and $hTRPV1_{222}$ indicated that at least one of the three mutations had to be responsible for the changes observed in the properties of the ion channel. By analysing the individual mutations in $hTRPV1_{222}$, it became apparent that the single missense SNP at T469I in hTRPV1 must have been responsible for this difference, as it was the only mutation which involved a change in polarity of an amino acid. It is well established that changes in the polarity of an amino acid in an ion channel, including TRPV1, often results in altered characteristics of the ion channel (Voets et al., 2007; Brauchi et al., 2006; Tombola et al., 2006; Gavva et al., 2004)

It has already been observed that TRPV1 ligands are able to reduce the heat threshold and the $V_{1/2}$ of TRPV1 (Voets et al., 2004; Babes et al., 2002). It was therefore postulated that ligand-binding activates TRPV1 either through reducing the heat or the voltage-activation threshold. Thus, either the heat-sensor, or the voltage-sensor, were postulated to be the ultimate activators of TRPV1 (Voets et al., 2004; Reeh and Petho, 2000). However, a recent publication has suggested that the voltage-sensor is not the ultimate activator of this ion channel, as high concentrations of ligands are able to open the ion channel independently of the voltage sensor (Matta and Ahern, 2007). Notwithstanding this latter study, I decided to assess both the heat and the voltage sensitivity of $hTRPV1_{121}$.

I found that the heat activation threshold of $hTRPV1_{121}$, which contains only the T469I mutation, was similar to that of $hTRPV1_{222}$ and significantly different from that of $hTRPV1_{111}$. Moreover, the voltage-sensitivity, for $hTRPV1_{121}$ with observing all the limitations, was similar to that of $hTRPV1_{222}$ and different from that of $hTRPV1_{111.}$ These data suggested that T469I may be responsible for the differences observed between $hTRPV1_{111}$ and $hTRPV1_{222}$. In order to verify the role of the T469I mutation in the generation of those changes, I also assessed the heat-activated responses of $hTRPV1_{211}$ and $hTRPV1_{112.}$ These studies showed that the heat activation threshold for $hTRPV1_{211}$ and $hTRPV1_{112}$ were similar to that of $hTRPV1_{111}$ and significantly lower than those of $hTRPV1_{222}$ and $hTRPV1_{121}$, respectively. These findings confirmed that the SNP, T469I, located in the extracellular loop between the first and second transmembrane domains is responsible for the increase in the sensitivity of the molecule to these activators. I postulated that the underlying mechanism of the changes associated with the T469I mutation likely to be the alteration of the charge distribution by this mutation. Since the voltage-sensitivity of voltage-gated ion channels, including the cold sensitive TRPM8, is known to depend on the distribution of charged amino acids (Voets et al., 2007), the T469I mutation associated changes could involve changes in the sensitivity of the voltage sensor. However, the voltage sensor in voltage-gated ion channels is in the fourth transmembrane domain (Voets et al., 2007; Papazian et al., 1991; Perez-Reyes, 2003; Stuhmer et al., 1989; Tombola et al., 2006), although the linker of the first and second transmembrane domains also contribute to voltage-sensing in hyperpolarisation-activated cationic channels (Ishii et al., 2001). Charge distribution also affects the gating apparatus of voltage-gated ion channels (Lecar et al., 2003; Elinder and Århem, 1999). Hence, as an alternative, the T469I mutation may affect the gating apparatus, although according to the 2-dimensional putative membrane topology of the TRPV1, the T469I is far from the location of the gating apparatus, T670 and A680, suggested in a recent publication (Susankova et al., 2007)

While the T469I mutation could result in an alteration in the voltage-sensitivity or in the gating apparatus, it *per se*, is unlikely to be responsible for the altered heat-sensitivity of the molecule, because the temperature-sensing region in

temperature-sensitive TRP channels has been found to be located in the C-terminal domain of the molecule (Brauchi et al., 2006). Therefore, a more plausible explanation for the T469I mutation-associated reduction in heat-sensitivity may be that the T469I mutation acts through either the coupling mechanism predicted to link the voltage-sensor and the heat sensor (Brauchi et al., 2004; Brauchi et al., 2006; Lattore et al., 2007; Voets et al., 2004; Voets et al., 2007) or the gating apparatus.

To further verify the role of the altered charge distribution in the T469I mutation-associated changes, I studied the heat threshold, and the $V_{1/2,}$ of $hTRPV1_{121\text{-}S}$, and $hTRPV1_{121\text{-}A}$, in which the polar threonine of $hTRPV1_{111}$ at position 469 was changed to a polar serine, or non-polar alanine. Data from these mutants showed that, as expected, the threonine to serine amino acid change did not alter the heat threshold. Furthermore, these data also showed that, the heat threshold of $hTRPV1_{121\text{-}A}$ was similar to that of $hTRPV1_{222}$ and $hTRPV1_{121.}$ These data on $hTRPV1_{121\text{-}S}$ and $hTRPV1_{121\text{-}A}$ are consistent with the predicted differential shift of the heat threshold of $hTRPV1_{111,}$ $hTRPV1_{222}$ and $hTRPV1_{121}$.

To further examine whether any of the mutations modify the hypothesised close link between the heat-sensitivity and the voltage-sensitivity of TRPV1, I studied the relationship between these properties in each of the five original clones. According to Voets and co-workers, depolarising the membrane to more positive potentials decreases the heat activation threshold. In fact, this relationship was seen in each of the 5 five clones. Furthermore, in agreement with the data that the T469I mutation results in lowering the heat threshold of hTRPV1, I found that $hTRPV1_{222}$ and $hTRPV1_{121}$ showed significantly lower thresholds at all four holding potentials when compared to $hTRPV1_{111}$, $hTRPV1_{211}$, and $hTRPV1_{112.}$

The alterations in the sensitivity to heat and possibly to voltage, respectively, in opposite directions is surprising, since a close link between these two activation sites has been suggested in earlier studies (Voets et al., 2004; Brauchi et al., 2006). There has been an on going debate whether TRPV1 is ultimately gated by temperature-dependent regulation or by voltage-dependent regulation. Thus, Voets

and co-workers have proposed that: (a) the heat sensor is directly coupled to the voltage sensor; (b) ligand-binding mimics heat activation; and (c) all TRPV1 activators activate this ion channel by shifting the voltage-dependence of channel activity from a physiologically non-relevant voltage range into a physiologically relevant one. However, other studies have shown that the temperature-sensor and the voltage-sensor are conserved in different modules and are able to modulate each others activity (Lattore et al., 2007). Furthermore, based on modelling and biophysical studies, it has been proposed that the stimulus integration occurs through an allosteric mechanism instead of by direct coupling. Subsequent studies by Matta and Ahern (2007) support this allosteric model as they show that voltage results in only a partial activation of TRPV1 and that a high concentration of capsaicin is able to elicit voltage-independent gating. These findings suggest that voltage does not constitute the ultimate gating mechanism of TRPV1 but is able to activate TRPV1 independently, as well as being able to modulate the effect of other stimuli on channel activation. Data from this present work also support the allosteric model of TRPV1 activation, as our findings suggest that, while the heat-sensor and voltage-sensor in TRPV1 are indeed coupled, that coupling may be indirect. Hence, the voltage-sensor is unlikely to be able to transmit all of the effects of each stimulus to the gating apparatus and it is also unlikely to be the main activator of TRPV1. The alterations in the sensitivity in opposing directions of TRPV1 for the heat-dependent and the voltage-dependent activation, respectively, in this study can therefore be explained by the temperature-sensor and the voltage-sensor being conserved in separate regions of the ion channel. Moreover, although they are linked, they may not necessarily shift in same direction due to a mutation. Interestingly, the acid-sensitivity of $hTRPV1_{111}$ was not changed by the mutations found in $hTRPV1_{222}$ in spite of a shift in heat-sensitivity and capsaicin-sensitivity. This finding is in agreement with a putative allosteric link between the various sensors because, if the sensors are linked directly, then the proton sensitivity of $hTRPV1_{222}$, should also be reduced since protons also mimic heat activation. (Voets et al., 2004; Jordt et al., 2000; Ryu et al., 2003).

Chapter 6

SIMMARY OF RESULTS AND CONCLUSION

6.1 Summary

The main findings of my research are as follows:

(i) DMSO activates TRPV1;
(ii) Amiloride affects TRPV1-mediated responses;
(iii) Polymorphisms alter the sensitivity of hTRPV1 to various activators; and
(iv) Polymorphisms induce differential changes in heat-sensitivity and voltage-sensitivity of hTRPV1.

Based on these results, it is considered that the following are the main conclusions of this thesis. First, the TRPV1 activating effect of DMSO should be observed when this lipophilic solvent is employed either *in vivo*, or *in vitro*, experiments. Second, amiloride may increase TRPV1-associated sensation in patients. Third, polymorphism(s) may underlie the differences in pain experience associated with TRPV1 activity reported by individuals. Finally, various sensors in TRPV1 are coupled allosterically, rather than directly.

6.2 DMSO activates TRPV1

As presented in Chapter Three, I found that DMSO concentration-dependently activates TRPV1 both in a heterologous system expressing human TRPV1 and in mouse primary sensory neurons. Further, I demonstrated that in the presence of Ca^{2+}, DMSO, like capsaicin, produced desensitisation of hTRPV1.

DMSO is not only used in laboratories to dissolve lipophilic compounds, but has also been employed in clinics to treat different painful conditions, including interstitial cystitis and inflammation of peripheral organs (Sant et al., 1991 and 1987; Rossberger et al., 2005; Malek et al., 2002; Shiga et al., 2007). In urology, intravesical instillations of high concentrations of DMSO, for example, 50 %, have been shown to alleviate bladder hyperactivity and pain associated with interstitial inflammation (Melchior et al., 2003). Although controversial, DMSO up to 70% has

been shown to alleviate pain associated with inflammation of joints (Muir, 2001; Rosenstein, 1999; Santos and Tipping, 1994; Matsumoto, 1967). However, the mechanism of these beneficial effects of DMSO has not yet been fully elucidated. Recently, Shiga and co-workers (2007) found that DMSO decreases calcium sensitivity of myo-filaments. Previously, Evans and co-workers (1993) showed that DMSO even at low concentration, for example, 5-7% could reduce nerve conduction in high threshold nociceptive C-fibers. As mentioned in the Introduction, the great majority of nociceptive C-fibers express TRPV1 (Caterina et al., 1997; Scotland et al., 2004; Christiansona et al., 2006; Avelino et al., 2002). Recent findings also show that TRPV1 is essential for the development of bladder hyper-reflexia and pain in cystitis and the development of heat hyperalgesia associated with inflammation (Charrua et al., 2007; Dinis et al., 2004; 2005; Davis et al., 2000; Caterina et al., 2000). Results of the present study show that repeated application of 0.2% DMSO in cells expressing TRPV1 resulted in desensitsation. Therefore, it is reasonable to assume that, in addition to reducing calcium sensitivity of myo-filaments and reducing the conduction velocity of nerve impulses in nociceptive C-fibers, DMSO-evoked TRPV1 desensitisation may also contribute to the beneficial effects of DMSO both in the urinary bladder and in joints. Thus my present finding may contribute to the elucidation of mechanisms through which DMSO used to control pain and bladder hyper-reflexia may occur. Of course, for a full elucidation, in vivo studies are needed. Our collaborator, Dr Antonio Avellino has started such studies by examining cFos expression in the spinal cord following intravesical application of DMSO.

6.3 Amiloride affects TRPV1-mediated responses

As presented in Chapter Four, I found that amiloride affects TRPV1-mediated responses. Amiloride is a prototypic inhibitor of epithelial sodium channels. It has also been shown that selected sodium channel mutations affect amiloride binding, provides critical clues towards defining sites within the channel that bind amiloride. Residues within the channel pore and within its extracellular domain participate in amiloride binding. These results suggest that sites that interact with amiloride within the channel's extracellular domain may be in close proximity to residues within the channel's pore (Katzman et al., 1988; Vidt, 1981).

Amiloride hydrochloride is an orally administered, potassium-sparing diuretic with mild natriuretic properties. Its primary site of action is the distal tubule of the nephron where it selectively blocks sodium transport, thereby inhibiting sodium-potassium exchange. The mechanism of action of amiloride is independent of aldosterone. It is excreted unmetabolized in the urine and faeces. Peak serum levels are seen at three hours, and the serum half-life is six hours. The drug can probably be safely administered to patients with hepatic dysfunction but should be used cautiously, if at all, in patients with renal insufficiency. Amiloride is well tolerated, and serious toxicity is rare. It should prove useful in edematous states and hypertension. When amiloride is used in fixed combination with a thiazide diuretic the risk of hypokalemia is minimal (Katzman et al., 1988; Vidt, 1981; Klayman et al., 1999).

However, my present data suggest that when TRPV1 is sensitised and activated for example by inflammatory processes, this agent might induce adverse effects. As discussed, TRPV1 is involved in the development of visceral hyper-reflexia and visceral pain associated by inflammation of various organs, including cystitis and colitis (Dinis et al., 2004). Since amiloride is excreted with urine and faeces it might increase the activity of TRPV1 and increase visceral hyper-reflexia and pain.

Therefore, my findings should be taken into account when using amiloride in patients with inflammatory conditions, particularly cystitis or colitis.

6.4 Polymorphisms alter the sensitivity of hTRPV1 to various activators

As presented in Chapter Five, I have found that certain naturally occurring TRPV1 polymorphs show altered sensitivity to various activators, including capsaicin and heat and possibly voltage. These changes in TRPV1 sensitivity might have profound consequences both in the development of pain associated with various pathologies and in controlling those prolonged pain experiences in the development of which TRPV1 plays a pivotal role. It has been believed that TRPV1 is activated in vivo during pathological conditions by several activators, including endovanilloids and reduction in heat threshold (Walker et al., 2003). Therefore, altered sensitivity to capsaicin and probably other vanilloids, including endovanilloids (though anandamide-sensitivity was not affected) as well as altered heat threshold, which are both associated with certain naturally occurring mutations, may play an important role in the severity of pain experienced by patients.

Several researchers have shown that ethnic differences influence the clinical appearance of pain experience (Riley et al., 2002; Rahim-Williams et al., 2007; Hastie et al., 2005), including the severity of pain associated with medical conditions such as arthritis (Creamer et al., 1999), postoperative pain (Faucett et al., 1994), joint pain (Rantanen et al., 1998), and the treatment of conditions such as low back pain (Taylor et al., 2005). Ethnic differences have also been seen in the responses to multiple experimental pain stimuli. For example, African Americans show significantly higher ratings in intensity and unpleasantness for supra-threshold heat stimuli than Caucasians (Campbell et al., 2005). A recent study has shown that ethnic identity predicts experimental pain sensitivity across multiple noxious stimuli (Rahim-Williams et al., 2007). The difference in pain perception experienced by various ethnic groups indicates that genetic factors may play a major role in the development of pain.

Data suitable for studying the correlation between ethnicity, allele frequency and pain ratings were not available during my PhD studies. However, given the heritable nature of SNPs and the ethnicity-associated pain-sensitivity, it is tempting to suggest that SNPs with possibly many other factors contribute to difference in the severity of pain experienced by people belonging to various ethnic groups. Although during my PhD studies I did not examine the effect of any of the novel TRPV1 antagonists, many of which are in clinical trials currently, on TRPV1-mediated responses, my findings regarding naturally occurring mutation-induced alterations of TRPV1 sensitivity suggest that genotyping may increase the efficacy of controlling pain in the development of which TRPV1 plays a pivotal role.

REFERENCES

Aggarwal SK, MacKinnon R (1996). Contribution of the S4 segment to gating charge in the Shaker K+ channel. *Neuron* 16:1169-77.

Ahern GP, Brooks IM, Miyares RL, Wang XB (2005). Extracellular cations sensitize and gate capsaicin receptor TRPV1 modulating pain signaling. *J Neurosci* 25:5109-5116.

Ahern GP, Wang X, Miyares RL (2006) J Biol Chem. 2006 Mar 31;281(13):8991-5. Epub 2006 Jan 23.

Ahluwalia J, Urban L, Bevan S, Nagy I (2003). Anandamide regulates neuropeptide release from capsaicin-sensitive primary sensory neurons by activating both the cannabinoid 1 receptor and the vanilloid receptor 1 in vitro. *Eur J Neurosci* 17:2611-2618.

Ahluwalia J, Urban L, Capogna M, Bevan S, Nagy I (2000). Cannabinoid 1 receptors are expressed in nociceptive primary sensory neurons. *Neuroscience* 100:685-688.

Aidley DJ, Stanfield PR (1996). Investigating channel activity: The patch clamp technique. In *Ion Channels: Molecules in Action* (pp. 46-51). Cambridge: Cambridge University Press.

Alberts B, Johnson A, Lewis J , Raff M, Roberts K, Peter Walter P (2002). *Molecular Biology of the Cell.* New York: Garland Publishing.

Aldenborg F, Fall M, Enerback L (1986). Proliferation and transepithelial migration of mucosal mast cells in interstitial cystitis. *Immunology* 58: 411.

Aloisi AM, Bonifazi M (2006). Sex hormones, central nervous system and pain. *Horm Behav* 50:1-7.

Amaya F, Shimosato G, Nagano M, Ueda M, Hashimoto S, Tanaka Y, Suzuki, Tanaka M (2004). NGF and GDNF differentially regulate TRPV1 expression that contributes to development of inflammatory thermal hyperalgesia. *Eur J Neurosci* 20:2303-2310.

Anand U, Otto WR, Casula MA, Day NC, Davis JB, Bountra C, Birch R, Anand P (2006). The effect of neurotrophic factors on morphology, TRPV1 expression and capsaicin responses of cultured human DRG sensory neurons. *Neurosci Lett* 399:51-56.

Anderson PA, Josephson RK (1983). Cobalt uptake and localization of putative calcium binding sites in striated muscle. Histochem Cytochem 31:591-600.

Andersson DA, Chase HW, Bevan S (2004). TRPM8 activation by menthol, icilin, and cold is differentially modulated by intracellular pH. *J Neurosci* 24:5364-9.

Angeletti PU, Levi-Montalcini R, Caramia F (1971). Analysis of the effects of the antiserum to the nerve growth factor in adult mice. Brain Res 27:343-55.

Ariano P, Baldelli P, Carbone E, Gilardino A, Lo Giudice A, Lovisolo D, Manfredotti C, Novara M, Sternschulte H, Vittone E (2005). Cellular adhesion and neuronal excitability on functionalised diamond surfaces. *Diamond and Related Materials* 14:669-674.

Arrhenius S (1889). On the Reaction Velocity of the Inversion of Cane Sugar by Acids (translated). *Z Phys Chem* 4:226–248

Avelino A, Cruz C, Nagy I, Cruz F (2002). Vanilloid receptor 1 expression in the rat urinary tract. *Neuroscience* 109:787-798.

Axon Guide (2008). A Guide to Electrophysiology & Biophysics Laboratory Techniques. MDS Analytical Technologies

Babes A, Amuzescu B, Krause U, Scholz A, Flonta ML, Reid G (2002). Cooling inhibits capsaicin-induced currents in cultured rat dorsal root ganglion neurones. *Neurosci Lett* 317:131-134.

Baccaglini PI, Hogan PG (1983). Some rat sensory neurons in culture express characteristics of differentiated pain sensory cells. *Proc Natl Acad Sci U S A* 80:594-8.

Bailey DW (1971). Recombinant-inbred strains. An aid to finding identity, linkage, and function of histocompatibility and other genes. *Transplantation* 11:325-7.

Baiou D, Santha P, Avelino A, Charrua A, Bacskai T, Matesz K, Cruz F, Nagy I (2007). Neurochemical characterization of insulin receptor-expressing primary sensory neurons in wild-type and vanilloid type 1 transient receptor potential receptor knockout mice. *J Comp Neurol* 503:334-47.

Balaban CD., Zhou J, Li HS (2003). Type 1 vanilloid receptor expression by mammalian inner ear ganglion cells. *Hear Res* 175:165-170.

Bannon AW, Seda J, Carmouche M, Francis JM, Norman MH, Karbon B, McCaleb ML (2000). Behavioral characterization of neuropeptide Y knockout mice. *Brain Res* 868:79-87.

Barclay J, Patel S, Dorn G, Wotherspoon G, Moffatt S, Eunson L, Abdel'al S, Natt F, Hall J, Winter J, Bevan S, Wishart W, Fox A, Ganju P (2002). Functional downregulation of P2X3 receptor subunit in rat sensory neurons reveals a significant role in chronic neuropathic and inflammatory pain. *J Neurosci* 22:8139-47.

Barrett AC, Cook CD, Terner JM, Roach EL, Syvanthong C, Picker MJ (2002) Sex and rat strain determine sensitivity to kappa opioid-induced antinociception. *Psychopharmacology (Berl)* 160:170-181.

Baumann TK, Martenson ME (2000). Extracellular protons both increase the activity and reduce the conductance of capsaicin- gated channels. *J Neurosci* 20:RC80.

Bautista DM, Movahed P, Hinman A, Axelsson HE, Sterner O, Högestätt ED, Julius D, Jordt SE, Zygmunt PM (2005). Pungent products from garlic activate the sensory ion channel TRPA1. *Proc Natl Acad Sci U S A* 102:12248-52.

Belknap JK, Haltli NR, Goebel DM, Lamé M (1983). Selective breeding for high and low levels of opiate-induced analgesia in mice. *Behav Genet* 13:383-96.

Benham CD, Gunthorpe MJ, Davis JB (2003). TRPV channels as temperature sensors. *Cell Calcium* 33:479-87.

Bennett DL, Averill S, Clary DO, Priestley JV, McMahon SB (1996). Postnatal changes in the expression of the trkA high-affinity NGF receptor in primary sensory neurons. *Eur J Neurosci* 8:2204-8.

Berjukow F, Doring M, Froschmayr M. Grabner, H. Glossmann Hering S (1996). Endogenous calcium channels in human embryonic kidney (HEK293) cells. *British Journal of Pharmacology* 118:748–754.

Berjukow S, Döring F, Froschmayr M, Grabner M, Glossmann H, Hering S (1996). Endogenous calcium channels in human embryonic kidney (HEK293) cells. *Br J Pharmacol* 118:748-54.

Bevan S, Hothi S, Hughes G, James IF, Rang HP, Shah K, Walpole CS, Yeats JC (1992). Capsazepine: a competitive antagonist of the sensory neurone excitant capsaicin. *Br J Pharmacol* 107:544-52.

Bevan S, Hothi S, Hughes G, James IF, Rang HP, Shah K, Walpole CS, Yeats JC (1991). Development of a competitive antagonist for the sensory neurone excitant, capsaicin. *Br J Pharmacol* 102(Suppl):77.

Bevan S, Winter J (1995). Nerve growth factor (NGF) differentially regulates the chemosensitivity of adult rat cultured sensory neurons. *J Neurosci* 15:4918-26.

Bevan S, Yeats J (1991). Protons activate a cation conductance in a sub-population of rat dorsal root ganglion neurones. *J Physiol* 433:145-61.

Bhave G, Hu HJ, Glauner KS, Zhu W, Wang H, Brasier DJ (2003). Protein kinase C phosphorylation sensitizes but does not activate the capsaicin receptor transient receptor potential vanilloid 1 (TRPV1). *Proc Natl Acad Sci (USA)* 100:12480-12485.

Bhave G, Zhu W, Wang H, Brasier DJ, Gereau RW (2002). cAMP-dependent protein kinase regulates desensitization of the capsaicin receptor (VR1) by direct phosphorylation. *Neuron* 35: 721-731.

Bilsky EJ, Bernstein RN, Pasternak GW, Hruby VJ, Patel D, Porreca F, Lai J (1994). Selective inhibition of [D-Ala2, Glu4]deltorphin antinociception by supraspinal, but not spinal, administration of an antisense oligodeoxynucleotide to an opioid delta receptor. *Life Sci* 55:PL37-43.

Birder LA, Kanai AJ, De Groat WC, Kiss S, Nealen ML, Burke NE, Kineley KE, Watkins S, Reynolds IJ, Caterina MJ (2001). Vanilloid receptor expression suggests a sensory role for urinary bladder epithelial cells. *Proc Natl Acad Sci U S A* 98:13396-13401.

Birnboim HC, Doly J (1979). A rapid alkaline extraction procedure for screening recombinant plasmid DNA. *Nucleic Acids Res* 7:1513-23

Bitner RS, Nikkel AL, Curzon P, Donnelly-Roberts DL, Puttfarcken PS, Namovic M, Jacobs IC, Meyer MD, Decker MW (2000). Reduced nicotinic receptor-mediated antinociception following in vivo antisense knock-down in rat. *Brain Res* 871:66-74.

Boiziau C, Kurfurst R, Cazenave C, Roig V, Thuong NT, Toulmé JJ (1991). Inhibition of translation initiation by antisense oligonucleotides via an RNase-H independent mechanism. *Nucleic Acids Res* 19:1113-9.

Bond C, LaForge KS, Tian M, Melia D, Zhang S, Borg L, Gong J, Schluger J, Strong JA, Leal SM, Tischfield JA, Kreek MJ, Yu L (1998). Single-nucleotide polymorphism in the human mu opioid receptor gene alters beta-endorphin binding and activity: possible implications for opiate addiction. *Proc Natl Acad Sci U S A* 95:9608-9613.

Borbély S, Dobó E, Czégé D, Molnár E, Bakos M, Szucs B, Vincze A, Világi I, Mihály A (2009). Modification of ionotropic glutamate receptor-mediated processes in the rat hippocampus following repeated, brief seizures. *Neuroscience 159:358-68.*

Bradford L (2002). CYP2D6 allele frequency in European Caucasians, Asians, Africans and their descendants. *Pharmacogenomics* 3:229–243.

Braman J, Papworth C, Greener A (1996). Site-directed mutagenesis using double-stranded plasmid DNA templates. *Methods Mol Biol* 57:31-44.

Brauchi S, Orio P, Latorre R (2004). Clues to understanding cold sensation: thermodynamics and electrophysiological analysis of the cold receptor TRPM8. *Proc Natl Acad Sci U S A* 101:15494-15499.

Brauchi S, Orta G, Mascayano C, Salazar M, Raddatz N, Urbina H, Rosenmann E, Gonzalez-Nilo F, Latorre R (2007). Dissection of the components for PIP2 activation and thermosensation in TRP channels. *Proc Natl Acad Sci U S A* 104:10246-10251.

Brauchi S, Orta G, Salazar M, Rosenmann E, Latorre R (2006). A hot-sensing cold receptor: C-terminal domain determines thermosensation in transient receptor potential channels. *J Neurosci* 26:4835-4840.

Brock TD, Freeze H (1969). Thermus aquaticus gen. n. and sp. n., a nonsporulating extreme thermophile. *J Bacteriol* 98: 289-97.

Butelman ER, Ball JW, Harris TJ, Kreek MJ (2003). Topical capsaicin-induced allodynia in unanesthetized primates: pharmacological modulation. *J Pharmacol Exp Ther* 306:1106-14.

Caicedo A, Kim KN, Roper SD (2000). Glutamate-induced cobalt uptake reveals non-NMDA receptors in rat taste cells. *J Comp Neurol* 417:315-24.

Callister LC, Khalaf I, Semenic S, Kartchner R, Vehvilainen-Julkunen K (2003). The pain of childbirth: perceptions of culturally diverse women. *Pain Manag Nurs* 4:145-154.

Campbell AM, Heyer LJ (2007). *Discovering Genomics, Proteomics and Bioinformatics 2nd edition*. San Francisco: Benjamin-Cummings Publishing Company.

Campbell CM, Edwards RR, Fillingim RB (2005). Ethnic differences in responses to multiple experimental pain stimuli. *Pain* 113:20-26.

Cao YQ, Mantyh PW, Carlson EJ, Gillespie AM, Epstein CJ, Basbaum AI (1998). Primary afferent tachykinins are required to experience moderate to intense pain. *Nature* 392: 390-394.

Capecchi MR (1989). Altering the genome by homologous recombination. *Science* 244:1288-92.

Carone DA, Barone DF (2001). A social cognitive perspective on religious beliefs: their functions and impact on coping and psychotherapy. *Clin Psychol Rev* 21:989-1003.

Carriedo SG, Yin HZ, Lamberta R, Weiss JH (1995). In vitro kainate injury to large, SMI-32(+) spinal neurons is Ca2+ dependent. *Neuroreport* 6:945-8.

Caterina MJ, Leffler A, Malmberg AB, Martin WJ, Trafton J, Petersen-Zeitz KR, Koltzenburg M, Basbaum AI, Julius D (2000). Impaired nociception and pain sensation in mice lacking the capsaicin receptor. *Science* 288: 306–313.

Caterina MJ, Rosen TA, Tominaga M, Brake AJ, Julius D (1999). A capsaicin-receptor homologue with a high threshold for noxious heat. *Nature* 398:436-41.

Caterina MJ, Schumacher MA, Tominaga M, Rosen TA, Levine J, Julius D (1997) The capsaicin receptor: A heat-activated ion channel in the pain pathway. *Nature* 389: 816–824.

Cesare P, McNaughton (1996). A novel heat-activated current in nociceptive neurons and its sensitization by bradykinin. *Proc Natl Acad Sci USA* 93:15435-15439.

Chalfie M (1995). Green fluorescent protein. *Photochem Photobiol* 62:651-6.

Chalfie M, Tu Y, Euskirchen G, Ward WW, Prasher DC (1994). Green fluorescent protein as a marker for gene expression. *Science* 263:802-5.

Chaney WG, Howard DR, Pollard JW, Sallustio S, Stanley P (1986). High-frequency transfection of CHO cells using polybrene. *Somat Cell Mol Genet* 12:237–244.

Chang L, Toner BB, Fukudo S, Guthrie E, Locke GR, Norton NJ, Sperber AD (2006). Gender, age, society, culture, and the patient's perspective in the functional gastrointestinal disorders. *Gastroenterology* 130:1435-46.

Charrua A, Cruz CD, Cruz F, Avelino A (2007). Transient receptor potential vanilloid subfamily 1 is essential for the generation of noxious bladder input and bladder overactivity in cystitis. *J Urol* 177:1537-15341.

Cheng CL, Liu JC, Chang SY, Ma CP, de Groat WC (1999). Effect of capsaicin on the micturition reflex in normal and chronic spinal cord-injured cats. *Am J Physiol* 277:786-94.

Cheng W, Yang F, Takanishi CL, Zheng J (2007). Thermosensitive TRPV channel subunits coassemble into heteromeric channels with intermediate conductance and gating properties. *J Gen Physiol* 129:191-207.

Cheung NF (1994). Pain in normal labor: A comparison of experiences in southern China and Scotland. *Midwives Chronicles* 107:212–216.

Chou MZ, Mtui T, Gao YD, Kohler M, Middleton RE (2004). Resiniferatoxin binds to the capsaicin receptor (TRPV1) near the extracellular side of the S4 transmembrane domain. *Biochemistry* 43:2501-2511.

Christiansona JA, McIlwrathb SL, Koerberb HR, Davis, BM (2006). Transient receptor potential vanilloid 1-immunopositive neurons in the mouse are more prevalent within colon afferents compared to skin and muscle afferents. *Neuroscience* 140:247-257.

Christoph T, Gillen C, Mika J, Grünweller A, Schäfer MK, Schiene K, Frank R, Jostock R, Bahrenberg G, Weihe E, Erdmann VA, Kurreck J (2007). Antinociceptive effect of antisense oligonucleotides against the vanilloid receptor VR1/TRPV1. *Neurochem Int* 50:281-90.

Christoph T, Gillen C, Mika J, Grunweller A, Schater MKH, Schiene K, Frank R, Jostock R, Bahrenberg G, Weihe E, Erdmann VA, Kurreck J (2007). Antinociceptive effect of antisense oligonucleotides against the vanilloid receptor VR1/TRPV1. *Neurochem Internat* 50:281-290.

Chu CJ, Huang SM, De Petrocellis L, Bisogno T, Ewing SA, Miller JD, Zipkin RE, Daddario N, Appendino G, Di Marzo V, Walker JM (2003). N-oleoyldopamine, a novel endogenous capsaicin-like lipid that produces hyperalgesia. *J Biol Chem* 278:13633-13639.

Chuang H., Prescott ED, Kong H, Shields S, Jordt SE, Basbaum AI, Chao MV, D Julius (2001). Bradykinin and nerve growth factor release the capsaicin receptor from PtdIns(4,5),P2-mediated inhibition. *Nature* 411: 957–962.

Chuang HH, Prescott ED, Kong H, Shields S, Jordt SE, Basbaum AI, Chao MV, Julius D (2001). Bradykinin and nerve growth factor release the capsaicin receptor from PtdIns(4,5)P2-mediated inhibition. *Nature* 411:957-62.

Chung KM, Lee SB, Heur R, Cho YK, Lee CH, Jung HY, Chung SH, Lee SP, Kim KN (2005). Glutamate-induced cobalt uptake elicited by kainate receptors in rat taste bud cells. *Chem Senses* 30:137-143.

Clapham DE (2003). TRP channels as cellular sensors. *Nature* 426:517-524.

Cline J, Braman JC, Hogrefe HH. (1996). PCR fidelity of Pfu DNA polymerase and other thermostable DNA polymerases. *Nucleic Acids Res* 24: 3546-3551.

Cody CW, Prasher DC, Westler WM, Prendergast FG, Ward WW (1993). Chemical structure of the hexapeptide chromophore of the Aequorea green-fluorescent protein. *Biochemistry* 32:1212-8.

Cohen SN, Chang AC, Hsu L (1972). Nonchromosomal antibiotic resistance in bacteria: genetic transformation of Escherichia coli by R-factor DNA. *Proc Natl Acad Sci U S A.* 69:2110-4.

Cole KS (1949). Dynamic electrical characteristics of the squid axon membrane. *Arch Sci physiol* 3:253-8.

Collins FS, Brooks LD, Chakravarti A (1998). A DNA polymorphism discovery resource for research on human genetic variation. *Genome Res* 8:1229-31.

Columb MO, Stevens A (2008). Power analysis and sample size calculations. *Current Anaesthesia & Critical Care.* 19:12-14.

Conrad DR (2008). Glutamine in Cell Culture. Importance and uses of glutamine in serum-free eucaryotic, including hybridoma and Chinese Hamster Ovary (CHO) cell, cultures. *Sigma-Aldrich product sheet*.

Contassot E, Tenan M, Schnuriger V, Pelte MF, Dietrick PY (2004). Arachidoyyl ethanolamide induces apoptosis of uterine cervix cancer cells via aberrantly expressed vanilloid receptor-1. *Gynecol Oncol* 93:182-188.

Coolican H (1995). Introduction to Research Methods and Statistics in Psychology London: Hodder and Stoughton.

Correll CC, Phelps PT, Anthes JC, Umland S, Greenfeder S (2004). Cloning and pharmacological characterization of mouse TRPV1. *Neurosci Lett* 370:55-60.

Craft RM (2003). Sex differences in opioid analgesia: "from mouse to man". Clin J *Pain* 19:175-186.

Creamer P, Lethbridge-Cejku M, Hochberg MC (1999). Determinants of pain severity in knee osteoarthritis: effect of demographic and psychosocial variables using 3 pain measures. *J Rheumatol* 26:1785-1792.

Cristino L, de Petrocellis L, Pryce G, Baker D, Guglielmotti V, Di Marzo V (2006). Immunohistochemical localization of cannabinoid type 1 and vanilloid transient receptor potential vanilloid type 1 receptors in the mouse brain. *Neuroscience* 139:1405-1415.

Crowley C, Spencer SD, Nishimura MC, Chen KS, Pitts-Meek S, Armanini MP, Ling LH, McMahon SB, Shelton DL, Levinson AD, et al (1994). Mice lacking nerve growth factor display perinatal loss of sensory and sympathetic neurons yet develop basal forebrain cholinergic neurons. *Cell* 76:1001-11.

Crowley C, Spencer SD, Nishimura MC, Chen KS, Pitts-Meek S, Armanini MP, Ling LH, McMahon SB, Shelton DL, Levinson AD, Phillips HS (1994). Mice lacking nerve growth factor display perinatal loss of sensory and sympathetic neurons yet develop basal forebrain cholinergic neurons. *Cell* 76:1001-1011.

Crusio WE (2004). Flanking gene and genetic background problems in genetically manipulated mice. *Biol Psychiatry* 56:381-5.

Culp WJ, Ochoa J, Cline M, and Dotson R (1989) Heat and mechanical hyperalgesia induced by capsaicin. *Brain* 112: 1317-1331.

Cummins TR, Renganathan M, Stys PK, Herzog RI, Scarfo K, Horn R, Dib-Hajj SD, Waxman SG (2003). The pentapeptide QYNAD does not block voltage-gated

sodium channels. J Pharmacol Toxicol Methods 51:187-200. *Neurology* 60:224-9

Dahan A, Sarton E, Teppema L, Olievier C (1998). Sex-related differences in the influence of morphine on ventilatory control in humans. *Anesthesiology* 88:903-913.

Dai Y, Moriyama T, Higashi T, Togashi K, Kobayashi K, Yamanaka H, Tominaga M, Noguchi K (2004) Proteinase-activated receptor 2-mediated potentiation of transient receptor potential vanilloid subfamily 1 activity reveals a mechanism for proteinase-induced inflammatory pain. *J Neurosci* 24:4293-9.

Dalby B, Cates S, Harris A, Ohki EC, Tilkins ML, Price PJ, Ciccarone VC (2004). Advanced transfection with Lipofectamine 2000 reagent: primary neurons, siRNA, and high-throughput applications. *Methods* 33:95-103.

Dalby B, Cates S, Harris A, Ohki EC, Tilkins ML, Price PJ, Ciccarone VC (2004). Advanced transfection with Lipofectamine 2000 reagent: primary neurons, siRNA, and high-throughput applications. *Methods* 33:95-103.

Davis JB, Gray J, Gunthorpe MJ, Hatcher JP, Davey PT, Overend P, Harries MH, Latcham J, Clapham C, Atkinson K, Hughes SA, Rance K, Grau E, Harper AJ, Pugh PL, Rogers DC, Bingham S, Randall A, Sheardown SA (2000). Vanilloid receptor-1 is essential for inflammatory thermal hyperalgesia. *Nature* 405: 183–187.

Davis ME, Davis RJ (2003). Rate constants of elementary reaction: Arrhenius temperature dependence of the rate constant. *Fundamentals of Chemical Reaction* (pp.54-56). Boston: McGraw-Hill Companies.

De Biasi S, Rustioni A (1988) Glutamate and substance P coexist in primary afferent terminals in the superficial laminae of spinal cord. *Proc Natl Acad Sci U S A* 85:7820-4.

De Petrocellis L, Harrison S, Bisogno T, Tognetto M, Brandi I, Smith GD, Creminon C, Davis JB, Geppetti P, Di Marzo V (2001).The vanilloid receptor (VR1)-mediated effects of anandamide are potently enhanced by the cAMP-dependent protein kinase. *J Neurochem* 77:1660-1663.

Denda M, Fuziwara S, Inoue K, Denda S, Akamatsu H, Tomitaka A, Matsunaga K (2001). Immunoreactivity of VR1 on epidermal keratinocyte of human skin. *Biochem Biophys Res Commun* 285:1250-1252.

Dever GEA (1991) Basic statistics measure. *Community Health Analysis: Global Awareness At the Local Level* (pp.100). Blvd, Rockville: Aspen Publishers. Inc.

Devor M, Raber P_(1990). Heritability of symptoms in an experimental model of neuropathic pain. *Pain* 42:51-67.

Di Marzo V, Fontana A, Cadas H, Schinelli S, Cimino G, Schwartz JC, Piomelli D (1994). Formation and inactivation of endogenous cannabinoid anandamide in central neurons. *Nature* 372:686-691.

Di MarzoV, Blumberg PM, Szallasi A (2002). Endovanilloid signalling in pain. *Curr Opin Neurobiol* 12:372 –379.

Diamond M (2002). Sex and Gender are Different: Sexual Identity and Gender Identity are Different. *Clinical Child Psychology and Psychiatry* 7: 320-334.

Dias N, Dheur S, Nielsen PE, Gryaznov S, Van Aerschot A, Herdewijn P, Hélène C, Saison-Behmoaras TE (1999). Antisense PNA tridecamers targeted to the

coding region of Ha-ras mRNA arrest polypeptide chain elongation. *J Mol Biol* 294:403-16.

Dichter MA, Fischbach GD (1977). The action potential of chick dorsal root ganglion neurones maintained in cell culture. *J Physiol* 267:281-98.

Dickenson AH (1995). Spinal cord pharmacology of pain. *Br J Anaesth* 75:193-200.

Dickenson AH, Dray A (1991). Selective antagonism of capsaicin by capsazepine: evidence for a spinal receptor site in capsaicin-induced antinociception. *Br J Pharmacol* 104:1045-1049.

Dickenson AH, Dray A., Hughes GA, Walpole CSJ (1991). The selective capsaicin antagonist capsazepine inhibits capsaicin-induced antinociception: electrophysiological studies in rodents. *Br J Pharmacol* 2:79.

Dinis P, Charrua A, Avelino A, Yaqoob M, Bevan S, Nagy I, Cruz F (2004). Anandamide-evoked activation of vanilloid receptor 1 contributes to the development of bladder hyperreflexia and nociceptive transmission to spinal dorsal horn neurons in cystitis. *J Neurosci* 24:11253-11263.

D'Mello R, Dickenson AH (2008). Spinal cord mechanisms of pain. *Br J Anaesth* 101:8-16.

Docherty RJ, Robertson B, Bevan S (1991). Capsaicin causes prolonged inhibition of voltage-activated calcium currents in adult rat dorsal root ganglion neurons in culture. *Neuroscience* 40:513-21.

Docherty RJ, Yeats JC, Bevan S, Boddeke HW (1996). Inhibition of calcineurin inhibits the desensitization of capsaicin-evoked currents in cultured dorsal root ganglion neurones from adult rats. *Pflugers Arch* 431:828-837.

Docherty RJ, Yeats JC, Piper AS (1997). Capsazepine block of voltage-activated calcium channels in adult rat dorsal root ganglion neurones in culture. *Br J Pharmacol* 121:1461-7.

Dogrul A, Gardell LR, Ma S, Ossipov MH, Porreca F, Lai J (2002). 'Knock-down' of spinal CB1 receptors produces abnormal pain and elevates spinal dynorphin content in mice. *Pain* 100:203-9.

Dray A, Patel IA, Perkins MN, Rueff A (1992). Bradykinin-induced activation of nociceptors: receptor and mechanistic studies on the neonatal rat spinal cord-tail preparation in vitro. *Br J Pharmacol* 107:1129-34.

Dray A, Perkins MN (1988). Bradykinin activates peripheral capsaicin-sensitive fibres via a second messenger system. *Agents Actions* 25: 214-215.

Duggan AW, Hendry IA, Morton CR, Hutchison WD, Zhao ZQ (1988). Cutaneous stimuli releasing immunoreactive substance P in the dorsal horn of the cat. *Brain Res* 451:261-73.

Edsall SA, Knapp RJ, Vanderah TW, Roeske WR, Consroe P, Yamamura HI (1996). Antisense oligodeoxynucleotide treatment to the brain cannabinoid receptor inhibits antinociception. *Neuroreport* 7:593-6.

Eilers H, Lee SY, Hau CW, Logvinova A, Schumacher MA (2007). The rat vanilloid receptor splice variant VR.5'sv blocks TRPV1 activation. *Neuroreport* 18:969-973.

Elinder F, Arhem P (1999). Role of individual surface charges of voltage-gated K channels. *Biophys J* 77:1358-1362.

Evans MS, Reid KH, Sharp JB (1993). Dimethylsulfoxide (DMSO) blocks conduction in peripheral nerve C fibers: a possible mechanism of analgesia. *Neurosci Lett* 150:145-148.

Evans W, McLeod H (2003). Pharmacogenomics - drug disposition, drug targets, and side effects. *N Engl J Med* 348:538–549.

Fabbro A, Nistri A (2004). Chronic NGF treatment of rat nociceptive DRG neurons in culture facilitates desensitization and deactivation of GABAA receptor-mediated currents. *J Pharmacol* 142:425-34.

Fairbanks CA, Stone LS, Kitto KF, Nguyen HO, Posthumus IJ, Wilcox GL (2002). alpha(2C)-Adrenergic receptors mediate spinal analgesia and adrenergic-opioid synergy. *J Pharmacol Exp Ther* 300:282-90.

Fang X, L. Djouhri, S. McMullan, C. Berry, S.G. Waxman, K. Okuse and S.N. Lawson (2006). Intense isolectin-B4 binding in rat dorsal root ganglion neurons distinguishes C-fiber nociceptors with broad action potentials and high Nav1 9 expression. *J Neurosci* 26: 7281–7292.

Faucett J, Gordon N, Levine J (1994). Differences in postoperative pain severity among four ethnic groups. *Pain Symptom Manage* 9:383-389.

Feine JS, Bushnell MC, Miron D, Duncan GH (1991). Sex differences in the perception of noxious heat stimuli. *Pain* 44:255-262.

Felgner PL, Gadek TR, Holm M, Roman R, Chan HW, Wenz M, Northrop JP, Ringold GM, Danielsen M (1987). Lipofection: a highly efficient, lipid-mediated DNA-transfection procedure.Proc Natl Acad Sci U S A 84:7413-7417.

Ferreira SH, Lorenzetti BB, Cunha FQ, Poole S (1993). Bradykinin release of TNF-alpha plays a key role in the development of inflammatory hyperalgesia. *Agents Actions* 38: C7-9.

Fillingim RB, Gear RW (2004). Sex differences in opioid analgesia: clinical and experimental findings. *Eur J Pain* 8:413-425.

Fillingim RB, Kaplan L, Staud R, Ness TJ, Glover TL, Campbell CM, Mogil JS, Wallace MR (2005). The A118G single nucleotide polymorphism of the mu-opioid receptor gene (OPRM1) is associated with pressure pain sensitivity in humans. *J Pain* 6:159-167.

Fischer MJ, Reeh PW (2007). Sensitization to heat through G-protein-coupled receptor pathways in the isolated sciatic mouse nerve. *Eur J Neurosci* 25:3570-35705.

Fukuoka T, Tokunaga A, Tachibana T, Dai Y, Yamanaka H, Noguchi K (2002). VR1, but not P2X3 increases in the spared L4 DRG in rats with L5 spinal nerve ligation. *Pain* 99:111-120.

Fulton JT (2000). Patch clamp measurements applied to neurons. Process in Animal Vision. Corona Del Mar, CA: Vision Concepts. Internet: URL: http://www.4colorvision.com.

Fundytus ME, Osborne MG, Henry JL, Coderre TJ, Dray A (2002). Antisense oligonucleotide knockdown of mGluR1 alleviates hyperalgesia and allodynia associated with chronic inflammation. *Pharmacol Biochem Behav* 73:401-10.

Fundytus ME, Yashpal K, Chabot JG, Osborne MG, Lefebvre CD, Dray A, Henry JL, Coderre TJ (2001). Knockdown of spinal metabotropic glutamate receptor 1 (mGluR(1)) alleviates pain and restores opioid efficacy after nerve injury in rats. *Br J Pharmacol* 132:354-67.

Gaedigk A, Bradford L, Marcucci K, Leeder J (2002). Unique CYP2D6 activity distribution and genotype-phenotype discordance in black Americans. *Clinical Pharmacology and Therapeutics* 72:76–89.

Galoyan SM, Petruska JC, Mendell LM (2003). Mechanisms of sensitization of the response of single dorsal root ganglion cells from adult rat to noxious heat. *Eur J Neurosci* 18:535-41.

García-Sanz N, Fernández-Carvajal A, Morenilla-Palao C, Planells-Cases R, Fajardo-Sánchez E, Fernández-Ballester G, Ferrer-Montiel A (2004). Identification of a tetramerization domain in the C terminus of the vanilloid receptor. *J Neurosci* 24:5307-5314.

Gavazzi I, Kumar RD, McMahon SB, Cohen J (1999). Growth responses of different subpopulations of adult sensory neurons to neurotrophic factors in vitro. *Eur J Neurosci* 11: 3405–3414.

Gavva NR, Klionsky L, Qu Y, Shi L, Tamir R, Edenson S, Zhang TJ, Viswanadhan VN, Toth A, Pearce LV, Vanderah TW, Porreca F, Blumberg PM, Lile J, Sun Y, Wild K, Louis JC, Treanor JJ (2004). Molecular determinants of vanilloid sensitivity in TRPV1. *J Biol Chem* 279:20283-20295.

Gerlai R (1996. Gene-targeting studies of mammalian behaviour: is it the mutation or the background genotype? *Trends Neurosci* 19:177-81.

Gilabert R, McNaughton P (1997). Enrichment of the fraction of nociceptive neurones in cultures of primary sensory neurones. *J Neurosci Methods* 71:191-8.

Gillam S, Astell CR, Smith M (1980). Site-specific mutagenesis using oligodeoxyribonucleotides: isolation of a phenotypically silent phi X174 mutant, with a specific nucleotide deletion, at very high efficiency. *Gene* 12:129-37.

Golan DE, Tashjian AH, Armstrong, AW (2007) Fundamental principles of neuropharmacology. In *Principles of Pharmacology: The Pathophysiologic Basis of Drug Therapy* (pp. 75-106). Baltimore:Lippincott Williams & Wilkins.

Gold MS, Dastmalchi S, Levine JD (1996), Co-expression of nociceptor properties in dorsal root ganglion neurons from the adult rat in vitro. *Neuroscience* 71:265-75.

Gold MS, Weinreich D, Kim CS, Wang R, Treanor J, Porreca F, Lai J (2003). Redistribution of Na(V)1.8 in uninjured axons enables neuropathic pain. *J Neurosci* 23:158-66.

Gram DX, Ahren B, Nagy I, Olsen UB, Brand CL, Sundler F, Tabanera R, Svendsen O, Carr RD, Santha P, Wierup N, Hansen AJ (2007). Capsaicin-sensitive sensory fibers in the islets of Langerhans contribute to defective insulin secretion in Zucker diabetic rat, an animal model for some aspects of human type 2 diabetes. *Eur J Neurosci* 25:213-223.

Granick S (1983). Psychologic assessment technology for geriatric practice. *J Am Geriatr Soc* 31:728-42.

Gravetter FJ, Wallnau LB (2006). Post Hoc Test. In *Statistics for the Behavioural Sciences* (pp. 418-422). Wadsworth :Wadsworth Publishing Company.

Güler AD, Lee H, Iida T, Shimizu I, Tominaga M, Caterina M (2002). Heat-evoked activation of the ion channel, TRPV4. *J Neurosci* 22:6408-14.

Gunthorpe MJ, Harries MH, Prinjha RK, Davis JB, Randall A (2000). Voltage- and time-dependent properties of the recombinant rat vanilloid receptor (rVR1). *J Physiol* 525:747-759.

Gunthorpe MJ, Smith GD, Davis JB, Randall AD (2001). Characterisation of a human acid-sensing ion channel (hASIC1a) endogenously expressed in HEK293 cells. *Pflugers Arch* 442:668-674.

Guia A, Remillard CV, Leblanc N (2001). Concepts for patch-clamp recording of the whole-cell and single-channel K+ currents in cardiac and vascular myocytes: Protocols to investigate gating mechanisms. In SL Archer, NJ Rusch (Eds.), *Potassium Channels in Cardiovascular Biology* (pp. 134). New York: Springer.

Guo A, Vulchanova L, Wang J, Li X, Elde R (1999). Immunocytochemical localisation of the vanilloid receptor (VR1): relationship to neuropeptides, the P2X3 purinoceptor and IB4 binding sites. *Eur J Neurosci* 11:946-958.

Hack N, Balázs R (1995). Properties of AMPA receptors expressed in rat cerebellar granule cell cultures: Ca2+ influx studies. *J Neurochem* 65:1077-1084.

Harmar A, Schofield JG, Keen P (1980). Cycloheximide-sensitive synthesis of substance P by isolated dorsal root ganglia. *Nature* 284:267-9.

Harper AA, Lawson SN (1985). Conduction velocity is related to morphological cell type in rat dorsal root ganglion neurones. *J Physiol* 359:31-46.

Hastie BA, Riley JL, Fillingim RB (2005). Ethnic differences and responses to pain in healthy young adults. *Pain Med* 6:61-71.

Hayes P, Meadows HJ, Gunthorpe MJ, Harries MH, Duckworth DM, Cairns W, Harrison DC, Clarke CE, Ellington K, Prinjha RK, Barton AJ, Medhurst AD, Smith GD, Topp S, Murdock P, Sanger GJ, Terrett J, Jenkins O, Benham CD, Randall AD, Gloger IS, Davis JB (2000). Cloning and functional expression of a human orthologue of rat vanilloid receptor-1. *Pain* 88:205-215.

Hellwig N, Albrecht N, Harteneck C, Schultz G, Schaefer M (2005). Homo- and heteromeric assembly of TRPV channel subunits. *J Cell Sci* 118:917-928.

Herness MS (2001). Researching isolated taste receptors cells: Deciphering transduction cascades with patch-clamp and calcium imaging techniques. In SA Simon, MAL Nicolelis (Eds), *Methods in Chemosensory Research* (pp. 178-179). Florida: CRC Press.

Hille B (2001). Classical biophysics of the squid giant axon. *Ion Channels of Excitable Membranes* (pp. 25-60). Massachusetts: Sinauer Associates.

Hilton A, Armstrong R (2006) Stat note 6: Post hoc ANOVA tests. *Microbiologis*t 7: 34–36.

Hinton P (2004). Statistics Explained: A Guide for Social Science Students. Sussex: Routledge.

Hodgkin AL, Huxley AF (1952). A quantitative description of membrane current and its application to conduction and excitation in nerve. *J Physiol* 117:500-44.

Hogan PG (1983). Expression of markers for pain sensory. *Ph.D. Dissertation*, Harvard University, Cambridge, MA, USA.

Hogrefe HH, Hansen CJ, Scott BR, Nielson KB (2002). Archaeal dUTPase enhances PCR amplifications with archaeal DNA polymerases by preventing dUTP incorporation. *Proc Natl Acad Sci U S A* 99:596-601.

Hökfelt T, Kellerth JO, Nilsson G, Pernow B (1975). Substance p: localization in the central nervous system and in some primary sensory neurons. *Science* 190:889-90.

Holzer P (1991). Capsaicin: cellular targets, mechanisms of action and selectivity for thin sensory neurones. *Pharmacol Rev* 43: 143–201.

Holzer-Petsche U, Lembeck F (1984). Systemic capsaicin treatment impairs the micturition reflex in the rat. *Br J Pharmacol* 83:935-941.

Honore P, Kage K, Mikusa J, Watt AT, Johnston JF, Wyatt JR, Faltynek CR, Jarvis MF, Lynch K (2002).Analgesic profile of intrathecal P2X(3) antisense oligonucleotide treatment in chronic inflammatory and neuropathic pain states in rats. *Pain* 99:11-9.

Hori T, Oka T, Hosoi M, Abe M, Oka K (2000). Hypothalamic mechanisms of pain modulatory actions of cytokines and prostaglandin E2. *Ann NY Acad Sci* 917:106-20.

Hou WY, Shyu BC, Chen TM, Lee JW, Shieh JY, Sun WZ (1997). Intrathecally administered c-fos antisense oligodeoxynucleotide decreases formalin-induced nociceptive behavior in adult rats. *Eur J Pharmacol* 329:17-26.

Huang J, Zhang Z, McNaughton PA (2006). Modulation of temperature-sensitive TRP channels. *Sem Cell & Biol* 17: 638-645.

Huang SM, Bisogno T, Trevisani M, Al-Hayani A, De Petrocellis L, Fezza F, Tognetto M, Petros TJ, Krey JF, Chu CJ, Miller JD, Davies SN, Geppetti P, Walker JM, Di Marzo V (2002). An endogenous capsaicin-like substance with high potency at recombinant and native vanilloid VR1 receptors. *Proc Natl Acad Sci (USA)* 99:8400-8405.

Huang W, Simpson RK Jr (1999). Antisense of c-fos gene attenuates Fos expression in the spinal cord induced by unilateral constriction of the sciatic nerve in the rat. *Neurosci Lett* 263:61-4.

Hudson LJ, Bevan S, Wotherspoon G, Gentry C, Fox A, Winter J (2001). VR1 protein expression increases in undamaged DRG neurons after partial nerve injury. *Eur J Neurosci* 13:2105-14.

Hudson LJ, Bevan S, Wotherspoon G, Gentry C, Fox A, Winter J (2001). VR1 protein expression increases in undamaged DRG neurons after partial nerve injury. *Eur J Neurosci* 13:2105-2114.

Huesa G, Ikenaga T, Böttger B, Finger TE (2008). Calcium-fluxing glutamate receptors associated with primary gustatory afferent terminals in goldfish (Carassius auratus). *J Comp Neurol* 506:694-707.

Hui K, Liu B, Qin F (2003). Capsaicin activation of the pain receptor, VR1: multiple open states from both partial and full binding. *Biophys* J 84:2957-2968.

Human Genome Project Information (2008). Cloning Fact Sheet. www.genomics.energy.gov

Hu-Tsai M, Woolf C, Winter J (1996). Influence of inflammation or disconnection from peripheral target tissue on the capsaicin sensitivity of rat dorsal root ganglion sensory neurones. *Neurosci Lett* 203:119-22.

Hwang SW, Cho H, Kwak J, Lee SY, Kang CJ, Jung J, Cho S, Min KH, Suh YG, Kim D, Oh U (2000) Direct activation of capsaicin receptors by products of lipoxygenases: endogenous capsaicin-like substances. *Proc Natl Acad Sci (USA)* 97:6155-6160.

Ichikawa H, Sugimoto T (2004). The co-expression of P2X3 receptor with VR1 and VRL-1 in the rat trigeminal ganglion. *Brain Res* 998:130-135.

Ide S, Kobayashi H, Tanaka K, Ujike H, Sekine Y, Ozaki N, Inada T, Harano M, Komiyama T, Yamada M, Iyo M, Ikeda K, Sora I (2004). Gene polymorphisms of the mu opioid receptor in methamphetamine abusers. *Ann N Y Acad Sci* 1025:316-24.

Inouye S, Tsuji FI (1994). Aequorea green fluorescent protein. Expression of the gene and fluorescence characteristics of the recombinant protein. *FEBS Lett* 341:277-80.

International Association for the Study of Pain (1979). Subcommittee on taxonomy of pain teams: A list with definitions and notes on usage. *Pain* 6:249-252.

Ioue K, Koizumi S, Fuziwara S, Denda S, Inoue K, Denda M (2002). Functional vanilloid receptors in cultured normal human epidermal keratinocytes. *Biochem Biophys Res Commun* 291:124-129.

Jackson MB (1997). Whole-Cell Voltage Clamp Recording. In M Rogowski (Ed), *Current Protocols in Neuroscience* (6.6.1-6.6.30). New York: John Wiley & Sons, Inc.

Jancsó N (1968). Desensitization with capsaicin and related acylamides as a tool for studying the function of pain receptors. In Lim RKS, Armstrong D, Pardo ED, (Eds.) *Pharmacology of pain* (pp 33-55). New York: Pergamon.

Jancsó N and Jancsó A (1949). Desensitization of sensory nerve endings (in Hungarian). *Kísérletes Orvostudomány* 2(Suppl): 15.

Jancso-Gabor A, Szolecsanyi J, Jancso N (1970). Stimulation and desensitization of the hypothalamic heat-sensitive structure by capsaicin in rats. *J Physiol* 208:444.

Jeske NA, Patwardhan AM, Gamper N, Price TJ, Akopian AN, Hargreaves KM (2006). Cannabinoid WIN 55,212-2 regulates TRPV1 phosphorylation in sensory neurons. *J Biol Chem* 281:32879-32890.

Johansson B, Halldner L, Dunwiddie TV, Masino SA, Poelchen W, Giménez-Llort L, Escorihuela RM, Fernández-Teruel A, Wiesenfeld-Hallin Z, Xu XJ, Hårdemark A, Betsholtz C, Herlenius E, Fredholm BB (2001). Hyperalgesia, anxiety, and decreased hypoxic neuroprotection in mice lacking the adenosine A1 receptor. *Proc Natl Acad Sci U S A* 98:9407-9412.

Johnson RA (1994). *Johnson, Miller & Freund's Probability & Statistics for Engineers* (pp. 342). New Jersey: Prentice-Hall.

Jones A, Reed R, Weyers J (2007). Statistical test for measuring the association between two variables. *Practical Skills in Biology* (pp. 380-381). Jones & Bartlett Publishers, Inc.

Jones J (2009). Statistics, Lecture notes. http://people.richland.edu/james/lecture/m170/ch13-def.html.

Jordt SE, Bautista DM, Chuang HH, McKemy DD, Zygmunt PM, Högestätt ED, Meng ID, Julius D (2004). Mustard oils and cannabinoids excite sensory nerve fibres through the TRP channel ANKTM1. *Nature* 427:260-265.

Jordt SE, Julius D (2002). Molecular basis for species-specific sensitivity to "hot" chili peppers. *Cell* 108:421-430.

Jordt SE, Tominaga M, Julius D (2000). Acid potentiation of the capsaicin receptor determined by a key extracellular site. *Proc Natl Acad Sci U S A* 97:8134-8139.

Julius D, Basbaum AI (2001). Molecular mechanisms of nociception. *Nature* 413:203-210.

Jung J, Lee SY, Hwang SW, Cho H, Shin J, Kang YS, Kim S, Oh U (2002) Agonist recognition sites in the cytosolic tails of vanilloid receptor 1. *J Biol Chem* 277:44448-44454.

Kanai Y, Nakazato E, Fujiuchi A, Hara T, Imai A (2005). Involvement of an increased spinal TRPV1 sensitization through its up-regulation in mechanical allodynia of CCI rats. *Neuropharmacology* 49:977-984.

Kao LS, Green CE (2007). Analysis of variance: is there a difference in means and what does it mean? *J Surg Res*. 144:158-70.

Kaplan DR, Martin-Zanca D, Parada LF (1991). Tyrosine phosphorylation and tyrosine kinase activity of the trk proto-oncogene product induced by NGF. *Nature* 350:158-60.

Kato S, Aihara E, Nakamura A, Xin H, Matsui H, Kohama K, Takeuchi K (2003). Expression of vanilloid receptors in rat gastric epithelial cells: role in cellular protection. *Biochem Pharmacol* 66:1115-1121.

Katzman PL , Henningsen NC, Hulthén UL (1988). Amiloride compared with nitrendipine in treatment of essential hypertension. *J Hum Hypertens* 2:147-51.

Kawai S, Nishizawa M (1984). New procedure for DNA transfection with polycation and dimethyl sulfoxide. *Mol Cell Biol* 4:1172-4.

Kelly S, Chapman V (2002). Spinal administration of capsazepine inhibits noxious evoked responses of dorsal horn neurons in non-inflamed and carrageenan inflamed rats. *Brain Res* 935:103-108.

Kerekes N, Landry M, Lundmark K, Hokfelt T (2000). Effect of NGF, BDNF, bFGF, aFGF and cell density on NPY expression in cultured rat dorsal root ganglion neurones. *J Auton Nerv Syst* 81:128–138.

Kerr BJ, Cafferty WB, Gupta YK, Bacon A, Wynick D, McMahon SB, Thompson SW (2000). Galanin knockout mice reveal nociceptive deficits following peripheral nerve injury. *Eur J Neurosci* 12:793-802.

Kest B, Palmese C, Hopkins E (2000). A comparison of morphine analgesic tolerance in male and female mice. *Brain Res* 879:17-2.

Keusch P (2009) http://www.uni-regensburg.de/Fakultaeten/nat_Fak_IV/Organische_ Chemie/Didaktik/Keusch/kinetics.html.

Khasar SG, Green PG, Levine JD (1993). Comparison of intradermal and subcutaneous hyperalgesic effects of inflammatory mediators in the rat. *Neurosci Lett* 153:215-8.

Kilo S, Forster C, Geisslinger G, Brune K, Handwerker HO (1994). Inflammatory models of cutaneous hyperalgesia are sensitive to effects of ibuprofen in man. *Pain* 62:187-93.

Kilo S, Schmelz M, Koltzenburg M, Handwerker HO (1994). Different patterns of hyperalgesia induced by experimental inflammation in human skin. *Brain* 117:385-96.

Kim H, Neubert JK, San Miguel A, Xu K, Krishnaraju RK, Iadarola MJ, Goldman D, Dionne RA (2004). Genetic influence on variability in human acute experimental pain sensitivity associated with gender, ethnicity and psychological temperament. *Pain* 109:488-96.

Kim KN, Caicedo A, Roper SD (2001). Glutamate-induced cobalt uptake reveals non-NMDA receptors in developing rat taste buds. *Neuroreport* 12:1715-8.

Kim S, Kang C, Shin CY, Hwang SW, Yang YD, Shim WS, Park MY, Kim E, Kim M, Kim BM, Cho H, Shin Y, Oh U (2006). TRPV1 recapitulates native

capsaicin receptor in sensory neurons in association with Fas-associated factor 1. *J Neurosci* 26:2403-12.

Kindgen-Milles D, Klement W (1992). Pain and inflammation evoked in human skin by bradykinin receptor antagonists. *Eur J Pharmacol* 218:183-5.

Kitao Y, Robertson B, Kudo M, Grant G (1996). Neurogenesis of subpopulations of rat lumbar dorsal root ganglion neurons including neurons projecting to the dorsal column nuclei. *J Comp Neurol* 371:249-57.

Klein R, Jing SQ, Nanduri V, O'Rourke E, Barbacid M (1991). The trk proto-oncogene encodes a receptor for nerve growth factor. *Cell* 65:189-97.

Kleppe K, Ohtsuka E, Kleppe R, Molineux I, Khorana HG (1971). Studies on polynucleotides. XCVI. Repair replications of short synthetic DNA's as catalyzed by DNA polymerases. *J Mol Biol* 56:341-61.

Kleyman TR, Sheng S, Kosari F, Kieber-Emmons T (1999). Mechanism of action of amiloride: a molecular prospective. *Semin Nephro* 19:524-32.

Kobayashi K, Fukuoka T, Obata K, Yamanaka H, Dai Y, Tokunaga A, Noguchi K (2005). Distinct expression of TRPM8, TRPA1, and TRPV1 mRNAs in rat primary afferent neurons with adelta/c-fibers and colocalization with trk receptors. *J Comp Neurol* 493:596-606.

Kolesnikov YA, Pan YX, Babey AM, Jain S, Wilson R, Pasternak GW (1997). Functionally differentiating two neuronal nitric oxide synthase isoforms through antisense mapping: evidence for opposing NO actions on morphine analgesia and tolerance. *Proc Natl Acad Sci U S A* 94:8220-5.

Koplas PA, Rosenberg RL, Oxford GS (1997). The role of calcium in the desensitization of capsaicin responses in rat dorsal root ganglion neurons. *J Neurosci* 17:3525-37.

Kozlova EN, Jansson L (2005). In vitro interactions between insulin-producing beta cells and embryonic dorsal root ganglia. *Pancreas* 31:380-4.

Kress M, Fetzer S, Reeh PW, Vyklicky L (1996). Low pH facilitates capsaicin responses in isolated sensory neurons of the rat. *Neurosci Lett* 211: 5-8.

Kress M, Koltzenburg M, Reeh PW, Handwerker HO (1992). Responsiveness and functional attributes of electrically localized terminals of cutaneous C-fibers in vivo and in vitro. *J Neurophysiol* 68:581–595.

Kress M, Reeh PW (1996). More sensory competence for nociceptive neurons in culture. *Proc Natl Acad Sci U S A* 93:14995-7.

Kunkel TA (1985). Rapid and efficient site-specific mutagenesis without phenotypic selection. *Proc Natl Acad Sci U S A* 82:488-92.

Kunkel TA, Roberts JD, Zakour RA (1987). Rapid and efficient site-specific mutagenesis without phenotypic selection. *Methods Enzymol* 154:367-82.

Kupers RC, Chen CC, and Bushnell MC (1997). A model of transient hyperalgesia in the behaving monkey induced by topical application of capsaicin. *Pain* 72: 269-275.

Kuzhikandathil EV, Wang H, Szabo T, Morozova N, Blumberg PM, Oxford GS (2001). Functional analysis of capsaicin receptor (vanilloid receptor subtype 1) multimerization and agonist responsiveness using a dominant negative mutation. *J Neurosci* 21:8697-8706.

Kuzmenkin A, Bezanilla F, Correa AM (2004). Gating of the bacterial sodium channel, NaChBac: voltage-dependent charge movement and gating currents. *J Gen Physiol* 124:349-56.

Kwak J, Wang MH, Hwang SW, Kim TY, Lee SY, Oh U (2000). Intracellular ATP increases capsaicin-activated channel activity by interacting with nucleotide-binding domains. *J Neurosci* 20:8298-8304.

Lai J, Bilsky EJ, Rothman RB, Porreca F (1994). Treatment with antisense oligodeoxynucleotide to the opioid delta receptor selectively inhibits delta 2-agonist antinociception. *Neuroreport* 5:1049-52.

Lai J, Gold MS, Kim CS, Bian D, Ossipov MH, Hunter JC, Porreca F (2002). Inhibition of neuropathic pain by decreased expression of the tetrodotoxin-resistant sodium channel, NaV1.8. *Pain* 95:143-52.

Lakhlani PP, MacMillan LB, Guo TZ, McCool BA, Lovinger DM, Maze M, Limbird LE (1997). Substitution of a mutant alpha2a-adrenergic receptor via "hit and run" gene targeting reveals the role of this subtype in sedative, analgesic, and anesthetic-sparing responses in vivo. *Proc Natl Acad Sci U S A* 94:9950-5.

Lam PM, McDonald J, Lambert DG (2001). Characterization and comparison of recombinant human and rat TRPV1 receptors: effects of exo- and endocannabinoids. *Br J Pharmacol* 132:1084-94.

Lane D (2009). http://davidmlane.com/hyperstat/A13660.html

Latorre R, Brauchi S, Orta G, Zaelzer C, Vargas G (2007). ThermoTRP channels as modular proteins with allosteric gating. *Cell Calcium* 42:427-438.

Lautenbacher S, Rollman GB (1993). Sex differences in responsiveness to painful and non-painful stimuli are dependent upon the stimulation method. *Pain* 53:255-264.

Lawson SN, Waddell PJ (1991). Soma neurofilament immunoreactivity is related to cell size and fibre conduction velocity in rat primary sensory neurons. *J Physiol* 435:41-63.

Lázár J, Szabó T, Marincsák R, Kovács L, Blumberg PM, Bíró T (2004). Sensitization of recombinant vanilloid receptor-1 by various neurotrophic factors. *Life Sci* 75:153-63.

Lecar H, Larsson HP, Grabe M (2003). Electrostatic model of S4 motion in voltage-gated ion channels. *Biophys J* 85:2854-2864.

Ledent C, Vaugeois JM, Schiffmann SN, Pedrazzini T, El Yacoubi M, Vanderhaeghen JJ, Costentin J, Heath JK, Vassart G, Parmentier M (1997). Aggressiveness, hypoalgesia and high blood pressure in mice lacking the adenosine A2a receptor. *Nature* 388: 674-678.

Lee IO, Yukhananov R, Standaert DG, Crosby G (2004). NMDA-R1 antisense oligodeoxynucleotides modify formalin-induced nociception and spinal c-Fos expression in rat spinal cord. *Pharmacol Biochem Behav* 79:183-8.

Lee JC, Greig A, Ravindranathan A, Parks TN, Rao MS (1998). Molecular analysis of AMPA-specific receptors: subunit composition, editing, and calcium influx determination in small amounts of tissue. *Brain Res Brain Res Protoc* 3:142-54.

Lee MC, Essoka G (1998). Patient's perception of pain: Comparison between Korean-American and Euro-American obstetric patients. *Journal of Cultural Diversity* 5:29–40.

Lee SP, Park MT, Kim SH, Jo EC, Lee GM (2001). Monolayer and suspension of HEK293 cells for recombinant adenovirus production for gene therapy: Effect of "cell passage number" pages 535-537. In E Lindner-Olsson, N

Chatzissavidou, E Lüllau (Eds.), *Animal Cell Technology: From Target to Market.* New York: Springer-Verlag

Lee SY, Lee JH, Kang KK, Hwang SY, Choi KD, Oh U (2005). Sensitization of vanilloid receptor involves an increase in the phosphorylated form of the channel. *Arch Pharm Res* 28:405-412.

Lee YJ, Zachrisson O, Tonge DA, McNaughton PA (2002). Upregulation of bradykinin B2 receptor expression by neurotrophic factors and nerve injury in mouse sensory neurons. *Mol Cell Neurosci* 19: 186-200.

Leffler A, Linte RM, Nau C, Reeh P, Babes A (2007). A high-threshold heat-activated channel in cultured rat dorsal root ganglion neurons resembles TRPV2 and is blocked by gadolinium. *Eur J Neurosci* 26:12-22.

Lever IJ, Robinson M, Cibelli M, Paule C, Santha P, Yee L, Hunt SP, Cravatt BF, Elphick MR, Nagy I, Rice AS (2009). Localization of the endocannabinoid-degrading enzyme fatty acid amide hydrolase in rat dorsal root ganglion cells and its regulation after peripheral nerve injury. *J Neurosci* 29:3766-80.

Levi-Montalcini R (1987). The nerve growth factor 35 years later. *Science* 237:1154-62.

Levi-Montalcini R, Angeletti PU (1963). Essential role of the nerve growth factor in the survival and maintenance of dissociated sensory and sympathetic embryonic nerve cells in vitro. *Dev Biol* 7:653-9.

Levi-Montalcini R, Cohen S (1960). Effects of the extract of the mouse submaxillary salivary glands on the sympathetic system of mammals. *Ann N Y Acad Sci* 85:324-41.

Levine JD, Fields HL, Basbaum AI (1993). Peptides and the primary afferent nociceptor. *Neurosci* 13:2273-2286.

Lewin GR, Mendell LM (1993). Nerve growth factor and nociception. *Trends Neurosci* 16:353-359.

Lewis R, Evans W (2006). The Graphical determination of the Arrhenius Activation Energy. *Chemistry* (pp. 247-253). New York: Palgrave Macmillan.

Li HH, Gyllensten UB, Cui XF, Saiki RK, Erlich HA, Arnheim N (1988). Amplification and analysis of DNA sequences in single human sperm and diploid cells. *Nature* 335: 414-417.

Liang YF, Haake B, Reeh PW (2001). Sustained sensitization and recruitment of rat cutaneous nociceptors by bradykinin and a novel theory of its excitatory action. *J Physiol* 523: 229-239.

Lieberman AR (1976). Sensory ganglia. In DN Landon (Ed.), *The peripheral nerve* (pp. 188-278) London: Chapman and Hall.

Lindsay RM, Harmar AJ (1989). Nerve growth factor regulates expression of neuropeptide genes in adult sensory neurons. *Nature Lond* 337:362–364.

Lindsay RM, Rang HP (1987). Effects of bradykinin on membrane currenls of rat sensory neurons in tissue culture. *J Physiol* 390(Suppl): 74P.

Lishko PV, Procko E, Jin X, Phelps CB, Gaudet R (2007). The ankyrin repeats of TRPV1 bind multiple ligands and modulate channel sensitivity. *Neuron* 54:905-918.

Liu B, Hui K, Qin F (2003). Thermodynamics of heat activation of single capsaicin ion channels VR1. *Biophys J* 85:2988-3006.

Liu B, Ma W, Ryu S, Qin F (2004). Inhibitory modulation of distal C-terminal on protein kinase C-dependent phospho-regulation of rat TRPV1 receptors. *J Physiol* 560:627-638.

Liu B, Zhang C, Qin F (2005). Functional recovery from desensitization of vanilloid receptor TRPV1 requires resynthesis of phosphatidylinositol 4,5-bisphosphate. *J Neurosci* 25:4835-4843.

Liu L, Simon SA (1996). Capsaicin-induced currents with distinct desensitization and Ca2+ dependence in rat trigeminal ganglion cells. *Journal of Neurophysiology* 75:1503–1514.

Llinás R, Sugimori M (2004). Electrophysiological properties of in vitro Purkinje cell somata in mammalian cerebellar slices. *Neurosci Lett* 370:55-60.

Lopshire JC, Nicol GD (1998). The cAMP transduction cascade mediates the prostaglandin E2 enhancement of the capsaicin-elicited current in rat sensory neurons: whole-cell and single-channel studies. *J Neurosci* 18:6081-6092.

Low JF (1997). Religious orientation and pain management. *Am J Occup Ther* 51:215-219.

Lu G, Henderson D, Lu L, Reinhart PH, Simon SA (2005). TRPV1b, a functional human vanilloid receptor splice variant. *Mol Pharmacol* 67:1119-1127.

Lu Z (2004). Mechanism of rectification in inward-rectifier K+ channels. *Annu Rev Physiol* 66:103-29.

Lucas JJ, Mellström B, Colado MI, Naranjo JR (1993).Molecular mechanisms of pain: serotonin1A receptor agonists trigger transactivation by c-fos of the prodynorphin gene in spinal cord neurons. *Neuron* 10:599-611.

Lue BH, Huang TS, Chen HJ (2008). Physical Distress, Emotional Status, and Quality of Life in Patients With Nasopharyngeal Cancer Complicated by Post-Radiotherapy Endocrinopathy. *Int J Radiat Oncol Biol Phys* 70:28-34.

Lukacs V, Thyagarajan B, Varnai P, Balla A, Balla T, Rohacs T (2007). Dual regulation of TRPV1 by phosphoinositides. *J Neurosci* 27:7070-7080.

Macpherson LJ, Geierstanger BH, Viswanath V, Bandell M, Eid SR, Hwang S, Patapoutian A (2005). The pungency of garlic: activation of TRPA1 and TRPV1 in response to allicin. *Curr Biol* 15:929-34.

MacQueen GM, Ramakrishnan K, Croll SD, Siuciak JA, Yu G, Young LT, Fahnestock M (2001). Performance of heterozygous brain-derived neurotrophic factor knockout mice on behavioral analogues of anxiety, nociception, and depression. *Behav Neurosci* 115:1145-1153.

Maggi CA, Santicioli P, Meli A (1984). The effects of topical capsaicin on rat urinary bladder motility in vivo. *Eur J Pharmacol* 103:41-50.

Mahmud A, Santha P, Paule CC, Nagy I (2009). Cannabinoid 1 receptor activation inhibits transient receptor potential vanilloid type 1 receptor-mediated cationic influx into rat cultured primary sensory neurons. *Neuroscience* 162:1202-11.

Malek RS, Wahner-Roedler DL, Gertz MA, Kyle RA (2002). Primary localized amyloidosis of the bladder: experience with dimethyl sulfoxide therapy. *J Urol* 168:1018-10120.

Malva JO, Vieira AP, Oliveira CR (2003). Understanding the physiology of glutamate receptors by use of a protocol for neuronal staining. *Adv Physiol Educ* 27:78-85.

Mandadi S, Numazaki M, Tominaga M, Bhat MB, Armati PJ, Roufogalis BD (2004). Activation of protein kinase C reverses capsaicin-induced calcium-dependent desensitization of TRPV1 ion channels. *Cell Calcium* 35:471-478.

Mandel M, Higa A (1970). Calcium-dependent bacteriophage DNA infection. *J Mol Biol* 53:159-62.

Marek P, Mogil JS, Belknap JK, Sadowski B, Liebeskind JC (1993). Levorphanol and swim stress-induced analgesia in selectively bred mice: evidence for genetic commonalities. *Brain Res* 608:353-7.

Marín-Burgin A, Reppenhagen S, Klusch A, Wendland JR, Petersen M (2000). Low-threshold heat response antagonized by capsazepine in chick sensory neurons, which are capsaicin-insensitive. *Eur J Neurosci* 12:3560-3566.

Marsh SJ, Stansfeld CE, Brown DA, Davey R, McCarthy D (1987). The mechanism of action of capsaicin on sensory C-type neurons and their axons in vitro. *Neuroscience* 23:275-89.

Martin M, Matifas A, Maldonado R, Kieffer BL (2003). Acute antinociceptive responses in single and combinatorial opioid receptor knockout mice: distinct mu, delta and kappa tones. *Eur J Neurosci* 17:701-708.

Martini G, Toniolo D, Vulliamy T, Luzzatto L, Dono R, Viglietto G, Paonessa G, D'Urso M, Persico MG (1986). Structural analysis of the X-linked gene encoding human glucose 6-phosphate dehydrogenase. *EMBO J* 5:1849–1855.

Martin-Zanca D, Barbacid M, Parada LF (1990). Expression of the trk proto-oncogene is restricted to the sensory cranial and spinal ganglia of neural crest origin in mouse development. *Genes Dev* 4:683-94.

Mather JP and Roberts PE (1998). Introduction to Cell and Tissue Culture: Theory and Technique. New York: Plenum Press.

Matthews GG (2000). Advance topic three: Analysis of channel gating. In *Neurobiology: Molecules, Cells and Systems* (pp 525-538). Oxford: Blackwell Science.

Matsumoto J (1967). Clinical trials of dimethyl sulfoxide in rheumatoid arthritis patients in Japan. *Ann NY Acad Sci* 141:560-568.

Matta JA, Ahern GP (2007). Voltage is a partial activator of rat thermosensitive TRP channels. *J Physiol* 585(Pt 2):469-482.

McCarthy PW, Lawson SN (1989). Cell type and conduction velocity of rat primary sensory neurons with substance P-like immunoreactivity. *Neuroscience* 28:745-53.

McCarthy PW, Lawson SN (1990). Cell type and conduction velocity of rat primary sensory neurons with calcitonin gene-related peptide-like immunoreactivity. *Neuroscience* 34:623-32.

McDonald JH (2009). Handbook of Biological Statistics). Baltimore, Maryland: Sparky House Publishing.

McEwen BS, Alves SE, Bulloch K, Weiland NG (1998). Clinically relevant basic science studies of gender differences and sex hormone effects. *Psychopharmacol Bull* 34:251-259.

McIntyre P, McLatchie LM, Chambers A, Phillips E, Clarke M, Savidge J, Toms C, Peacock M, Shah K, Winter J, Weerasakera N, Webb M, Rang HP, Bevan S, James IF (2001). Pharmacological differences between the human and rat vanilloid receptor 1 (VR1). *Br J Pharmacol* 132:1084-94.

McKemy DD, Neuhausser WM, Julius D (2002). Identification of a cold receptor reveals a general role for TRP channels in thermosensation. *Nature* 416:52-8.

McLatchie LM, Bevan S (2001). The effects of pH on the interaction between capsaicin and the vanilloid receptor in rat dorsal root ganglia neurons. *Br J Pharmacol* 132:899-908.

McMahon S B, Armanini, MP Ling, L H Phillips H S (1994) Expression and coexpression of Trk receptors in subpopulations of adult primary sensory neurons projecting to identified peripheral targets. *Neuron* 12: 1161-1171.

McMahon SB, Bennett DL, Priestley JV, Shelton DL (1995). The biological effects of endogenous nerve growth factor on adult sensory neurons revealed by a trkA-IgG fusion molecule. *Nat Med* 1:774-80.

Melchior D, Packer CS, Johnson TC, Kaefer M (2003). Dimethyl sulfoxide: does it change the functional properties of the bladder wall? *J Urol* 170:253-258.

Mendell LM (1999). Neurotrophin action on sensory neurons in adults: an extension of the neurotrophic hypothesis. *Pain* Suppl 6:S127-32.

Mense S. (1981). Sensitization of group IV muscle receptors to bradykinin by 5-hydroxytryptamine and prostaglandin E 2. *Brain Res* 225:95-105.

Mezey E, Toth ZE, Cortright DN, Arzubi MK, Krause JE, Elde R, Guo A, Blumberg PM, Szallasi A (2000). Distribution of mRNA for vanilloid receptor subtype 1 (VR1), and VR1-like immunoreactivity, in the central nervous system of the rat and human. *Proc Natl Acad Sci (USA)* 97:3655-3660.

Michael GJ, Priestley JV (1999). Differential expression of the mRNA for the vanilloid receptor subtype 1 in cells of the adult rat dorsal root and nodose ganglia and its downregulation by axotomy. *J Neurosci* 19: 1844-1854.

Miczek KA, Thompson ML, Shuster L (1982). Opioid-like analgesia in defeated mice. *Science* 215:1520-2.

Millan MJ (1999) The induction of pain: an integrative review. *Prog Neurobiol* 57:1-164.

Millar N (2001). Biology statistics made simple using Excel. *School Science Review* 83(303)

Miller C, Newton SE (2006) Pain perception and expression: the influence of gender, personal self-efficacy, and lifespan socialization. *Pain Manag Nurs* 7:148-52.

Mizumura K, Minagawa M, Tsujii Y, Kumazawa T (1990). The effects of bradykinin agonists and antagonists on visceral polymodal receptor activities. *Pain* 40:221-7.

Mogil JS, Chesler EJ, Wilson SG, Juraska JM, Sternberg WF (2000). Sex differences in thermal nociception and morphine antinociception in rodents depend on genotype. *Neurosci Biobehav Rev* 24:375-389.

Mogil JS, Max MB (2006). The genetics of pain. In McMahon SB, Koltzenburg M, Wall PD (Ed.) *Wall and Melzack's Textbook of Pain: Edition 5* (pp 159-174). Philadelphia: Elsevier Science Health Science Division.

Mogil JS, McCarson KE (2000). Identifying pain genes: bottom-up and top-down approaches. *J Pain* 1(3 Suppl):66-80.

Mogil JS, Wilson SG, Bon K, Lee SE, Chung K, Raber P, Pieper JO, Hain HS, Belknap JK, Hubert L, Elmer GI, Chung JM, Devor M (1999). Heritability of nociception I: responses of 11 inbred mouse strains on 12 measures of nociception. *Pain* 80:67-82.

Mohapatra DP, Nau C (2003). Desensitization of capsaicin-activated currents in the vanilloid receptor TRPV1 is decreased by the cyclic AMP-dependent protein kinase pathway. *J Biol Chem* 278:50080-50090.

Mohapatra DP, Nau C (2005) Regulation of Ca2+-dependent desensitization in the vanilloid receptor TRPV1 by calcineurin and cAMP-dependent protein kinase. *J Biol Chem* 280:13424-13432.

Mohapatra DP, Trimmer JS (2006). The Kv2.1 C terminus can autonomously transfer Kv2.1-like phosphorylation-dependent localization, voltage-dependent gating, and muscarinic modulation to diverse Kv channels. *J Neurosci* 26:685-95.

Mohapatra DP, Wang SY, Wang GK, Nau C (2003). A tyrosine residue in TM6 of the Vanilloid Receptor TRPV1 involved in desensitization and calcium permeability of capsaicin-activated currents. *Mol Cell Neurosci* 23:314-324.

Molleman A (2002). The platform: Anti-vibration tables. In *Patch Clamping: An Introductory Guide to Patch Clamp Electrophysiology* (pp. 46). Chichester: Wiley, John & Sons, Incorporated.

Moore S, Steve C, Dave A (2005). Gender and Identity. *Sociology AS for OCR* (pp 30-33). London: Harper Collins Publsihers.

Morcos PA (2000). Gene switching: analyzing a broad range of mutations using steric block antisense oligonucleotides. *Methods Enzymol* 313:174-89.

Morenilla-Palao C, Planells-Cases R, Garcia-Sanz N, Ferrer-Montiel A (2004). Regulated exocytosis contributes to protein kinase C potentiation of vanilloid receptor activity. *J Biol Chem* 279:25665-25672.

Moriyama T, Higashi T, Togashi K, Iida T, Segi E, Sugimoto Y, Tominaga T, Narumiya S, Tominaga M (2005). Sensitization of TRPV1 by EP1 and IP reveals peripheral nociceptive mechanism of prostaglandins. *Mol Pain* 1:3.

Morley M, Molony CM, Weber TM, Devlin JL, Ewens KG, Spielman RS, Cheung VG (2004). Genetic analysis of genome-wide variation in human gene expression. *Nature* 430:733-734.

Morse JM, Park C (1988). Differences in cultural expectations of the perceived painfulness of childbirth. In: KL. Michaelson (Ed). *Childbirth in America: Anthropological perspectives* (pp. 121–129). South Hadley, MA: Bergin & Garvey.

Motulsky HJ (2007). Prism 5 Statistics Guide. San Diego CA :GraphPad SoftwareInc. www.graphpad.com.

Movahed P, Jonsson BAG, Birnir B, Wingstrand JA, Jorgensen TK, Ermund A, Sterner O, Zygmunt PM, Hogestatt ED (2005). Endogenous unsaturated C18 N-acylethanolamines are vanilloid receptor (TRPV1) agonists. *J Biol Chem* 280:38496-38504.

Muir M (2001) DMSO: Many Uses, Much Controversy. http://www.dmso.org/articles/information/ muir.htm.

Mullis KB (1987). Process for amplifying nucleic acid sequences. U.S. Patent #4,683,202.

Mullis KB, Erlich HA, Arnheim N, Horn GT, Saiki RK, and Scharf SJ (1987). Process for amplifying, detecting, and/or cloning nucleic acid sequences. U.S. Patent #4,683,195.

Mullis KB, Faloona FA (1987). Specific synthesis of DNA in vitro via a polymerase-catalyzed chain reaction. *Methods Enzymol* 155:335-50.

Nagy I (2004). Sensory processing: primary afferent neurons/DRG. In AS Evers, M Maze (Eds.) *Anesthetic Pharmacology:Physiologic Principles and Clinical Practice* (pp. 187–197). Philadelphia: Chirchill Livingstone.

Nagy I, Pabla R, Matesz C, Dray A, Woolf CJ, Urban L (1993). Cobalt uptake enables identification of capsaicin- and bradykinin-sensitive subpopulations of rat dorsal root ganglion cells in vitro. *Neuroscience* 56:241-246.

Nagy I, Rang HP (1999). Similarities and differences between the responses of rat sensory neurons to noxious heat and capsaicin. *J Neurosci* 19:10647-55.

Nagy I, Woolf CJ, Dray A, Urbán L (1994). Cobalt accumulation in neurons expressing ionotropic excitatory amino acid receptors in young rat spinal cord: morphology and distribution. *J Comp Neurol* 344:321-35.

Negri L, Lattanzi R, Borsodi A, Toth G, Salvadori S (1999). Differential knockdown of delta-opioid receptor subtypes in the rat brain by antisense oligodeoxynucleotides targeting mRNA. *Antisense Nucleic Acid Drug Dev* 9:203-11.

Nelson DJ, Fozzard HA (2000). Ion channels. In PM Conn, AR Means (Eds.) *Principles of Molecular Regulation* (pp. 135-148). New York: Springer-Verlag.

Nelson EK (1919). The constitution of capsaicin-the pungent principle of capsicum. *J Am Chem Soc* 41:1115–1117.

Nelson M, McClelland M (1992). Use of DNA methyltransferase/endonuclease enzyme combinations for megabase mapping of chromosomes. *Methods Enzymol* 216:279-303.

Ni D, Gu Q, Hu HZ, Gao N, Zhu MX, Lee LY (2006). Thermal sensitivity of isolated vagal pulmonary sensory neurons: role of transient receptor potential vanilloid receptors. *Am J Physiol Regul Integr Comp Ph*ysiol 291:R541-50.

Nicol GD, Klingberg DK, Vasko MR (1992). Prostaglandin E2 increases calcium conductance and stimulates release of substance P in avian sensory neurons. *J Neurosci* 12:1917-27.

Nikcevic G, Kovacevic-Grujicic N, Stevanovic M (2003). Improved transfection efficiency of cultured human cells. *Cell Biol Int* 27:735-7.

Nilius B, Talavera K, Owsianik G, Prenen J, Droogmans G, Voets T (2005). Gating of TRP channels: a voltage connection? *J Physiol*. 567:35-44.

Numazaki M, Tominaga T, Takeuchi K, Murayama N, Toyooka H, Tominaga M (2003). Structural determinant of TRPV1 desensitization interacts with calmodulin. *Proc Natl Acad Sci U S A* 100:8002-8006.

Numazaki M, Tominaga T, Toyooka H, Tominaga M (2002). Direct phosphorylation of capsaicin receptor VR1 by protein kinase C epsilon and identification of two target serine residues. *J Biol Chem* 277:13375-13378.

Ogun-Muyiwa P, Helliwell R, McIntyre P, Winter J (1999). Glial cell line derived neurotrophic factor (GDNF) regulates VR1 and substance P in cultured sensory neurons. *Neuroreport* 10:2107-2111.

Oh U, Hwang SW, Kim D (1996). Capsaicin activates a nonselective cation channel in cultured neonatal rat dorsal root ganglion neurons. *J Neurosc*i 16:1659-67.

Olah Z, Karai L, Iadarola MJ (2001). Anandamide activates vanilloid receptor 1 (VR1) at acidic pH in dorsal root ganglia neurons and cells ectopically expressing VR1. *J Biol Chem* 276:31163-31170.

OriginLab (2007). Origin 9 User Manaul OriginLab Corporation. Northampton, MA www.OriginLab.com http://www.llas.ac.cn/upload/Origin_8_User_Guide.pdf

Otten U, Lorez HP, Businger F (1983). Nerve growth factor antagonizes the neurotoxic action of capsaicin on primary sensory neurones. *Nature* 301:515-7.

Ou J, Geiger T, Ou Z, Ackerman AW, Oldham KT, Pritchard KA Jr (2003). AP-4F, antennapedia peptide linked to an amphipathic alpha helical peptide, increases the efficiency of Lipofectamine-mediated gene transfection in endothelial cells. *Biochem Biophys Res Commun* 305:605-610.

Panet A, Khorana HG (1974). Studies on polynucleotides. The linkage of deoxyribopolynucleotide templates to cellulose and its use in their replication. *J Biol Chem* 249:5213-21.

Panocka I, Marek P, Sadowski B (1986). Inheritance of stress-induced analgesia in mice. Selective breeding study. *Brain Res* 397:152-5.

Papazian DM, Timpe LC, Jan YN, Jan LY (1991). Alteration of voltage-dependence of Shaker potassium channel by mutations in the S4 sequence. *Nature* 349:305-310.

Papworth C, Bauer JC, Braman J, Wright DA (1996). QuikChange site-directed mutagenesis. *Strategies* 9:3-4.

Pare M, Elde R, Mazurkiewicz JE, Smith AM, Rice FL (2001). The Meissner corpuscle revised: a multiafferented mechanoreceptor with nociceptor immunochemical properties. *J Neurosci* 21:7236-7246.

Pari GS, Keown WA (1997). Experimental strategies in efficient transfection of mammalian cells. Calcium phosphate and DEAE-dextran. *Methods Mol Biol* 62:301-6.

Park MT, Lee MS, Kim SH, Jo EC, Lee GM (2004). Influence of culture passages on growth kinetics and adenovirus vector production for gene therapy in monolayer and suspension cultures of HEK 293 cells. *Appl Microbiol Biotechnol* 65:553-8.

Passmore GM (2005). Dorsal root ganglion neurones in culture: a model system for identifying novel analgesic targets? *J Pharmacol Toxicol Methods* 51:201-8.

Patel TD, Jackman A, Rice FL, Kucera J, Snider WD (2000). Development of sensory neurons in the absence of NGF/TrkA signaling in vivo. *Neuron* 25:345-57.

Paul D, Yao D, Zhu P, Minor LD, Garcia MM (2001). 5-hydroxytryptamine3 (5-HT3) receptors mediate spinal 5-HT antinociception: an antisense approach. *J Pharmacol Exp Ther* 298:674-8.

Pazdrak K, Shi XZ, Sarna SK (2004). TNFalpha suppresses human colonic circular smooth muscle cell contractility by SP1- and NF-kappaB-mediated induction of ICAM-1. *Gastroenterology* 127:1096-109.

Peier AM, Reeve AJ, Andersson DA, Moqrich A, Earley TJ, Hergarden AC, Story GM, Colley S, Hogenesch JB, McIntyre P, Bevan S, Patapoutian A (2002). A heat-sensitive TRP channel expressed in keratinocytes. *Science* 296:2046-9.

Penner R (1995). A practical guide to patch clamping. In B Sakmann, E Neher (Eds.), *Single-Channel Recording* (pp. 1-30). New York: Plenum Press.

Pérez-García MT, López-López JR, González C (1999). Kvbeta1.2 subunit coexpression in HEK293 cells confers O2 sensitivity to kv4.2 but not to Shaker channels. *J Gen Physiol* 113:897-907.

Perez-Reyes E (2003). Molecular physiology of low-voltage-activated t-type calcium channels. *Physiol Rev* 83:117-61.

Piper AS, Yeats JC, Bevan S, Docherty RJ (1999). A study of the voltage dependence of capsaicin-activated membrane currents in rat sensory neurones before and after acute desensitization. *J Physiol* 518:721-733.

Pitchford S, Levine JD (1991). Prostaglandins sensitize nociceptors in cell culture. *Neurosci Lett* 132:105-8.

Pogatzki-Zahn EM, Shimizu I, Caterina M, Raja SN (2005). Heat hyperalgesia after incision requires TRPV1 and is distinct from pure inflammatory pain. *Pain* 115:296-307.

Polikov V, Block M, Zhang C, Reichert M, Hong JS (2007). In Vitro Models for Neuroelectrodes: A Paradigm for Studying Tissue–Materials Interactions in the Brain. In WM Reichert (Ed.), *Indwelling Neural Implants: Strategies for Contending with the in Vivo Environment* (pp. 89-116). Florida: CRC Press

Polit DF, Beck CT (2008). Power analysis and sample size calculations. In *Nursing Research: Generating and Assessing Evidence for Nursing Practice* (pp.602). Philadelphia: Lippincott Williams and Wilkins.

Porreca F, Lai J, Bian D, Wegert S, Ossipov MH, Eglen RM, Kassotakis L, Novakovic S, Rabert DK, Sangameswaran L, Hunter JC (1999). A comparison of the potential role of the tetrodotoxin-insensitive sodium channels, PN3/SNS and NaN/SNS2, in rat models of chronic pain. *Proc Natl Acad Sci U S A* 96:7640-4.

Prasher DC, Eckenrode VK, Ward WW, Prendergast FG, Cormier MJ (1992). Primary structure of the Aequorea victoria green-fluorescent protein. *Gene* 111:229-33.

Premkumar LS (2001). Interaction between vanilloid receptors and purinergic metabotropic receptors: pain perception and beyond. *Proc Natl Acad Sci (USA)* 98: 6537-6539.

Premkumar LS, Ahern GP (2000). Induction of vanilloid receptor channel activity by protein kinase C. *Nature* 408:985-990.

Prescott ED, Julius D (2003). A modular PIP2 binding site as a determinant of capsaicin receptor sensitivity. *Science* 300: 1284-1288.

Pruss RM, Akeson RL, Racke MM, Wilburn JL (1991). Agonist-activated cobalt uptake identifies divalent cation-permeable kainate receptors on neurons and glial cells. *Neuron* 7:509-518.

Przewlocka B, Sieja A, Starowicz K, Maj M, Bilecki W, Przewlocki R (2002). Knockdown of spinal opioid receptors by antisense targeting beta-arrestin reduces morphine tolerance and allodynia in rat. *Neurosci Lett* 325:107-10.

Puntambekar P, Mukherjea D, Jajoo S, Ramkumar V (2005). Essential role of Rac1/NADPH oxidase in nerve growth factor induction of TRPV1 expression. *J Neurochem* 95:1689-1703.

Purves D, Augustine GA, Fitzpatrick D, Katz LC, LaMantia AS, McNamara JO (2001). Ion channels underlying action potentials. In *The patch clamp method. Neuroscience.* Sunderland, MA: Sinauer Associates.

Rahim-Williams FB, Riley JL 3rd, Herrera D, Campbell CM, Hastie BA, Fillingim RB (2007). Ethnic identity predicts experimental pain sensitivity in African Americans and Hispanics. *Pain* 129:177-184.

Raisinghani M, Pabbidi RM, Premkumar LS (2005). Activation of transient receptor potential vanilloid 1 (TRPV1) by resiniferatoxin. *J Physiol* 567:771-86.

Rami HK, Thompson M, Wyman P, Jerman JC, Egerton J, Brough S, Stevens AJ, Randall AD, Smart D, Gunthorpe MJ, Davis JB (2004). Discovery of small molecule antagonists of TRPV1. Bioorg Med Chem Lett 14:3631-4.

Rantanen T, Guralnik JM, Leveille S, Izmirlian G, Hirsch R, Simonsick E, Ling S, Fried LP (1998). Racial differences in muscle strength in disabled older women. *J Gerontol A Biol Sci Med Sci* 53:355-661.

Razavi R, Chan Y, Afifiyan FN, Liu XJ, Wan X, Yantha J, Tsui H, Tang L, Tsai S, Santamaria P, Driver JP, Serreze D, Salter MW, Dosch HM (2006). TRPV1+ sensory neurons control beta cell stress and islet inflammation in autoimmune diabetes. *Cell* 127:1123-35.

Reeh PW, Pethö G (2000). Nociceptor excitation by thermal sensitization--a hypothesis. *Prog Brain Res* 129:39-50.

Riley JL, Robinson ME, Wise EA, Myers CD, Fillingim RB (1998). Sex differences in the perception of noxious experimental stimuli: a meta-analysis. *Pain* 74:181-187.

Riley JL, Wade JB, Myers CD, Sheffield D, Papas RK, Price DD (2002). Racial/ethnic differences in the experience of chronic pain. *Pain* 100:291-298.

Rippentrop EA, Altmaier EM, Chen JJ, Found EM, Keffala VJ (2005). The relationship between religion/spirituality and physical health, mental health, and pain in a chronic pain population. *Pain* 116:311-321.

Ritter AM, Mendell LM (1992). Somal membrane properties of physiologically identified sensory neurons in the rat: effects of nerve growth factor. *J Neurophysiol* 68:2033-41.

Roberts JC, Davis JB, Benham CK (2004). [3H]Resiniferatoxin autoradiography in the CNS of wild-type and TRPV1 null mice defines TRPV1 (VR-1) protein distribution. *Brain Res* 995:176-183.

Rosenbaum T, Gordon-Shaag A, Munari M, Gordon SE (2004). Ca2+/calmodulin modulates TRPV1 activation by capsaicin. *J Gen Physiol* 123:53-62.

Rosenstein ED (1999). Topical agents in the treatment of rheumatic disorders. *Rheum Dis Clin North Am* 25:899-918.

Ross RA (2003). Anandamide and vanilloid TRPV1 receptors. *Br J Pharmacol* 140:790-801.

Rössberger J, Fall M, Peeker R (2005). Critical appraisal of dimethyl sulfoxide treatment for interstitial cystitis: discomfort, side-effects and treatment outcome. *Scand J Urol Nephrol* 39:73-77.

Rossi GC, Su W, Leventhal L, Su H, Pasternak GW (1997). Antisense mapping DOR-1 in mice: further support for delta receptor subtypes. *Brain Res* 753:176-9.

Routtenberg A (1996). Reverse piedpiperase: is the knockout mouse leading neuroscientists to a watery end? *Trends Neurosci* 19:471-2.

Ruit KG, Elliott JL, Osborne PA, Yan Q, Snider WD (1992). Selective dependence of mammalian dorsal root ganglion neurons on nerve growth factor during embryonic development. *Neuron* ;8:573-87.

Rukwied R, Chizh BA, Lorenz U, Obreja O, Margarit S, Schley M, Schmelz M (2007). Potentiation of nociceptive responses to low pH injections in humans by prostaglandin E2. *J Pain* 8:443-451.

Rutter AR, Ma QP, Leveridge M, Bonnert TP (2005). Heteromerization and colocalization of TrpV1 and TrpV2 in mammalian cell lines and rat dorsal root ganglia. *Neuroreport* 16:1735-9.

Rydh-Rinder M, Berge OG, Hökfelt T (2001). Antinociceptive effects after intrathecal administration of phosphodiester-, 2'-O-allyl-, and C-5-propyne-modified antisense oligodeoxynucleotides targeting the NMDAR1 subunit in mouse. *Brain Res Mol Brain Res* 86:23-33.

Ryu S, Liu B, Qin F (2003). Low pH potentiates both capsaicin binding and channel gating of VR1 receptors. *J Gen Physiol* 122:45-61.

Sacharczuk M, Jaszczak K, Sadowski B (2003). Cytogenetic comparison of the sensitivity to mutagens in mice selected for high (HA) and low (LA) swim stress-induced analgesia. *Mutat Res* 535:95-102.

Sacharczuk M, Jaszczak K, Sadowski B (2003). Cytogenetic comparison of the sensitivity to mutagens in mice selected for high (HA) and low (LA) swim stress-induced analgesia. *Mutat Res* 535:95-102.

Sachidanandam R, Weissman D, Schmidt SC, Kakol JM, Stein LD, Marth G, Sherry S, Mullikin JC, Mortimore BJ, Willey DL, Hunt SE, Cole CG, Coggill PC, Rice CM, Ning Z, Rogers J, Bentley DR, Kwok PY, Mardis ER, Yeh RT, Schultz B, Cook L, Davenport R, Dante M, Fulton L, Hillier L, Waterston RH, McPherson JD, Gilman B, Schaffner S, Van Etten WJ, Reich D, Higgins J, Daly MJ, Blumenstiel B, Baldwin J, Stange-Thomann N, Zody MC, Linton L, Lander ES, Altshuler D; (2001). A map of human genome sequence variation containing 1.42 million single nucleotide polymrphisms. *Nature* 409: 928–933.

Sambrook J, Fritsch EF, Maniatis T (1989). Site directed mutagenesis. *Molecular Cloning: A Laboratory Manual*. New York: Cold Spring Harbor Laboratory.

Sambrook J, Russell DW (2001). Molecular Cloning: A Laboratory Manual, 3rd ed. Cold Spring Harbor, NY: Cold Spring Harbor Laboratory Press.

Sanchez JF, Krause JE, Cortright DN (2001). The distribution and regulation of vanilloid receptor VR1 and VR1 5' splice variant RNA expression in rat. *Neuroscience* 107:373-381.

Sanchez MG, Sangchez AM, Collado B, Malagarie-Cazenave S, Olea N, Carmena MJ, Prieto JC, Diaz-Laviada I (2005). Expression of the transient receptor potential vanilloid 1 (TRPV1) in LNCaP and PC-3 prostate cancer cells and in human prostate tissue. *Eur J Pharmacol* 515:20-7.

Sandor Z, Szallasi A (2005). Vanilloid receptor-mediated hyperalgesia and desensitization. In AB Malmberg, KR Bley (Eds), *Turning up the Heat on Pain: TRPV1 Receptors in Pain and Inflammation* (pp. 95-115). Basel: Birkhäuser.

Sant GR (1987). Intravesical 50% dimethyl sulfoxide (Rimso-50) in treatment of interstitial cystitis. *Urology* 29:17-21.

Sant GR (1991). Interstitial cystitis. *Monogr. Urol* 12: 37

Sant GR, LaRock DR (1994). Standard intravesical therapies for interstitial cystitis. *Urol Clin North Am* 21:73-83.

Santos, L., Tipping, P.G (1994). Attenuation of adjuvant arthritis in rats by treatment with oxygen radical scavengers. *Immunol Cell Biol* 72:406-414.

Sarton E, Olofsen E, Romberg R, den Hartigh J, Kest B, Nieuwenhuijs D, Burm A, Teppema L, Dahan A (2000). Sex differences in morphine analgesia: an experimental study in healthy volunteers. *Anesthesiology* 93:1245-1254.

Sasamura T, Sasaki M, Tohda C, Kuraishi Y (1998). Existence of capsaicin-sensitive glutamatergic terminals in rat hypothalamus. *Neuroreport* 9:2045-2048.

Sathianathan V, Avelino A, Charrua A, Santha P, Matesz K, Cruz F, Nagy I (2003). Insulin induces cobalt uptake in a subpopulation of rat cultured primary sensory neurons. *Eur J Neurosci* 18:2477-2286.

Sauer SK, Reeh PW, Bove GM (2001). Noxious heat-induced CGRP release from rat sciatic nerve axons in vitro. *Eur J Neurosci* 14: 1203–1208.

Schadt EE, Monks SA, Drake TA, Lusis AJ, Che N, Colinayo V, Ruff TG, Milligan SB, Lamb JR, Cavet G, Linsley PS, Mao M, Stoughton RB, Friend SH (2003). Genetics of gene expression surveyed in maize, mouse and man. *Nature* 422:297-302.

Schmidt R, Schmelz M, Forster C, Ringkamp M, Torebjörk HE, Handwerker HO (1995). Novel classes of responsive and unresponsive C nociceptors in human skin. *J Neurosci* 15:333-341.

Schoppa NE, McCormack K, Tanouye MA, Sigworth FJ (1992). The size of gating charge in wild-type and mutant Shaker potassium channels. *Science* 255:1712-5.

Schuel H, Goldstein E, Mechoulam R, Zimmerman AM, Zimmerman S (1994). Anandamide (arachidonylethanolamide), a brain cannabinoid receptor agonist, reduces sperm fertilizing capacity in sea urchins by inhibiting the acrosome reaction. *Proc Natl Acad Sci U S A* 91:7678-7682.

Schumacher MA, Moff I, Sudanagunta SP, Levine JD (2000). Molecular cloning of an N-terminal splice variant of the capsaicin receptor. Loss of N-terminal domain suggests functional divergence among capsaicin receptor subtypes. *J Biol Chem* 275:2756-2762.

Schwarz S, Greffrath W, Büsselberg D, Treede RD (2000). Inactivation and tachyphylaxis of heat-evoked inward currents in nociceptive primary sensory neurones of rats. *J Physiol* 528:539-49.

Scotland RS, Chauhan S, Davis C, De Felipe C, Hunt S, Kabir J, Kotsonis P, Oh U, Ahluwalia A (2004). Vanilloid Receptor TRPV1, Sensory C-Fibers, and Vascular Autoregulation: A Novel Mechanism Involved in Myogenic Constriction. *Circulation Research* 95:1027-1034.

Sengupta JN, Gebhart GF (1994). Characterization of mechanosensitive pelvic nerve afferent fibers innervating the colon of the rat. J Neurophysiol 71:2046-60.

Sharif Naeini R, Witty MF, Séguéla P, Bourque CW (2006). An N-terminal variant of Trpv1 channel is required for osmosensory transduction. *Nat Neurosci* 9:93-98.

Sharif RN, Osborne M, Coderre TJ, Fundytus ME (2002). Attenuation of morphine tolerance after antisense oligonucleotide knock-down of spinal mGluR1. *Br J Pharmacol* 136:865-72.

Shaw G, Morse S, Ararat M, Graham FL (2002). Preferential transformation of human neuronal cells by human adenoviruses and the origin of HEK 293 cells. *FASEB J* 16:869-71.

Shen W (2005). Repetitive light stimulation inducing glycine receptor plasticity in the retinal neurons. *J Neurophysiol* 94:2231-8.

Shiga KI, Hirano K, Nishimura J, Niiro N, Naito S, Kanaide H (2007). Dimethyl sulphoxide relaxes rabbit detrusor muscle by decreasing the Ca2+ sensitivity of the contractile apparatus. *Br J Pharmacol* 151:1014-1024.

Shimomura O, Johnson FH, Saiga Y (1962). Extraction, purification and properties of aequorin, a bioluminescent protein from the luminous hydromedusan, Aequorea. *J Cell Comp Physiol* 59:223-39.

Shin JS, Wang MH, Hwang SW, Cho H, Cho SY, Kwon MJ, Lee SY, Oh U (2001). Differences in sensitivity of vanilloid receptor 1 transfected to human embryonic kidney cells and capsaicin-activated channels in cultured rat dorsal root ganglion neurons to capsaicin receptor agonists. *Neurosci Lett* 299:135–139.

Shu XQ, Mendell LM (1999). Neurotrophins and hyperalgesia. *Proc Natl Acad Sci U S A* 96:7693-7696.

Sigmund CD (2000). Viewpoint: are studies in genetically altered mice out of control? *Arterioscler Thromb Vasc* Biol 20:1425-9.

Sigworth FJ (1994). Voltage gating of ion channels. *Q Rev Biophys* 27:1-40.

Simmons DD, Song C, Giboney P (1994). Kainic acid stimulates uptake of divalent cations in postnatal cochlear neurons. *Neuroreport* 5:1433-7.

Singh Tahim A, Sántha P, Nagy I (2005). Inflammatory mediators convert anandamide into a potent activator of the vanilloid type 1 transient receptor potential receptor in nociceptive primary sensory neurons. *Neuroscience* 136:539-548.

Sirkin R (2005). One-way Analysis of variance. *Statistics for the Social Sciences* (pp. 318-343). California: Sage Publications, Inc.

Smart D, Gunthorpe MJ, Jerman JC, Nasir S, Gray J, Muir AI, Chambers JK, Randall AD, Davis JB (2000). The endogenous lipid anandamide is a full agonist at the human vanilloid receptor (hVR1). *Br J Pharmacol* 129:227-230.

Smeraski CA, Böttger B, Finger TE (2001). Kainate-activated cobalt uptake in the primary gustatory nucleus in goldfish: visualization of the morphology and distribution of cells expressing AMPA/kainate receptors in the vagal lobe. *J Comp Neurol* 431:59-74.

Smith GD, Gunthorpe MJ, Kelsell RE, Hayes PD, Reilly P, Facer P, Wright JE, Jerman JC, Walhin JP, Ooi L, Egerton J, Charles KJ, Smart D, Randall AD, Anand P, Davis JB (2002). TRPV3 is a temperature-sensitive vanilloid receptor-like protein. *Nature* 418:186-190.

Sonnergaard JM (2006). On the misinterpretation of the correlation coefficient in pharmaceutical sciences. *Int J Pharm* 321:12-7.

Sontheimer H, Ransom BR (2002). Whole-cell patch-clamp recording. In W Walz, AA Boulton, GB Baker (Eds), *Patch-Clamp Analysis: Advanced Techniques* (pp. 35-68). New York: Springer-Verlag.

Sopasakis VR, Nagaev I, Smith U (2005). Cytokine release from adipose tissue of non-obese individuals. *Int J Obes (Lond*) 29:1144-7.

Sora I, Takahashi N, Funada M, Ujike H, Revay RS, Donovan DM, Miner LL, Uhl GR (1997). Opiate receptor knockout mice define mu receptor roles in

endogenous nociceptive responses and morphine-induced analgesia. *Proc Natl Acad Sci U S A* 94:1544-1549.

Southall MD, Li T, Gharibova Ls, Pei Y, Nicol GD, Travers JB (2003). Activation of epidermal vanilloid receptor-1 induces release of proinflammatory mediators in human keratinocytes. *J Pharmacol Exp Ther* 304:217-222.

Spielman RS, Bastone LA, Burdick JT, Morley M, Ewens WJ, Cheung VG (2007). Common genetic variants account for differences in gene expression among ethnic groups. *Nat Genet* 39:226-231.

Ständer S, Moormann C, Schumacher M, Buddenkotte J, Artuc M, Shpacovitch V, Brzoska T, Lippert U, Henz BM, Luger TA, Metze D, Steinhoff M (2004). Expression of vanilloid receptor subtype 1 in cutaneous sensory nerve fibers, mast cells, and epithelial cells of appendage structures. *Exp Dermatol* 13:129-39.

Starowicz K, Maione S, Cristino L, Palazzo E, Marabese I, Rossi F, de Novellis V, Di Marzo V (2007). Tonic endovanilloid facilitation of glutamate release in brainstem descending antinociceptive pathways. *J Neurosci* 27:13739-13749.

StatSoft, Inc. (2001). STATISTICA (data analysis software system), version 6. www.statsoft.com

Steen KH, Steen AE, Kreysel HW, Reeh PW (1996). Inflammatory mediators potentiate pain induced by experimental tissue acidosis. Pain 66:163-70.

Steen KH, Steen AE, Reeh PW (1995). A dominant role of acid pH in inflammatory excitation and sensitization of nociceptors in rat skin, in vitro. *J Neurosci* 5:3982-9.

Stone LS, MacMillan LB, Kitto KF, Limbird LE, Wilcox GL (1997). The alpha2a adrenergic receptor subtype mediates spinal analgesia evoked by alpha2 agonists and is necessary for spinal adrenergic-opioid synergy. *J Neurosci* 17:7157-65.

Stone LS, Vulchanova L (2003). The pain of antisense: in vivo application of antisense oligonucleotides for functional genomics in pain and analgesia. *Adv Drug Deliv Rev* 55:1081-112.

Story GM, Peier AM, Reeve AJ, Eid SR, Mosbacher J, Hricik TR, Earley TJ, Hergarden AC, Andersson DA, Hwang SW, McIntyre P, Jegla T, Bevan S, Patapoutian A (2003). ANKTM1, a TRP-like channel expressed in nociceptive neurons, is activated by cold temperatures. *Cell* 112:819-829.

Strachan T, Read A (1999). PCR, DNA sequencing and in vitro mutagenesis. *Human Molecular Genetics 2* (pp. 119-138). Oxford: Bios Scientific Publishers Ltd.

Stuhmer W (1997). Electrophysiological recording from Xenopus oocytes. In RB Bernardo, LE Iverson (Eds.), *Ion Channels: Methods in enzymology* (pp. 319-338). San Diego: Academic Press.

Stühmer W, Conti F, Suzuki H, Wang XD, Noda M, Yahagi N, Kubo H, Numa S (1989). Structural parts involved in activation and inactivation of the sodium channel. *Nature* 339:597-603.

Sugimoto M, Esaki N, Tanaka H, Soda K (1989). A simple and efficient method for the oligonucleotide-directed mutagenesis using plasmid DNA template and phosphorothioate-modified nucleotide. *Anal Biochem* 179:309-11.

Sugiura T, Tominaga M, Katsuya H, Mizumura K (2002). Bradykinin lowers the threshold temperature for heat activation of vanilloid receptor 1. *J Neurophysiol* 88:544-548. Susankova K, Ettrich R, Vyklicky L, Teisinger J,

Vlachova V (2007). Contribution of the putative inner-pore region to the gating of the transient receptor potential vanilloid subtype 1 channel (TRPV1). *J Neurosci* 27:7578-7585.

Sutton KG, Garrett EM, Rutter AR, Bonnert TP, Jarolimek W, Seabrook GR (2005). Functional characterisation of the S512Y mutant vanilloid human TRPV1 receptor. *Br J Pharmacol* 146:702-11.

Suzuki M, Sato J, Kutsuwada K, Ooki G, Imai M (1999). Cloning of a stretch-inhibitable nonselective cation channel. J Biol Chem 274:6330-6335. Tian W, Fu Y, Wang DH, Cohen DM (2006) Regulation of TRPV1 by a novel renally expressed rat TRPV1 splice variant. *Am J Physiol Renal Physiol* 290:F117-26.

Szallasi A, Blumberg PM (1990a). Resiniferatoxin and its analogs provide novel insights into the pharmacology of the vanilloid (capsaicin) receptor. *Life Sci* 47(16):1399-408.

Szallasi A, Blumberg PM (1990b). Specific binding of resiniferatoxin, an ultrapotent capsaicin analog, by dorsal root ganglion membranes. *Brain Res* 524:106-111.

Szallasi A, Blumberg PM (1991). Characterization of vanilloid receptors in the dorsal horn of pig spinal cord. *Brain Res* 547:335-338.

Szallasi A, Blumberg PM (1993). [3H]resiniferatoxin binding by the vanilloid receptor: species-related differences, effects of temperature and sulfhydryl reagents. *Naunyn Schmiedebergs Arch Pharmacol* 347:84-91

Szallasi A, Conte B, Goso C, Blumberg PM, Manzini S (1993). Characterization of a peripheral vanilloid (capsaicin) receptor in the urinary bladder of the rat. *Life Sci* 52:221-226.

Szallasi A, Joo F, Blumberg PM (1989). Duration of desensitization and ultrastructural changes in dorsal root ganglia in rats treated with resiniferatoxin, an ultrapotent capsaicin analog. *Brain Res* 503:68-72.

Székely G, Lévai G, Matesz K (1983). Primary afferent terminals in the nucleus of the solitary tract of the frog: an electron microscopic study. *Exp Brain Res* 53:109-17.

Szeto CY, Tang NL, Lee DT, Stadlin A (2001). Association between mu opioid receptor gene polymorphisms and Chinese heroin addicts. *Neuroreport* 12:1103-6.

Szolcasanyi J (1993). Actions of capsaicin on sensory neurones. In JN Wood, *Capsaicin in the study of pain* (pp. 1–26). London: Academic Press.

Szolcsanyi J, Anton F, Reeh PW, Handwerker HO (1988). Selective excitation by capsaicin of mechano-heat sensitive nociceptors in rat skin. *Brain Res* 446:262-8.

Takahashi T, Otsuka M (1975).Regional distribution of substance P in the spinal cord and nerve roots of the cat and the effect of dorsal root section. *Brain Res* 87:1-11.

Tanaka E, Ishii K, Akagi T, Hirai K, Motelica-Heino I, Katayama Y, Higashi H, Hashikawa T, Tsuji S (2004). A new cytochemical method for ultrastructural localization of Co2+ in rat hippocampal CA1 pyramidal neurons in vitro. *J Neurosci Method*s 135:1-8.

Taylor BA, Casas-Ganem J, Vaccaro AR, Hilibrand AS, Hanscom BS, Albert TJ (2005). Differences in the work-up and treatment of conditions associated

with low back pain by patient gender and ethnic background. *Spine* 30:359-364.

Taylor JW, Ott J, Eckstein F (1985). The rapid generation of oligonucleotide-directed mutations at high frequency using phosphorothioate-modified DNA. *Nucleic Acids Res* 13:8765-85.

Thomas P, Smart TG (2005). HEK293 cell line: a vehicle for the expression of recombinant proteins. *J Pharmacol Toxicol Methods* 51:187-200.

Thresh LT (1846). Isolation of capsaicin. *Pharm J* 6:941.

Tian W, Fu Y, Wang DH, Cohen DM (2006). Regulation of TRPV1 by a novel renally expressed rat TRPV1 splice variant. *Am J Physiol Renal Physiol* 290:117-126.

Tombola F, Pathak MM, Isacoff EY (2006). How does voltage open an ion channel? *Annu Rev Cell Dev Biol* 22:23-52.

Tominaga M, Caterina MJ, Malmberg AB, Rosen TA, Gilbert H, Skinner K, Raumann BE, Basbaum AI, Julius D (1998). The cloned capsaicin receptor integrates multiple pain-producing stimuli. *Neuron* 21:531-543.

Tominaga M, Julius D (2000). Capsaicin receptor in the pain pathway. *Jpn J Pharmacol* 83:20-24.

Tominaga M, Tominaga T (2005). Structure and function of TRPV1. *Pflugers Arch* 451:143-150.

Tominaga M, Wada M, Masu M: Potentiation of capsaicin receptor activity by metabotropic ATP receptors as a possible mechanism for ATP-evoked pain and hyperalgesia. roc Natl Acad Sci U S A 2001, 98:6951-6956.

Toomim CS, Millington WR (1998). Regional and laminar specificity of kainate-stimulated cobalt uptake in the rat hippocampal formation. *J Comp Neurol* 402:141-54.

Traub RJ, Mendell LM (1988). The spinal projection of individual indentified A6- and C-fibers. *J Neurophysiol* 59:41-55.

Trouet D, Nilius B, Voets T, Droogmans G, Eggermont J (1997). Use of a bicistronic GFP-expression vector to characterise ion channels after transfection in mammalian cells. *Pflugers Arch* 434:632-8.

Tsien RY (1998). The green fluorescent protein. *Annu Rev Biochem* 67:509-44.

Unruh A M (1996). Gender variations in clinical pain experience. *Pain* 65: 123–167.

Urdan TC (2005). One-Way Analysis of Variance. In Statistics *in Plain English* (pp. 120-138). Mahwah, NJ: Lawrence Erlbaum Associates.

van der Stelt M, Di Marzo V (2005). Anandamide as an intracellular messenger regulating ion channel activity. *Prostaglandins Other Lipid Mediat* 77:111-122.

Vandeyar MA, Weiner MP, Hutton CJ, Batt CA (1988). A simple and rapid method for the selection of oligodeoxynucleotide-directed mutants. *Gene* 65:129-33.

Vasko MR, Campbell WB, Waite KJ (1994). Prostaglandin E2 enhances bradykinin-stimulated release of neuropeptides from rat sensory neurons in culture. *J Neurosci* 14:4987–97.

Vellani V, Mapplebeck S, Moriondo A, Davis JB, and McNaughton PA (2001). Protein kinase C activation potentiates gating of the vanilloid receptor VR1 by capsaicin, protons, heat and anandamide. *J Physiol* 534: 813-825.

Vidt DG (1981). Mechanism of action, pharmacokinetics, adverse effects, and therapeutic uses of amiloride hydrochloride, a new potassium-sparing diuretic. *Pharmacotherapy* 1:179-87.

Vlachová V, Teisinger J, Susánková K, Lyfenko A, Ettrich R, Vyklický L (2003). Functional role of C-terminal cytoplasmic tail of rat vanilloid receptor 1. J *Neurosci* 23:1340-1350.

Vlachová V, Vyklický L (1993). Capsaicin-induced membrane currents in cultured sensory neurons of the rat. *Physiol Res* 42:301-11.

Voets T, Droogmans G, Wissenbach U, Janssens A, Flockerzi V, Nilius B (2004). The principle of temperature-dependent gating in cold- and heat-sensitive TRP channels. *Nature* 430:748-754.

Voets T, Owsianik G, Janssens A, Talavera K, Nilius B (2007). TRPM8 voltage sensor mutants reveal a mechanism for integrating thermal and chemical stimuli. *Nat Chem Biol* 3:174-182.

Vos MH, Neelands TR, McDonald HA, Choi W, Kroeger PE, Puttfarcken PS, Faltynek CR, Moreland RB, Han P (2006). TRPV1b overexpression negatively regulates TRPV1 responsiveness to capsaicin, heat and low pH in HEK293 cells. *J Neurochem* 99:1088-1102.

Vyklický L, Knotková-Urbancovä H (1996). Can sensory neurones in culture serve as a model of nociception? *Physiol Res* 45:1-9.

Vyklicky L, Lyfenko A, Kuffler DP, Vlachova V (2003). Vanilloid receptor TRPV1 is not activated by vanilloids applied intracellularly. *Neuro Report* 14: 1061-1065.

Vyklický L, Vlachová V, Vitásková Z, Dittert I, Kabát M, Orkand RK (1999). Temperature coefficient of membrane currents induced by noxious heat in sensory neurones in the rat. *J Physiol* 517:181-192.

Wach J, Marín-Burgin A, Klusch A, Forster C, Engert S, Schwab A, Petersen M (2003). Low-threshold heat receptor in chick sensory neurons is upregulated independently of nerve growth factor after nerve injury. *Neuroscience* 117:513-519.

Walder RY, Walder JA (1988). Role of RNase H in hybrid-arrested translation by antisense oligonucleotides. *Proc Natl Acad Sci U S A* 85:5011-5.

Waldmann R, Champigny G, Bassilana F, Heurteaux C, Lazdunski M (1997). A proton-gated cation channel involved in acid-sensing. *Nature* 386:173-177.

Walker K, Urban L, Medhurst SJ, Patel S, Panesar M, Fox AJ, McIntyre P (2003). The VR1 antagonist, capsazepine, reverses hyperalgesia in models of inflammatory and neuropathic pain. *J Pharmacol Exp Ther* 304:56-62.

Wan Y-J, Poland R, Han G (2001). Analysis of CYP2D6 polymorphism and enzyme activity in African-Americans in Southen California. *Pharmacogenetics* 11:489–499.

Wang SY, Mitchell J, Wang GK (2007). Preferential block of inactivation-deficient Na+ currents by capsaicin reveals a non-TRPV1 receptor within the Na+ channel. *Pain* 127:73–83.

Wang XM, Zhang ZJ, Bains R, Mokha SS (2002). Effect of antisense knock-down of alpha(2a)- and alpha(2c)-adrenoceptors on the antinociceptive action of clonidine on trigeminal nociception in the rat. *Pain* 98:27-35.

Wang Y, Hassouna MM (2000). Neuromodulation reduces c-fos gene expression in spinalized rats: a double-blind randomized study. *J Urol* 163:1966-1970.

Ward SM, Bayguinov J, Won KJ, Grundy D, Berthoud HR (2003). Distribution of the vanilloid receptor (VR1) in the gastrointestinal tract. *J Comp Neurol* 465:121-135.

Warren S, Yezierski RP, Capra NF (2006) The Somatosensory System II: Touch, Thermal Sense, and Pain. In: DE Haines (Ed.) *Fundamental Neuroscience for Basic and Clinical Applications* (pp. 280-301). Philadelphia: Elsevier Science Health Science Division.

Watanabe H, Vriens J, Suh SH, Benham CD, Droogmans G, Nilius B (2002). Heat-evoked activation of TRPV4 channels in a HEK293 cell expression system and in native mouse aorta endothelial cells. *J Biol Chem* 277:47044-51.

Wedding U, Koch A, Röhrig B, Pientka L, Sauer H, Höffken K, Maurer I (2008). Depression and functional impairment independently contribute to decreased quality of life in cancer patients prior to chemotherapy. *Acta Oncol* 47:56-62.

Weinshilboum R (2003). Inheritance and drug response. *N Engl J Med* 348:529–537.

Weisenberg M, Caspi Z (1989). Cultural and educational influences on pain of childbirth. *Journal of Pain and Symptom Management* 4:13–19.

Welch JM, Simon SA, Reinhart PH (2000). The activation mechanism of rat vanilloid receptor 1 by capsaicin involves the pore domain and differs from the activation by either acid or heat. *Proc Natl Acad Sci U S A* 97:13889-13894.

Werner T (2003). Functional in silico analysis of non-coding SNPs. In: MR. Barnes and IC. Gray (Ed.) *Bioinformatics for Geneticists* (pp273-287). West Sussex: John Wiley & Sons, Ltd.

Whalley ET, Clegg S, Stewart JM, Vavrek RJ (1987). The effect of kinin agonists and antagonists on the pain response of the human blister base. *Naunyn Schmiedebergs Arch Pharmacol* 336:652-5.

White DM (1996). Mechanism of prostaglandin E2-induced substance P release from cultured sensory neurons. *Neuroscience* 70:561-5.

White DM, Basbaum AI, Goetzl EJ, Levine JD (1990). The 15-lipoxygenase product, 8R,15S-diHETE, stereospecifically sensitizes C-fiber mechanoheat nociceptors in hairy skin of rat. *J Neurophysiol* 63: 966-70.

White J, Calcott G, Jenes A, Paule CC, Hossein M, Maze M, Santha P, Ma D, Nagy I (2008) Xenon reduces responses mediated through the transient receptor potential vanilloid type 1 receptor (TRPV1). 12th World Congress of the International Association of Studying Pain, Glasgow, UK.

Williams LR, Pregenzer JF, Oostveen JA (1992). Induction of cobalt accumulation by excitatory amino acids within neurons of the hippocampal slice. *Brain Res* 581:181–189.

Wilson K, Walker K (2005). Cell culture techniques. Principles and techniques of biochemistry and molecular biology (pp.71-76). Cambridge: Cambridge University Press.

Wingerd BD, Stein G (1988). The nervous system. In *Rat Dissection Manual* (pp. 38-39). Baltimore: Johns Hopkins University Press.

Winston J, Toma H, Shenoy M, Pasricha PJ (2001). Nerve growth factor regulates VR-1 mRNA levels in cultures of adult dorsal root ganglion neurons. P*ain* 89:181-6.

Winter J (1987). Characterization of capsaicin-sensitive neurones in adult rat dorsal root ganglion cultures. *Neurosci Lett* 80:134-140.

Winter J, Forbes CA, Sternberg J, Lindsay RM (1988). Nerve growth factor (NGF) regulates adult rat cultured dorsal root ganglion neuron responses to the excitotoxin capsaicin. *Neuron* 1:973-81.

Wise EA, Price DD, Myers CD, Heft MW, Robinson ME (2002). Gender role expectations of pain: relationship to experimental pain perception. *Pain* 96:335-342.

Wolfer DP, Crusio WE, Lipp HP (2002). Knockout mice: simple solutions to the problems of genetic background and flanking genes. *Trends Neurosci* 25:336-40.

Wood JN, Winter J, James IF, Rang HP, Yeats J, Bevan S (1988). Capsaicin-induced ion fluxes in dorsal root ganglion cells in culture. *J Neurosci* 8:3208-3220.

Woolf CJ, Costigan M (1999). Transcriptional and posttranslational plasticity and the generation of inflammatory pain. *Proc Natl Acad Sci USA* 96: 7723–7730.

Wuttke H, Rau T, Heide R, Bergmann K, Böhm M, Weil J, Werner D, Eschenhagen T (2002). Increased frequency of cytochrome P450 2D6 poor metabolizers among patients with metoprolol-associated adverse effects. *Clin Pharmacol Ther* 72:429–437.

Xia YX, Ikeda T, Xia XY, Ikenoue T (2000). Differential neurotrophin levels in cerebrospinal fluid and their changes during development in newborn rat. *Neurosci Lett* 280:220-2.

Xu GY, Huang LY, Zhao ZQ (2000). Activation of silent mechanoreceptive cat C and Aδ sensory neurons and their substance P expression following peripheral inflammation. *J Physiol* 528:339–348.

Xu H, Ramsey IS, Kotecha SA, Moran MM, Chong JA, Lawson D, Ge P, Lilly J, Silos-Santiago I, Xie Y, DiStefano PS, Curtis R, Clapham DE (2002). TRPV3 is a calcium-permeable temperature-sensitive cation channel. *Nature* 418:181-6.

Xu H, Tian W, Fu Y, Oyama TT, Anderson S, Cohen DM (2007). Functional effects of nonsynonymous polymorphisms in the human TRPV1 gene. *Am J Physiol Renal Physiol* 293:1865-1876.

Xue Q, Yu Y, Trilk SL, Jong BE, Schumacher MA (2001). The genomic organization of the gene encoding the vanilloid receptor: evidence for multiple splice variants. *Genomics* 76:14-20.

Yaksh TL, Jessell TM, Gamse R, Mudge AW, Leeman SE (1980). Intrathecal morphine inhibits substance P release from mammalian spinal cord in vivo. *Nature* 286:155-7.

Yin HZ, Lindsay AD, Weiss JH (1994). Kainate injury to cultured basal forebrain cholinergic neurons is Ca21 dependent. *Neuroreport* 5:1477–1480.

Yoon YH, Jeong KH, Shim MJ, Koh JY (1999). High vulnerability of GABA-immunoreactive neurons to kainate in rat retinal cultures: correlation with the kainate-stimulated cobalt uptake. *Brain Res* 823:33-41.

Yoshiki A, Moriwaki K (2006). Mouse phenome research: implications of genetic background. *ILAR J* 47:94-102.

Yoshimura N, Erdman SL, Snider MW, de Groat WC (1998). Effects of spinal cord injury on neurofilament immunoreactivity and capsaicin sensitivity in rat dorsal root ganglion neurons innervating the urinary bladder. *Neuroscience* 83:633-43.

Yoshimura N, Seki S, Novakovic SD, Tzoumaka E, Erickson VL, Erickson KA, Chancellor MB, de Groat WC (2001). The involvement of the tetrodotoxin-resistant sodium channel Na(v)1.8 (PN3/SNS) in a rat model of visceral pain. *J Neurosci* 21:8690-6.

Young MR, Blackburn-Munro G, Dickinson T, Johnson MJ, Anderson H, Nakalembe I, Fleetwood-Walker SM (1998). Antisense ablation of type I metabotropic glutamate receptor mGluR1 inhibits spinal nociceptive transmission. *J Neurosci* 18:10180-8.

Yu SP, Kerchner GA (1998). Endogenous voltage-gated potassium channels in human embryonic kidney (HEK293) cells. *J Neurosci Res* 52:612-7.

Yu SP, Kerchner GA (1998). Endogenous voltage-gated potassium channels in human embryonic kidney (HEK293) cells. *Journal of Neuroscience Research* 52:612–617.

Yukhananov R, Guan J, Crosby G (2002). Antisense oligonucleotides to N-methyl-D-aspartate receptor subunits attenuate formalin-induced nociception in the rat. *Brain Res* 930:163-9.

Zborowski M, Herzog E (1952). Life Is with People: The Jewish Little-Town of Eastern Europe. New York: International Universities Press.

Zhang X, Huang J, McNaughton PA (2005). NGF rapidly increases membrane expression of TRPV1 heat-gated ion channels. *The EMBO Journal* 24:4211-4223.

Zheng J, Dai C, Steyger PS, Kim Y, Vass Z, Ren T, Nuttall AL (2003). Vanilloid receptors in hearing: altered cochlear sensitivity by vanilloids and expression of TRPV1 in the organ of corti. *J Neurophysiol* 90:444-455.

Zhong J, Dietzel ID, Wahle P, Kopf M, Heumann R (1999). Sensory impairments and delayed regeneration of sensory axons in interleukin-6-deficient mice. *J Neurosci* 19:4305-4313.

Zhou N, Taylor DA and Parks TN (1995) Cobalt-permeable non-NMDA receptors in developing chick brainstem auditory nuclei. *Neuroreport* 6:2273–2276.

Zhou N, Taylor DA, Parks TN (1995). Cobalt-permeable non-NMDA receptors in developing chick brainstem auditory nuclei. *NeuroReport* 6:2273–2276.

Zhuang ZY, Xu H, Clapham DE, Ji RR (2004). Phosphatidylinositol 3-kinase activates ERK in primary sensory neurons and mediates inflammatory heat hyperalgesia through TRPV1 sensitization. *J Neurosci* 24:8300-8309.

Zimmer A, Zimmer AM, Hohmann AG, Herkenham M, Bonner TI (1999). Increased mortality, hypoactivity, and hypoalgesia in cannabinoid CB1 receptor knockout mice. *Proc Natl Acad Sci U SA* 96:5780-5785.

Zoller MJ, Smith M (1983). Oligonucleotide-directed mutagenesis of DNA fragments cloned into M13 vectors. *Methods Enzymol* 100:468-500.

Zygmunt PM, Peterson J, Anderson DA, Chuang H, Sorgard M, Di Marzo V (1999). Vanilloid receptors on sensory nerves mediate the vasodilator action of anandamide. *Nature* 400:452-457.

The end.